

The role of Class I Histone deacetylases in the formation of chromosome translocations

Dissertation

Zur Erlangung des Grades

Doktor der Naturwissenschaften

Am Fachbereich Biologie

Der Johannes Gutenberg-Universität Mainz

Rossana Piccinno

geboren am 12.04.1988

in Taranto, Italien

Mainz, 2022

Dekan der Fakultät für Biologie:

1. Berichterstatter:

2. Berichterstatter:

Tag der mündlichen Prüfung:

Table of Contents

| | |
|--|----|
| Summary | 8 |
| Zusammenfassung | 10 |
| Chapter 1 – Introduction..... | 12 |
| 1.1 Double-strand breaks pose a major threat to genome integrity | 12 |
| 1.2 DSB repair pathways | 13 |
| 1.2.1 DSB repair pathways: a chromatin-based choice | 16 |
| 1.3 Chromosome translocations are associated with cancer..... | 18 |
| 1.4 Cellular and chromatin determinants for the formation of chromosome translocations | 20 |
| 1.4.1 DNA & chromatin features affect breakage susceptibility | 20 |
| 1.4.1.1 DNA features which facilitate chromosome breakage | 20 |
| 1.4.1.2 Chromatin features associated with breakpoint regions | 22 |
| 1.4.2 Nuclear positioning of DSBs | 24 |
| 1.4.2.1 Motion properties of DSBs: “...and yet, it moves” | 25 |
| 1.4.2.2 DSB pairing | 29 |
| 1.4.3 The role of DSB repair pathways | 33 |
| 1.5 Class I histone deacetylases..... | 36 |
| 1.5.1 The role of HDAC1 and HDAC2 in genome integrity | 38 |
| 1.5.2 Drug-targeting HDACs in cancer therapy | 40 |
| 1.6 Open questions | 42 |
| 1.6.1 Goals of the study | 43 |
| Chapter 2 – Results..... | 46 |
| 2.1 Screen for epigenetic inhibitors reveals modulators of translocation frequency..... | 46 |
| 2.1.1 Class I HDAC inhibition, decreases the frequency of translocations..... | 47 |
| 2.2 Time and space control of DSBs induction | 50 |
| 2.2.1 Strategy | 50 |
| 2.2.2 Selection of DD-I-SceI-GR cell line (Superduo cells) | 51 |
| 2.3 Local chromatin changes in the proximity of a DSB | 57 |
| 2.3.1 Artificial tethering of chromatin modifiers to induce specific chromatin domains..... | 57 |
| 2.3.2 Functional validation of chromatin domains upon tethering of chromatin modifiers | 59 |
| 2.3.2.1 HDAC1-tethering causes chromatin condensation of the locus | 61 |
| 2.3.2.2 Artificial tethering of HDAC1 or TIP60 does not influence the accessibility of the locus | 62 |
| 2.3.2.3 HDAC1 and TIP60-tethering induces depletion and enrichment of panacetylation of histone H4 (H4panAc), respectively | 63 |
| 2.4 HDAC1 facilitates the formation of chromosome translocations..... | 65 |
| 2.4.1 HDAC1 depletion decreases LacO-TetO translocation frequency..... | 65 |
| 2.4.2 Tethering of HDAC1 at DSBs increases translocation frequency..... | 67 |

| | |
|---|-----|
| 2.5 Histone hyper-acetylation decreases DSB motility | 69 |
| 2.5.1 HDAC inhibition decreases DSB mobility..... | 69 |
| 2.5.2 HDAC1 depletion decreases DSB mobility | 70 |
| 2.6 A hypo-acetylated chromatin environment leads to high frequency of chromosome translocations..... | 71 |
| 2.6.1 Induction of DSBs in various chromatin contexts..... | 71 |
| 2.6.2 Repair of DSBs in various chromatin contexts..... | 74 |
| 2.6.3 Decitabine and NU7441 treatments are used as controls to screen for suppressors or enhancers of AsiSI-induced genome instability | 76 |
| 2.6.4 Modelling of AsiSI – induced breakage and translocations by C-Fusion 3D upon decitabine or NU7441 treatment..... | 76 |
| 2.6.5 Chromosome translocations occur preferentially at sites with hypo-acetylated histones upon the formation of DSBs..... | 79 |
| 2.6.5.1 Fast and slow repair rates of DSBs do not correlate with difference in acetyl histone marks | 82 |
| 2.7 HDAC inhibition reduces the frequency of Etoposide-induced <i>MLL</i> translocations | 84 |
| 2.8 Investigating key determinants of etoposide-mediated genome instability..... | 87 |
| 2.8.1 Etoposide–induced genome instability depends on both Topoisomerase 2 alpha and beta.. | 88 |
| 2.8.2 Transcription and replication are contributors of Etoposide-induced DNA damage | 91 |
| 2.8.3 VCP and proteasome system are enhancers of Etoposide-induced genome instability..... | 93 |
| Chapter 3 – Discussion..... | 97 |
| 3.1 Chromatin – related functions influence chromosome translocation frequency | 97 |
| 3.2 A cell-based system for the spatial and temporal controlled formation of I-SceI-induced DSBs | 98 |
| 3.3 HDAC1 plays a major role in the formation of chromosome translocations | 99 |
| 3.4 Functional validation of tethering of mCherryLacR-chromatin modifiers..... | 100 |
| 3.5 AsiSI endonuclease induces DSBs in various chromatin contexts..... | 102 |
| 3.6 HDACs inhibition decreases etoposide-induced <i>MLL</i> translocations | 104 |
| Chapter 4 – Material & Methods..... | 105 |
| 4.1 Material | 105 |
| 4.2 Methods | 105 |
| 4.2.1 Generation of Dox-inducible cell line for space and time control of I-SceI enzyme | 105 |
| 4.2.1.1 Cloning of GR-I-SceI degron constructs in lentiviral pLenti CMV TRE 3G..... | 105 |
| 4.2.1.2 Infection of NIH3T3 duo cells with Dox-inducible lentiviral vectors for the expression of GR-I-SceI constructs..... | 109 |
| 4.2.2 Generation of stable cells lines for the overexpression of mCherry-LacR-chromatin modifiers..... | 110 |
| 4.2.2.1 Two steps cloning strategy | 110 |
| 4.2.2.2 Infection with retroviral vectors to over-express mCherry-LacR-chromatin modifiers | 111 |
| 4.2.3 Cell Maintenance..... | 112 |

| | |
|---|-----|
| 4.2.4 Drug treatments | 113 |
| 4.2.4.1 Induction and repair of DSBs | 113 |
| 4.2.4.2 Induction of chromatin domains | 113 |
| 4.2.4.3 Chemical Inhibitors | 113 |
| 4.2.5 Immunofluorescence assay | 114 |
| 4.2.6 Cytoskeletal extraction | 115 |
| 4.2.7 siRNAs knockdown | 116 |
| 4.2.8 Silencing of Top2A and Top2B via shRNAs in CD34+ | 117 |
| 4.2.9 Western blot analysis | 118 |
| 4.2.10 TOP2ccs detection assay | 119 |
| 4.2.11 Screening set up | 120 |
| 4.2.12 qPCR | 120 |
| 4.2.13 Chromatin condensation assay | 121 |
| 4.2.14 Chromatin enrichment or depletion of acetyl-histone marks measured by IF | 121 |
| 4.2.15 Chromatin accessibility by Ligation-Mediated PCR | 122 |
| 4.2.16 DSB Motion: experimental procedure and analysis | 123 |
| 4.2.17 Fluorescent labelling of BAC probes | 124 |
| 4.2.18 Fluorescence <i>In Situ</i> Hybridization (FISH) | 125 |
| 4.2.19 Imaging and image analysis | 125 |
| 4.2.19.1 FISH image analysis | 127 |
| 4.3. Supplementary methods | 128 |
| 4.3.1 ChIP-seq data analysis | 128 |
| 4.3.2 DSB repair kinetics by sBLISS | 128 |
| 4.3.2.1 AsiSI-DSB repair kinetics - model | 129 |
| Chapter 5 – References | 134 |
| List of abbreviations arranged in alphabetical order | 159 |
| List of figures | 161 |
| List of tables | 162 |

Summary

Exposure to DNA damaging agents and failure of safeguarding genome integrity mechanisms could lead to accumulation of DNA Double strands breaks (DSBs) that increase the risk of forming chromosome translocations. Chromosome translocations are low in frequency gene fusions, which could provoke deregulation of gene expression of oncogenes and tumor suppressor genes, and thereby, drive tumorigenesis. Chromosome translocations are the result of a multistep process, which lead to illegitimate fusion of spatially proximal DSBs from different chromosomes. However, because of their rare occurrence and the lack of research efforts in investigating upstream events of DSB illegitimate repair, molecular players and pathways dictating the formation of chromosome translocations are not fully elucidated. For instance, although DSBs and chromosome translocations occur in the context of highly ordered chromatin organization, whether and how chromatin-related functions influence the frequency of chromosome translocations remain unclear. Here, we raised the hypothesis that chromatin-related functions might affect also the propensity of two DSBs to pair within the nucleus and, then, to engage in an illegitimate repair fusion, thereby influencing the frequency of chromosome translocations. To address this, we performed a screening to identify epigenetic inhibitors that influence the frequency of chromosome translocations. We found that Class I HDACs inhibitors act as suppressors of chromosome translocations. In particular, both global loss-of-function experiments and local tethering of HDAC1 in proximity of breakpoints revealed that HDAC1 facilitates the formation of chromosome translocations. To reveal the molecular mechanisms underlying HDAC1-dependent increase in translocation frequency, we have used the DIvA system by which we could monitor changes in chromosome translocation frequencies in correlation with acetylation levels in the vicinity of DSBs-induced via AsiSI endonuclease. Using sBLISS to profile repair kinetics of AsiSI-DSBs genome-wide, we correlated translocation frequency, acetylation levels in the vicinity of induced DSBs and DSB repair rates. However, we found that change in acetylation levels in the vicinity of induced DSBs does not influence the DSB repair kinetics.

To dissect DSBs dynamics in cells with global perturbed levels of HDACs we developed a system to spatially and temporally control the formation of DSBs. Since translocating DSBs show higher mobility compared to non-translocating DSBs, we sought to dissect whether DSB-motion properties are influenced by changes on the levels of histone acetylation, in a degree to affect the frequency of translations. We demonstrated that HDACs inhibitors or depletion of HDAC1 lead to retention of histone acetyl marks onto chromatin and provoke decreased mean square displacement compared to control conditions, suggesting that HDAC1-dependent acetylation might facilitate the propensity of a DSB to move faster and synapse with a translocation-partner. Finally, we validated that HDACs inhibition suppresses the occurrence of recurrent oncogenic *MLL* translocations upon chemotherapeutic treatment with etoposide, without decreasing the cytotoxic effect of TOP2 poison.

Together, our results indicate that histone hyper-acetylation due to lack of HDAC1 activity decreases the frequency of chromosome translocations by decreasing DSB mobility.

Zusammenfassung

Die Exposition gegenüber DNA-schädigenden Stoffen und der Verlust von Mechanismen, die die Genomintegrität schützen, können zur Häufung von DNA-Doppelstrangbrüchen (DSBs) führen, die das Risiko von Chromosomentranslokationen erhöhen. Diese sind das Ergebnis eines mehrstufigen Prozesses, der zu einer illegitimen Fusion räumlich benachbarter DSBs von verschiedenen Chromosomen führt. Translokationen treten selten auf, können aber eine Deregulierung der Expression von Onkogenen und Tumorsuppressorgenen hervorrufen und dadurch die Tumorentstehung vorantreiben. Aufgrund ihrer Seltenheit und des Mangels an Forschungsanstrengungen bei der Untersuchung von Translokationen vorgeschalteter DSB-Reparaturmechanismen, sind molekulare Akteure, die die Bildung von Translokationen diktieren, noch nicht vollständig aufgeklärt. Obwohl DSBs und Translokationen im Zusammenhang der übergeordneten Chromatinorganisation auftreten, bleibt unklar, ob und wie die Chromatinumgebung die Häufigkeit von Translokationen beeinflussen. Hier stellen wir die Hypothese auf, dass die Chromatinumgebung die Neigung zweier DSBs beeinflussen könnte, im Zellkern aufeinander zutreffen und dann illegitim zu fusionieren, was die Häufigkeit von Chromosomentranslokationen beeinflusst.

Durch Screening epigenetischer Inhibitoren durch die die Häufigkeit von Translokationen potentiell beeinflusst wird, fanden wir heraus, dass Inhibitoren von Histondeacetylasen (HDACs) der Klasse I Translokationen verhindern. Die Untersuchung einer lokalen Anreicherung von HDAC1 in der Nähe von DSBs zeigte, dass HDAC1 die Bildung von Translokationen begünstigt. Mit Hilfe von sBLISS, profilierten wir die genomweite Reparaturkinetik von AsiSI-induzierten DSBs im zellulären Modell der DiVA-Zellen und korrelierten Translokationshäufigkeit, Acetylierungsniveau in der Nähe von induzierten DSBs und DSB-Reparaturraten. Wir fanden heraus, dass eine Änderung des Acetylierungsniveau in der Nähe von DSBs deren Reparaturkinetik nicht beeinflusst.

Um die DSB-Mobilität in Zellen mit veränderten HDAC-Leveln zu analysieren, entwickelten wir ein System, mit dem die Bildung von DSBs räumlich und zeitlich kontrollierbar ist. Da DSBs, welche zur Translokationsbildung neigen, eine höhere Mobilität aufweisen, analysierten wir, Änderungen der Histonacetylierung deren Bewegungseigenschaften so beeinflusst, dass sie die Häufigkeit von Translokationen beeinflussen. Wir zeigten, dass fehlende HDAC1 Aktivität Acetylmarkierungen auf Histonen stabilisiert und eine geringere mittlere quadratische Verschiebung hervorruft, was darauf hindeutet, dass ein DSB durch die HDAC1-abhängige Acetylierung mobiler ist und eher Teil einer Chromosomentranslokation wird. Schließlich haben wir validiert, dass die HDAC-Hemmung das Auftreten onkogener MLL-Translokationen nach Chemotherapie mit Etoposid unterdrückt, ohne die Zytotoxizität von Etoposid zu verringern. Zusammengefasst zeigen unsere Ergebnisse, dass fehlende HDAC1-Aktivität die Häufigkeit von Chromosomentranslokationen durch eine Reduktion der DSB-Mobilität verringert.

Chapter 1 – Introduction

1.1 Double-strand breaks pose a major threat to genome integrity

Throughout evolution, cells have matured mechanisms to safeguard genome integrity in order to ensure a faithful transmission of the genetic material during cell division or a correct inheritance by the offspring.

Every day, however, our genome is threatened with $\sim 10^5$ DNA lesions per cell, which are the results of endogenous and environmental insults (Hoeijmakers 2009; Tubbs and Nussenzweig 2017). During DNA replication, dNTPs can be erroneously incorporated and generally, during normal cellular metabolism, abasic sites, DNA base alkylation or deamination can spontaneously accumulate on DNA sequence. Oxidation of DNA bases can also provoke chromosome breaks and increased genome instability, both reduced in anaerobic conditions. Endogenous damage can also arise from abortive reaction cycles of Topoisomerase enzymes, stalled and collapsed replication forks, head on collisions between replication forks and the transcription bubble. Certain DNA features might pose a threat to genome stability, for instance, repetitive sequences can be intrinsically fragile and thereby hotspots of chromosome breakage or they cause DNA polymerase slippage; finally, DNA can configure in harmful non-canonical B-DNA structures. Numerous works have recently witnessed a role for R-loops and G-quadruplex in eliciting genome instability (Aguilera and Gómez-González; 2017; Cristini et al. 2018; S. Cohen et al. 2018; Cristini et al. 2019; Mosler et al. 2021; Crossley, Bocek, and Cimprich 2019; Niehrs and Luke 2020; Y. Wang et al. 2019; De Magis et al. 2019; Galati et al. 2021).

Pervasive source of exogenous hazards to DNA are ultraviolet light (UV) and ionizing radiation (IR); cigarette smoke, crosslinking agents and chemotherapeutics, such as Topoisomerase poisons are also associated with tumorigenesis.

All these types of DNA insults become highly cytotoxic when they are converted into DNA Double-Strand Breaks (DSBs). Persistent DSBs are particularly deleterious because of their potential to induce structural changes at chromosomal level, such as deletions, inversions, duplications and chromosome translocations, which are hallmarks of cancer.

However, at cellular level, genome is preserved by a fine orchestration of evolutionary conserved metabolic reactions that go under the name of DNA damage response (DDR), during which a polyphony of post-translation modifications on damaged chromatin and on DDR factors themselves, regulates the accessibility of repair proteins to the DNA lesion. This provides a spatial and temporal control of DNA damage signaling and repair. Cascade of events constitutes the response to a DNA lesion: briefly, sensor proteins detect the damage on DNA, then mediators transduce the signals to effectors proteins eliciting not only DNA repair, but also a multitude of cellular responses, which have the final goal to tune down the cellular metabolism until the lesion is repaired. Because DDR is integral to chromatin organization, chromatin changes, occurring in response to DNA damage, present another level of DDR regulation. For instance, rapid phosphorylation at Ser139 of H2A.X (γ H2AX) mediated by master sensor kinases,

Introduction

such as ATM, ATR and DNAPKs, constitutes one of the earliest events upon DSB formation (Rogakou et al. 1998). Therefore, γ H2AX is used as *bona fide* marker for DSBs detection and DDR activation. Phosphorylation at the level of histone variant H2A.X spreads for megabases on both sides of the lesion allowing signaling amplification and it represents a docking site for the recruitment of the mediator protein, MDC1 that, in turn, serves as scaffold for the recruitment of downstream transducers proteins.

The level of complexity of DDR regulation does not end with the interplay of chromatin-related factors. In fact, maintenance of genome integrity is a sophisticated affair as DDR can operate also during physiological cellular metabolisms. For instance, during V(D)J recombination, RAG1-RAG2 complex generates a blunt DSB at recombination-signal sequences; whereas in class-switch recombination, AID induces deamination of cytosine to uracil, then mismatches generate SSBs, finally converted into DSBs. Both are cases of programmed DNA damage, where DNA repair factors contribute to generate immune receptors diversity. Similarly, during meiotic recombination, initiated by Spo11-bound DSBs, DDR components coordinate gametes diversification. Finally, telomeres ends have a 3' single strand DNA overhang, DNA structures that resemble a DSB; thereby it is not surprising that active mechanisms exist to refrain DDR at telomeres in physiological conditions (De Lange 2005).

1.2 DSB repair pathways

Non-homologous ends joining (NHEJ) and Homologous Recombination (HR) are the two main DSB repair mechanisms, which differ for the extension of ends processing and, thereby, for the usage or not of a homologous template to copy faithfully the genetic information. In fact, HR-mediated end-resection of DSBs has the ultimate goal to generate a 3' single strand DNA substrate to perform strand invasion and to repair the damaged strand in error-free manner. Because HR relies on the presence of the sister chromatid, it is utilized mainly during S/G2 phase of the cell cycle. Vice versa, the mere re-ligation of unprocessed double strand ends secures NHEJ as main DSB repair pathway that can operate throughout the cell cycle, but with the cost of possible insertions, deletions or chromosome translocations during the end-joining of heterologous DSBs.

End-processing highly depends on DSBs sensors, which compete for the binding of double-strand ends and convey DSBs repair through recruitment of specific downstream signaling and repair factors. In fact, Ku70-Ku80 dimer rapidly engages the double strand ends into its toroidal structure and it assists to DNA-PK loading, thereby forming a holoenzyme that tethers DSB, protecting the ends from resection, and initiates c-NHEJ (Figure 1). Non-homologous end-joining repair progresses via DNAPKcs phosphorylation of ARTEMIS, which processes unligatable DNA ends; then, Ku-dependent recruitment of LIG4/XRCC4 promotes re-ligation of the double strand ends. Finally, auto-phosphorylation of DNAPKcs promotes its dissociation from Ku proteins.

Introduction

Binding of Ku70-Ku80 has a further function of keeping in place the double strand ends, thereby during NHEJ, DSBs mobility is generally restrained (Soutoglou et al. 2007; Roukos et al. 2013), with some important exceptions, such as at telomeric ends (Dimitrova et al. 2008; S. Difilippantonio et al. 2008).

On other hand, PARP1 facilitates alt-EJ and competes with Ku binding (M. Wang et al. 2006). However, it might also promote MRN recruitment, shifting towards a type of homologous directed repair that requires homology search and strand invasion: these moments of DSBs repair are characterized by an enhanced mobility of DSBs (Miné-Hattab and Rothstein 2012).

MRN is a trimeric complex composed of MRE11-RAD50-NBS1. While MRE11 has endonuclease and exonuclease activities important for end processing of DSBs, NBS1 binds ATM at DSB. ATM is a master kinase, and together with DNA-PKcs and ATR, belongs to the family of phosphoinositide 3-kinase (PI3K)-related kinases (PIKKs), which phosphorylate many targets in DNA damage response. Among those, ATM sustains DSB signaling through phosphorylation of H2AX that leads to MDC1 recruitment, which serves as docking platform for the recruitment of MRN itself but also of RNF8 (in complex with UBC13) and RNF168 that, together with BRCA1, are E3 ligases regulating 53BP1 accessibility to DSB lesion (Doil et al. 2009; Kolas et al. 2007; Huen et al. 2007). 53BP1 increases chromatin mobility, thereby favoring synapsis of distal chromosome ends and, in G1 phase, it antagonizes with BRCA1-CtIP-mediated DSB resection, by doing so it supports end-joining of double strand ends (Dimitrova et al. 2008; S. Difilippantonio et al. 2008; Escribano-Díaz et al. 2013).

During Homologous Recombination, MRN complex together with CtIP promote the formation of single strand DNA (Sartori et al. 2007), that, after RPA-coating, becomes substrate for RAD51-mediated strand invasion Figure 1 and recombinases-driven reactions can take place.

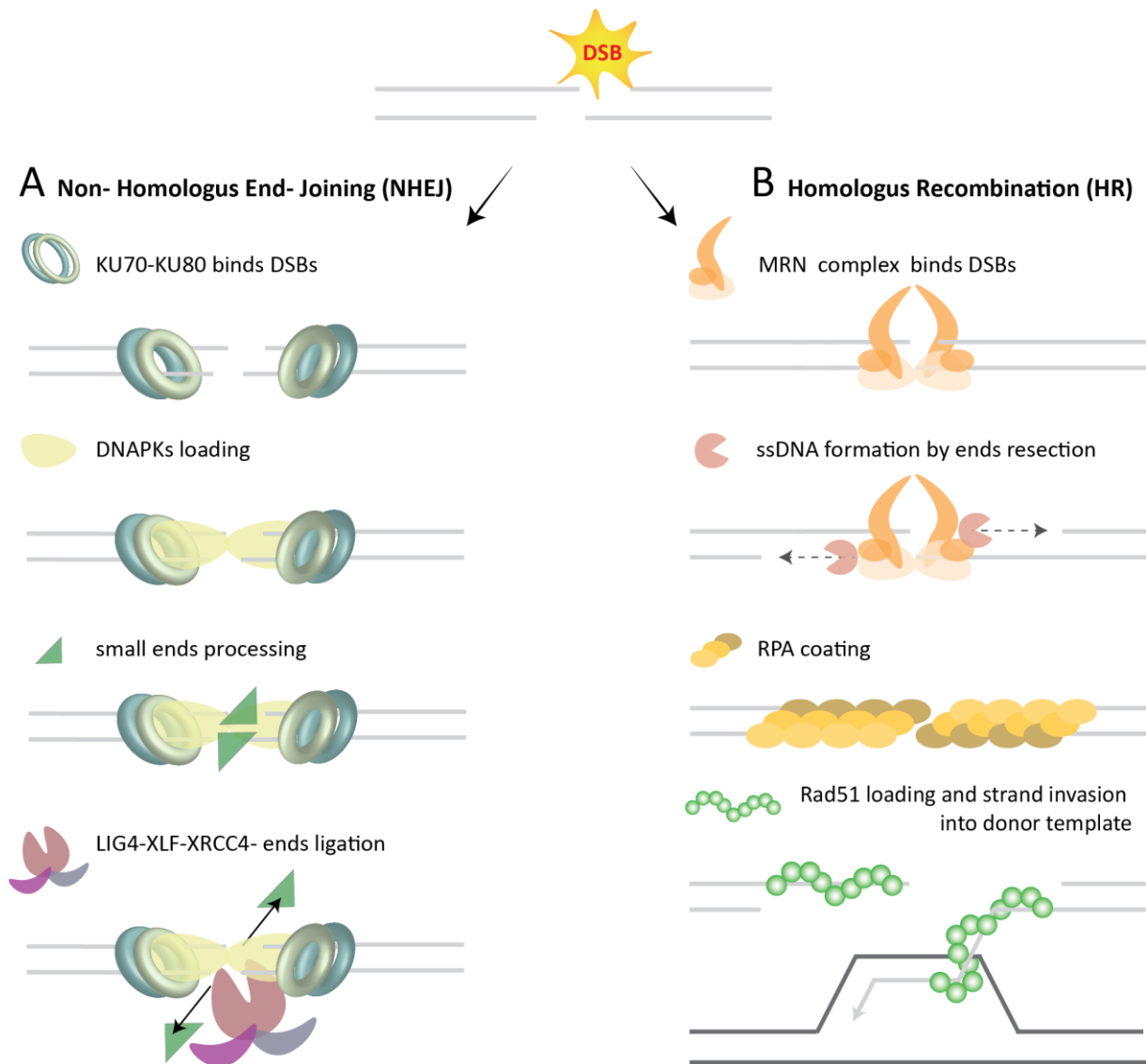


Figure 1: DSB-repair pathways. DSBs formation triggers DNA damage response, which senses the damage, transmits signaling effectors and mediates the repair through two main mechanisms, Non-Homologous End Joining (NHEJ) and Homologous Recombination (HR). **A.** During NHEJ, Ku70-Ku80 heterodimer binds DSBs, keeps in place the double strand ends within its toroidal structure and prevents ends-processing. This step helps recruitment of DNAPK, a PI3K – like kinase, which phosphorylates downstream effectors and sustains signaling. This allows accrual of other factors involved more in the processing and repair of double strand ends: for instance, in G1 phase, MRE11 and ARTEMIS mediate end-processing of unligatable ends; then, LIG4 together with XLF and XRCC4 mediates sealing of the double strand ends, via end ligation. **B.** During HR, MRN complex competes with Ku70-Ku80 for the binding of double strand ends. MRE11 binding stimulates CtIP-EXO1 resection that generates a ssDNA; this structure is stabilized by RPA coating prior RAD51 filaments formation which, together with helicase activity, assists strand invasion in a donor template, from which the genetic information is copied and restored into the damaged double helix.

Although, KU dimer and NBS1 recruit respectively, DNA-PK and ATM or MDC1 in order to scaffold the accrual of many downstream effectors, DDR factors accumulate at DSB not only via protein-protein interactions. In fact, accrual and disassociation of DNA damage factors takes place through recognition of chemical groups, which are post-translationally added or removed at the level of DDR factors' or histone proteins' residues.

Introduction

Among the post translation modifications regulating assembly and activity of repair factors at DSB site, phosphorylation is undeniably largely represented: several hundreds of phosphorylated targets have been identified and numerous DDR factors contain phospho-binding motifs to participate in the signaling cascade of a DSB lesion.

Sumoylation and ubiquitination are other modifications determining both the accrual of DDR factors to the double strand ends and dynamics of the broken chromosomes (Ryu et al. 2015; Torres-Rosell et al. 2007; Churikov et al. 2016; Horigome et al. 2016; Whalen et al. 2020; Hauer et al. 2017). PARylation rapidly occurs during a DSB response and it regulates not only the accumulation and dissociation of DDR factors, but also it is involved in local modulation of the chromatin structure (Luijsterburg et al. 2016). Methylation and acetylation are post-translation modifications that mainly occur at the level of residues of histone proteins and, therefore, they are revisited in the next paragraph where I am describing chromatin changes as steps of a DNA damage response. However it is noteworthy that histone modifiers can operate also by depositing or removing chemical groups at residues of DNA damage signaling factors, for example the master kinase ATM gets acetylated at Lys3016 by the histone acetyltransferase TIP60, and loss of Tip60 blocks ATM auto-phosphorylation at Ser 1981 and activation (Sun et al. 2007; 2005).

1.2.1 DSB repair pathways: a chromatin-based choice

When analyzing the cascade of events in response to DSBs formation, one must consider that chromatin structure constitutes the ground where DSB repair takes place. Chromatin does not constitute a physical barrier to DSB repair, rather important changes at nucleosomes surrounding a DNA lesions are integral moments of the response to DNA damage. These modifications occur either at the level of histone proteins, which are the base units of nucleosomes, or at the level of non-histone proteins associated with chromatin, and together ensure the high-order folding of the chromatin fibers. Upon a DNA lesion, changes of the surrounding chromatin environment are mediated by ATP-dependent remodeling complexes, histone chaperones and chromatin modifiers, which, respectively, slide or evict nucleosomes, assist exchange of DDR-specific histone variants, or mediate chemical modifications at specific residues, thereby regulating which proteins converge at the site of lesion.

During DDR, Tip60-mediated acetylation of histone H2A and H4 rapidly occurs at damaged chromatin (Ikura et al. 2000) with the scope to promote the accessibility of repair factors. Tip60, as part of NuA4 complex, gets recruits via Arp4 - binding of H2A-Ser129 phosphorylated (Downs et al. 2004). This interaction is important for the recruitment of other remodeling complexes such as Ino80 and Swr1 and, altogether they regulate H2A.Z/H2A exchange. H2A.Z, together with deposition of the specialized H3.3 histone variant lead to destabilization of the nucleosome fiber and enhance H4-acetylation. Depletion of histone linker H1 has the effect to increase nucleosome spacing, and, together, these events have the scope to open chromatin structure and to promote DSB repair. However, chromatin remodeling does not

Introduction

produce exclusively a more relaxed configuration to ensure accessibility to DDR factors, in fact KAP1 and HP1, typical of heterochromatic regions are actively recruited at DSB, where they are important for 53BP1 and BRCA1 loading (Baldeyron et al. 2011; Luijsterburg et al. 2009), supporting a model where transient chromatin condensation has the effect of promoting full DDR activation (Burgess et al. 2014). On the other hand, loss of HP1 further stimulates Tip60 - mediated acetylation of histone H3 at DSB site (Sun et al. 2009), and in heterochromatin domains, both HP1 and H3K9 methyltransferase knockdowns facilitate the repair of DSBs that persist in absence of ATM (Goodarzi et al. 2008), whereas expansion of HP1 domain facilitates DSB relocation at the periphery of the domain (Chiolo et al. 2011). These pieces of evidence demonstrate not only that chromatin is integral to DDR and promotes an environment permissive for the recruitment of repair factors, but also it highlights that chromatin changes affect the mobility of a broken chromosome end. Another example of DSBs-induced “chromatin breathing” is given by NurD complex, which counteracts the chromatin relaxation induced by CHD7 chromatin remodeler, fostering an accurate repair (Rother et al. 2020).

Importantly, chromatin is primed in different ways that dictate the pathway choice to repair a given DSB, according to the cell cycle stage and the nuclear context in which the lesion is arisen. For instance, 53BP1 is a bivalent histone mark reader, in fact, it accumulates to DSB via binding of RNF168-mediated K15 ubiquitination of H2A and through its tandem Tudor domain that recognizes H4K20me2 (Fradet-Turcotte et al. 2013). The affinity of this binding is reduced in presence of Tip60-mediated H4K16ac (Tang et al. 2013). Moreover, MBTD1 subunit of NuA4 complex competes with 53BP1 for H4K20me2 binding and Tip60 subunit mediates acetylation of H2AK15, which lose the ability to anchor 53BP1 through RNF168-ubiquitination (Jacquet et al. 2016). In fact, in this scenario the interplay between histone acetylation and histone ubiquitination is fundamental to assure chromatin dynamics (Ikura et al. 2007). In S and G2 phase, Tip60-phosphorylation prevents 53BP1 accumulation at break site (M. L. Li et al. 2019). Together this highlights a critical role of Tip60 in limiting BRCA1-blocker, 53BP1, and, therefore, favoring HR. Likewise to chromatin writers, erasers of histone modifications guide toward a specialized type of repair. For instance, histone deacetylases 1 and 2 are quickly recruited at laser-induced lesion to deacetylate H3K56 and H4K16, this latter is a well-characterized DNA-damage responsive marker. The same authors have found that depletion of HDAC1 and HDAC2 elicits a persistent DNA damage response and impairs NHEJ repair similarly to Lig4 depleted cells (Miller et al. 2010), again supporting the active role or repressive chromatin complex in DDR. Role of histone deacetylases in DSB repair is similarly revealed by another work showing that SIRT7 deficient mice die perinatally, while the survivors display accelerated aging and increased genomic instability due to accumulation of H3K18Ac, that impair NHEJ (Vazquez et al. 2016).

1.3 Chromosome translocations are associated with cancer

In 1960, a minute chromosome (Philadelphia chromosome) was described as first chromosomal abnormality associated with hematological disorders (Nowell 1962). Almost a decade later, through banding analysis of metaphase chromosomes, Philadelphia chromosome was identified to be the result of a balanced chromosomal translocation between chromosome 9 and chromosome 22, where rearrangements between long chromosome arms occurred at level of bands 34 and 11, respectively ($t(9;22)(q34;q11)$) (Rowley 1973).

Bypassing the surveillance and repair mechanisms that take care of a faithful restoration of DNA lesions, chromosome translocations arise when persistent double strand breaks are illegitimately repaired leading to ectopic fusions of portions of distinct chromosomes. By doing so, chromosome translocations might lead to gene inactivation when coding regions are separated by their regulatory elements; otherwise, gene fusions can lead to deregulation of the expression of certain genes either because these become juxtaposed to a strong promoter, or because the gene fusion gives rise to a chimeric product with neoplastic potential (Roukos and Misteli 2014). Examples of pathogenetic chromosome translocations are gene truncations that led to inactivation of NF1 gene ($t(4;17)(q21.3; q11.2)$) or haploinsufficient production of RUNX1, ($t(8;21)(q22;q22)$, *RUNX1–RUNX1T1*). Instead, swapping MYC gene with promoter elements of immunoglobulin chain loci (translocations: $t(2;8)(p11;q24)$, $t(8;14)(q24;q32)$ and $t(8;22)(q24;q11)$) leads to an aberrant expression of transcription factor MYC in Burkitt lymphoma. Finally, the Philadelphia chromosome represents an example of gene fusions determining the formation of a hybrid product with oncogenic potential: in fact fusion of the 5' end of BCR gene with the 3' end of ABL1 gene leads to an exacerbated activity of the tyrosine kinase ABL1, ($t(9;22)(q34;q11)$) (Figure 2).

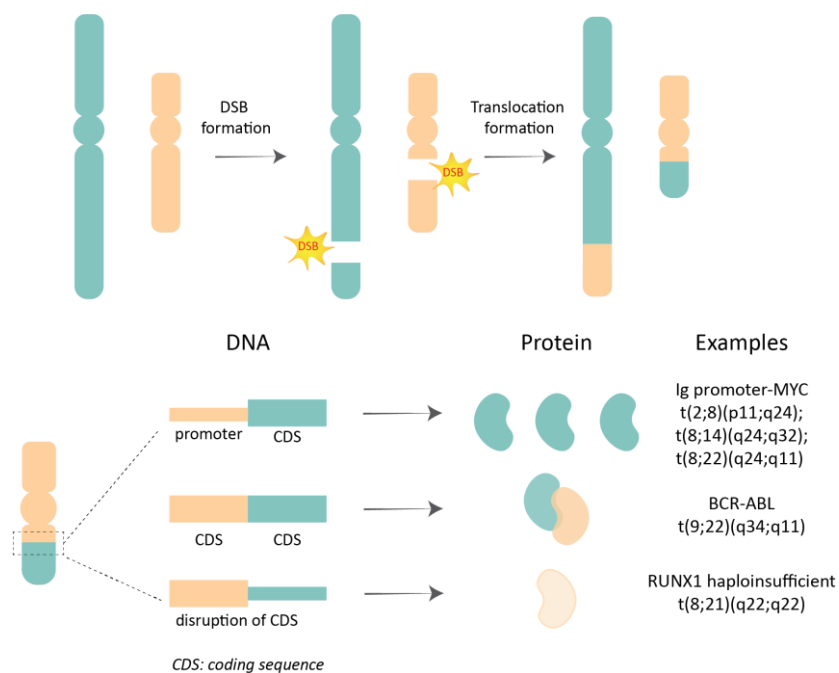


Figure 2: Chromosome translocations can cause gene deregulation. DSBs hitting two distinct chromosomes increase the chances that the broken chromosomes are miss-joined and form chromosome translocations. Balanced

Introduction

translocations (like the one depicted at upper right side of the figure) are the results of a mutual exchange of chromosomes pieces. Depending on its genomic location, a translocations junction can disrupt the function because the following three scenarios can occur: if a gene A translocates in proximity of strong regulatory elements of a gene B, this might abrogate the function of gene B, while gene A results exacerbatly expressed (an example of this rearrangements is given by MYC oncogene undergoing the control of Ig genes' promoters). If two genes are fused together, at protein level this might lead to a chimeric product with oncogenic capability (a classic example is represented by BCR-ABL fusion). Finally, chromosome translocations can lead to gene inactivation or to the haploinsufficient expression of a gene (examples are NF1 inactivation of haploinsufficient production of RUNX1). Adapted from (Roukos and Misteli 2014).

Because associated to gene deregulation, gene fusions are first or second hits in cancer initiation; thereby they are particularly important in cancer diagnostics and in monitoring the efficacy of therapeutic treatments.

Taking into consideration indices of cancer incidence, it was suggested that chromosome translocations are causal of 20% of clinical cases with same proportions among hematological disorders, sarcomas and carcinomas, even though in this latter subgroup of neoplasia, frequency of *TMPRSS2-ERG* and *TMPRSS2-ETV1* fusions in prostate cancer accounts for the majority of cases (Mitelman, Johansson, and Mertens 2007).

Nevertheless, gene fusions are mostly represented in lymphomas and leukemia; however, this bias is not only due to the high genome complexity and low input material available to sequence solid tumors. In fact, last decades bore witness of consolidation of deep sequencing techniques, which have allowed large detection of gene fusions over more guided approaches (Mertens et al. 2015). Moreover, the high recurrence of gene fusions in hematological disorders hardly results only by the acquisition of a clonal advantage in growth and survival as these features are commonly shared across tumor types, defining the neoplastic transition of a normal cell. High frequency of chromosome translocations in lymphoma can rather be attributed to processes dedicated to the development and maturation of immune system, that require scheduled formation of DSBs. In fact, during antigen receptor diversification, V(D)J loci are recombined through RAG1/RAG2 activity, and in mature lymphocytes, activation-induced cytidine deaminase, AID, assures the introduction of point mutations in the variable regions of Ig genes or allow switching of isotypes during Somatic Hypermutation and during Class Switch Recombination, respectively. The direct introduction of DSBs (via RAG enzymes) or lesions convertible in DSBs (via AID deaminase) largely increase the risk of chromosome translocations at immunoglobulin loci. Furthermore, while RAG1/2 activity requires the recognition of a start sequence (RSS), AID is exploited also at non-Ig genes, thereby increasing the chances of fusions, such as between c-myc proto-oncogene and the 3' regulatory elements of immunoglobulin heavy chain (IgH) in B lymphocytes (Robbiani et al. 2008), where the deaminase is mainly expressed. Moreover, failure in the mechanisms of repair of RAG- and AID-lesions can contribute to the formation of Ig-translocations. Finally, the closest nuclear positioning between c-myc and IgH genes in primary B cells, but not in other cell types, is further key-determinant of the etiology of such chromosomal rearrangements (Nussenzweig and Nussenzweig 2010).

Introduction

Chromosome translocations involving Ig-genes primarily found in B-cells malignancies have served here as paradigm to emphasize basic principles of biogenesis of chromosome translocations: persistent DSBs at given genes greatly increase the chance for chromosomal rearrangements between those genomic loci, especially in conditions where chromosome breaks lie spatially proximal and/or when repair mechanisms fail in their resolution. In the next paragraphs, we aimed to delve into cellular and chromatin determinants underlying the formation of chromosome translocations.

1.4 Cellular and chromatin determinants for the formation of chromosome translocations

Given that during the process of formation of gene fusions, double strand break lesions arise on distinct chromosomes, which come together in the nuclear space to be finally joined, here, we aim to discuss cellular features that impinge on chromosome fragility, that influence loci-nuclear positioning, and finally, that skew toward, or protect from, illegitimate fusion. Because DSBs occur and are resolved in the context of higher folding chromatin structure, steps underlying the formation of chromosome translocations can also be influenced by chromatin features and chromatin-based factors. Intriguingly, although specific chromatin signatures are found enriched at breakpoint regions, chromatin based-molecular mechanisms, which directly affect frequency of chromosome translocations by influencing mobility and repair of frequently translocating DSBs, have not yet been reported.

1.4.1 DNA & chromatin features affect breakage susceptibility

1.4.1.1 DNA features which facilitate chromosome breakage

Among DNA features that might influence the formation of translocating-DSBs, we have already mentioned that RAG enzymes via recognition of a recombination start sequence (RSS) exhibit their endonuclease activity and trigger rearrangements of V(D)J loci. However other genomic loci have shown a sort of degenerated motif sequence where RAG1/2 can initiate DSBs, increasing the frequency of chromosome translocations elsewhere than Ig- genes (Raghavan, Kirsch, and Lieber 2001) (Figure 3.2). Conversely from RAG enzymes, AID does not recognize specific sequences and in fact its activity has been at promiscuous loci, which share similar features with Ig- genes (Kato et al. 2012; Staszewski et al. 2011). For instance, a common DNA characteristic between non-Ig and Ig sites, targeted by AID-deamination activity, is the presence of repetitive regions (Figure 3.3) that can span from dinucleotide repeats up to short elements, such as SINEs (Short Interspersed Nuclear Elements).

Repetitive elements per se can also be sources of genomic instability; in fact, they can be sites of replications stress due to slippage of DNA polymerase and, therefore, are normally included in so-called class of common fragile sites, CFS. Another class of fragile sites, called “early replication fragile sites”,

Introduction

are described to differ from CFS, because dense of early replication origins, GC and genes rich and normally in more open configuration, yet constitute still a threat for genome integrity (Barlow et al. 2013). Both fragile sites (Krummel et al. 2000; G. Gao and Smith 2014; Barlow et al. 2013) and repeated sequences (Huang et al. 2010) have been described as sources of structural rearrangements, such as translocations and insertions.

Intriguingly, repetitive sequences not only impinge on DNA polymerizations causing stalling of the replisome, but they can also assume topological distortions of the canonical DNA double helix and therefore being more susceptible to breakage. Among the diverse non-canonical configurations of DNA, R-loops are acquiring more and more scientific interest because of their dual ability to regulate transcription and also to originate DSBs (Marnef and Legube 2021) (Figure 3.4). The involvement of non-B DNA structure, and specifically of R-loops, in chromosome rearrangements has been documented by the fact that these DNA structures synergistically stimulate the activity of RAG complex and AID enzymes at sites of accumulation and that undergo chromosome translocations (Raghavan et al. 2004; Yu et al. 2003; Ruiz, Gómez-González, and Aguilera 2011; Duquette et al. 2005). In yeast, defects in mRNA metabolism have been associated with hyper-recombination phenotype, suppressed by RNase H1 overexpression, hinting the detrimental role of R-loops in driving transcription associated recombination (Aguilera and Huertas 2003). Intriguingly, R-loops accumulate at CpG islands promoters (Ginno et al. 2012; Arab et al. 2019) and these sequences are breakpoint regions of 40-70% of chromosome translocations occurred in a specific cell division stage of progenitors B cells (Tsai et al. 2008).

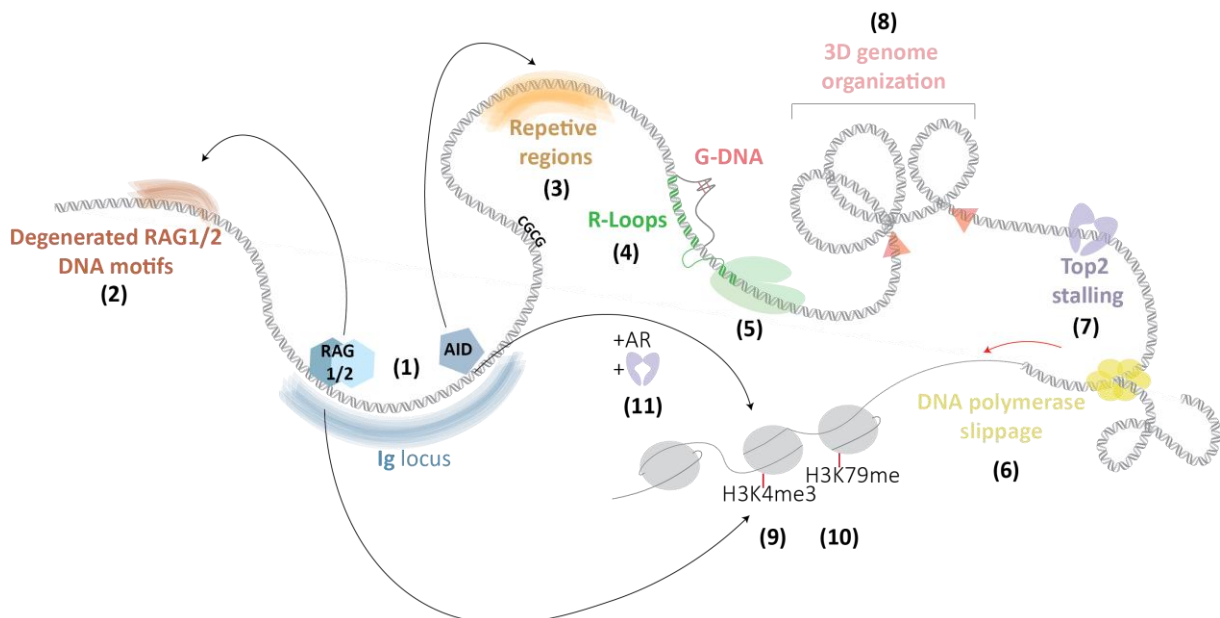


Figure 3: DNA and chromatin features influencing breakage susceptibility and translocation formation. RAG1/2 complex and AID can trigger DSBs formation at Ig Loci (1). RAG1/2 can recognize non canonical Recombination Signal Sequences (RSSs) and initiates formation of a harping structure where it cleaves forming DSBs and aberrant rearrangements (2). AID deamination occur without motif recognition, and it gets stimulated at off-target sites by certain genomic regions such as repetitive sequences (3) non-B DNA structures (such as R-loops and G-quadruplexes) promoting the synergistic activity AID and RAGs, making them prone to translocations

Introduction

formation (4). Breaks and translocation are often found at sites with open chromatin marks. Knowledge of loci engaged in the same transcription hub together with the discovery that lesions at active sites tend to cluster raise a model in which transcription might be indeed a determinant for translocation formation (5). DNA polymerase slippage can be also a threat for genome integrity and both head on collisions between replication fork and transcriptional bubble can be sources of DNA damage (not shown in figure) (6). TOP2-cleavage complex (TOP2cc) stalling increase breaks and translocation frequency at actively transcribed units and at sites proximal to chromatin loops (7). Late replicated regions in proximity of TAD boundaries provide also source DNA fragility (8). Not only DNA features, DNA structures and genome configuration, can influence predisposition of a certain locus to break and to translocate, but recently role of specific histone modifications in translocation formation has been highlighted. H3K4me3 stimulates RAG activity both in *cis* and *trans*, and it is enriched at sites targeted by AID (9). Similarly, H3K79me enriches at active loci undergoing V(D)J recombination and at translocations junction of *TMPRSS2* fusions (10). Upon Androgen Receptor-ligand binding, AID is recruited at sites enriched of H3Kme3 and H3K79me and, together with Top2, triggers *TMPRSS2* formation (11).

Topoisomerase enzymes are also considered another source of chromosome fragility, and potential drivers of chromosome rearrangements. In the genome, sites of supercoiling accumulation are targeted by Top2 enzymes where they introduce DSB (Figure 3.7), through which Topoisomerases let DNA molecule pass, thereby resolving topological tensions. When Topoisomerases are stalled in a DNA-covalently bound conformation, they cannot reseal the cleaved double strand, thus collisions with transcription or replication machineries or proteolytic hydrolysis can expose the now free chromosome ends and increase the probability of forming chromosome translocations. Chemotherapeutics can exploit this mechanism, in fact, their cytotoxicity implies to pause Topoisomerases, therefore stalling of Top2 in a form covalently bound to DNA makes the genomic locus prone to DSBs formation. The strong association between Top2 stalling and formation of chromosome breakage, upon chemotherapeutic treatment, such as etoposide, is revealed by the fact that treated patients have a brief relapse time before they develop a secondary therapy-related tumor, caused by etoposide-induced translocations (Cowell et al. 2012; Gothe et al. 2019).

Finally, 3D genome organization can also hamper genome integrity and initiate tumorigenesis (Figure 3.8). Disruption of confined domains and aberrant expression of certain proto-oncogenes (Hnisz et al. 2016), or TADs boundaries (Sarni et al. 2020) and chromatin loops (Canela et al. 2017; 2019; Gothe et al. 2019) at large transcribed units and in combination with delayed replication time (Sarni et al. 2020) or Top2 stalling (Gothé et al. 2019; Canela et al. 2019), can drive genome fragility (Canela et al. 2019; Gothe et al. 2019; Sarni et al. 2020; Canela et al. 2017) leading to the formation of chromosome translocations (Gothé et al. 2019; Canela et al. 2019).

1.4.1.2 Chromatin features associated with breakpoint regions

Modifications at level of chromatin structure regulate spatially and temporally many cellular processes that require DNA as template. In fact, not only serving as markers for chromatin modifiers and chromatin remodelers, which directly operate on histone code and nucleosome positioning, but also histone modifications guide transcriptional factors to promoter regions, prime damaged chromatin for specialized repair pathways and, more generally, create distinct environments to allow targeted binding

Introduction

and activity of certain factors. For instance, programmed DNA rearrangements, such as the ones during antibodies diversification, must be fine regulated in order to avoid unscheduled formation of DSBs.

In this regard, it has been demonstrated that, although RAG complex acts at specific DNA sequence, methylation at the level of H3 histone tails ensures a further layer to control and direct its activity. Furthermore, it has been characterized that PHD finger domain of RAG2 has specificity to bind H3K4 methylation and the strength of the binding correlates with the numbers of methyl groups (Matthews et al. 2007; Liu et al. 2007; Ramón-Maiques et al. 2007). In particular, reduced binding between RAG2 and H3K4me3, due to PHD domain mutations (Liu et al. 2007; Matthews et al. 2007), or knockdown of methyltransferases, or transient expression of histone demethylase (Matthews et al. 2007), lead to impaired recombination levels. Furthermore, crystal structure of RAG2 PHD domain alone or in complex with differently modified H3 tail peptides, had revealed that this finger domain is a bivalent reader of K4me3 and R2me2 of histone H3 and this latter modification seems to enhance the binding of RAG2 with H3K4me3 (Ramón-Maiques et al. 2007). A further implication in the formation of chromosome translocations is provided by a study showing that H3K4me3 does not merely stimulate RAG activity at *cis* RSS-bound sequences, but H3K4me3-binding induces such conformational changes to unlock RAG complex to bind at *trans* DNA sequences independently of RSS recognition (Shimazaki, Tsai, and Lieber 2009) (Figure 3.9). However, enrichment in this histone modification is not a prerequisite of immunoglobulin loci, in fact not only other genomic sites, yet targeted by AID, are enriched in H3K4me3 (Kato et al. 2012), but also prostate tumors, positive for *TMPRSS2-ERG* gene fusions, show significant enrichment of H3K4me3 (Berger et al. 2011) (Figure 3.9 and Figure 3.11). At translocation sites, prostatic *TMPRSS2* fusions are also characterized by co-occupancy of H3K36me3, H3 acetylation and PolII at breakpoint regions (Berger et al. 2011).

Importantly, the observed deposition of active chromatin marks at sites that underwent chromosome rearrangements upon binding of transcription factor, might be the result of migration into shared transcriptional factories, thereby increasing spatial proximity between potential translocating partners (Osborne et al. 2004). Another piece of evidence supporting the role of transcription in proximity of DSBs, comes from a recent study, which highlights that lesions at active genes tend to cluster, even though this mechanism was proposed to favor a more faithful repair and prevents the formation of chromosome translocations (Aymard et al. 2017) (Figure 3.5). In agreement with a positive role of transcription activation and chromatin marks at sites which undergo chromosome translocations, it has been found that H3K79me is enriched at active loci undergoing V(D)J recombination (Ng et al. 2003) (Figure 3.10).

Methylation on K79 of H3 was also found increased at translocating junctions of *TMPRSS2* fusions (Lin et al. 2009), upon binding of transcription factor. Intriguingly, changes in the transcriptional status of certain loci can trigger chromatin unfolding and, in line with this, it was shown that methylation of histone H3 on Lys 79 could induce refolding of higher-order chromatin structure to recruit 53BP1 at DSB lesion (Huyen et al. 2004). Therefore, it might be possible that rather than susceptibility to

Introduction

breakage, H3K79me might be involved in downstream steps of translocation formation, such as influencing spatial proximity (by transcription-induced repositioning) or repair outcomes.

Regarding the link of chromatin and aberrant repair outcomes due to chromosomal rearrangements, it has been observed that impairment of H4K20 di- and tri-methylation leads to aberrant embryonic development with perinatal lethality of mice animals, because of a defective CSR process (Schotta et al. 2008). This defect comes along with a deficiency in DSBs repair, thereby DSBs persistency leads to chromosome aberrations involving Ig locus. Because 53BP1 is a reader of H4K20me2, the authors speculate that the defect in DNA repair might be due to a failed 53BP1-lesion recognition.

Finally, enrichment of open chromatin marks such as H3K4me3 and K4me2, H3K9ac, H3K27ac and H3K79me positively correlates with etoposide-induced fragility in K562, suggesting that etoposide induces DSBs mainly at transcribing units and specifically at promoters regions (Gothe et al. 2019), again supporting a positive role of transcriptional output in DSBs formation.

Nevertheless, computational analysis of certain chromatin marks profiled in 74 frequently translocating genes have scored enrichments in H3K4me1 and K4me3 and H3K27ac, compared to control genes with similar features regarding gene length, expression level and exons/ introns density. Importantly, these chromatin marks even though associated with open chromatin status (as observed by the correlation of DNaseI sensitivity signal), were not dependent on the transcriptional status of these genes (Burman et al. 2015). Enrichment of H3K4me, via overexpression of histone methyltransferases such as ASH2L and SET7/9, predisposes NPM1 and ALK genes to break and to translocate via a mechanism, which is uncoupled from the transcriptional program of those genes, but rather it is sustained by the open chromatin configuration at those sites, which allowed a greater accessibility of the DSBs inducing mean.

1.4.2 Nuclear positioning of DSBs

A chromosome translocation results from juxtaposition of heterologous breaks, therefore shedding light on cellular components and mechanisms that influence how translocating DSBs might come together in the nuclear space is pivotal in the ultimate effort to counteract the arising of these rearrangements. In this regard, the role of chromatin environment in influencing DSBs synapsis has not been fully understood. Researchers foresee two scenarios: the “contact first” hypothesis predicts that genomic loci undergoing chromosome rearrangement lie in close proximity at the moment of DSBs formation and do not travel long-range distance before being fused in a translocation junction, as instead, is postulated by “breakage first” model (Savage 1996; Meaburn, Misteli, and Soutoglou 2007). Experimental evidence hint that, presumably, both motion properties and spatial proximity of chromosome ends play a role in the formation of chromosome translocations.

1.4.2.1 Motion properties of DSBs: “...and yet, it moves”

Based on the sources of DSBs inducing agents, different levels of displacement have been scored. Linear tracking of DSBs, induced by α -particles, had shown rapid changes of trajectories indicating movement of broken chromosome loci and clustering of the same DSB lesions (Aten 2004). On the contrary, Neutrons or X-rays irradiation led to GFP-53BP1 foci confinement within minutes, no long-range displacements of damaged chromatin and rather rare clustering events (Jakob et al. 2009). Recently, however, it has been shown that immediately after break induction, damaged chromatin might become stiffer, like in a sort of “needle in a ball of yarn”, allowing a more efficient nuclear exploration at larger time scale (Miné-Hattab et al. 2017). In yeast, nuclear roaming upon DSBs formation has been widely associated with search for a donor template in order to carry out homology-directed repair (Miné-Hattab and Rothstein 2012; Smith, Bryant, and Rothstein 2018; Neumann et al. 2012; Dion et al. 2012) and, thereby, it comes along with increased DSB mobility. When, for instance, the lesion is caused by stalling of replication, the broken chromosome end is already tethered to the sister chromatid that can serve as repair donor, thus DSB mobility is unchanged (Dion et al. 2012).

Despite DSBs mobility might have been tightly associated with homology search, it is erroneous considering NHEJ as a repair pathway with confined chromatin movement. For instance, 53BP1, known player in NHEJ, is responsible for long range mobility of deprotected telomeres and aberrant end-joining fusions between chromosome ends (Dimitrova et al. 2008). Similar conclusions can be drawn by investigating the role of 53BP1 in joining distal V(D)J segments (S. Difilippantonio et al. 2008). Furthermore, in mammalian nuclei, chromosome translocations are notoriously the result of illegitimate end joining process, and observations on motion properties of translocating DSBs highlighted that those ends are characterized by increased mean square displacement in comparison with non-translocating DSBs (Roukos et al. 2013).

Other evidence, that support a “contact-first” view in the formation of chromosome rearrangements, suggest that chromosome translocations might occur preferentially between neighbor loci. In support of this, it has been also observed that a single DSB does not elicit chromatin mobility, but it is rather positionally stable (Soutoglou et al. 2007) and therefore, does not migrate through chromatin compartments (Lemaître et al. 2014). Stable positioning of broken chromosomes occur in a manner dependent on end-joining factors, such as Ku80, which keeps shield the double strand breaks from end processing. However, knockdown of Ku80 lead to an increase formation of chromosomal aberrations, such as chromosome translocations (Soutoglou et al. 2007; Roukos et al. 2013), suggesting that nonetheless chromosome translocations preferable occur between proximal DSBs, loss of constrain is associated with increased genome instability.

Determinants that might account for differences in motion among DSBs with propensity to translocate compared others that are faithfully repaired are not well known, but it is possible that the surrounding chromatin, where a DSB lies, plays a role in this process. So far, there is not a direct evidence on the

Introduction

role of chromatin environment on the movement of translocation partners, although it has been proposed that changes in the chromatin status can govern positioning and movement of loci within the nucleus. In this regard, it has been shown that gene activation by tethering of a potent viral transactivator domain of transcription factor, VP16, led to repositioning from the periphery to the interior of the nucleus (Tumbar, Sudlow, and Belmont 1999; Tumbar and Belmont 2001; Therizols et al. 2014) (Figure 4A). Intriguingly, this movement was observed also with a small acidic peptide of this domain, which was unable to initiate transcription, but that it conserved its properties on chromosome decondensation (Chuang et al. 2006; Therizols et al. 2014). In fact, upon targeting of VP16 not only splicing factors accumulate on the tethered locus but also histone acetyltransferases (Tumbar, Sudlow, and Belmont 1999), thereby, changes in the chromatin status are likely the causes in the observed gene repositioning. Intrigued by the possibility that local chromatin changes might elicit chromatin movement, without need of large unfolding of chromatin structure, Neumann and colleagues tried first to recapitulate the involvement of active transcription in this process. By using tethering of a strong transcription activator or a temperature-sensitive allele for *rpb4*, they assessed that nor transcription activation nor ongoing transcription, could induce chromosome movement of a trackable locus (Neumann et al. 2012). Given that chromatin displacement co-occurs with changes at chromatin levels (Tumbar, Sudlow, and Belmont 1999), and that VP16 stimulates ATP-dependent INO80-mediated nucleosome loss (Shen et al. 2003), they demonstrate that, indeed, INO80-remodeler is responsible of enhanced movement of an intact or broken locus to elicit ectopic recombination (Figure 4B). During homologous recombination, search for a donor template is possible through enhanced global chromatin mobility, regulated by checkpoint kinases and INO80-dependent chromatin remodeling (Seeber, Dion, and Gasser 2013). Recently, it has been uncovered the molecular mechanism underlying this *trans* mobility induced by INO80 complex relies also on the co-orchestrated histone degradation by the ubiquitin-proteasome system (UPS) that together lead to nucleosome loss and thereby to an increased chromatin expansion and recombination rate (Hauer et al. 2017) (Figure 4D).

Introduction

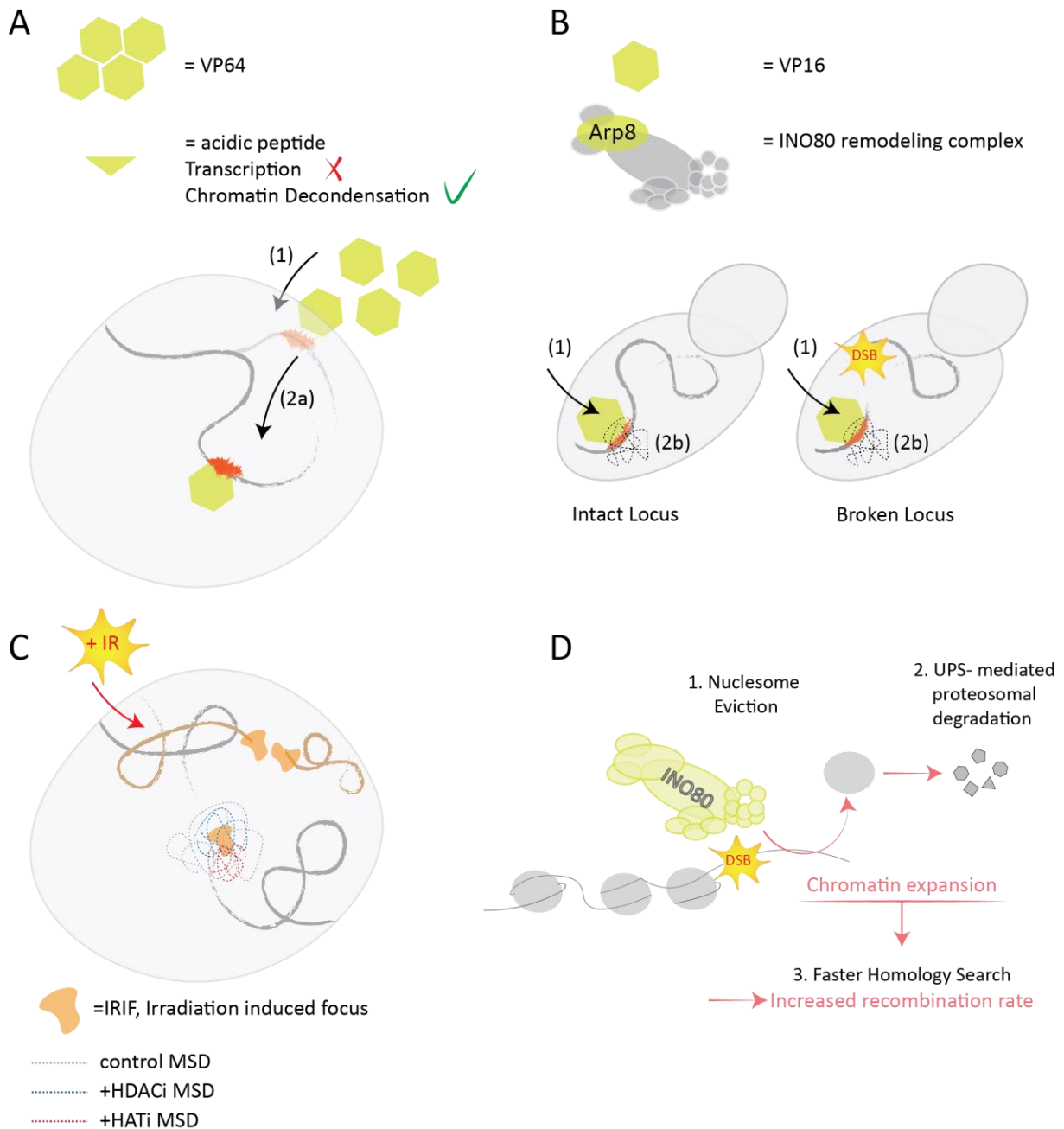


Figure 4: Changes in chromatin organization influence mobility and locus positioning in eukaryotes. A. Artificial tethering of viral transactivator VP16 (1) induces transcription activation and chromatin changes such as repositioning of the locus (2a), in human cells. Tethering of the acidic peptide of the transactivator was able to trigger the same repositioning: importantly, the peptide enables to trigger transcription activation but it conserves the capability to induce chromatin decondensation. **B.** In budding yeast, VP16-induced transcription activation was able to enhance mobility of the target locus (2b). However, it was not transcription activation per se to induce such changes (tethering of Gal4 on inducible promoter did not score changes in mobility), rather changes at chromatin levels were able to influence the displacement of the investigated locus. In line with this, Arp8-tethering was able to mimic VP16-triggered mobility, suggesting that INO80-induced remodeling activity was responsible to enhance the mobility of an intact or broken locus. Together these works hint that change at the level of chromatin structure affects chromatin positioning and mobility of a certain locus. **C.** Upon irradiation, mobility of irradiation induced foci is influenced (actually restrained) when chromatin perturbation using epigenetic inhibitors for histone deacetylases or histone acetyltransferases is applied. **D.** In response to DSBs, global chromatin mobility is the result of remodeling activity by INO80 and of proteasome degradation; both these effects contribute to chromatin expansion, which result in a faster search for a homologous template and, thereby, increased recombination rate.

Introduction

Global mobility is uncoupled from local DSB mobility (Cheblal et al. 2020). This latter is controlled by a fine balance between cohesin loading at double-strand ends and SUMO-target ULS1, which constrain or increase the motility of a DSB, respectively. Intriguingly, upon DSBs, ULS1 can enrich at telomeric TG-repeats, whereas MRE11 asymmetrically binds the other strand end (Marcomini et al. 2018). By doing so, ULS1 provokes enhanced DSB mobility and the formation of ectopic rearrangements, which resemble non-reciprocal translocations found in human cancer (Marcomini et al. 2018). Finally, in line with a role of chromatin organization in DSBs mobility, it has been shown that treatments with inhibitors of histone acetyltransferases and deacetylases reduce the mobility of IR-induced lesions (Krawczyk et al. 2012) (Figure 4C).

Altogether, these works suggest that local DSB mobility and global chromosome mobility are triggered by changes in the status of chromatin; alteration of such processes can ultimately increase the risk for unscheduled rearrangements.

Other cellular processes might also affect DSBs movements and thereby increasing the risk of unscheduled chromosomal rearrangements. For instance, during the reestablishment of chromatin architecture upon mitotic exit (Csink and Henikoff 1998; Baarlink et al. 2017), gene activation (Chuang et al. 2006) or association of the transcribed gene to preexisting Cajal bodies (Dundr et al. 2007), long range mobilization of those loci was precluded by chemical block of microtubules polymerization or by using a polymerization-defective mutant of actin protein.

The long distances covered during these processes are in the same range of the ones crossed by translocating DSBs (Roukos et al. 2013), hinting to the possibility that a shared molecular machinery based on nuclear forces might be responsible for long range movements of intact and damaged loci. The scientific literature is becoming more and more studded with examples describing nucleoskeleton-based activities in DSBs dynamics and repair. Microtubules (Lottersberger et al. 2015; Oshidari et al. 2018), factors that connect nucleoplasm and cytoskeleton forces (Lottersberger et al. 2015; Marnef et al. 2019; Aymard et al. 2017), actin filaments (Caridi et al. 2018; Schrank et al. 2018; Pinzaru et al. 2020; Belin, Lee, and Mullins 2015) and associated nucleator complexes (Belin, Lee, and Mullins 2015; Zhu et al. 2020; Oshidari et al. 2018; Chung et al. 2015), have all being found involved in DSB mobilization (Lottersberger et al. 2015; Caridi et al. 2018; Schrank et al. 2018; Pinzaru et al. 2020; Marnef et al. 2019; Oshidari et al. 2018), in repositioning lesions through chromatin compartments (Caridi et al. 2018; Pinzaru et al. 2020) and in assisting the clustering of repair foci (Schrank et al. 2018; Aymard et al. 2017).

Moreover, mobility of DSBs triggered by the nucleoskeleton has been implicated in the formation of chromosome rearrangements. For instance, RNAi for arp3, myo1a and myo1b leads to accumulation of heterochromatin DSBs, which cannot relocate to Nuclear Pore Complex and being faithfully repaired. Persistency of these lesions leads to micronuclei formation both in flies and mouse cells; and chromosomal abnormalities, such as aneuploidy, satellites expansions and chromosome fusions, are

Introduction

largely found in early development stages of flies (Caridi et al. 2018). With a more direct role in DSB mobility rather than in DSB repair deficiency, ARP2/3 have found to promote end resection and thereby clustering of resected DSBs through a sort of mechanism which is self-sustained (Schrack et al. 2018). On the other hand, ARP2/3-induced clustering affects 3D genome compartmentalization by enhancing local chromatin insulation and thereby mediating more homotypic interactions within the clustered regions. Reinforcing of contacts occurs also at level of distal DSB and in turn, this increases the formation of intra and inter-chromosomal rearrangements (Zagelbaum et al. 2021). Finally, 53BP1 has been shown to enhance mobility and thereby increases end-fusions of de-protected telomeres (Dimitrova et al. 2008), in a manner also dependent on LINC complex (Linkers of the nucleoskeleton to the cytoskeleton complex) and microtubules filaments (Lottersberger et al. 2015). However, 53BP1 foci have been shown to feature properties typical of phase separated condensates with fission and fusion behavior (Kilic et al. 2019). Thus, it is intriguing to hypothesize that the coordinated action of microtubules dependent forces (Lottersberger et al. 2015) and the biophysical properties of 53BP1 phase separated compartments (Kilic et al. 2019) lead to transient clustering of repair foci and dramatic end-fusion of telomeric breaks. In this regard, formation of transient repair hubs is starting to emerge as common feature of many proteins involved in lesion recognition and repair of DSBs and thereby fusion, bouncing, dripping and wetting behavior of these droplet-like condensates might unleash strengths that provoke movement of DSB lesion itself. A similar effect has been described when active RNAPII dissociates from promoter proximal regions eliciting enhanced chromatin movement, which is conversely constrained during RNAPII-Ser5 engagement within P-TEFb hub (Nagashima et al. 2019).

Finally, post-translation modifications (PTMs) at level of histone tail or repair factors serve as switch not only to regulate accrual and dissociation of proteins to the lesion site, but also to induce DSB mobilization and assembling of condensates where DSB repair occurs (Aguzzi and Altmeyer 2016). SUMOylation of repair factors, for example, fosters the repair of difficult lesions by generating “preferential lanes” for DSB relocation to the nuclear edge (Lamm, Rogers, and Cesare 2021; Amaral et al. 2017). Moreover, deficiency in SUMOylation turnover has been associated with increase rate of gross chromosomal rearrangements (Claudio P. Albuquerque et al. 2013; Claudio Ponte De Albuquerque et al. 2016; Hwang et al. 2008).

1.4.2.2 DSB pairing

Formation of resected double strand ends is associated either with increased DSBs displacement, or with DSBs pairing. In fact, to initiate homology search, ssDNAs can both increase DSBs motility and/or lead to coalescence of multiple DNA lesions in a shared RAD52 focus (Lisby, Mortensen, and Rothstein 2003). These repair centers highly accumulated in S/G2-M phases of cell cycle, furtherly hinting their dependency on the presence of a sister chromatid template for homologous recombination. Nonetheless,

Introduction

increased DSBs mobility (Smith et al. 2019) and DSBs clustering (Aymard et al. 2017) were scored also in G1 phase in a manner dependent on RAD51 binding at DSBs. However, because ends resection precedes RAD51 filaments formation, once again, it is likely that formation of ssDNA is the cause of increased foci mobility and elicited DSBs-contacts. Importantly, interfering with the processing of double strand ends, leads to defect in DSB relocalization across chromatin and nuclear compartments (Chiolo et al. 2011; Tsouroula et al. 2016; Marnef et al. 2019) and it disrupts the formation of synapsis (Roukos et al. 2013) and clustering (Schrack et al. 2018) of broken ends. Finally, DSBs pairing not only occurs because of homologous search and strand invasion during HR, but breaks repaired by NHEJ might synapse with other DSBs and undergoing cycles of transient association and dissociation and eventually being engaged in a persistent pairing, synonymous of the formation of a chromosomal translocation (Roukos et al. 2013).

Both DSBs mobility and coalescence of repair foci can influence the probability of two chromosome ends to come in contact; however, cell lineage, cell cycle phase and global gene activity can also influence the non-random nuclear positioning of chromosomes and genomic loci within the nuclear space and thereby can be determinants of chromosome translocations frequencies and of their recurrence in a given cell type. In this regards, Bickmore and Teague analyzed more than 10^5 translocations from two independent databases for cytogenetic abnormalities and they found that translocations frequencies predominantly correlate with chromosome size and low gene density, suggesting a negative pressure for rearrangements on gene-rich loci (Bickmore and Teague 2002). These parameters are typical of a radial distribution of chromosomes within the nucleus (Meaburn, Misteli, and Soutoglou 2007), however, careful analysis of their results highlighted that the relative nuclear positioning highly impinge on translocations etiology (Bickmore and Teague 2002).

In line with this, measuring of the intergenic distances between frequently translocating genes, at different stages of cell differentiation and cell cycle, had revealed that BCR and ABL or PML and RAR α are significantly associated during S-G2 transition compared to ABL or PML paired with control locus (Neves et al. 1999). Moreover, the scored gene proximity was detected in hematopoietic precursors, even though they observed differences between BCR-ABL and PML- RAR α association in unstimulated or Interlukin-3-treated CD43 + cells. In fact Interlukin-3 treatment stimulates differentiation of hematopoietic stem cells in myeloid progenitor cells and indeed BCR-ABL rearrangement arises in very-early hematopoietic precursor, whereas PML-RAR α is an oncogenic lesion that hits precursors already committed to myeloid differentiation. These results argue for an involvement of cell type commitment and cell cycle stage in influencing the spatial contiguity of loci found recurrently rearranged in the corresponding tumor type. Similar, in interphase nuclei, 3D analysis of intrachromosomal distances between RET and H4 genes that commonly rearrange in thyroid cancer, have revealed that those loci were found closer in thyroid normal cells seven time more often than unrelated normal cells (Nikiforova et al. 2000). Not only genes which frequently fuse are spatially closer compared to genes not involved

Introduction

in translocations, but also their spatial arrangement, and thereby their relative positioning into the nucleus, was found conserved between normal and the corresponding transformed cells (Parada et al. 2002): both parameters can directly contribute to the frequency of chromosome translocations. For example, in Burkitt Lymphoma, Ig-rearrangements disrupt the physiological expression of c-myc when it translocates with immunoglobulin genes, encoding for heavy chain IgH, and light chains λ , IgL and κ , IgK. Interestingly, translocations between Ig- loci and c-myc occur at different frequencies, which mirror the relative spatial distance between c-myc locus and each of these translocation partners (Roix et al. 2003). This work links the physical proximity to a potential translocations partner with its incidence of clinical translocations and, further, it highlights that differential and relative vicinity is related to the whole topology of 3D genome, and does not solely depend on the physical distance of individual pairs. Altogether, these works show correlative findings of the association between nuclear proximity and rate of rearrangements. However, a casual effect has also been described during the formation of Androgen Receptor-induced *TMPRSS2* intra and inter-chromosomal rearrangements which are triggered by induced spatial proximity upon Androgen Receptor-binding at these loci (Mani et al. 2009; Lin et al. 2009). In fact, prostate cells are responsive to androgen signaling, so as spatial proximity between *TMPRSS2* and *ETV* or *TMPRSS2* and *ERG* depends on androgen receptor binding. This corroborates one more time that because 3D spatial genome organization is a distinct characteristics of a given type of cell, the probability to translocate of certain loci can be highly influenced by the relative spatial arrangement of those chromosome loci and, thereby, constitutes an individual mark for that cell type.

Moreover, changes in the transcriptional program of certain genes and in general gene activation can be contributor of changes in the chromatin status that leads to gene repositioning (Tumbar, Sudlow, and Belmont 1999; Tumbar and Belmont 2001; Chuang et al. 2006; Therizols et al. 2014) and, thereby, might bring spatially distant genomic loci in physical proximity. Findings by Osborne and colleagues proposed that active transcribing genes co-occupy the same “transcription factory”, suggesting that ongoing transcription can contribute to the physical interaction of transcribing loci in the same discrete focus. In prostatic cancer, ligand-dependent binding of androgen receptors to intronic regions of genes undergoing rearrangements, activates such transcriptional changes to cause alterations of the local chromatin structure, which elicit both mono- or biallelic proximity with intra- or interchromosomal loci. This latter, in combination with more accessibility to genotoxic enzymes are drivers of *TMPRSS2* translocations formation (Lin et al. 2009). Importantly, movements that led interchromosomal proximity were controlled via a nuclear myosin I (NMI)/actin-dependent mechanism, likewise, components that organize actin nucleation and LINC complex, are found to regulate clustering of lesions at active transcribing loci (Aymard et al. 2017), suggesting that a common mechanism based on nuclear motors might assist how chromosome loci or DSBs lesion come in proximity.

When Branco and Pombo assessed the level of intermingling between chromosomes, they proposed a new model to describe chromosomal arrangement in the nuclear volume. Even though conserving the

Introduction

definition of territoriality of each individual chromosomes (Cremer and Cremer 2010), they hypothesized that chromosomes do not occupy discrete domains with few interactions occurring in the interchromosomal domain space, rather they form a network with deep extension of chromosome loops in others territories (Branco and Pombo 2006). This model well espouses the positive correlation they scored between frequency of translocations and level of intermingling for each of the 24 chromosomes pairs they analyzed in human lymphocytes. Intriguingly, in agreement with previous pieces of evidence already discussed, they also found transcription influencing the interchromosomal interactions, which they analyzed as level of chromosome intermingling upon treatment with α -amanitin. Transcription inhibition led both to an increase or to a decrease of the degree of chromosome overlap between different pairs (while no significant changes on nuclear or chromosome volumes were detected), which confirmed the general role of transcriptional status in genome organization.

Translocations capture sequencing based methodologies have broadly confirmed the role of transcription in driving the formation of chromosome translocations. In B lymphocytes, genome wide analysis of the full spectra of translocation partners of a bait DSB have revealed that translocations are highly frequent in transcribed units, mainly at Transcription Start Site (TSS) rich in open chromatin marks (H3K4me3, H3ac, H3K36me3 and PolII). Moreover, it has been found that in absence of AID enzyme, which plays a dominant role in the formation of recurrent translocations in B cells, proximity to the breakpoint sites, further promotes the formation of the majority of intrachromosomal rearrangements that indeed occur within 350 Kbp around the DSB (Chiarle et al. 2011; Klein et al. 2011). Together, these findings highlight that linear vicinity to a DSB plays a preferential role in the formation of intra-chromosomal rearrangements, but it does not add information on the role of 3D genome configuration, namely, how the relative positioning of two genomic loci in the 3D volume affects the probability of these loci to form a translocation. Zhang and colleagues decided to investigate the role of spatial proximity in the formation of chromosome translocations in unbiased manner. For this purpose, they utilized High-Throughput Genome-wide Translocation Sequencing (HTGTS), HiC contact map on pro B-mouse cells and irradiation as DSBs-inducing agents. Because DSBs are major drivers of chromosome translocations, they decided to normalize translocations frequency at a certain locus for the breakage frequency of the same locus. They could recapitulate the recurrence of translocations at TSS of transcribing genes; however, they conclude that even though transcription plays a relevant role in those rearrangements, it is not the main drive for translocations to occur. Instead, they could show that when DSBs acceptors (translocation partners) are widely available along all chromosomes, like for instance upon irradiation, spatial conformation of the chromosome where the DSBs lies is the main predictor of translocation frequency. To conclude, physical intra or interchromosomal proximity influence rearrangements between DSBs on the “true” *cis* chromosome, which is not the one dictated by linear distance, but the one occupying the same volume (Y. Zhang et al. 2012). One can envision that this has tremendous consequences in understanding phenomena like chromothripsis, where pre-existing spatial proximity might determine how chromosome segments are reasserted/reshuffled. Finally, findings from

Introduction

Klein and Chiarle regarding rearrangements in B cells are revisited by works from Hakim and Rocha that emphasized on the role of spatial proximity in AID-mediated rearrangements, rather than on transcriptional influence. Hakim and colleagues suggested that in absence of DNA damage, physical proximity, chromatin accessibility and gene expression greatly determine the frequency of chromosome translocations. However, when DNA damage is inflicted, proximity and the absolute number of rearrangements lack of correlation, whereas RPA deposition at a given locus positively correlates with the numbers of rearrangements at the same locus, suggesting that DSBs formation is rate-limiting of translocations (Hakim et al. 2012). On the other side, Rocha and colleagues discovered that “off-target” activity of AID enzyme occurred at loci occupying the same topological domain during class switch recombination, confirming the role of spatial proximity in the formation of AID-mediated translocations (Rocha et al. 2012).

1.4.3 The role of DSB repair pathways

DSBs repair mechanisms can also impinge on the probability of two DNA lesions being faithfully repaired or engaging in a chromosome rearrangement. Employing genetic tools to generate defective alleles of certain repair factor, reporter systems for the usage of specific pathway or sequencing of translocations junctions have shed light on the role of DSB repair pathways as contributors or suppressors of the formation of chromosome rearrangements. Taccioli and colleagues were among the firsts to associate impairment of CSR with defective repair machinery, suggesting that repair pathways might influence the process of formation of scheduled chromosome rearrangements (Taccioli et al. 1993).

In yeast, recombination-based repair processes are prevalent mechanisms to restore genome integrity, however chromosome translocations are not formed by canonical gene conversion that requires homologous sequences for both double strand ends, but they result from Single Strand Annealing (SSA), when DSBs flank directly repeated regions, or by Break Induced Replication (BIR), based on single strand invasion by one double strand end. Multi-invasion recombination is another type of mechanism forming chromosome translocations, based on two-strand invasion of a broken DNA. This mechanism relies on HR factors, and while homology lengths and spatial proximity of donor templates further stimulate the process, DNA Helicases and Topoisomerases, by resolving the heteroduplex structure, act as negative regulators in this process (Piazza, Wright, and Heyer 2017). Multi-invasion-induced rearrangements (MIRs) come with the cost of possible insertions in the final translocation junction; furthermore, resolution of MIRs intermediates lead to formation of new breaks with the potential of triggering additional rearrangements. Complex structural variations have been also scored as the results of heterologous recombination between not identical but similar homologous sequences (León-Ortiz et al. 2018). This type of heterologous recombination is different from the “homeologous” recombination for the extension of the homology (sequence divergency higher than 70 % in the first type of

Introduction

rearrangements) and on the dependency on mismatch repair factors and structure specific endonucleases. Mismatch repair factors suppress “homeologous” recombination, but they are responsible of heterologous rearrangements in mutants of structure - specific helicases such as BLM and RTEL1 (León-Ortiz et al. 2018; LaRocque and Jasin 2010). Intriguingly, genome rearrangements can arise also upon replication stress. Rescue of stalled replication forks has been also shown to cause structural abnormality and generation of complex fusions, due to repetitive template switching between micro-homology sequences (F. Zhang et al. 2009; Mizuno et al. 2013; Watanabe et al. 2017).

In mammals, end-joining signatures characterize translocation junctions, which arise throughout the cell cycle, suggesting that NHEJ is the predominant repair mechanism underlying the illegitimate joining of heterologous breaks. This finding was quite surprising giving that factors involved in repair of DNA lesions, are normally considered genome *caretakers* and animal models carrying alleles null for those factors, are lethal at embryonic stages, or their development is associated with enhanced genome instability, due to increased sensitivity to DNA damage agents (M. J. Difilippantonio et al. 2000; Ferguson et al. 2000; Y. Gao et al. 2000).

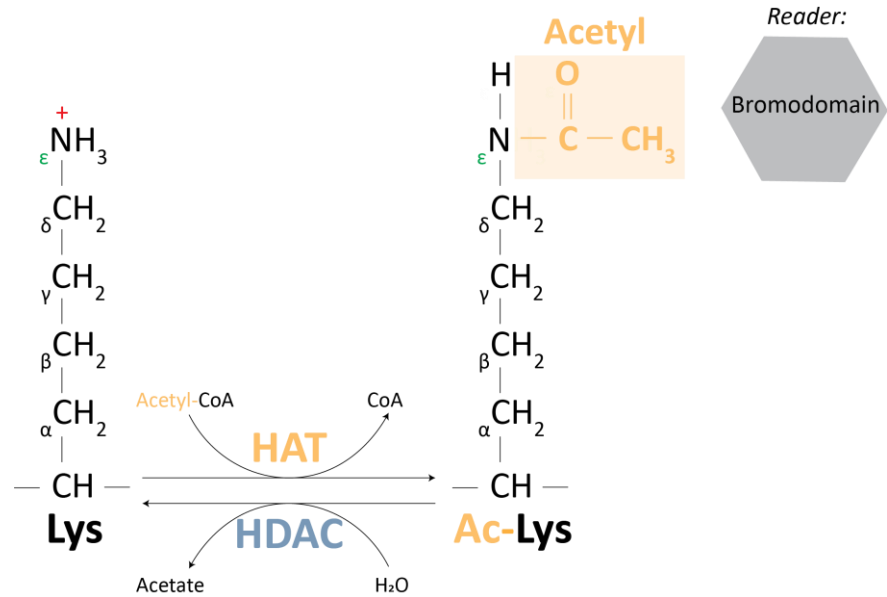
For instance Ku80^{-/-} mice are characterized by chromosome aberrations and cycling defects, which are partially restored upon additional mutation of p53, even though the double mutant for Ku80 and p53 holds higher sensitivity to ionizing radiation (M. J. Difilippantonio et al. 2000). Normally, p53 mutation predisposes to T-cell lymphoma, however, probably due to the enhanced sensitivity to DNA damage, mice carrying double mutations in p53 and Ku80 alleles develop even earlier proB-lymphomas, characterized by IgH and c-myc fusion and amplification of both genes (M. J. Difilippantonio et al. 2000). Similarly, XRCC4^{-/-} mice show defects in cellular proliferation and present premature senescence; when this mutation is crossed with animals carrying alleles mutated in p53 gene, the embryonic lethality is rescued and mice were born nearly as predicted. However, defects in B and T cells development are not restored and it comes along with constant appearance of IgH/c-myc fusions (Y. Gao et al. 2000). While, Ku80 acts early on during NHEJ, therefore loss of its ends-tethering function might lead to increase illegitimate joining with non-homologous ends, which can still be catalyzed through NHEJ pathway, XRCC4 acts in the final end-joining step, suggesting that likely alternative pathways are mediators of rearrangements formation. Over the decades, in fact, more and more evidence have shown that NHEJ suppresses chromosome translocations, rather than mediates them. Cells defective for XRCC4 accumulate translocations, however overexpression of WT isoform for XRCC4 rescues the increase in chromosome translocations (Simsek and Jasin 2010). Furthermore, analysis of translocations junctions shows shared feature in rodents with genetic backgrounds WT, Ku70^{-/-}, XRCC4^{-/-} or XRCC4^{-/-} but complemented with a functional XRCC4, such as insertions and deletions characterized by few base pairs microhomologies, hinting alt-EJ-based mechanisms for the formation of chromosome translocations. XRCC4-LIG4 and Ku are pathway choice regulators and play role in suppressing HR and SSA (Weinstock and Jasin 2006; Pierce et al. 2001), by protecting DNA ends from nucleolytic processing and it is tempting to speculate that suppression of alt-EJ mediated translocations

Introduction

is sustained by blocking end-processing disfavoring the access of alt-EJ factors. Hence, researchers had tried to interfere with end-resection process and because the HR factor CtIP (Sae2, yeast homologous), was also identified as alt-EJ component (Lee and Sang 2007; Bennardo et al. 2008), its role in the formation of chromosome translocations has been assayed by knock down experiments (Y. Zhang and Jasin 2011). CtIP depletion lead to decreased translocation frequency, suggesting that defects in end resection lead to impairment in the usage of microhomologies underlying translocation formation. Involvement of alt-EJ in generating translocations is supported by other studies where mice deficient of LIG3 show reduced translocation frequency, while LIG1 has a marginal role in physiological condition, but an additive effect in reduction of translocation frequency was detected in double mutants for LIG1 and LIG3 (Simsek et al. 2011). The previous examples have highlighted that in mice, translocations are suppressed by classical NHEJ and arise from erroneous repair mediated by an alternative-end joining mechanism. However, human cell lines homozygotes for mutations at *xrcc4* and *lig4* genes showed a decreased formation of chromosome translocations and the few rearrangements detected, have presented large deletions and microhomologies at recombined junctions of endonuclease-inflicted DSBs. Furthermore, in this set up, lack of CtIP impairs translocation formation only when classical NHEJ is already compromised, but not in condition of intact end-joining machinery (Ghezraoui et al. 2014). Conversely, upon irradiation translocations accumulate in LIG4 and/or RAD54 deficient background (Soni et al. 2014), suggesting that nevertheless in case of impaired NHEJ and HR, illegitimate fusions of heterologous DSBs occur by different means. Therefore, Iliakis's laboratory proposed that also in human cells alt-EJ constitutes the back-up pathway to cover for NHEJ and HR defects. Cells depleted of KU show a rapid accumulation of translocation rearrangements (already after 1h versus the 4h upon IR in *lig4* and *rad54* mutants), suggesting that lack of DSBs tethering provokes a quick engagement in erroneous repair. Importantly, PARP-1 inhibition rescues translocations accumulation in all repair defective backgrounds, hinting, thereby, that PARP-1 is required for the formation of these DSBs miss-joining events (Soni et al. 2014; 2015) and co-treatment with a potent LIG1 and LIG3 inhibitor, L67, synergistic decreases translocations frequency, suggesting that PARP-1 and LIG1/3 operate on the same subset of DSBs repaired through alt-EJ. Intriguingly, HCT WT cells treated only with LIG1/3 inhibitor do not show a significant decrease in translocations 4h after irradiation, while combined treatment with LIG4 inhibitors, further decrease translocations, even if not completely (Soni et al. 2015). Altogether, these results hint that different repair pathway might contribute to different fraction of translocations, as was already proposed (Y. Zhang and Jasin 2011) and it highlights that chemical inhibition is often not the best tool to dissect the relative contribution to a given event, due to a possible incomplete block of the investigated factors. In conclusion, these experimental works have taught us that in the attempt of defining a comprehensive model system describing determinants of translocation frequency, one must take in considerations that parameters as DSBs location, frequency, persistency and characteristics of double strand ends, highly determine the outcomes whereon the model will be based.

1.5 Class I histone deacetylases

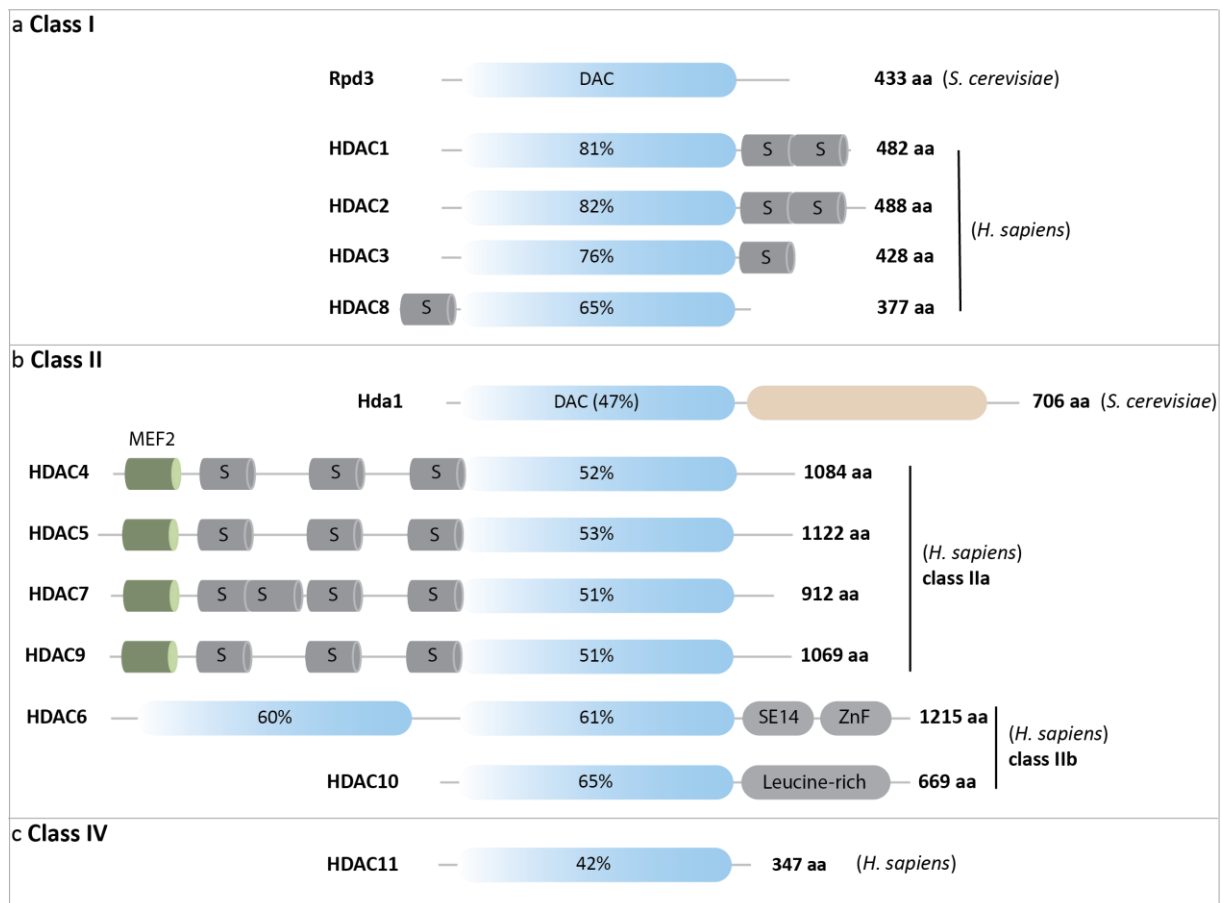
DSBs arise, move, are properly repaired or are engaged in translocations junction within the context of chromatin organization, therefore dissecting the mechanism underlying the formation of chromosome rearrangements cannot be untied from understanding how chromatin structure is regulated and in turn affect the aforementioned steps of DSB “lifetime”. As already discussed, chromatin is organized at different levels: nucleosomes can be evicted, slide or deposited by the activity of ATP-dependent remodeling complexes and, together with histone chaperones, attend to the turnover of specific histone variants; finally histone modifying enzymes participate in “decorating” the histone tails by adding or removing specific chemical groups, thereby tuning the activity of DNA-interacting factors. These modifications are made “*after* completion” of histone synthesis (Allfrey, Faulkner, and Mirsky 1964), thereby “post-translationally” added and removed, dictate so-called chromatin dynamics. Among the first discovered PTMs, acetylation consists in the addition of an acetyl group (-COCH₃) on the ε-amino group of lysine residues of histones and other proteins (Figure 5). At the level of chromatin, the negative charges carried by the acetyl group tend to neutralize the positively charged histone tails, thereby weakening the electrostatic interactions with DNA and provoking a looser chromatin status, often associated with active transcription. In fact, a pioneer work could show that incubation of isolated calf thymus nuclei with radiolabeled sodium acetate-2-C¹⁴ triggered acetylation incorporation and diminished the capacity of histones to inhibit RNA synthesis (Allfrey, Faulkner, and Mirsky 1964). In line with this, before identifying acetyltransferase domain (Brownell et al. 1996) and deacetylase activity (Taunton, Hassig, and Schreiber 1996) in enzymes involved in transcription regulation, histone acetylation and hypo-acetylated nucleosomes were already associated with promoter activation (Durrin et al. 1991) and gene silencing, respectively (Braunstein et al. 1993; Thompson, Ling, and Grunstein 1994). Mammalian histone acetyltransferases (HATs) are classified among 3 families: the first cloned and identified HAT1 have sequence and structure similarity with GCN5 (Brownell et al. 1996), both belonging to GNATs family (GCN5 N-Acetyltransferases), which includes PCAF, ELP3, HPA2, and NUT1 too. The MYST family of HATs has named based on the first identified members: MORF, YBF2, SAS2 and TIP60. This class includes a yeast homolog of Tip60, ESA1, which has the peculiarity to share a sequence motif with the yeast HDAC, RPD3. Others known MYST proteins are the fruit flies MOF and the yeast SAS2 and SAS3 that counteract SIR2-SIR3 mediated silencing. To the so-called “orphan class” belong p300/CBP and TAF1 that although having HAT activity do not hold a canonical HAT domain. Most HATs alone are unable to efficiently acetylate histones and in fact they are found in multisubunit complexes with enzymes carrying other domains, such as bromodomains which are actually the *readers* of K-acetylated, or chromo-, PHD and WD40 domains to bind mostly methylated residues, thus providing substrate specificity. The reverse reaction is the removal of acetylated group and it is catalyzed by histone deacetylases (HDACs), that alike their counterparts, do not exhibit their activity only on K-residues of histone tails, but they have a variety of non-histone targets, including co-regulators (Glozak et al. 2005).



Adapted from (X. J. Yang and Seto 2007; Gong and Miller 2013)

Figure 5: Lysine Acetylation is a chemical reaction catalyzed by acetyltransferase that, through the cofactor Acetyl-CoA, transfers an acetyl group on the ϵ -amminogroup of lysine residues of histones and non-histone proteins. Acetylated-lysines are recognized, most commonly, by bromodomains of a variety of multisubunit complexes. The inverse reaction, histone deacetylation, consisted of hydrolysis of the acetyl group via histone deacetylase enzymes and a molecule of water.

The first human HDAC purified was inferred by homology sequence to the yeast deacetylase, RPD3 (Taunton, Hassig, and Schreiber 1996). Moreover, because histone deacetylases are well-conserved enzymes across model organisms, their classification is based mainly on the similarity with their yeast homologues and their dependency on cofactors. To date, 4 classes of histone deacetylases exist in mammals: Class I, II and IV belong to the classical family and are Zn-dependent proteins, whereas Class III includes the *silent information regulator 2* (Sir2)-related proteins (Sirtuins) and require NAD⁺ for their deacetylase activity. While Class IV contains only one member HDAC11 and shares homology with both Class I and II, Class I includes proteins related to the yeast RPD3 and members of this class are HDAC1, HDAC2, HDAC3 and HDAC8, all ubiquitously expressed and with nuclear localization. Homologous to yeast HDA1 are members of Class II, which are tissue-specific and can shuttle between nucleus and cytoplasm. Class II can be divided in two subclasses: Class IIa, whose members are HDAC4, 7 and 9, whereas HDAC6 and HDAC10 belong to Class IIb (Figure 6) (X.-J. Yang and Seto 2008; Haberland, Montgomery, and Olson 2009).



Adapted from (X.-J. Yang and Seto 2008; Haberland, Montgomery, and Olson 2009)

Figure 6: Organization of human Histone Deacetylase family and domains similarity with *S. cerevisiae* Rpd3 enzyme. In figure, NAD⁺ independent HDACs are listed and grouped in classes according to their similarity with the deacetylase domain similarity of yeast Rpd3. To class I belong Rpd3-like enzymes: HDAC1, HDAC2, HDAC3 and HDAC8. Members of class II show higher sequence similarity with *S. cerevisiae* Hda1, which in turn holds 47% of sequence similarity with Rpd3 DAC domain. Then, percentages indicated in DAC domains of members of Class II and IV show similarity with yeast Hda1. HDAC11 is the orphan member of Class IV. Class II can be subdivided in two subclasses: Class IIa differs from Class IIb for the presence of Myocyte enhancer factor-2 (MEF2)-binding motifs (green cylinders) and 14-3-3 binding motifs containing Serines at N-terminal (gray cylinders). HDAC4, HDAC5, HDAC7 and HDAC9 are members of Class IIa, whereas HDAC6 and HDAC10 belong to class IIb. Deacetylase domain is depicted in gradient light blue; Rpd3, stays for “reduced potassium dependency-3”; Hda1 for “histone deacetylase-1”; SE14, Ser-Glu- containing tetradecapeptide repeats; ZnF, ubiquitin-binding zinc finger.

1.5.1 The role of HDAC1 and HDAC2 in genome integrity

Because of their nuclear localization, members of class I of HDACs are the more likely to play a role in the formation of chromosomal rearrangements. Defects in HDAC3 (Bhaskara et al. 2008) and HDAC8 (Haberland et al. 2009) lead to embryonic or perinatal lethality of mice and have been also linked to genome maintenance, but in the context of replication and cell cycle progression (Bhaskara et al. 2008; 2010; Wells et al. 2013); whereas, HDAC1 and HDAC2 have been more tightly associated with DSB repair (Miller et al. 2010; Chou et al. 2010; Rother et al. 2020) and resolution of replication stress (Sirbu et al. 2011).

Introduction

Although HDAC1 and HDAC2 share around 85% of sequence identity and around 80% of similarity with the yeast homolog RPD3 (Figure 6) (Taunton, Hassig, and Schreiber 1996; W. M. Yang et al. 1996), loss of function of one of those enzymes only partially is compensated from the other enzyme. This might also explain why, in fact, HDAC1 and HDAC2 are often found together to carry out deacetylase activity in multimeric repressive complexes, such as SIN3 complex, the Nucleosome Remodeling Deacetylase NuRD complex, and the Corepressor of RE1-silencing transcription factor (CoREST) complex (X.-J. Yang and Seto 2008). Moreover, null alleles for HDAC1 and HDAC2 highlighted different phenotypes, a hint that indeed HDAC1 and HDAC2 hold not redundant functions. For example, HDAC1 *-/-* results in embryonic lethality before E10.5 (Montgomery et al. 2007; Lagger et al. 2002), due to differentiation defects, because of overall hyper-acetylation of histones H3 and H4, and proliferation abnormalities, as result of increased p21 and p27 activity, both negative regulators of CDK activity (Lagger et al. 2002; Yamaguchi et al. 2010). Pups mice lacking of HDAC2 die perinatally or show cardiac malformations (Montgomery et al. 2007). Lack of both HDAC1 and HDAC2 in pre-B cells block B-cells development at early stage, whereas in mature B cells, loss of both histone deacetylases becomes unsustainable when cells are induced to proliferate as consequences of missregulated G1 to S transition (Yamaguchi et al. 2010), anticipating possible role of histone deacetylase 1 and 2 in DNA replication process. HDAC1 and 2 (and HDAC3) have been found enriched on nascent DNA (Sirbu et al. 2011; Bhaskara et al. 2013; Wells et al. 2013), where they regulate replication speed and counteract accumulation of H4K16ac. By doing so, and in concert with ATP-dependent chromatin remodeler activity, HDAC1 and 2 play an inhibitory effect on chromatin relaxation yet assuring proper chromatin configuration for fork progression (Shogren-Knaak et al. 2006; Bhaskara et al. 2013).

Indirect evidences highlighted that HDAC1 and 2 might have a role also in the PARP-dependent response to DNA damage. In fact, in a screen for proteins that increase ubiquitination upon DNA damage, two components of NuRD complex, CHD4 and MTA1, were found rapidly and transiently accumulating at site of microirradiation and the fast kinetics of recruitment prompt the author to investigate whether the accrual of components of NuRD complex was regulated by parylation. Indeed, treatment with Parp inhibitor prevented MTA1 to localize at damage site (Chou et al. 2010). This ultimately hints that HDAC1 and HDAC2, as NuRD subunits, might be also implicated in the response to DNA lesions. In line with this, it has been shown that HDAC1 and HDAC2 not only travel along with the replisome, but they are recruited at laser-induced damage where they promote DSBs repair by leading deacetylation of H3K16 and H3K56 (Gong and Miller 2013). Cells depleted of HDAC1/2 bear persistent DSBs and DDR activation and impaired NHEJ-repair events. A recent model gathers together the previous discoveries proposing, in fact, that upon DNA damage, PARP triggers CHD7-chromatin relaxation, to which follow HDAC1/2 localized deacetylation which fosters canonical NHEJ (Rother et al. 2020). SIRT7-mediated H3K18 deacetylation at DNA damage site is also PARP-regulated (Vazquez et al. 2016). Complementary evidences have shown that Tip60-mediated acetylation, or knockdown of

Introduction

both HDAC1 and HDAC2, impair 53BP1 recruitment, while shifting the balance for BRCA1 accrual at mCherry-LacR-FokI-induced DSBs (Tang et al. 2013). As previously discussed, histone acetyltransferase and deacetylases act also on non-histone proteins; for instance Tip60 targets ATM, promoting its full activation and autophosphorylation, whereas it has been shown that SIRT1 directly interacts with Ku70 and by promoting its deacetylation contribute to apoptosis attenuation (H. Y. Cohen, Miller, et al. 2004; H. Y. Cohen, Lavu, et al. 2004).

Regarding the role of histone deacetylases in homologous recombination repair no compelling evidence have been proposed so far: a work had attempted proposing that SIRT6-dependent CtIP deacetylation could promote end resection, however this paper has been retracted (Kaidi et al. 2019). Furthermore, HDAC2 depletion or HDACs inhibition by MS275, or PCI-24781, have shown to decrease RAD51 levels (Krumm et al. 2016; Adimoolam et al. 2007) restoring cell-drug sensitivity, whereas, an independent study has also observed that upon SAHA treatment (pan HDACi), RAD51 and Ku80 were both downregulated suggesting a more general effect of HDAC inhibitor molecules in attenuating key factors of DSB repair processes (Blattmann et al. 2010).

1.5.2 Drug-targeting HDACs in cancer therapy

Histone deacetylases are involved in several biological processes (included DNA repair, differentiation and apoptosis), therefore it comes with no surprise that in several cancer types, members of different classes are upregulated and specifically overexpression of HDAC1, HDAC2 or HDAC3 account for the most represented in various tumors hitting for instance Colorectal, Stomach, Oesophagus, Breast, Ovaries, Lung, Pancreas, Thyroid and Prostate.

Inhibitors targeting HDACs from class I, II or IV have anti proliferative effects and they have been tested in clinical trials for cancer therapy (Bolden, Peart, and Johnstone 2006). For example, Vorinostat or SAHA (Suberoylanilide Hydroxamic Acid) has been the first FDA-approved HDACs inhibitor to be used in clinical treatment of T-cell Lymphoma (Mann et al. 2007), because of its antitumor properties. In prostatic cancer cells, dose-dependent treatment with SAHA has shown to increase the fraction of G2-arrested cells, by decreasing expression levels of cyclin B and cyclin A2, and to enhance FOXO3a-regulated apoptosis, while inhibiting AKT- signaling pathway (Shi et al. 2017).

Loss of H4K16Ac, regulator of high-order chromatin structure (Shogren-Knaak et al. 2006), seems to be a shared feature among different cancer types (Fraga et al. 2005) and, more generally, upregulation of histone modifiers in tumor cells is considered a responsive mechanism to elude genotoxicity, on which many chemotherapeutics based their efficacy in cancer treatment. As matter of fact, it has been found that combined use of histone deacetylases inhibitors and chemotherapeutics can abolish, or even prevent, the drug-tolerant state and restore sensitivity to therapeutic agents (S. V. Sharma et al. 2010). Similar cellular responses are triggered upon combined treatment between HDAC inhibitors and ionizing

Introduction

radiation, used as radiotherapeutic agent (Karagiannis and El-Osta 2006). Importantly, although histone deacetylases inhibitors have a well-known impact on gene transcription, mounting evidences describe that this “repriming” toward drug sensitiveness rises from the enhanced DDR triggered by the new chromatin-state induced by HDACs inhibitor (TSA, in the study), together with checkpoint bypass and, as consequence, cell death (S. V. Sharma et al. 2010).

It was found that the combined use of etoposide and TSA (pan HDACs inhibitor) stimulates apoptosis, of drug-resistant non-small cell lung carcinomas. Indeed, usage of caspase inhibitor or depletion of pro-apoptotic factors, such as AIF (apoptosis inducing factor), abolishes etoposide/TSA triggered apoptosis, as monitored by measuring the levels of caspases activity, PARP cleavage and DNA fragmentation (Hajji et al. 2008). The restored cell death seems to be due to reestablished levels of H4K16ac upon HDAC inhibition as well as overexpression of hMOF, responsible to specifically acetylate Lys16 on histone H4 (Taipale et al. 2005), is sufficient to restore sensitization to etoposide treatment (Hajji et al. 2010). Same effect was observed upon SIRT1 inhibition, whereas when the authors overexpressed SIRT1, they observed low levels of H4K16ac and cell apoptosis; suggesting that the ratio between hMOF1/SIRF1 (and H4K16ac levels) might regulate drug sensitization (Hajji et al. 2008; 2010). Other researchers, by using Valproate (a Valproic Acid sodium salt), observed a synergized cytotoxicity of cisplatin and etoposide, when in combination with this histone deacetylase inhibitor, without increasing H2AX phosphorylation (Groh et al. 2015). Additive cytotoxic effect and decreased cell viability due to caspases activity was observed also upon co-treatment with Vorinostat and Topoisomerases inhibitors (Gray et al. 2012) and/or cisplatin (Pan et al. 2016). Cellular senescence of prostatic cancer cell lines is also increased upon combined treatment with a pan-Aurora Kinase inhibitor (Paller et al. 2014).

Increased H3-Ac, along with decreased expressions and activity of members of class I HDACs, and enhanced apoptosis were also observed upon combined treatment with CI-994 and etoposide of primary cells derived from patients with Atypical teratoid/rhabdoid (AT/AR) tumor (Kim et al. 2021). Another pan-histone deacetylase inhibitor, Panobinostat (formerly called LBH589), showed reduced cell proliferation in dose dependent manner (G. Wang et al. 2013) and, *in vitro* and *in vivo*, it can trigger up to 62% of reduction of tumor growth, in mesothelioma and lung cancer models (Crisanti et al. 2009). HDACs inhibitors can also count for veterinary applications: in fact similar effects, to the ones just described, were observed in mouse models carrying canine lymphoma xenografts, showing dose-dependent reduction of tumor size, linked with increased H3-Ac and apoptosis (Dias et al. 2018). Moreover, when Panobinostat is combined with chemotherapeutics, such as etoposide, doxorubicin, or cisplatin, increases cytotoxicity in high risk neuroblastoma-cells and small cell lung carcinoma cells (G. Wang et al. 2013; Crisanti et al. 2009). The mechanisms underlying this synergistic effect seem due to downregulation of CHK1, ATM/ATR substrate and cell cycle arrest due to low levels of CDK1 and thereby abrogation of G2 cell cycle checkpoint (G. Wang et al. 2013). However, treatment of patients with lung cancer with a combination of Panobinostat, carboplatin and etoposide in the context of a Phase

Introduction

I trial revealed high intolerability even at the lowest dose levels tested, along with thrombocyto- and neutro- penia, so that the study was suspended (Tarhini et al. 2013).

However, dissecting the molecular mechanism by which these inhibitors carry out their anticancer activity is quite challenging because HDACs inhibitors trigger “umbrella” of effects, varying from DNA damage and repair, regulation of reactive oxygen species and thereby apoptosis, to changes in chromatin structure, cell cycle progression and chromosome segregation (Bolden, Peart, and Johnstone 2006; Eot-Houllier et al. 2009).

1.6 Open questions

It has been well understood that formation of chromosome translocations can give rise to neoplasia and lots of efforts have been devoted to shed lights on how gene fusions trigger aberrant processes by eluding various cellular controls, however rudimentary remains our knowledge regarding the mechanisms which ultimately drive the formation of such chromosomal rearrangements. Regarding factors influencing the frequency of chromosome translocations it has been highlighted that null alleles for DSB repair factors, in cellular and animal systems, demonstrated their involvement in suppressing or facilitating formation of chromosome translocations: when the repair machinery is disrupted, translocations can be recovered at different frequencies compared physiological conditions.

Nonetheless, when dissecting mechanisms and pathways playing a role in translocations formation, one must consider not only what does affect the joining of double strand ends, because this constitutes only the final step in “DSBs life cycle”. In fact, chromosome translocations formation mechanisms rely as wells on what brings in proximity or keeps together two DSBs, what affects the movement and, *in primis*, what triggers the breakage of genomic loci. Intriguingly, chromosome translocations occur in the context of high-ordered chromatin organization and experimental evidences have demonstrated that chromatin related functions might affect individually each of the aforementioned moments of DSBs life span. In fact, as discussed throughout the introduction of this dissertation, chromatin signatures have been found enriched at genes which frequently undergo chromosome rearrangements (see 1.4.1.2 Chromatin features associated with breakpoint regions), chromatin remodelers activity or changes in condensation status of chromatin environment of certain loci influence their motion characteristics and nuclear positioning (see 1.4.2.1 Motion properties of DSBs: “...and yet, it moves”). Finally, chromatin dynamics is integral moment of DDR and specific histone modifications can dictate repair efficiencies or whether repair of a DSB occurs via end-joining rather than homologous-directed mechanism (see 1.2.1 DSB repair pathways: a chromatin based-choice). Recently, DSBs-induced chromatin changes have been map corroborating the hypothesis that a reshaping of the chromatin context upon DSBs formation is, indeed, need to set permissive states to DNA repair machineries (Clouaire et al. 2018).

Introduction

Altogether, this hints that chromatin environment is a key determinant of dynamic properties and repair of DSBs, however so far it has been not well established whether chromatin organization affects chromosome translocations formation, nor it has been found how the chromatin environment surrounding a DSB affects its propensity to translocate, nor in which specific moments of translocation process chromatin features play a role.

This highlights the need of a cellular system, which allows to induce perturbation in the chromatin environment and to probe whether it affects the formation of chromosome translocations, by influencing DSB formation, DSB motion and pairing or repair of targeted loci.

1.6.1 Goals of the study

The present research project had the goal to elucidate the involvement of chromatin factors and/or chromatin related mechanisms in the formation of chromosome translocations. To investigate the role of chromatin factors in modulating DSB-induced chromosome translocations, we have performed experiments to:

1. Screen for epigenetic drugs in modulating chromosome translocations frequencies, so that to infer which chromatin player might influence the formation of chromosome translocations.
2. Validate the selected hits by chemical inhibition and knock down experiment; this allows to assess whether perturbation of the levels and/or activity of candidates influence chromosome translocations (global chromatin changes). However, whether local changes in the chromatin environment surrounding a DSB, dictate its probability to translocate, it remains unsolved at this stage of the study.
3. Address whether local chromatin changes, by induction of chromatin domains in proximity of DSB, perturb its frequency to form translocations.
4. Investigate the molecular mechanisms by which chromatin players influence the formation of chromosome translocations (for instance do global or local changes in the chromatin context influence mobility of a given DSB? Do they affect DSBs repair kinetics?)
5. Validate gained insights with complementary tools and/or by assessing the involvement of chromatin changes in the formation of recurrent oncogenic chromosome translocations.

To achieve these goals we have employed previously characterized cell based systems to introduce DSBs at targeted loci, by mean of endonucleases.

The first cellular tool carries, on different chromosomes, genomic integration of one LacO and three TetO repeats flanking I-SceI cutting sequences. Thereby, upon DSB-induction, it is possible to quantify LacO-TetO translocations by qPCR or alternatively by employing fluorescently tagged versions of Lac and Tet Repressors (Figure 7).

Introduction

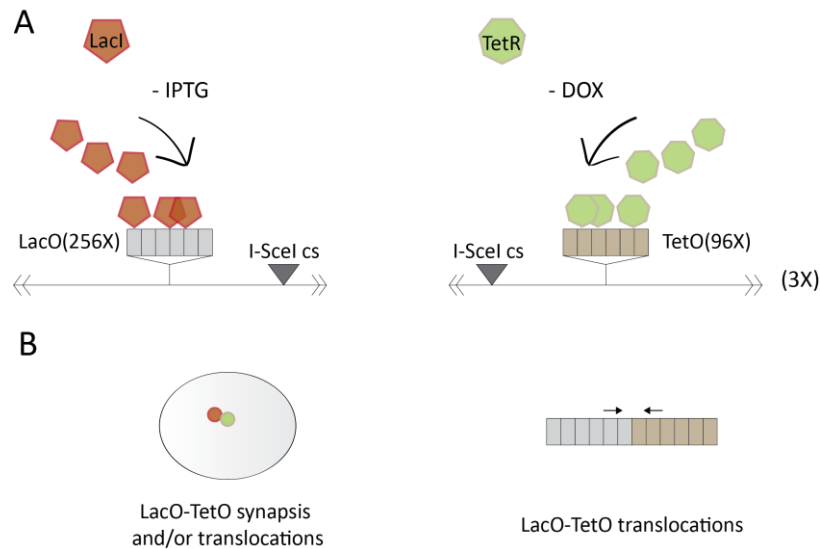


Figure 7: Cell system to induce and to quantify mechanistic steps of chromosome translocations in real time.

A. NIH3T3 cells are genetically modified to carry I-SceI cut sites flanking one integration of Lac Operator and three of Tet Operator, as repeats (NIH3T3 cells carrying these integration are renamed Parentalduo cells). Fluorescently modified versions of Lac Repressor and Tet Repressor, tagged with mCherry or GFP, can bind with high affinity their cognate operator sequences, in absence of IPTG and doxycycline, respectively. **B.** Upon induction of I-SceI-DSBs, movement of chromosome ends, DSBs synapsis and chromosome translocations can be monitored by time lapse microscopy and high-throughput imaging; alternatively translocations junctions can be quantified by qPCR, using oligos pair on the repeats, flanking the cut sites.

The high binding affinity of Lac (or Tet) Repressor for its cognate operator, in combination with fluorescent proteins such as mCherry or GFP have previously allowed either to measure motion characteristics of the said locus, or to tether any protein of interest and measure whether the enzymatic activity of the given protein can impact on locus mobility and its nuclear localization (Tumbar and Belmont 2001; Chubb et al. 2002; Soutoglou et al. 2007; Neumann et al. 2012; Roukos et al. 2013). Therefore, we have decided to use this system in combination with perturbation of the chromatin state, which can be induced either globally, via chemical inhibitors of classes or family of chromatin modifiers or via knock down of specific chromatin factors, or locally, by fusing chromatin factors in tandem with Lac Repressor and measure their relative contribution to the mobility of a broken LacO locus or in its propensity in forming translocations. For this purpose, we thought to finely regulate DSBs formation by controlling the expression and cellular localization of I-SceI endonuclease (Figure 10).

The system will be employed initially to identify chromatin factors influencing the frequency of formation of LacO-TetO translocations; further, to assess whether differences in chromosome translocations are regulated by local changes at chromatin surrounding the tethered-DSB. Finally, to investigate how chromatin perturbation affects DSBs mobility, thereby playing a role in movement of translocating-DSBs.

Similarly to the first one, the second cellular system, we have employed in the project, allows also control of DSBs formation through restriction of cellular localization of AsiSI endonuclease. Upon

Introduction

nuclear shuttling, the enzyme can cut, potentially, a thousand sites throughout the genome, thereby generating DSBs in different chromatin environments. Given that the system has been already used to monitor chromatin changes upon DSBs formation, we decided to investigate whether genomic sites bearing such DSBs-induced changes show differences in their translocations frequency, measured by HT-FISH methodology. Particularly, we focus on changes at chromatin levels triggered by chromatin factors that results as candidate modulators of LacO-TetO translocations and we aim to employ the system as part of our effort to mechanistically understand which step of chromosome translocations the identified chromatin factors play a role in.

For this purpose, we would like to verify whether genomic sites with certain chromatin changes and determined propensity to translocate, show defective repair. To do so, a variant of this cellular system allows degrading AsiSI endonuclease and thereby to monitor DSBs clearance overtime. Therefore, in collaboration with another PhD student and IMB bioinformatics core facility, we decided to profile AsiSI-DSBs over time using ssBLISS (Bouwman et al. 2020). These repair kinetics experiments aim to address whether differences in translocation frequencies, at the level of the analyzed chromatin changes, correspond to differences in DSBs repair rates.

Ultimate goal is to understand whether the same chromatin changes probed throughout the research with various cellular tools, can also impinge the formation of recurrent cancer initiating translocations. For this reason we decided to focus on modelling the formation of therapy related translocations, such as the one that arise as dramatic secondary effect upon chemotherapeutic treatment of the primary tumor. In particular we strived to understand whether combined treatment with drugs inhibiting chromatin related functions could hinder the formation of etoposide-induced *MLL* translocations

Chapter 2 – Results

2.1 Screen for epigenetic inhibitors reveals modulators of translocation frequency

Chromosome translocations occur in the context of chromatin structure and, similarly to other DNA transaction, is it likely that the chromatin modifying enzymes might play a tight control on DSBs lesions which turn into a translocation junction. However, so far, we had indirect evidence of the role of chromatin environment in the formation of chromosome translocations and the key molecular events, underlying this level of regulation, remain elusive (Lin et al. 2009; Berger et al. 2011; Burman et al. 2015).

Tracking of broken chromosome ends in space and in time has allowed not only to study dynamics of DSBs engaging or not in translocations in real time, but also to define some key features of the process (Roukos et al. 2013; Roukos, Burgess, and Misteli 2014). For instance, it has been already observed that translocations occur independently of the cell cycle phases and prevalently form between DSBs within 2,5 μm ; only sporadically persistent LacO-TetO arrays juxtaposition (indicative of translocation) were observed between distal breaks (up to 5 μm). Moreover, it has been observed that faster moving DSBs are likely more prone to form fusions.

One asset of the system resides in the possibility to combine it with perturbation of certain cellular function and study how this alteration might influence DSBs dynamics and chromosome translocations. For instance, disruption of DNA repair pathways, by using inhibiting molecules or siRNA technology, has shown that DNAPK suppress chromosome translocations, confirming previous results, without influencing tethering of DSBs, where MRE11 seems involved (Roukos et al. 2013). These previous data confirmed that the system can be used to identify modulators of the translocation frequency.

To shed light on a possible role of chromatin structure in modulating the occurrence of chromosome translocations, we carried out a screening for epigenetic inhibitors. Specifically, NIH3T3 cells (Parentalduo cells) were electroporated with I-SceI coding vector to induce the formation of I-SceI-DSBs at sites flanking the LacO and TetO arrays and released in different drugs-containing medium, each of them targeting and inhibiting specific class or family of chromatin modifiers. These drugs belong to an Epigenetic Screening Library composed of a wide range of chemical compounds that modulate the activity of methyltransferases, demethylases, histone acetyltransferases (HATs), histone deacetylases (HDACs), and acetylated lysine reader proteins. Because it was previously shown that DNAPK is essential to suppress chromosome translocations, the inhibition of the kinase activity of DNAPK (through NU7441 treatment) served as positive control to screen for modulators of the frequencies of chromosome translocations. Contrarily, MRE11 might facilitate the pairing of broken ends contributing to the formation of chromosome translocations, therefore its inhibition, through the compound Mirin, was used to screen for decreases in translocations frequencies compared to control condition (untreated cells).

Results

Translocations frequencies were quantified by qPCR using primers specific for the LacO and TetO repeats, and genomic DNA extracted 24h after the electroporation with I-SceI vector and released in drug-containing media.

The screen has revealed a variety of modulators that influence the formation of chromosome translocations in different ways (Figure 8): some drugs seems to target suppressors of chromosome translocations, as their inhibition led to an increase in the formation of chromosome translocations; others seems to target factors which facilitate the translocations process because their inhibition decrease the frequency of translocations detected by qPCR. Furthermore, inhibition of Class I HDACs seems greatly correlate with a decrease in LacO-TetO translocations frequency.

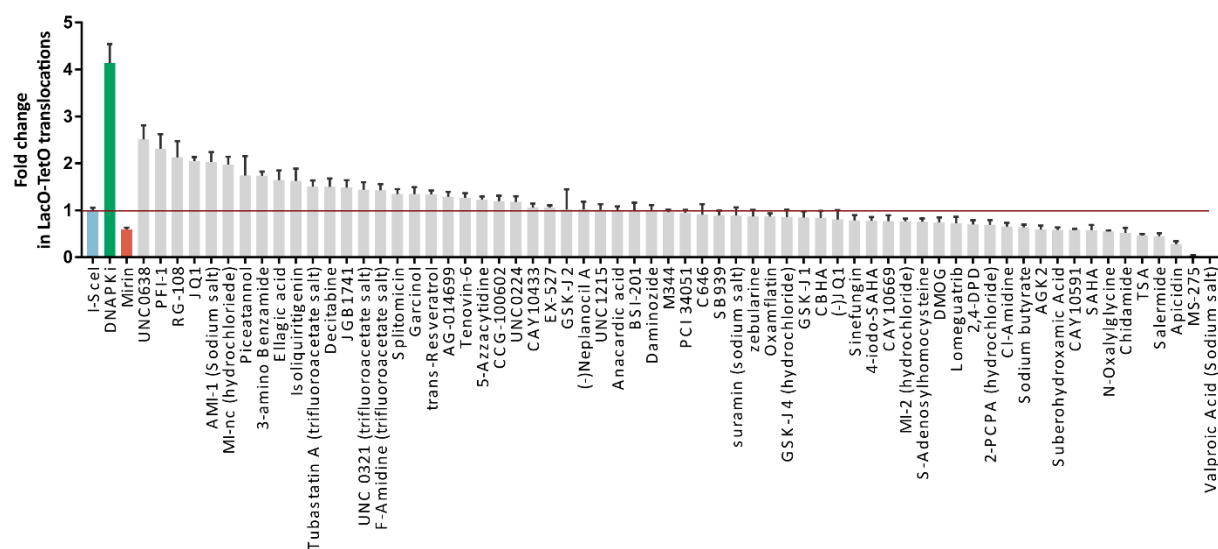


Figure 8: Epigenetic inhibitors screening revealed many modulators of the translocations frequency. NIH3T3 duo cells were electroporated with I-SceI construct and cultured for 24h in presence or not of epigenetic inhibitors. Positive and negative controls of the screening were genomic DNA extracted from cells treated with DNAPK inhibitor and Mre11 inhibitor, respectively. Class I HDACs inhibition led to a decrease of translocation frequency.

2.1.1 Class I HDAC inhibition, decreases the frequency of translocations

In our screen, the specific inhibition of class I histone deacetylases led to a reduction of LacO-TetO translocations. To rule out that the decrease in translocations is not an indirect consequence of the drugs, we measured if the inhibitory effect occurs on the deacetylase activity of the inhibited chromatin modifiers. To do so, we quantified the intensity of fluorescent reporters integrated in the cellular system, namely mCherry-TetR and GFP-LacR, as surrogate of their expression level and thereby as proxy of the state chromatin condensation. We have observed that increasing concentrations of certain histone deacetylase inhibitors correspond to higher fluorescent intensity (Figure 9B), suggesting higher expression of the fluorescent reporters probably due to more loose and hyper-acetylated chromatin state, triggered by histone deacetylases inhibition, mediated by Suberohydroxamic Acid, Sodium Butyrate, Apicidin, TSA, Pimelic Diphenylamide 106, (S)-HDAC-42 and MS275. Importantly, this dose-

Results

dependent increase of mCherry and GFP intensities, truly reflects the reduction in chromosome translocations frequencies (Figure 9A). Noteworthy, inhibition of HDAC8, via a specific inhibitor PC 34051, does not trigger variation in mCherry or GFP fluorescence, nor it seems perturbing the level of chromosome translocations, at least at doses of drugs tested in our study. Intriguingly, M344, SB939 and CBHA were not scored hits of decreased translocations frequency in the initial screening, but during validation they also led a reduction in translocations quantification and a correspondent increase in the fluorescence signal of mCherry and GFP. Therefore, we conclude that the decrease in chromosome translocations frequency occurs at doses which lead to chromatin de-condensation, hinting that the change in the chromatin environment, induced by the inhibition of the activity of these acetyl histone “erasers”, affecting the propensity of two DSBs to form a chromosome translocations.

We sought to focus our future efforts to shed light on the role of histone deacetylases into the biogenesis of chromosome translocations. In fact, the common pattern observed upon their inhibition, bring us to exclude pleiotropic effect due to a single drug treatment, but, instead, it underlies a biological and clinical relevance especially in the choice of chemotherapeutic treatment.

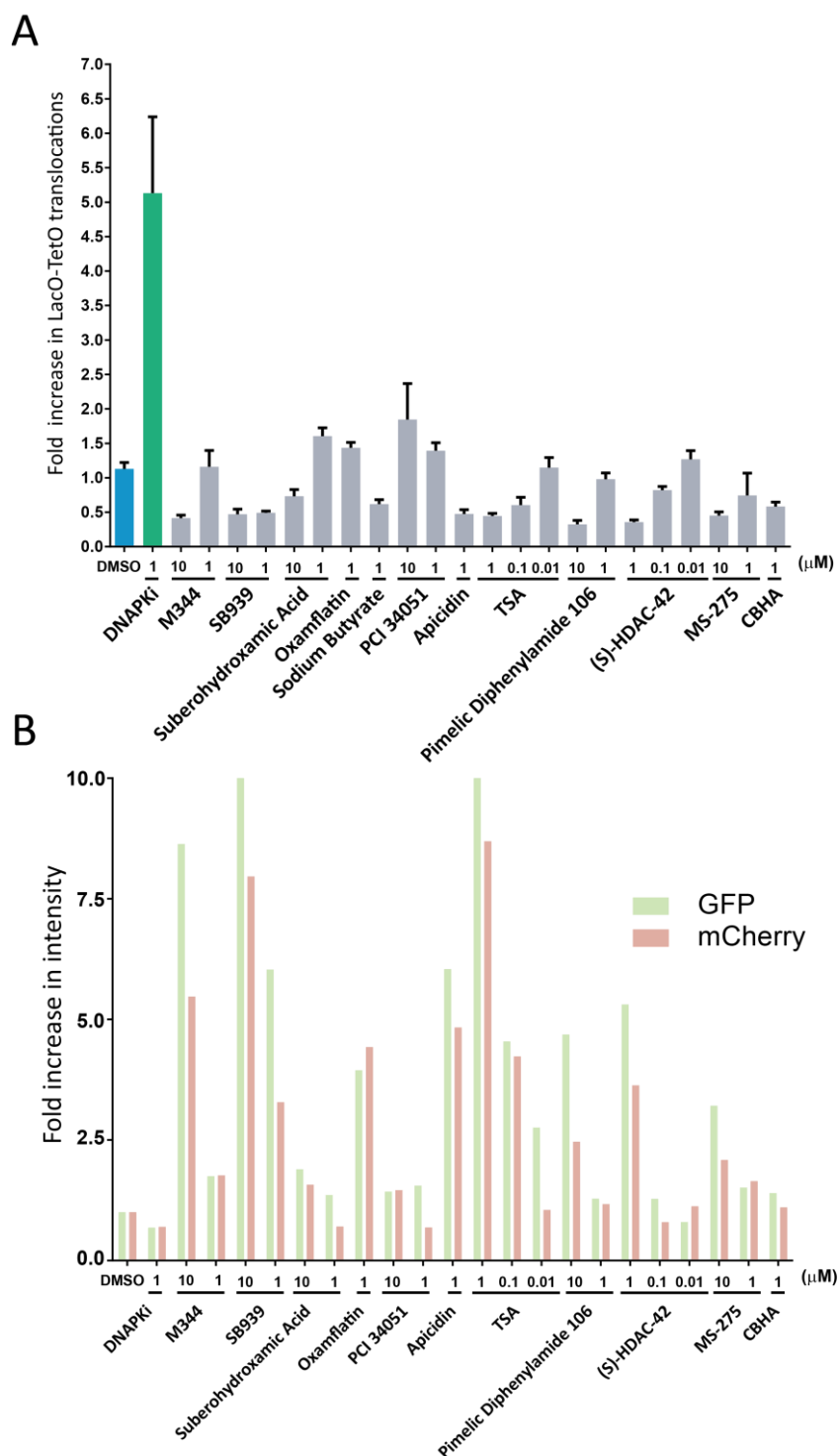


Figure 9: Translocation frequency decreases upon reduction of the condensation state of chromatin structure. **A.** HDAC inhibition decreases translocation frequency in a dose dependent manner. **B.** and in condition promoting chromatin decondensation. The increase in the intensity of an integrated in the genome fluorescent reporter is used as a surrogate of increased transcription rate due to chromatin decondensation triggered by HDACs inhibitors.

2.2 Time and space control of DSBs induction

2.2.1 Strategy

To dissect the relative contribution of chromatin factors in the formation of chromatin translocations, we thought it was important to control the timing of inducing DSBs via control of I-SceI expression, nuclear localization and DSB-repair. So far, DSBs were generated upon electroporation of a vector encoding for I-SceI endonuclease, but to trigger homogenously DSBs in the pool of cells, we strategized to control I-SceI expression under a doxycycline responsive promoter and to integrate the full constructs in the genome of the cells. Furthermore, we sought to integrate I-SceI coding region as a fusion construct with the nuclear binding domain of the glucocorticoid receptor and with an inducible degradation tag or with a destabilization tag.

Therefore, upon adding doxycycline to the media culture, I-SceI is expressed and it is anchored in the cytoplasm. When the steroid hormone, dexamethasone (Dex), binds the nuclear domain of glucocorticoid receptor, it induces a conformational change, which allows the chimeric construct to travel into the nucleus, where I-SceI can recognize its integrated target sequences and generates DSBs in proximity of the Lac and Tet operator repeats (Figure 10).

Together, this allows a time control of DSBs induction, however we envision also two approaches to trigger I-SceI degradation, allowing monitoring of DSBs repair events.

A possible way to direct degradation of I-SceI enzyme is via auxin-induced recruitment of TIR1 E3 ligases, which, together with an E2 conjugating enzyme, mediate the poly-ubiquitination of the I-SceI endonuclease and direct it to the ubiquitin proteasome system (Figure 10A). Another way consists of employing as tag a destabilization domain (DD) of FKBP protein. In presence of a stabilizing ligand (Shield1), DD-tagged I-SceI gets stabilized; contrarily when Shield1 is washed out from the cell culture media, the destabilization tag gets unfolded and accessible to the UPS (Figure 10B).

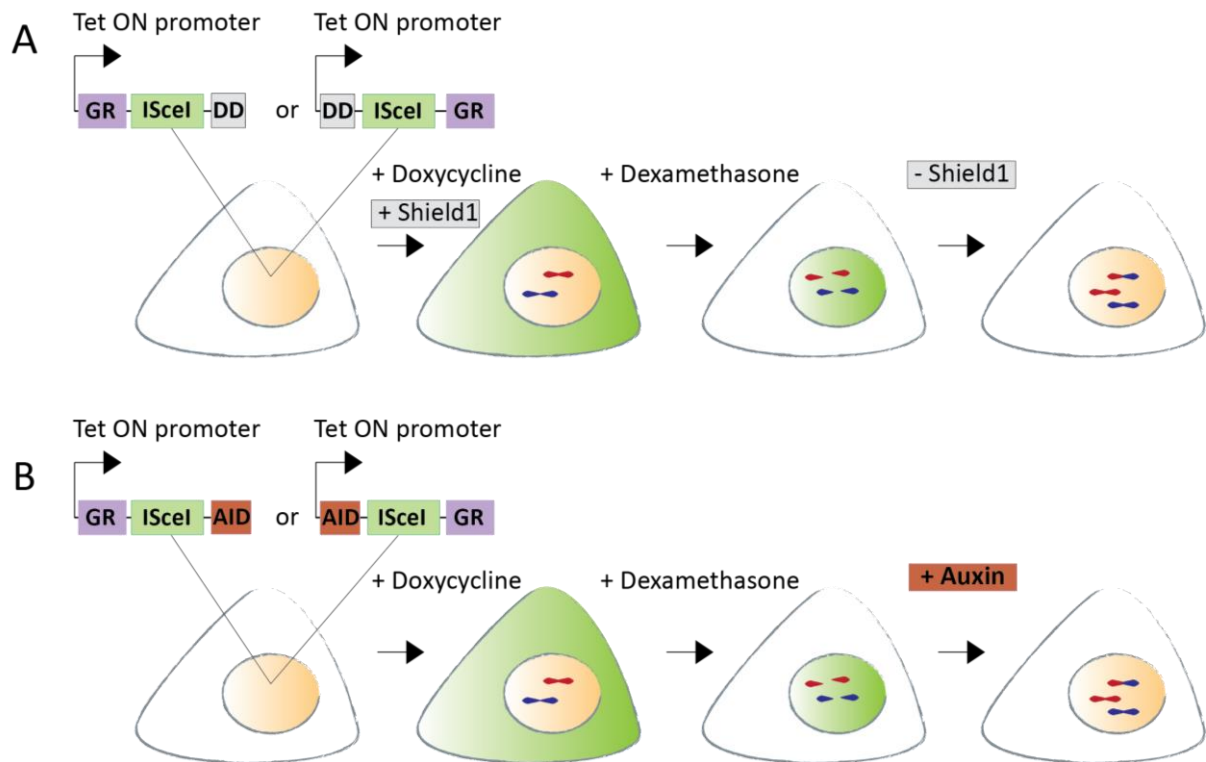


Figure 10: Dox- inducible system to generate DSBs in time and space controlled manner. Schematic workflow for the controlled induction and repair of I-SceI mediated DSBs. Four different configurations of the constructs GR-I-SceI and degron tags are cloned in lentiviral vectors and employed to generate stable cell lines. I-SceI is expressed by a Dox- inducible promoter and it resides in the cytoplasm until dexamethasone stimulation, which binds the nuclear domain of the glucocorticoid receptor and it triggers the nuclear shuttling of the enzyme. Monitor of DSBs repair can be followed upon degradation of I-SceI, which can be achieved, as in **A.**, by removing Shield1 ligand from the media culture so that it destabilizes the degron domain, now prone for degradation; in **B.** an alternative way for I-SceI degradation is depicted: addition of auxin triggers TIR1-mediated ubiquitination, which enables proteolysis degradation.

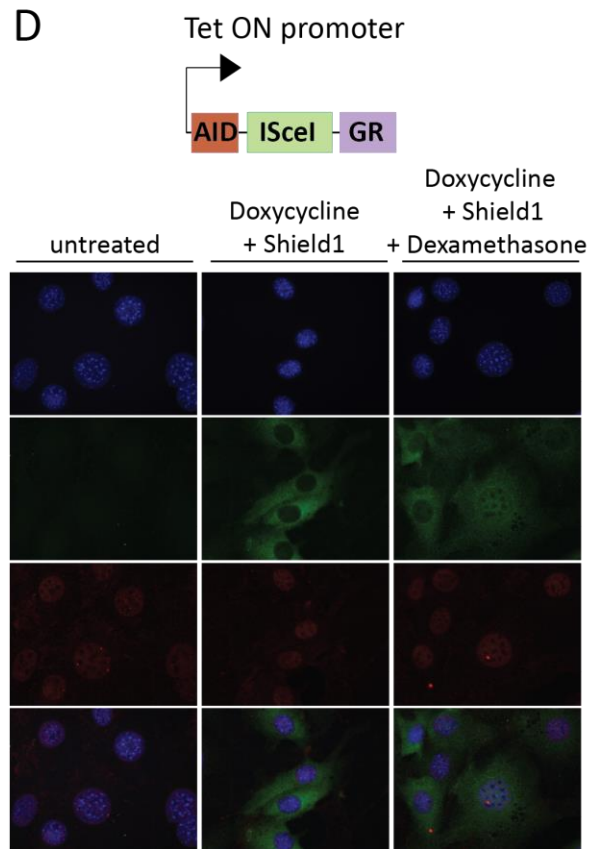
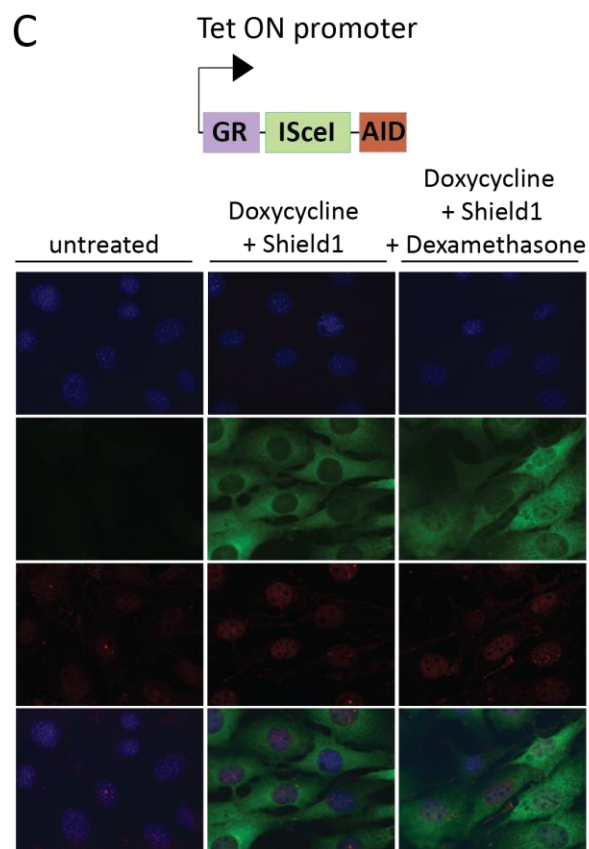
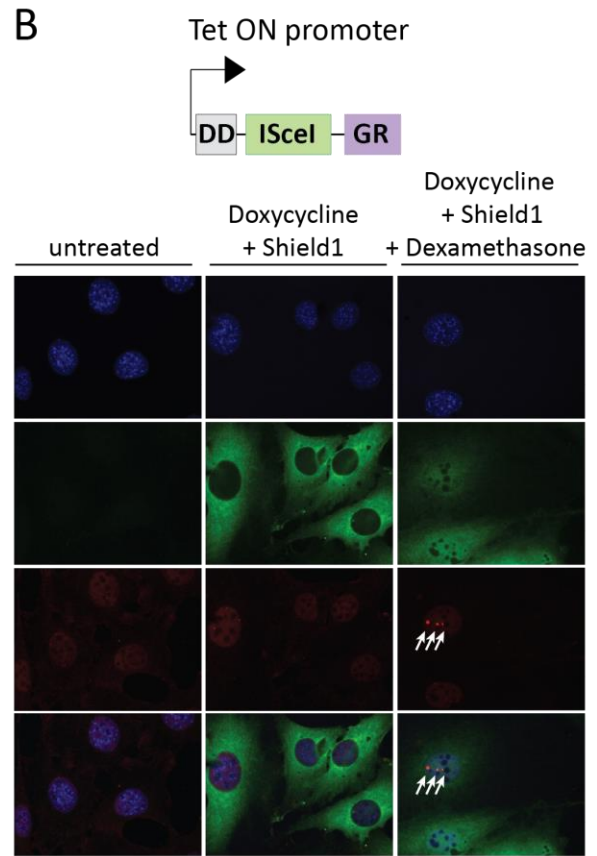
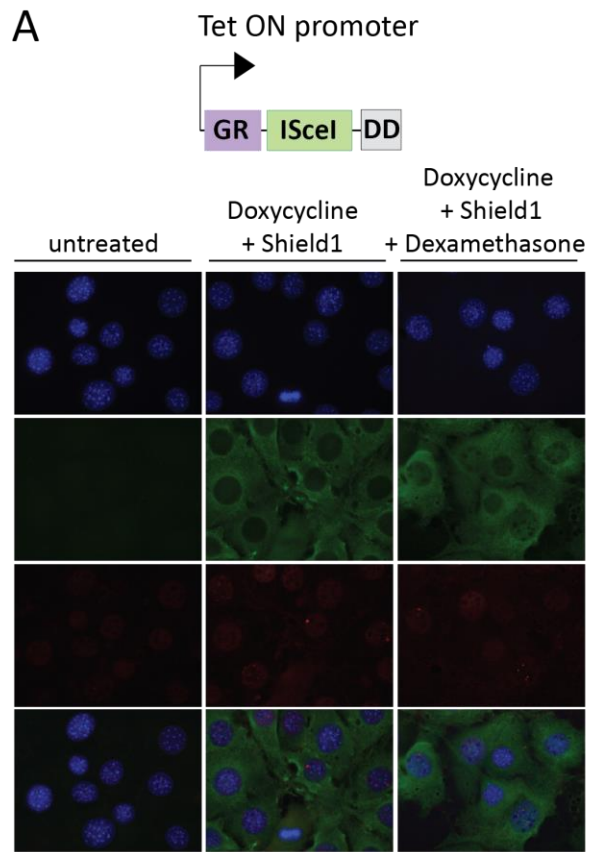
2.2.2 Selection of DD-I-SceI-GR cell line (Superduo cells)

To achieve a fine spatial and temporal control of the induction and the degradation of I-SceI of DSBs, the three basic elements, namely HA-tagged version of I-SceI endonuclease, glucocorticoid receptor domain, degron tag, were cloned in various configurations in lentiviral vectors.

Stably expressing cells lines for each of the constructs configuration were generated via viral transduction. Upon neomycin selection and colony formation, the best clones were selected based on HA-I-SceI intensity and its ability to induce up to four 53BP1 foci, surrogates of DSBs induction (Schultz et al. 2000) at the correspondent four I-SceI sites integrated in the cell system (specifically, one LacO-I-SceI and three TetO-I-SceI).

A clone for the stable integration of Dox-inducible **DD-I-SceI-GR** construct was chosen because of the higher expression level of I-SceI and the formation of distinct 53BP1 foci, and renamed “Superduo” cells. Representative images of the selected clones are shown below (Figure 11).

Results



Results

Figure 11: Dox-inducible expression of I-SceI endonuclease in various constructs configurations and controlled-induction of I-SceI-mediated DSBs. Immunofluorescence to monitor the expression of HA-GR-I-SceI-DD, HA-DD-I-SceI-GR (respectively panel **A** and **B**) and HA-GR-I-SceI-AID, HA-AID-I-SceI-GR (respectively panel **C** and **D**) after 24 h of doxycycline treatment (4 μ g/ml) and stimulation with dexamethasone 1 μ M. The chimeric constructs are tagged with HA sequence, whereas 53BP1 foci represent DSBs formation.

After assessing the expression (HA intensity signal), cellular localization (nuclear transfer of the chimeric construct upon adding dexamethasone to the medium) and enzymatic activity of the chimeric I-SceI construct (presence of 53BP1 foci), we tested whether we could induce degradation of the endonuclease and, thereby, monitor DSBs resolution.

Therefore, we washed out all drugs from the cell culture media, so that no trigger for I-SceI expression was present, but rather the chimeric construct could get destabilized and unfolded by proteasome. As readout of repair events, we monitored the disappearance of 53BP1 foci in a time course experiment.

When cells were stimulated with Dox, Dex and Shield1, the fraction of cells with intact I-SceI loci (in gray) drops dramatically (Figure 12B, 3rd condition), in fact the majority of cells show at least one or more than one 53BP1 focus, underlying to a “DSBs prone” condition. As said, because we do expect that upon I-SceI nuclear transfer, the enzyme induces 4 DSBs at integrated four I-SceI recognition/cut sites, we decided to count up to 4 53BP1 foci (which indeed represent the majority of DSB-induced nuclei).

On the other hand, when cells were replenished with fresh, drugs-free medium, we could observed lower levels of 53BP1 already 14h later, suggesting that the system is suitable for the controlled induction and the repair of I-SceI induced DSB. Finally, we have also observed that the ligand, Shield1, at 1 μ M concentration, is important to stabilize I-SceI protein, which, otherwise, would fade away, even if cells were stimulated with doxycycline and dexamethasone (Figure 12A, 3rd column).

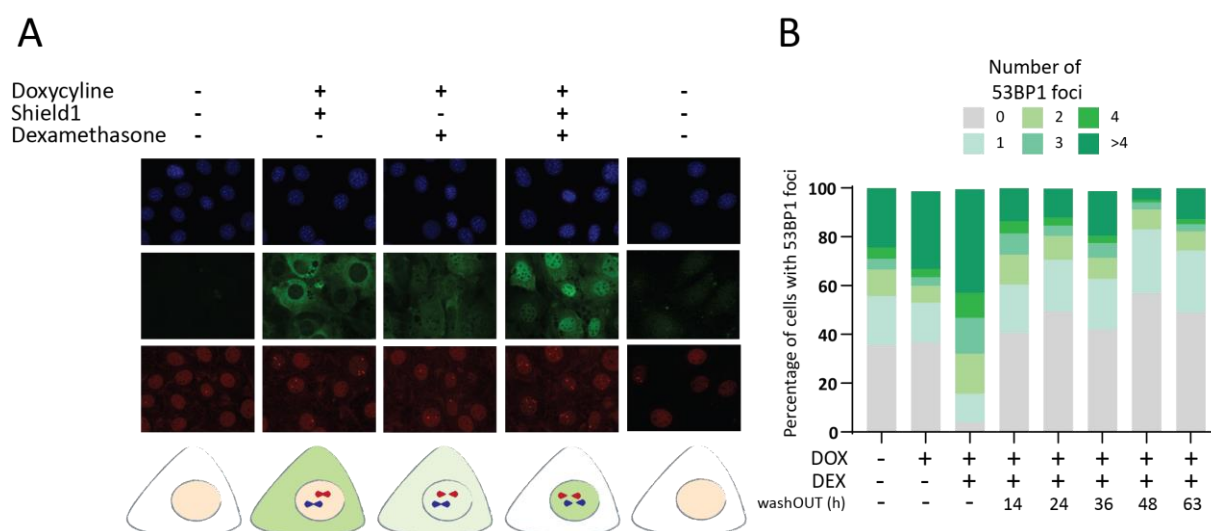


Figure 12: Repair of I-SceI-induced DSBs. Formation of DSBs by I-SceI endonuclease is confirmed by quantification of 53BP1 foci upon 24h induction of I-SceI nuclear transfer. Washing the drug (doxycycline) and the ligands (dexamethasone and Shield1) allows to degrade the protein and to repair the DSBs as results in

Results

decreased detection of 53BP1 foci already 12h after induction of degradation of the endonuclease. To monitor DSBs/53BP1 resolution cells were fixed 12h, 24h, 36h and 48h after the maximum cut (considered t=0).

To easily detect chromosome translocations, we sought to maximize the amount of DSBs by optimizing time of doxycycline and dexamethasone treatment; in other words, we thought to assess for how long I-SceI has to be expressed and anchored in the cytoplasm, to, then, optimally lead to I-SceI-DSBs accumulation, once the endonuclease is shuttled into the nucleus. For this purpose, doxycycline was added to the cells and different time treatments with dexamethasone were tested, ranging from 30 minutes up to 12 hours, after which cells were fixed and immunofluorescence against HA-I-SceI and 53BP1 foci was performed. Because doxycycline was added, in each condition, at the same time (and then, cells were fixed together), we should be aware that the kinetic of accumulation of 53BP1 upon different Dex- treatment is affected by the fact that time of doxycycline exposure was different at the moment of induction of I-SceI nuclear shuttling. Nonetheless, the total time of doxycycline- stimulation was identical among conditions. Disregarding this caveat, it is possible to observe a progressive accumulation of HA-I-SceI into the nucleus (Figure 13A), to which it correlates with a higher fraction of cells with 1, 2, 3, or 4 53BP1 foci (Figure 13B). Moreover, because one I-SceI sequence is adjacent LacO repeats, we controlled cut specificity by quantifying up to 4 times increased colocalization events between 53BP1 focus and mCherryLacR/lacO array (in 80% of nuclei, a 53BP1 focus overlaps with a mCherry spot), when I-SceI is expressed and transferred to the nucleus (Figure 14B, Figure 14C), reinforcing the feasibility of I-SceI as mean to induce DSBs and securing 53BP1 as proxy for DSBs detection.

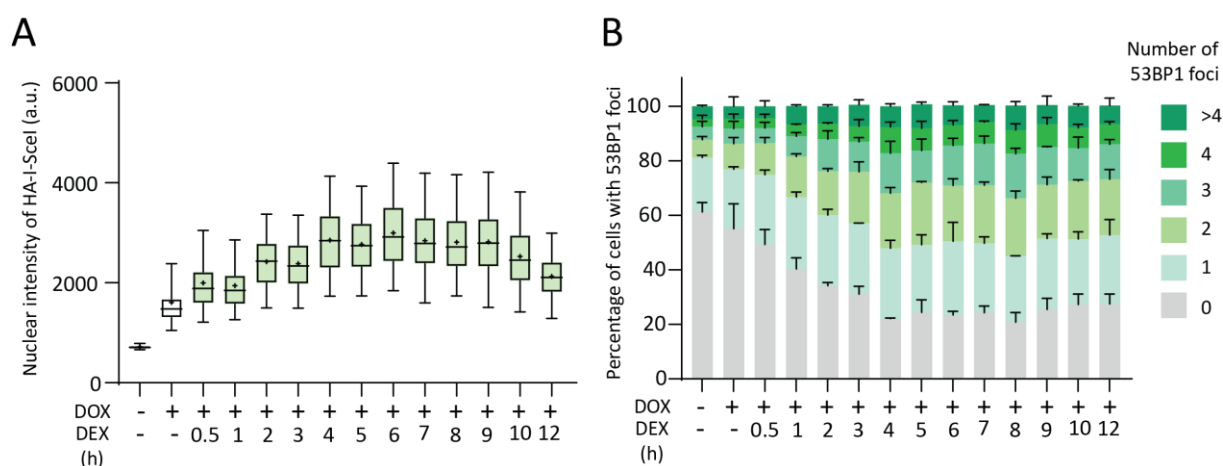


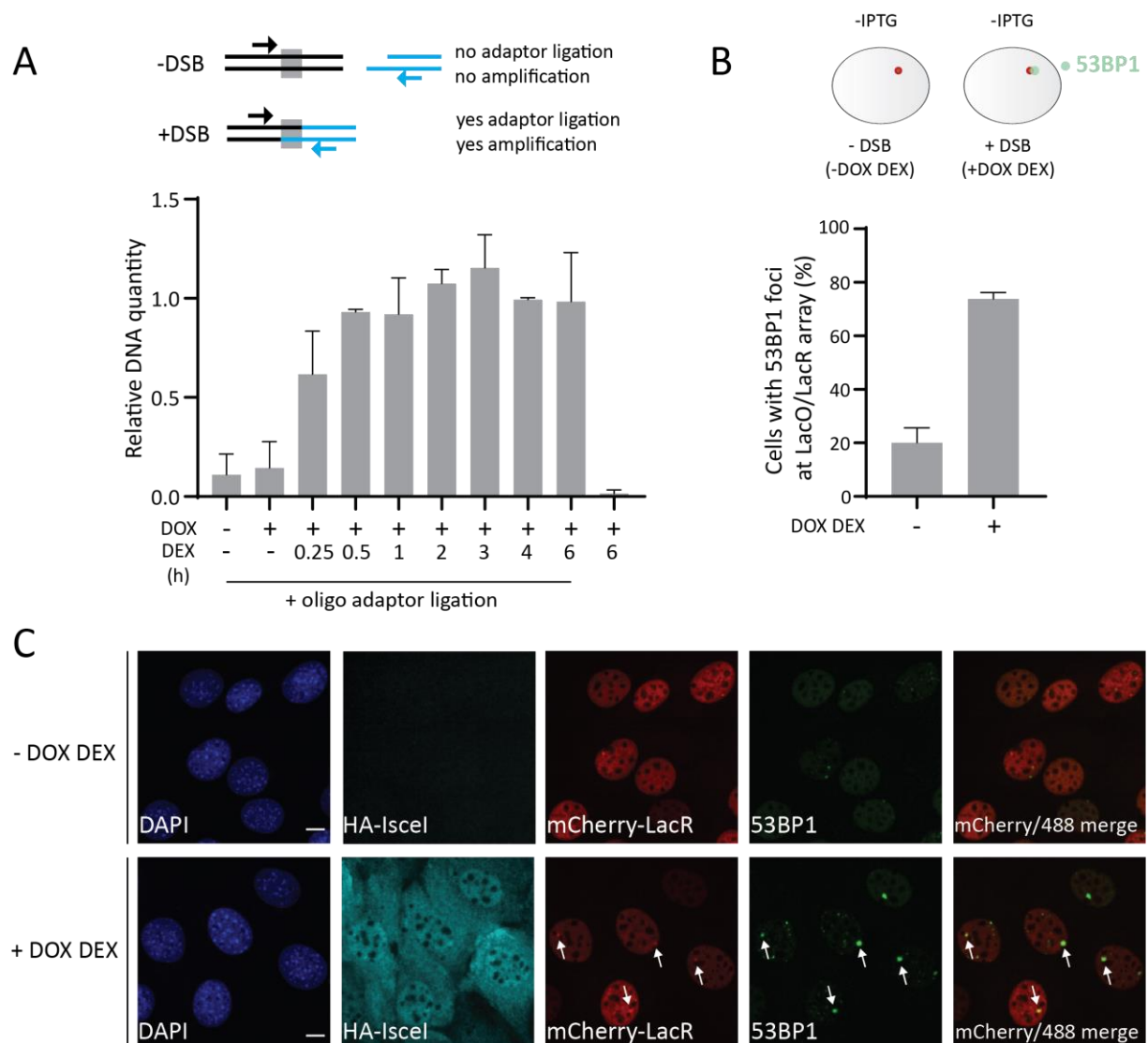
Figure 13: Time and space control of I-SceI-DSBs. **A.** Doxycycline and Shield1 (DOX) are added to the cell culture media for a total time of stimulation of 12h, to induce expression and stabilization of HA-I-SceI chimeric protein. Upon dexamethasone stimulation (DEX), HA-I-SceI progressively accumulates in the nucleus, reaching a plateau after 4 hours. **B.** Frequency distribution of cells with increased number of 53BP1 foci at different times of dexamethasone treatment. Bin window of 1 shows percentage of cells with 0, 1, 2, 3, 4 and more than 4 (>4) 53BP1 foci. Error bars represent standard deviations of the mean of two biological replicates.

Results

Importantly, we have observed that the effects of dexamethasone stimulus reach a plateau at time points higher than 4 hours, with a slight reversion at late time points, possibly suggesting that the endonuclease gets extruded as cells move in other cycle phases.

Another way to test directly the formation of DSBs via inducible-I-SceI, is based on ligation of adaptors to the double strands broken ends, followed by qPCR using primers designed on the genomic region next to DSB and on the ligated adaptor itself. In presence of a I-SceI-generated cut, 50 nM of a phosphorylated adaptors can be ligated giving rise to a productive amplification, vice versa few or background levels of ligation-mediated amplification might occur in conditions with no breaks or no T4 ligase.

Our results show a rapid accumulation of DSBs overtime, peaking at 3 hours after I-SceI is shuttled into nucleus and being stable up to 3 hours later (Figure 14A). This result well agrees with the observed frequency of accumulation from one to four 53BP1 foci, which peaks 4 hours after I-SceI starts nuclear shuttling. Therefore, for future experiments we have considered 4 hours of dexamethasone treatment as condition of maximum I-SceI cleavage activity.



Results

Figure 14: I-SceI nuclear transfer progressively induces DSBs formation at LacO locus. **A.** LM-PCR of I-SceI-DSBs shows that DSBs accumulate overtime when dexamethasone triggers nuclear localization of I-SceI enzyme. In untreated condition few DSBs are amplified; similarly Dox-treated cells show background level of ligatable and amplifiable DSBs. gnDNA from 6h dexamethasone, not ligated with the asymmetric adaptors serve as negative control of the assay. **B.** Upon Dox-inducible expression and Dex-mediated nuclear localization of I-SceI, I-SceI-DSBs accumulates 53BP1 colocalizing with lacO/LacR array. In **A** and **B**, error bars represent standard deviation of two biological replicates. **C.** Example image of colocalization of 53BP1 and lacO/LacR array in cells treated with doxycycline and dexamethasone. Scale bar indicates 10 μm .

Once known that DD-I-SceI-GR constructs could properly fold and translocate to the nucleus (Figure 12) to trigger DSBs accumulation already 3-4 hours after the nuclear shuttling of the enzyme (Figure 13, Figure 14), we verified whether we were able to induce translocations with similar frequency as the one observed upon cells electroporation of I-SceI vector.

Therefore, Superduo cells were electroporated with I-SceI vectors (expressing wt isoform or the catalytic inactive mutant of the enzyme), then were harvested 16, 24 and 36 hours later; alternatively, by using Dox and Dex, we stimulated the expression and the nuclear shuttling of the enzyme for 4h (which we consider as time 0 corresponding to the maximum percentage of cells with I-SceI DSBs), and we collected time points 12, 24 and 36 hours later.

LacO-TetO amplicons were normalized on GAPDH and translocation frequencies are shown as fold difference compared to the detected ones after 24h cell electroporation (9th bar in the plot).

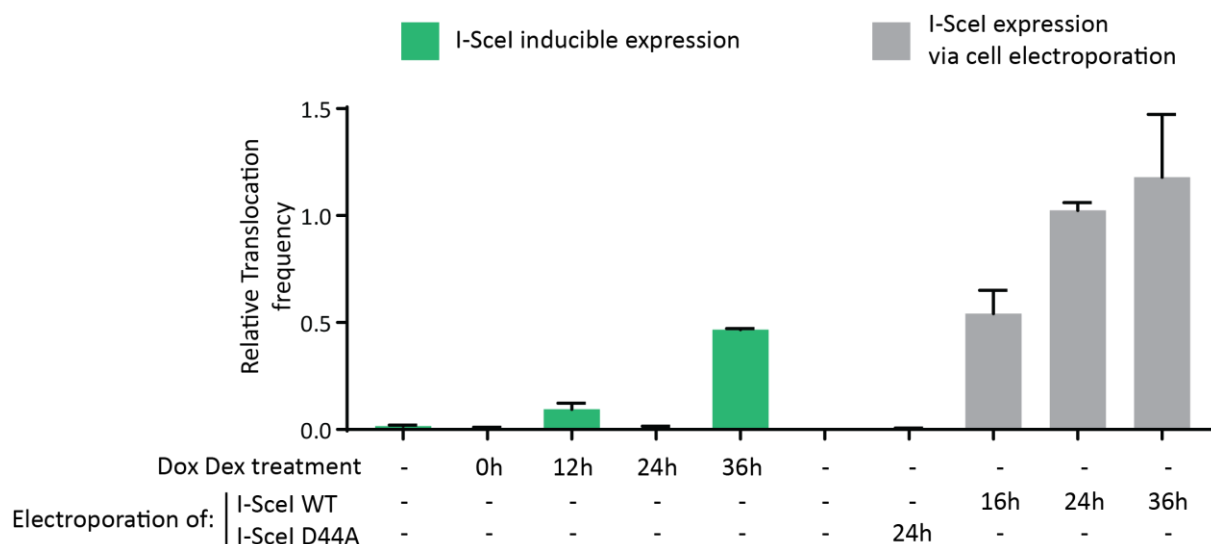


Figure 15: Comparison of two systems to induce DSBs and chromosome translocations. Induction of DSBs was triggered for at least 4h (maximum cut) and then genomic DNA was extracted immediately (time 0) or 12h, 24h and 36h (green bars). In parallel electroporation with vectors expressing I-SceI WT or catalytic dead isoform (D44A) was performed and genomic DNA extracted after 16h, 24h and 36h later (from cells with electroporation of WT isoform; DNA from cells electroporated with D44A mutant was isolated after 24h; gray bars). LacO-TetO translocations were detected by qPCR. Error bars represent standard deviations of the mean of two technical replicates.

Results

While I-SceI catalytic dead mutant (I-SceI D44A) precludes to detect any I-SceI-DSBs-induced rearrangements, cells electroporated with vector encoding for I-SceI WT accumulate chromosome translocations overtime. At each time point, higher frequencies were counted than the ones quantified using Dox- inducible system for DSBs and translocations. For instance, comparison of last collected time points, for both ways of I-SceI-DSBs induction, shows upon 2.5 fold higher recovery of chromosome translocations upon 36h of electroporation with I-SceI WT vector (10th bar) than translocations quantified 36h after the max cut of Dox- induced I-SceI (15th bar) (Figure 15 in gray color, DSBs are formed upon electroporation of I-SceI vector; in green color, DSBs are triggered via Dox-inducible I-SceI).

This suggests that, although Dox-Inducible I-SceI provokes a robust DNA damage response (53BP1 foci promptly accumulate at broken ends), likely it is still not sufficient for the formation of aberrant rearrangements.

Hence, we conclude that time and spatial control of DSBs induction via Dox-inducible expression of I-SceI is a powerful tool to study DSBs dynamics and how changes on chromatin layer influence it; however to understand the relative contribution of chromatin modifiers in translocation formations, we decided to pursue with the electroporation of a vector expressing I-SceI tagged with GFP. Fluorescent tag has allowed to sort GFP positive cells (Figure 21A) or to control the efficiency of transfection (Fig 22B), so that to enrich for a pool of cells that, uniformly, experience DSBs formation.

2.3 Local chromatin changes in the proximity of a DSB

To ascertain whether not merely HDAC1-dependent signaling, but rather changes in the acetylation status of the chromatin environment surrounding I-SceI-DSBs, do affect the formation of chromosome translocations, we decided to assess the contribution of a hyper-acetylated or hypo-acetylated chromatin domains on translocation frequency. Because, in our epigenetic inhibitors screening we have observed a decrease in chromosome translocations frequency at doses of HDACs inhibitors that trigger chromatin de-condensation, we promptly hypothesize that the formation of a hypo-acetylated chromatin domain surrounding the DNA lesions influences the propensity of those DSBs to translocate, rather than HDAC1-mediated protein-protein interactions.

2.3.1 Artificial tethering of chromatin modifiers to induce specific chromatin domains

To verify this hypothesis we sought to generate specific chromatin domains by artificial tethering of histone deacetylase and histone acetylase enzymes in proximity of I-SceI-DSBs. To assess the relative contribution of specific chromatin environments into the formation of chromosome translocations, we sought to derive cell lines overexpressing specific chromatin modifiers, starting from “Superduo” cells

Results

carrying the integration of Dox-inducible HA-DD-I-SceI-GR construct and from “Parental duo” cells carrying only the integration of Lac and Tet arrays. We took advantage of the integration of Lac Operator repeats flanking an I-SceI site to induce chromatin changes proximal to an I-SceI-DSB, by tethering chromatin modifiers as fusions with the Lac Repressor. The LacO - tethering system has been extensively used in various eukaryotic systems to drive any protein of interest to a certain locus and assess its involvement in chromosome dynamics (Belmont et al. 1999; Verschure et al. 2005; Burgess et al. 2014; Burman et al. 2015) (Fig. 16A).

Therefore, we decided to clone histone deacetylases and histone acetyltransferase in tandem with Lac repressor and mCherry coding regions and stable cell lines were derived for each of the chimeric constructs. NIH3T3 cells are fibroblasts isolated from mouse embryos; thus we decided to use mouse and the corresponding human isoforms of Histone deacetylase 1, to induce a hypo-acetylated chromatin environment; as controls, beside the tethering of the Lac Repressor alone, we thought to tether the histone acetyltransferase TIP60 to serve as counterpart to induce a hyper-acetylated chromatin domain and also a N-terminal truncated form of mHDAC1 (Figure 16B). In fact, mHDAC1 mutant, lacking of the first 50 amino acids, was previously characterized to be unable to homo-oligomerize with the endogenous mHDAC1 and other interacting proteins (HDAC2, and HDAC3), and thereby it shows reduced enzymatic activity (Taplick et al. 2001).

The expression of the abovementioned chimeric fusions is regulated, in cells, by CMV promoter and nuclear transfer of the full constructs is achieved via a SV40-nuclear localization sequence (PKKKRKV), cloned downstream the lac repressor and upstream each chromatin modifier.

Binding of the mCherry-LacR-Histone Modifiers chimeric fusions is tightly regulated by the presence of IPTG in the culture medium that in allosteric manner regulates the otherwise high affinity binding ($K_d^{\text{Lac}} \sim 10 \text{ pM}$) of the Lac Repressor to the Lac Operator (Sadler, Sasmor, and Betz 1983). Therefore, upon washout of IPTG from the culture medium, binding of mCherry-LacR-chromatin modifiers constructs to the LacO repeats was visible 12h later, thereby confirming the proper nuclear localization of the constructs.

Upon I-SceI nuclear transfer, the tethered mCherry-LacR constructs colocalized with a 53BP1 focus, as further proof of DDR-triggered by I-SceI cleavage of sites flanking LacO repeats (Figure 16C, Figure 16D). However, we did not observed an increase of colocalization between the Tip60-tethered array and 53BP1, as one can expect upon tethering of histone acetyltransferases which lead to more open chromatin configuration (Figure 16D), nor a decreased colocalization between 53BP1 and HDAC1-tethered array, which might indicate a more condensed chromatin status.

Results

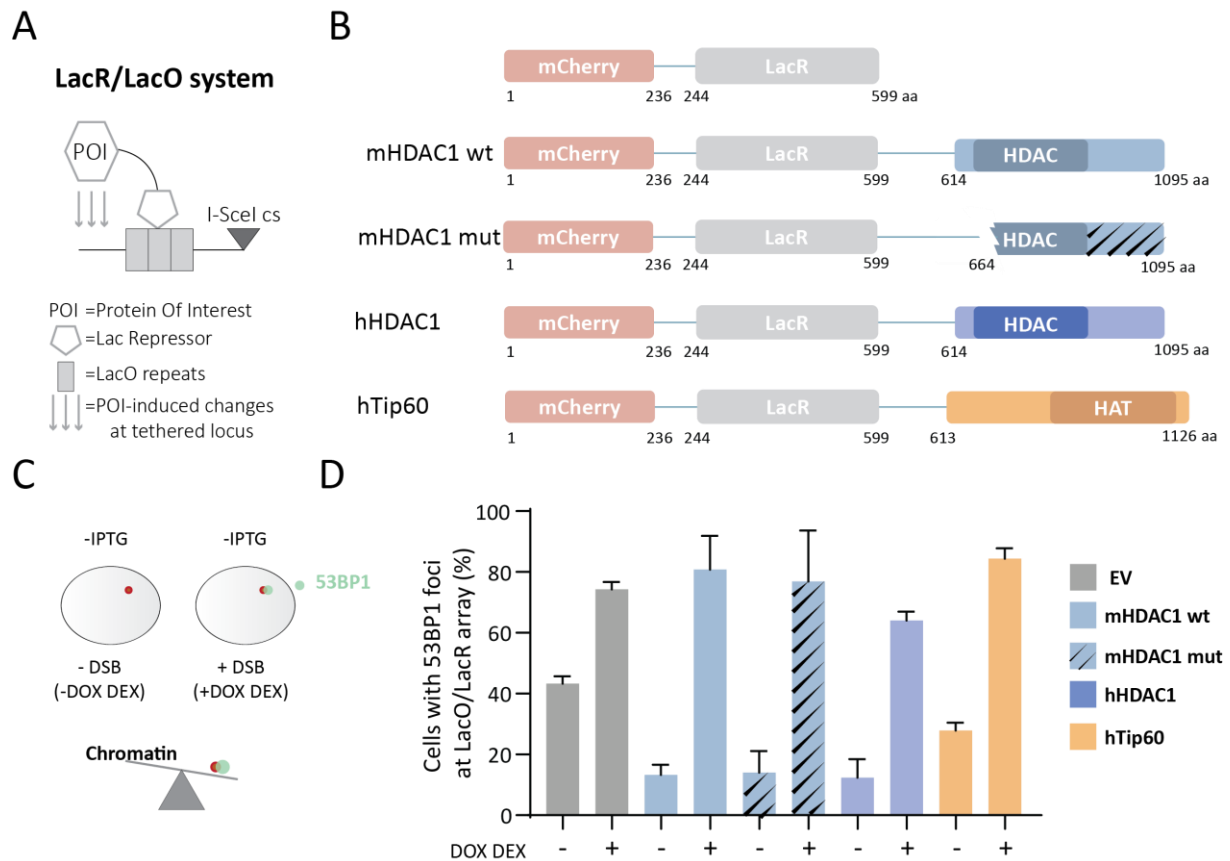


Figure 16: Artificial tethering of specific chromatin modifiers at LacO-I-SceI site. **A.** Schematic representation of how LacO/LacR tethering system operates: in absence of IPTG, chimeric fusion of protein of interest with Lac Repressor is tethered on DNA in proximity of LacO repeats because of high affinity binding of LacR for its operator locus. Arrows represent quantifiable changes induced by the tethered-protein of interest. **B.** Cartoon representing the chimeric fusion constructs (expression vectors and cell lines) generated and used to induce chromatin changes locally near an I-SceI-DSB. **C.** Upon Dox-inducible expression and Dex-mediated nuclear localization of I-SceI, 53BP1 colocalizing with LacO/LacR array in a manner dependent on the tethered chromatin modifiers. **D.** Percentage of cells with 53BP1 colocalizing with the LacO/LacR array upon 12h tethering of the respective chromatin modifiers. Assessment of more than 100 arrays per condition was performed. Error bars represent standard deviation of the mean of two independent experiments.

2.3.2 Functional validation of chromatin domains upon tethering of chromatin modifiers

For a complete characterization of the cell lines, beside the expression, the nuclear localization and the binding to the LacO repeat of each chromatin modifier construct, it was important to assess that the chimeric fusions were functional, meaning that upon artificial tethering, the changes in the surrounding chromatin environment were induced and quantifiable.

Results

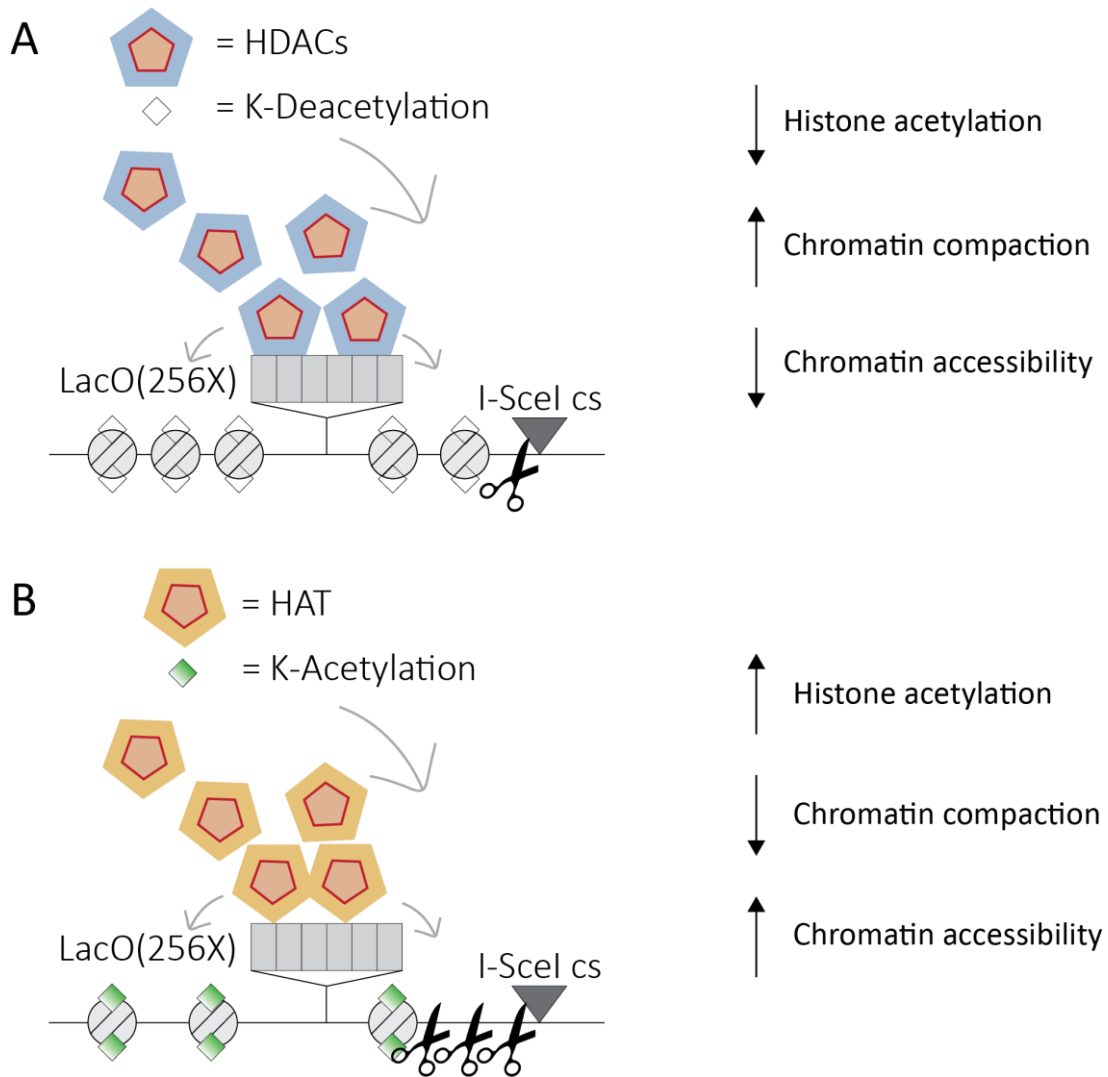


Figure 17: Chromatin changes upon tethering of histone deacetylases or histone acetyltransferases enzymes in proximity of a DSB. **A.** Functional tethering of histone deacetylases to a given locus might result in decreased acetyl marks at the level of lysine residues of H3 and H4 tails. This might lead to a more condensed locus, with the consequence of a reduced accessibility by certain factors. **B.** Functional tethering of a histone acetyltransferase enzyme leads to deposition of acetyl marks on the K-residues of histone tails. This might open up the chromatin locus to which it can follow a more accessibility by a given factor.

If a hypo-acetylated chromatin domain is induced at a given locus, one can expect a depletion of acetyl histone marks, which, then, might lead to a more condensed genomic region and thereby a decreased level of accessibility to various DNA binding proteins (Figure 17A). On the other hand, when we trigger a hyper-acetylated chromatin environment, we should be able to quantify an increased deposition of acetyl histone marks, following a chromatin relaxation of the locus, which, in this scenario, becomes more prone to the binding of various enzymes (Figure 17B). Depletion or enrichment of acetyl histone modifications (Figure 20), degree of chromatin condensation of the LacO array (Figure 18), and level of susceptibility of the locus to the activity of a given enzyme (Figure 19), are the parameters measured to assess the formation of chromatin domains upon tethering of TIP60, HDAC1 wild type and mutant isoforms (Figure 17).

Results

We decided to pursue different approaches that, directly or indirectly, could enable us to probe changes of the chromatin environment surrounding the I-SceI-induced DSB.

2.3.2.1 HDAC1-tethering causes chromatin condensation of the locus

We have already assessed that, after 12h after IPTG washout, binding of mCherry-LacR-Chromatin Modifiers to the Lac Operator occurs and it is visible as a bright nuclear spot under microscope inspection. To determine the formation of a functional chromatin domain upon tethering of the chimeric construct to the lac array, we decided to perform paraformaldehyde fixation of cells upon 16 h of tethered constructs, and quantify the size of the LacO/LacR array. The results are normalized for the area of the nucleus in order to rule out changes in the array's size due to cell progression into cycle phases characterized by double amount of DNA and thereby larger nucleus.

When the truncated form of the mouse isoform of HDAC1 binds the array, we could not observe any difference compared to a situation where the LacR alone binds the LacO repeats. However, tethering of the WT mouse or human isoform of HDAC1 shows significant reduction of the size of the Lac array compared to control conditions (tethering of the LacR construct alone) and we interpret this decrease as measure of increased chromatin compaction due to the hypo-acetylated status of the induced chromatin domain (Figure 18B).

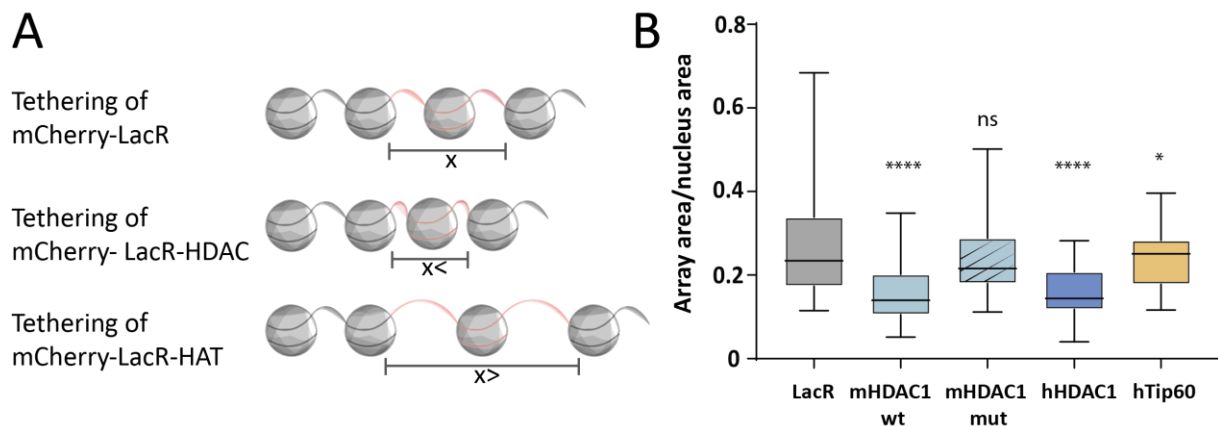


Figure 18: Artificial tethering of specific chromatin modifiers influence the status of chromatin condensation of the locus. **A.** Chromatin changes upon induction of hypo- and hyper-acetylated chromatin environments result in change in the status of compaction of the given locus. As depicted in the schematic: tethering of histone deacetylase might result in a reduction of the array size (compared to control condition), while tethering of histone acetyltransferases might lead to expansion of the LacO-LacR spot. **B.** Ratios between size of array and nuclear area were computed for 25 to 33 cells for each tethered construct. Unpaired t tests evaluate the average distribution of each condition compared to the average distribution of ratios of the control condition (mCherry-LacR): mCherry-LacR-mHDAC1 WT, P value=0.0003 (****); mCherry-LacR-mHDAC1 mut, P value=0.1522 (non-significant); mCherry-LacR-hHDAC1, P value=0.0003 (****); mCherry-LacR-hTip60, P value=0.1538 (non-significant).

2.3.2.2 Artificial tethering of HDAC1 or TIP60 does not influence the accessibility of the locus

In case of a more condensed chromatin environment, we hypothesized that also the accessibility to this chromatin region is restrained. In an opposite scenario, acute deposition of acetyl histone marks due to the tethering of histone acetyltransferase, can elicit increased binding of certain factors.

In our system, changes in the chromatin accessibility to the Lac array can be directly evaluated by ligation-mediated PCR, measuring the degree of I-SceI binding and activity to the juxtaposed genomic region, which contains sites sensitive to I-SceI endonucleolytic cleavage (Figure 19A, Figure 19B). Briefly, when I-SceI binds at LacO flanking sites, it recognizes and cuts genomic sites forming DSBs, which can be detected by ligation of a cohesive oligos adaptor coupled with quantitative PCR. In a situation where the Lac array is hypo-acetylated, the higher level of nucleosomal compaction, compared to a control condition, refrains I-SceI to bind and to generate DSBs, resulting in a poor amplification. Vice versa, due to a larger chromatin relaxation induced by histone-tails deposition of acetyl groups, I-SceI would bind more commonly increasing the frequency of DSBs, detectable as higher amplification signal in RealTime-PCR.

To test our hypothesis, we induced tethering of mCherry-LacR-chromatin modifiers constructs by washing out IPTG from the cell culture medium; then 16h later we triggered the expression and the nuclear transfer of the I-SceI by adding Dox, Dex and Shield1. Genomic DNA was extracted and ends-ligation with a compatible adaptor was tested in qPCR.

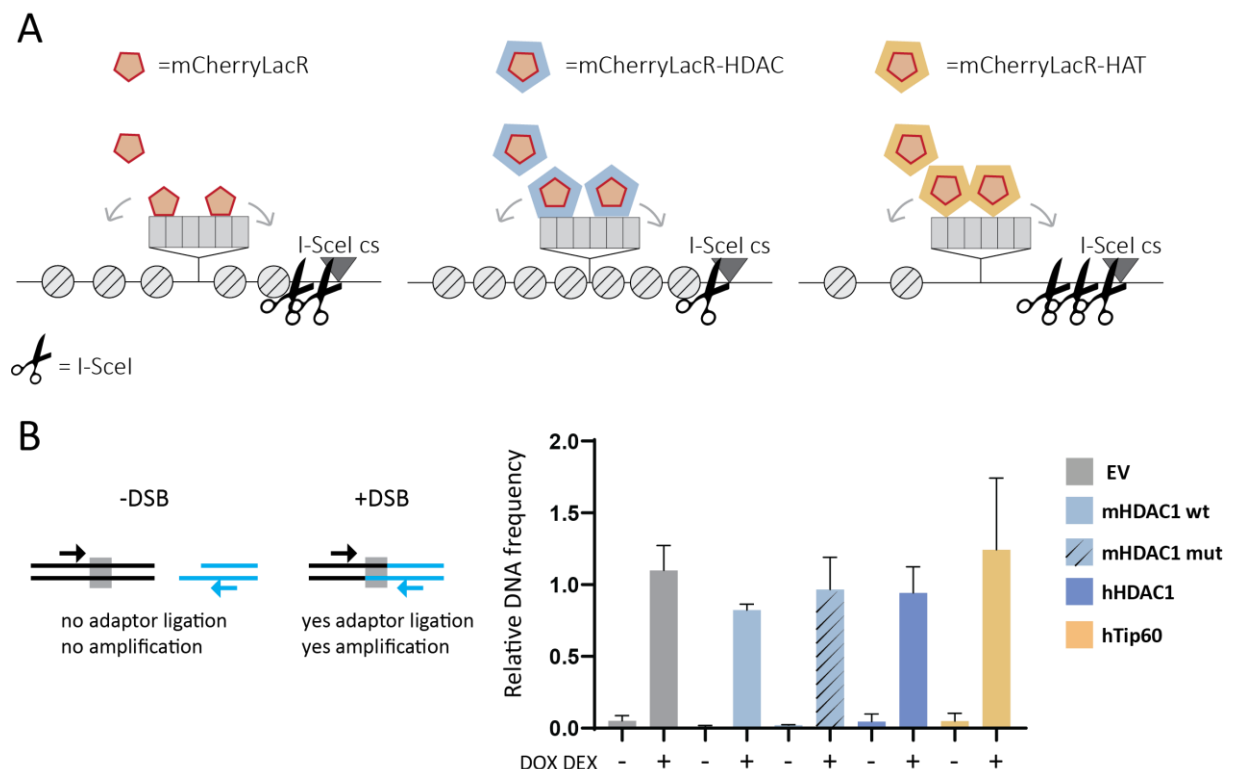


Figure 19: Artificial tethering of HDAC1 or TIP60 does not lead to difference in chromatin accessibility. A. Chromatin changes upon tethering of histone deacetylase or histone acetyltransferase might influence the accessibility of the locus by certain factors. For instance, tethering of HDAC might lead to a more condensed locus,

Results

hampering I-SceI accessibility to the locus, resulting in lower I-SceI activity (low DSBs formation). On the other hand, tethering of TIP60 might result in a more opened chromosome locus, favoring I-SceI binding and generation of DSBs. **B.** Tethering of the indicated constructs was triggered 16h before Dox-inducible induction of DSBs. Then, gndNA was extracted and LM-PCR served to quantify DSBs frequency upon ligation of an asymmetric adaptor to the broken ends, generated by I-SceI enzyme. qPCR results do not show statistical changes in locus accessibility across the various tethering of the constructs. Error bars indicate standard deviation of the mean of three biological experiments.

Firstly, we could observe that upon Dox- and Dex- treatment, we were able to enrich for specific amplicons corresponding to ligated double strands ends, compared to untreated conditions (Figure 19C). However, difference in DSBs frequency as measure of changes of the accessibility of the locus are difficult to interpret. In fact, although tethering of mHDAC1 accounts for ~20% less breaks, this difference does not pass statistical test; similarly tethering of acetyltransferase TIP60 led to an increase in chromosome accessibility not reproducible across experiments, as standard deviation of the mean indicates (Figure 19C). This negative result is in agreement with what we observed regarding colocalization rates between 53BP1 and HDAC1- or Tip60-tethered arrays (Figure 16D), upon DSBs formation via Dox- and Dex- treatments.

2.3.2.3 HDAC1 and TIP60-tethering induces depletion and enrichment of panacetylation of histone H4 (H4panAc), respectively

We decided to pursue the functional characterization of mCherryLacR-Chromatin modifiers constructs by immunofluorescence and quantification of acetyl histone marks signals specifically at Lac array sites (Figure 20A), to have a more direct esteem of the induced hypo- or hyper-acetylated chromatin domains. For this purpose, we used U2OS cells with integrated LacO-I-SceI-TetO at two genomic loci. In this cell line, the lac array is larger than the one integrated in NIH3T3 duo cells, therefore it is more suitable for screening of enrichment or depletion (*lacunas*) of specific acetyl histone marks via immunostaining of the chromatin bound fraction.

Thus, cells were electroporated with vectors expressing mCherry-LacR-Chromatin Modifiers and pre-extraction of the soluble pool was carried out prior fixation, so that we could do immunostaining only of the chromatin bound fraction. Immunofluorescence with antibodies raised against H3K56Ac, H4K12Ac, H4K16Ac and H4panAc was carried out, but only the latter one presented discernable results, while the others presented an even more diffuse background. Cells electroporated with different constructs showed all range of events, no changes in the H4pan acetylation signal, lacuna or enrichment at the LacO/LacR array; therefore we thought that differences might be outlined measuring the frequency of these events upon formation of the respective chromatin domains. Indeed, when we tethered HDAC1, mouse and human isoforms, we observed three times more *lacunas* (from 11% in control cells up to ~32% in HDAC1-tethered cells), which, instead, are not enriched upon tethering of TIP60. On the other hand,

Results

tethering of TIP60 provokes ~ threefold enrichment of H4-pan Acetylation at the array (from 8% of LacR-tethered cells to 25% in LacR-Tip60 tethered cells) (Figure 20B, Figure 20C).

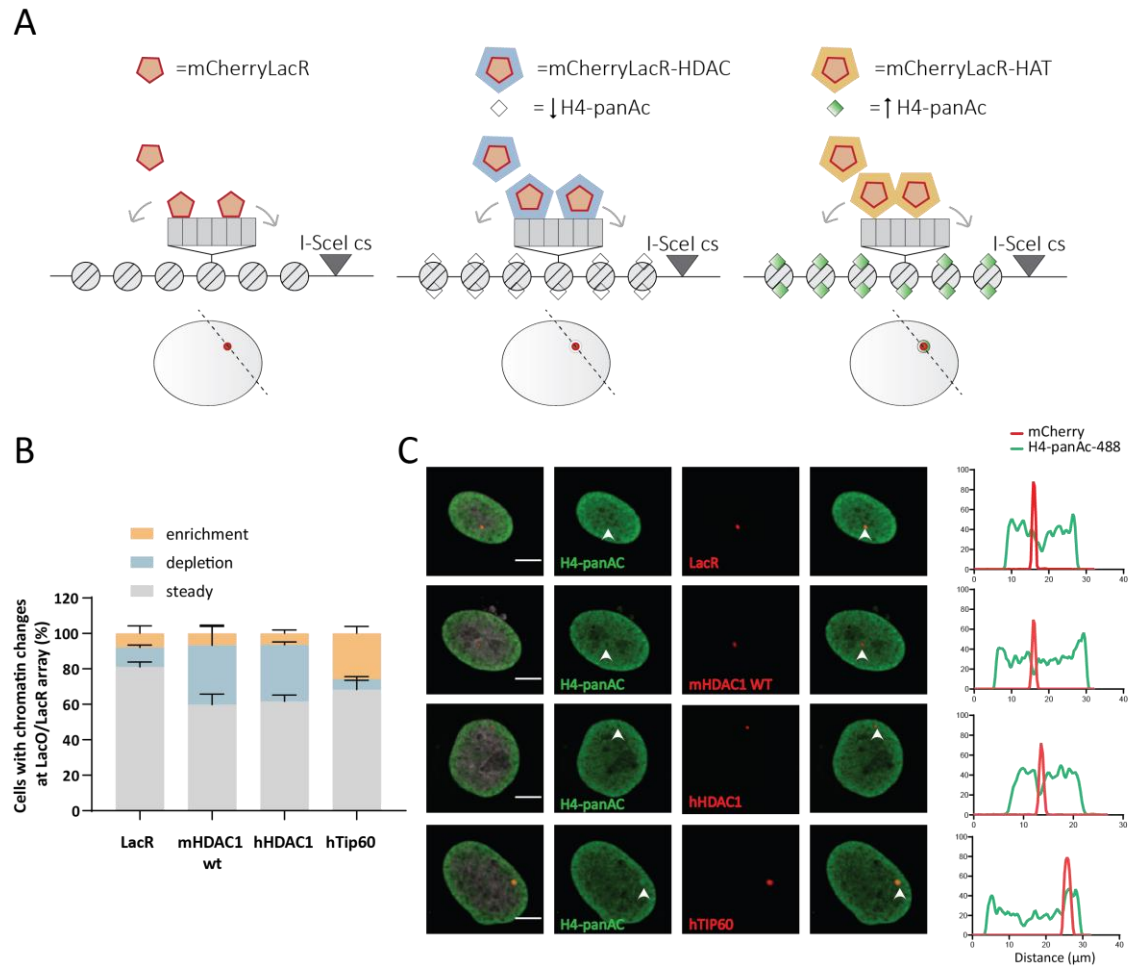


Figure 20: Artificial tethering of HDAC1 and TIP60 induce changes in H4 Acetylation levels at Lac array. **A.** At LacO/LacR array, tethering of histone deacetylase or histone acetyltransferase might induce hypo-acetylation or hyper-acetylation of the chromatin environment, respectively, compared to steady condition. **B.** U2OS cells, with double integration of LacO-I-SceI-TetO were electroporated with constructs encoding for chimeric fusions, mCherry-LacR-chromatin modifiers. After 24 hours, cytosol and nucleoplasmic fractions were washed out with CSK buffer, before fixation. Then, immunofluorescence against H4-panAc was carried out. Images analysis has revealed cells with different percentage of H4panAc enrichment, depletion or no changes (compared to background signal) at array site. Assessment of ~140 arrays in average has been carried out in two independent experiments. **C.** Example images of the scored changes for the indicated tethered constructs. To confirm, mCherry and 488-H4panAc signal were measured in a region of interest for representative images.

Overall, we have observed that tethering of histone deacetylase and histone acetyltransferase, can induce detectable changes in the acetylation of K-residues of histone tails, thereby stimulating changes in the status of condensation of the tethered locus. However, the different status of chromatin compaction presumably does not influence the accessibility of the locus itself by a given factor, as we could not detect significant differences in I-SceI cleavage.

Results

Taken together these results hint to a possible induction of chromatin domains upon tethering of the chromatin modifiers. However, it is quite relevant to consider that the induced changes in chromatin environments occur in a small fraction of cells.

Nevertheless, we decided to employ cell lines overexpressing mCherry-LacR-Chromatin Modifiers in order to tackle whether perturbation of the chromatin environment surrounding a DSB could affect its probability to pair with another broken end, forming a chromosome translocation.

To do so, we induced both local perturbation of the chromatin status, and global changes in the chromatin environment to finally dissect whether chromatin translocations are affected by changes in the acetylation apparatus of chromatin structure.

2.4 HDAC1 facilitates the formation of chromosome translocations

2.4.1 HDAC1 depletion decreases LacO-TetO translocation frequency

Members of the class I of histone deacetylases are HDAC1, HDAC2, HDAC3 and HDAC8. However, when we used a potent and specific inhibitor for HDAC8 (PCI-34051), we could not observe a decrease in chromosome translocations for any of the compound's concentrations utilized (Figure 9A). Therefore, we decided to target other components of class I HDACs by depleting the level of HDAC1, HDAC2, HDAC3 and HDAC6 (from class II HDACs), this latter we chose as negative control of chromatin - dependent modulation of chromosome translocations frequency. In fact, histone deacetylase 6 belongs to class II of HDACs, it is a microtubule-associated deacetylase, largely resident into the cytoplasm, but with capability to transit into the nucleus and thereby considered to deacetylate other cellular substrates rather than histone proteins (Bertos et al. 2004; Verdel et al. 2000; G. Li, Tian, and Zhu 2020).

To be able to deplete HDAC1, HDAC2, HDAC3 and HDAC6 with almost 100% efficacy, we carried out two reverse transfections with siRNAs, then we electroporated those cells with a vector encoding for I-SceI with GFP N-terminal tag. In order to have an unbiased relative quantification of chromosome translocations, it is preferable that cells could experience the same amount of DSBs. Thus, we decided to have cells that homogeneously express I-SceI endonuclease, by sorting only GFP positive cells and genomic DNA was extracted from this pool of cells (Figure 21A). Our result shows that the depletion of HDAC1 led to a significant decrease in the formation of chromosome translocations, which develop upon I-SceI-mediated DSBs (Figure 21C). Changes in chromosome translocation frequencies, observed upon depletion of the histone deacetylase enzymes HDAC2, HDAC3 and HDAC6 result to be not significant.

Results

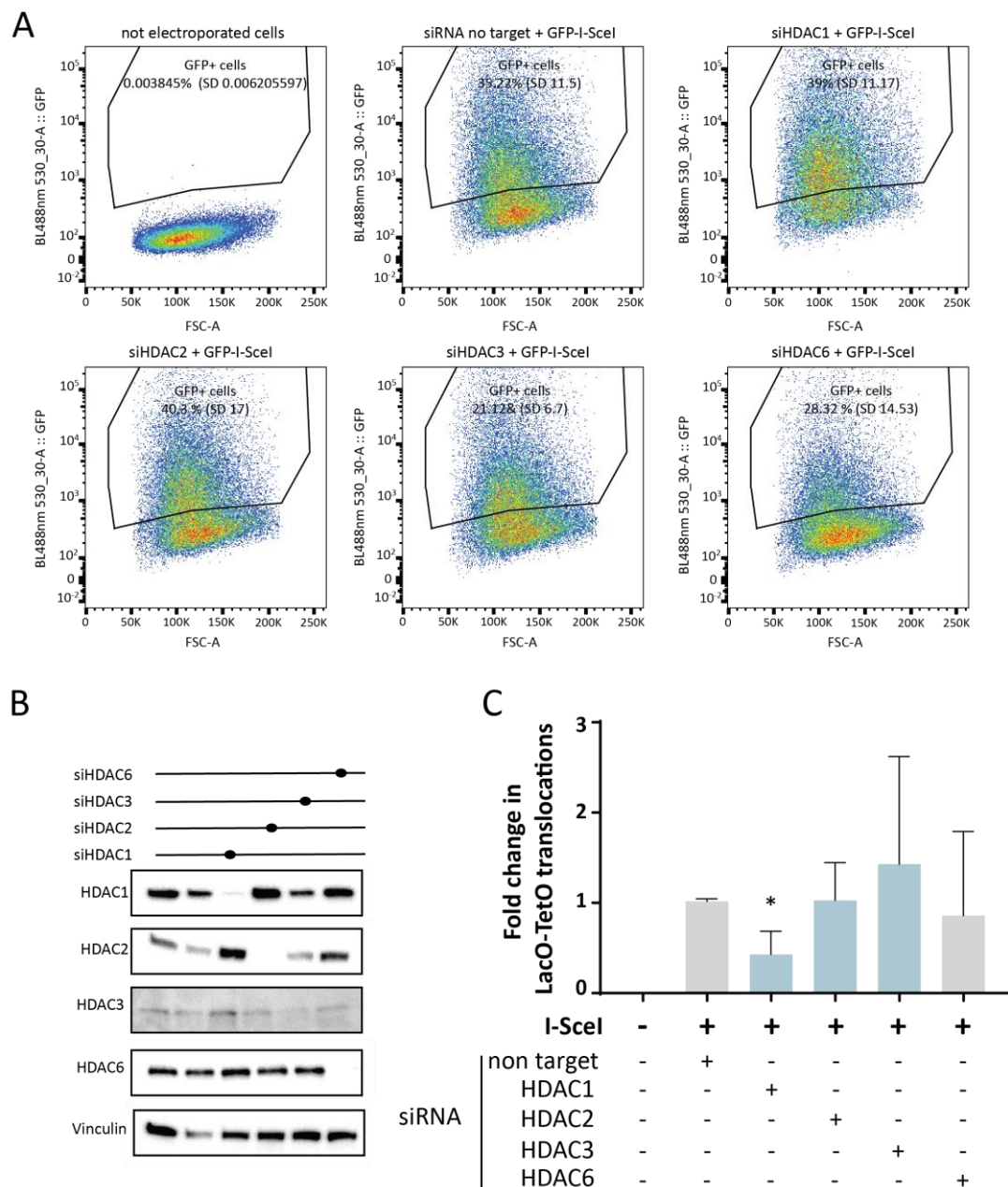


Figure 21: HDAC1 depletion significantly decreases LacO-TetO translocation frequency. **A.** Depletion of HDAC1, HDAC2, HDAC3 and HDAC6 was achieved through two cycles of reverse transfection; then NIH3T3 duo cells were electroporated with GFP-I-SceI vector and 24h later, GFP positive cells were sorted out for translocations frequency quantification assay. Percentage of GFP positive cells and (standard deviation of three independent sorting) is indicated. **B.** Efficiency of knockdown of HDAC1, HDAC2, HDAC3 and HDAC6 via on target siRNAs, was checked by Western blot analysis of total protein extract. Representative images of at least two biological experiments. **C.** Translocations frequencies were quantified by qPCR on genomic DNA extracted from sorted GFP positive cells (n=3). Star indicates statistical significance with P value= 0.02.

Noteworthy, HDAC1 and HDAC2 can work together as part of same multi protein corepressor complex that regulates epigenetics through chromatin deacetylation, ATP-dependent nucleosome remodeling and transcriptional silencing. As result of a genetic compensation mechanism, it is not surprising, and already reported (Zupkovitz et al. 2006; Lagger et al. 2002), that upon HDAC1 perturbation, HDAC2 gets

Results

stabilized (Figure 21B) and the opposite is also true: when we depleted cells of HDAC2, HDAC1 seemed to be highly retained.

Nonetheless, we conclude that HDAC1 depletion, as such, affects the formation of chromosome translocation, hinting to a possible role of HDAC1-dependent chromatin landscape, which favor the formation of chromosome translocations and that we decided to investigate.

2.4.2 Tethering of HDAC1 at DSBs increases translocation frequency

To assess how local changes in the chromatin environment surrounding the DSBs affect the formation of chromosome translocations, we checked whether the formation of chromatin domain influences chromosome translocation frequency.

When we perturbed globally HDACs levels by siRNAs, we have sorted GFP-I-SceI cells so to assess how HDACs specific changes influence chromosome translocations, starting from a pool of cells, which experienced similar levels of DSBs (Figure 21A). However, by doing so, we have noticed a quite important variation on the amount of GFP+ cells, across experiments and siRNAs conditions (see standard deviation reported on graphs in Figure 21A). Thus, we thought to optimize the electroporation of GFP-I-SceI vector in a way to obtain higher frequency of GFP + cells, 24 hours after transfection. Our goal was to reach nearly 90% of transfection efficiency to avoid cell sorting of GFP + cells. We observed that increasing amounts of GFP-I-SceI DNA led to a linear improvement in the transfection efficiency: thereby we used 20 μg of GFP-I-SceI plasmid to electroporate 1.2×10^6 cells (Figure 22A).

Then, we tethered mCherryLacR-mHDAC1 and the mutant isoform, mCherryLacR-hHDAC1, mCherryLacR-hTIP60 and the control, mCherryLacR, on the Lac Operator, for at least 16 hours. DSBs were induced via overexpression of GFP-I-SceI and GFP + cells were detected by microscope and quantified based on a threshold value of the GFP background intensity of control cells (non electroporated). We did not observe significant differences in percentage of transfected cells, among the different tethered constructs, with the exception of cells with mHDAC1 mutant tethering (Figure 22B). However, because the percentage of transfected cells was similar and above 85% for all the conditions, we decided to continue and extracted gnDNA from cells harvested at 12, 24 and 36 hours after the electroporation performed upon 16h tethering of Chromatin Modifiers. LacO-TetO translocations frequency was quantified by qPCR and values were normalized on the housekeeping gene GAPDH (Figure 22C).

In line with our data from chemical inhibition of class I HDACs and depletion of HDAC1, upon induction of an hypo-acetylated chromatin domain via tethering of wild-type human or mouse HDAC1, a DSB translocates more frequently compared to a broken locus, where the status of chromatin environment was not changed (Figure 22D, comparison between 2nd or 4th condition with the 1st condition). As expected, tethering of a mutant isoform of HDAC1 did not cause similar effect, but in

Results

this case I-SceI-DSB translocates with similar frequency as I-SceI-DSB proximal to an unmodified chromatin environment (tethering of the LacR alone, comparison between 3rd and 1st condition).

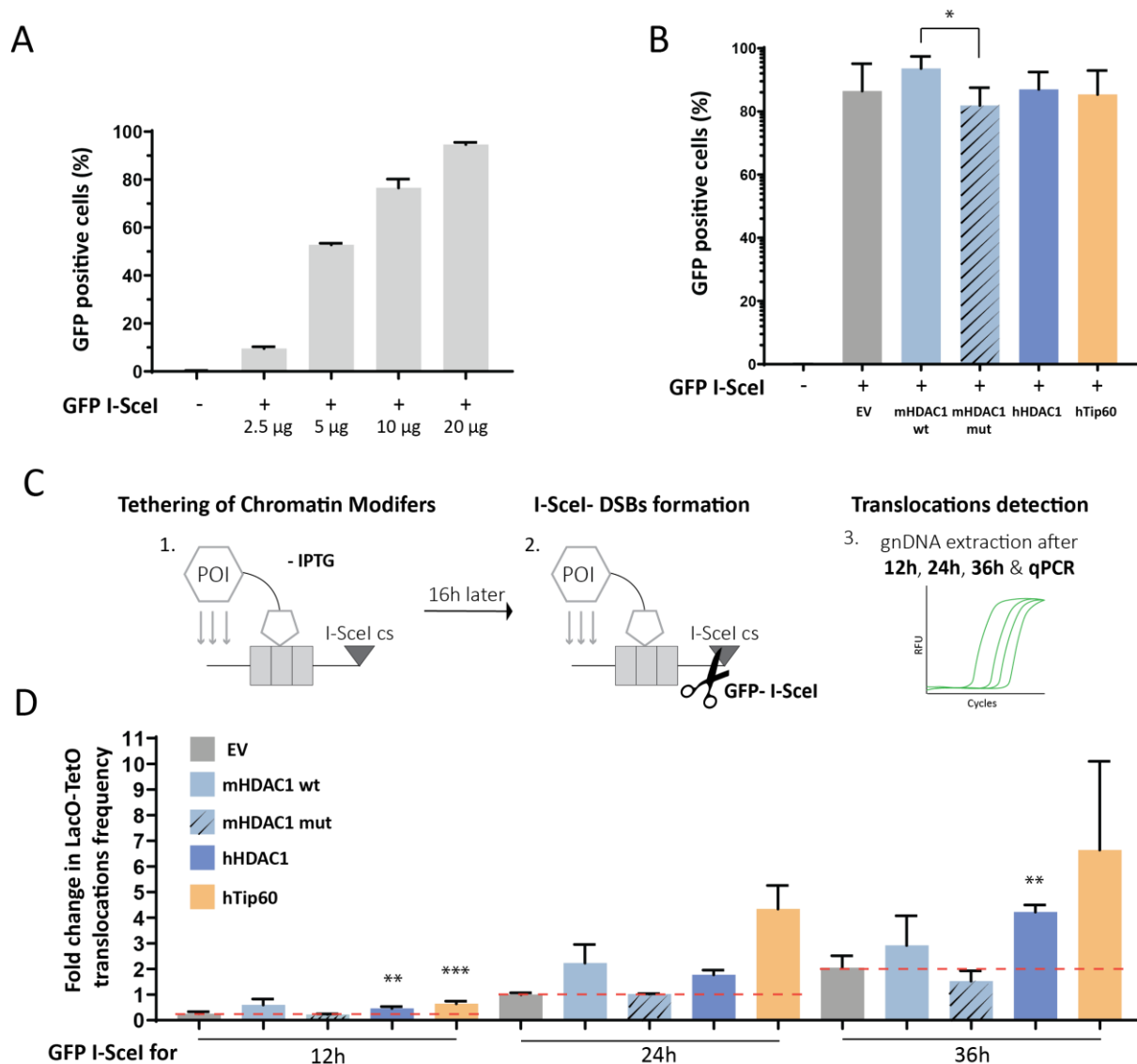


Figure 22: Induction of chromatin domains influences the formation of LacO-TetO translocations. **A.** NIH3T3 cells (1.2×10^6) were electroporated with increasing amounts of GFP-I-SceI vector as indicated in the bar plot. GFP+ nuclei were selected based on mean intensity of 488 channel higher than 600. 20 µg of GFP-I-SceI DNA was used for further analysis. Error bars represent standard deviation of the mean of technical triplicates. **B.** GFP-I-SceI was electroporated in the different cell lines and electroporation efficiency across cell lines was compared by counting GFP+ cells, as just described. Error bars represent standard deviation of the mean values of biological duplicates. No significant difference among conditions was observed with the exception of mHDAC1 WT and MUT (P value= 0.03). **C.** Artificial tethering of mCherryLacR-Chromatin modifiers was performed 16h prior I-SceI-DSBs induction, to induce chromatin changes in proximity of I-SceI cut site. At indicated time points after I-SceI electroporation cells were harvested, genomic DNA was extracted and frequency of chromosome translocations was analyzed by qPCR. **D.** Frequency of LacO-TetO translocations upon tethering of chromatin modifiers, is shown as relative difference compared to control condition (translocations detected upon tethering of LacR at 24h). Error bars represent standard deviation of 4 biological replicates. Stars indicate statistical significance in comparison with LacR control conditions (12h hHDAC1-tethered P value = 0.0027; 12h hTip60-tethered P value= 0.0005; 36h hHDAC1-tethered P value= 0.0024). Red dash lines serve to help comparison between fold change in translocations frequency compared to control conditions (translocations recovered at each time points from cells with tethering of LacR alone was triggered).

Results

Surprisingly, tethering of the histone acetyltransferase TIP60 led also to an increase in chromosome translocations, suggesting a complex involvement of histone modifiers across different steps of the translocations biogenesis. Together these data pointed out that remodeling of the chromatin environment influences the process of formation of chromosome translocations.

Because lack of HDAC1 led to a decrease in translocation frequency (Figure 21C), whereas the delivering of HDAC1 in proximity to DSBs site increases the propensity of the same DSB to translocate (Figure 22D), we conclude that HDAC1 acts as facilitator in the formation of chromosome translocations.

However, so far, we have not explored yet the mechanism underlying HDAC1-dependent effect in chromosome rearrangement.

2.5 Histone hyper-acetylation decreases DSB motility

The advantages of our system go beyond the mere quantification of DSBs and chromosome translocations, but they extend to the possibility of measuring and identifying key steps of the translocation process. We can quantify, for instance, how perturbation of the chromatin environment affects the synapsis of two broken chromosome ends or DSB dynamics, which both influence translocation frequency.

2.5.1 HDAC inhibition decreases DSB mobility

To investigate the mechanism behind the reduction in chromosome translocation upon HDAC1 perturbation, we have postulated that the formation of an hypo-acetylated chromatin environment could influence how chromatin loci explore the nuclear space, affecting, for instance, the propensity of DSBs to synapse and illegitimately join, thereby increasing the probability to form chromosome translocations. Vice versa, we expected that in absence of HDAC1, DSBs are less mobile, decreasing the space (and/or time) window of forming translocations.

In our system, I-SceI-induced DSBs can be tracked in time and space because they lie adjacent to the LacO/LacR array or the TetO/TetR array, which can be visualized by fusing the respective repressor proteins with a fluorescent reporter. For this reason, we performed time-lapse microscopy assays in the derivative cell line from “Superduo” cells, carrying mCherry-LacR overexpression. To induce perturbation of the chromatin environment we decided to inhibit class I of HDACs via TSA or SAHA treatment and follow how a DSB moves in the nuclear space compared to a condition where no perturbation of the chromatin state was triggered. We have observed that treatments with TSA and SAHA decrease the mean square displacement of a broken genomic locus (I-SceI-induced DSB), flanking the lac array (Figure 23B, left panel), while it does not affect the motion of an intact

Results

chromosome locus (Figure 23B, right panel). Importantly, we have observed that H3K56ac, H4K12ac and -K16ac are retained onto chromatin at doses of HDACs inhibitors that led to decreased DSB motion (Figure 23A), suggesting that the global accumulation of acetyl histone marks makes a DSB less mobile and potentially it reduces the propensity of a given DSB to translocate.

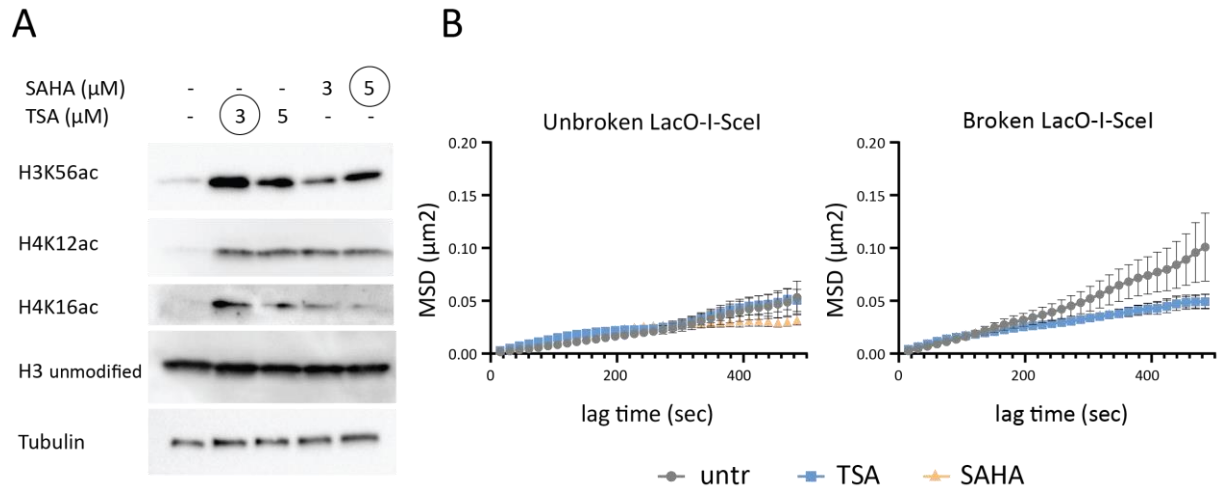


Figure 23: HDACs inhibition enhanced the motion properties of a broken LacO-I-SceI locus. **A.** Western blot inspection of the level of H3K56ac, H4K12ac and H4K16ac upon treatment with TSA or SAHA at the indicated concentrations. **B.** After 4h having induced I-SceI-DSBs, live cell imaging was carried out (33 frames with 15 sec of lag time). A region of interest was drawn around the max projection of individual cells. Rotation of cells was corrected with the stackreg Image J plugin and trackmate was used to calculate x and y coordinates of each selected spot (LacO/LacR) and mean square displacement was computed with a customized script. Plots show the mean square displacement of array from cells challenged or not with TSA, or SAHA in uncut or cut conditions (+Dox, +Dex, +Shield1). Results show the mean values of at least 30 tracks per condition from two independent experiments. Error bars indicate standard error of the mean.

2.5.2 HDAC1 depletion decreases DSB mobility

To exclude that this observation was due to a plethora of indirect effects of HDACs inhibition, we decided to dissect which histone deacetylase enzymes of class I are responsible for the reduced mobility of a broken LacO-I-SceI locus. Lack of HDAC1, upon double siRNA depletion, has shown reduced motion properties of the DSB compared to control conditions (siRNA non target, cut) (Figure 24B), suggesting that, in absence of HDAC1, constrained DSB movement might protect from the formation of chromosome translocations. In fact, a decreased mobility of DSBs well promotes a reduced propensity of DSBs to pair in a translocation junction, which we have observed in HDAC1 loss of function experiments.

A previous work provides a link between the two events by showing that DSBs with high motion properties have also high propensity to synapse and translocate (Roukos et al. 2013). Together, these observations suggest that HDAC1-induced chromatin environment, by enhancing motion properties of broken ends, might facilitate the frequency of certain DSBs to pair and translocate.

Results

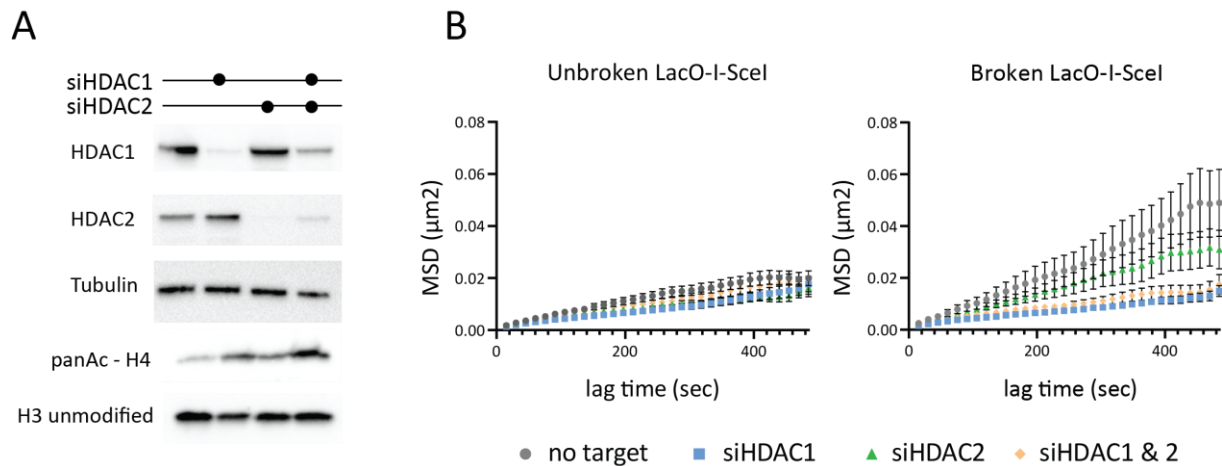


Figure 24: HDAC1 depletion enhanced the motion properties of a broken LacO-I-SceI locus. **A.** Western blot detection of HDAC1 and HDAC2 knock down upon a double reverse transfection of NIH3T3 Superduo cells and retention of H4-pan Ac, upon KD of HDAC1 and -2 functions. **B.** Experiment set up and track analysis for cells depleted of specific chromatin modifiers was computed as in Fig. 23. Plots show the mean square displacement (MSD) of intact or broken arrays (+Dox, +Dex, +Shield1) from cells carrying HDAC1 and/or HDAC2 KD. At least 35 tracks per condition were computed for two biological experiments. Errors bars show standard error of the mean.

We have observed that inhibition or depletion of HDAC1 leads to a decreased translocation frequency probably because of less mobility of DSBs, thereby the lower volume explored impairs the probability of pairing with another DSB. However, we cannot exclude that HDAC1 loss of function does not affect the nuclear volume explored by DSBs, but rather it makes the repair more effective, reducing the time during which broken chromosome ends can pair and form chromosome translocations. In other words, it is possible that HDAC1 increases either the volume explored by heterologous chromosome ends, or might provoke a defective repair process, which results in a slower DSBs repair kinetics and, thereby, in an increased time during which chromosome ends stay unrepaired and likely engage in the formation of chromosome translocations.

2.6 A hypo-acetylated chromatin environment leads to high frequency of chromosome translocations

2.6.1 Induction of DSBs in various chromatin contexts

To address this last possibility, we used a different cell based system which allow both to induce DSBs and to monitor repair events, at different genomic locations, so that to dissect how translocations frequencies are affected by the surrounding chromatin contexts where those DSBs occur.

This system is named DIvA cells, which stays for DSBs-Induced via AsiSI (Iacovoni et al. 2010; Aymard et al. 2014) and it has been developed and characterized by Gaele Legube's laboratory to induce and repair DSBs at annotated positions across the genome. In fact, DSBs are induced by AsiSI endonuclease, which potentially can cleave 1211 sites in the genome, however few hundreds of DSBs

Results

are detected with DSBs-genome wide mapping techniques, such as BLESS, BLISS or END-Seq (Clouaire et al. 2018; Iannelli et al. 2017; Canela et al. 2016).

HA-AsiSI enzyme is constitutively expressed and it resides in the cytoplasm, but because it is tagged with the nuclear domain of estrogen receptor, the enzyme can be shuttled in the nucleus when 4-Hydroxytamoxifen (4-OHT) is added to the cell culture media (Figure 25A), with a similar rationale to I-SceI-GR system, which depends on dexamethasone for the nuclear localization of the endonuclease.

When 300 nM of 4-Hydroxytamoxifen is added to the cell culture media, HA-AsiSI is transferred into nucleus and it cleaves sites, generating DSBs which start to accumulate 53BP1 and γ H2AX foci. As previously shown, we could confirm that already after 30 min of OHT treatment, AsiSI endonuclease forms DSBs that accumulate reaching a plateau in 4 hours (Figure 25B, Figure 25C).

Results

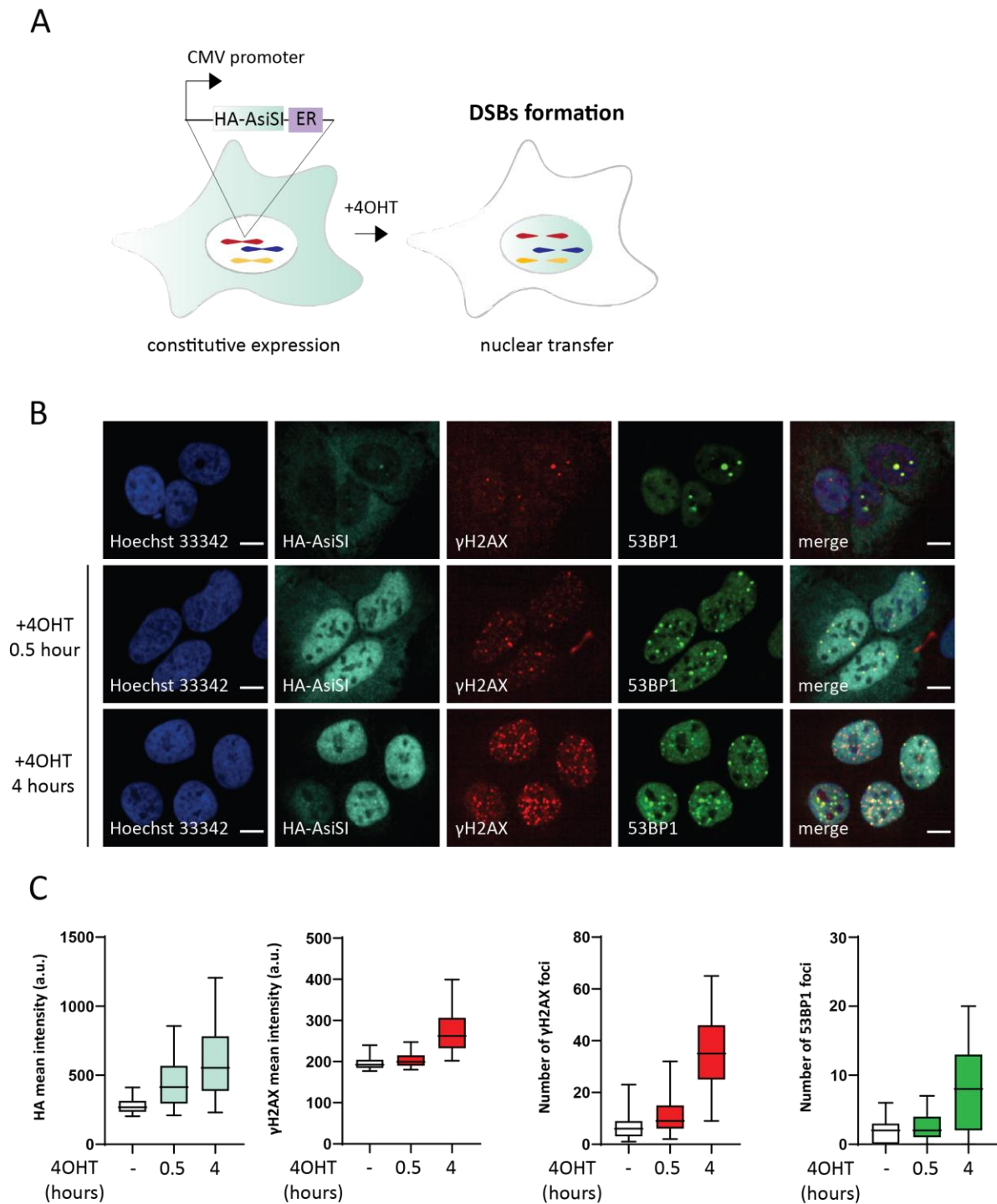


Figure 25: Controlled induction of AsiSI-DSBs. **A.** HA-AsiSI-ER expression is controlled by CMV promoter and it is anchored in the cytoplasm in absence of the steroid ligand. When 4-OHT is added to the cells, conformational changes induce nuclear transfer of the endonuclease, which can now cleave AsiSI sites, generating DSBs **B.** Example images of 30 minutes and 4 hours treatment with 300 nM of OHT. Scale bar indicates 10 μ m. HA-AsiSI, 53BP1 foci and γ H2AX foci accumulate overtime in the cell nucleus. **C.** Quantification of HA intensity, intensity and number of foci per nucleus of γ H2AX and 53BP1 are shown for more than 3000 nuclei.

2.6.2 Repair of DSBs in various chromatin contexts

A variant of this system consists of HA-AsiSI-ER in frame with an auxin-inducible degron; this version makes the tool suitable not only for DSBs induction (and monitoring of translocations formations), but also to study AsiSI-DSBs repair and how this process might be affected by various genomic and chromatin contexts (Aymard et al. 2014). Adding indole-3-acetic acid (IAA, commonly known as auxin) to the cell culture media at the final concentration of 500ng/ μ l leads to AsiSI degradation and repair of DSBs (Figure 26A), within 2 hours.

We confirmed the functionality of the auxin responsive tag and in the context of treatments with DNAPKI and DNA methyltransferases inhibitors that we used, respectively, as positive and negative controls in a screen for epigenetic modulators of AsiSI translocations (not shown here). Specifically, we used NU7441 (5 μ M) to inhibit DNAPK and decitabine (2 μ M), a cytosine analog used as demethylating agent in myelodysplastic syndrome and acute myeloid leukemia (Fenaux 2005; Gore 2005; Flotho et al. 2009).

The choice to use a hypo-methylating agent, such as decitabine, to negatively screen for reduction of AsiSI-DSBs and AsiSI-induced translocations might be surprising because AsiSI enzyme is sensitive to methylated cytosine, therefore using a DNMT inhibitors should enrich hypo-methylated DNA template and presumably exacerbates AsiSI endonucleolytic activity. Paradoxically, we have observed that when cells were pretreated with decitabine, levels of DSBs induction were not increased, instead, we quantified a reduction of γ H2AX foci, independent of the nuclear level of HA-AsiSI enzyme, which was comparable to control condition (cells treated with only 4-OHT) (Figure 26B, Figure 26C).

Upon IAA treatment, γ H2AX levels were restored to background levels, with exception of cells pretreated with NU7441, which do not show reduction of γ H2AX, after 2 hour degradation of AsiSI enzyme (Figure 26B, Figure 26C). Indeed, inhibition of DNAPK has been shown both to delay repair of DSBs lesions, evoking a persistence DNA damage response, and to increase I-SceI induced chromosome translocations frequency (Lu et al. 2019; Roukos et al. 2013; Soutoglou et al. 2007).

Results

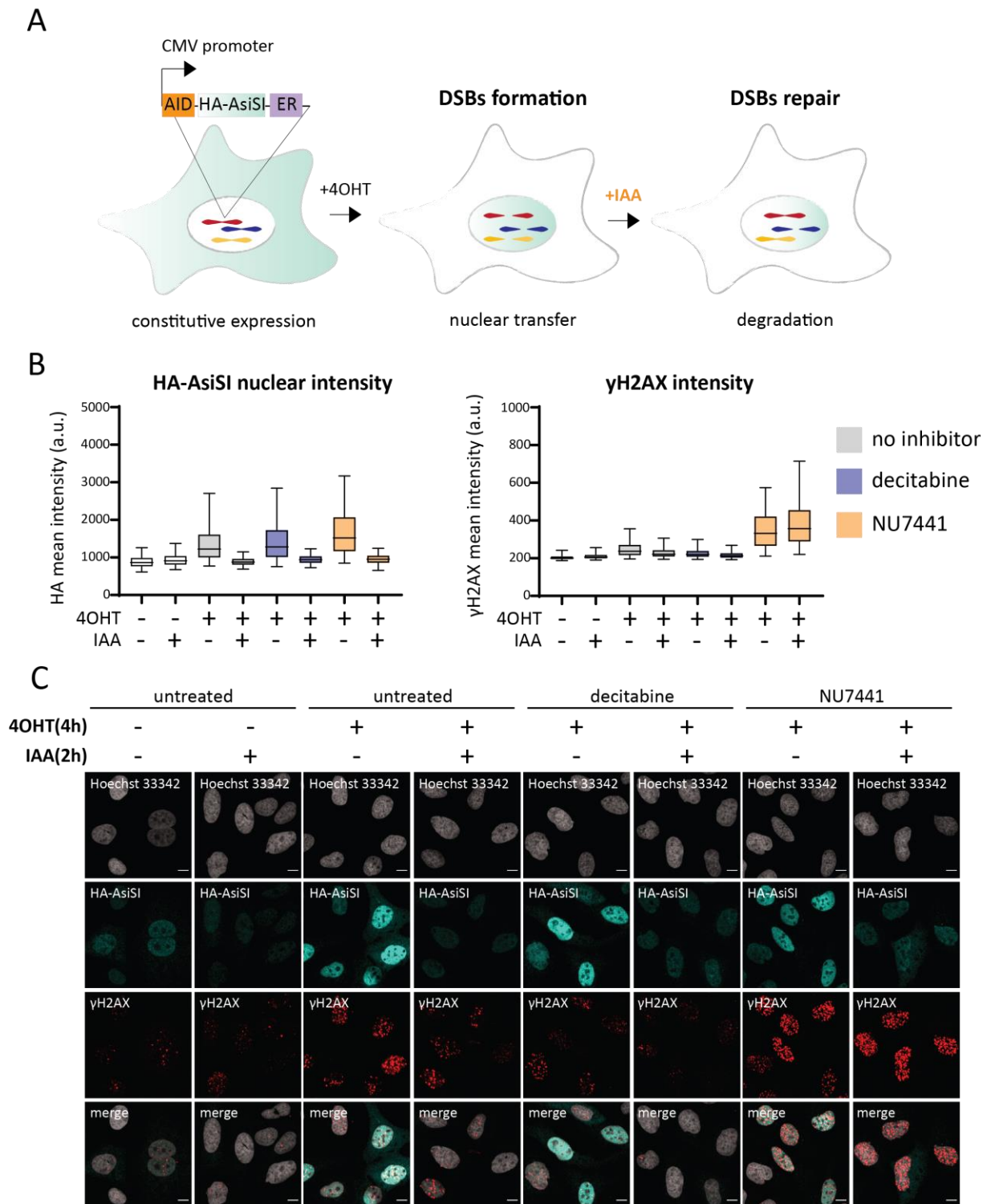


Figure 26: AsiSI-induced γ H2AX is reduced upon decitabine treatment, while DNAPKi delays γ H2AX restoration. **A.** An auxin-inducible degron controls degradation of AsiSI enzyme and allows to study repair of AsiSI-DSBs. **B.** Nuclear background levels of AsiSI enzyme are reached 2 hours upon auxin-induced degradation (500 ng/ μ l). Also γ H2AX foci are resolved, indicating repair of cleaved sites. Cells pretreated with decitabine (2 μ M) fail to trigger AsiSI-induced γ H2AX foci after six hours of 4-OHT treatment. Two hours after inducing degradation of DSBs forming agent, cells pretreated with DNAPK inhibitor (5 μ M) showed persistent phosphorylation of H2AX. Decitabine and NU7441 will serve as negative and positive controls of AsiSI-DSBs formation and AsiSI induced chromosomal translocations. **C.** Example images of cells pretreated or not with

Results

decitabine and DNAPKi, challenged or not with 4-OHT for 6 hours and treated or not for 2 hours with IAA. Scale bar indicates 10 μm .

2.6.3 Decitabine and NU7441 treatments are used as controls to screen for suppressors or enhancers of AsiSI-induced genome instability

To rule out that the low induction of AsiSI-triggered DDR observed upon decitabine treatment was due to a delay in AsiSI cleavage activity, due to increased cytosine methylation, we have monitored the accumulation of γH2AX foci at later time point of 4-OHT treatment. In this time course, we included 5-azacytidine, used also as DNMT inhibitor, to check whether we could achieve similar effect (Figure 27). While decitabine treatment precludes the formation of γH2AX foci also at later time points, we have observed that 5-aza treatment (2 μM final) provokes a small delay in DDR signaling only after 4 hours. At later time points, 5-azacytidine triggers higher accumulation of AsiSI-DSBs compared to cells challenged only with 4-OHT, suggesting more susceptibility to AsiSI-breakage of increased hypomethylated DNA templates.

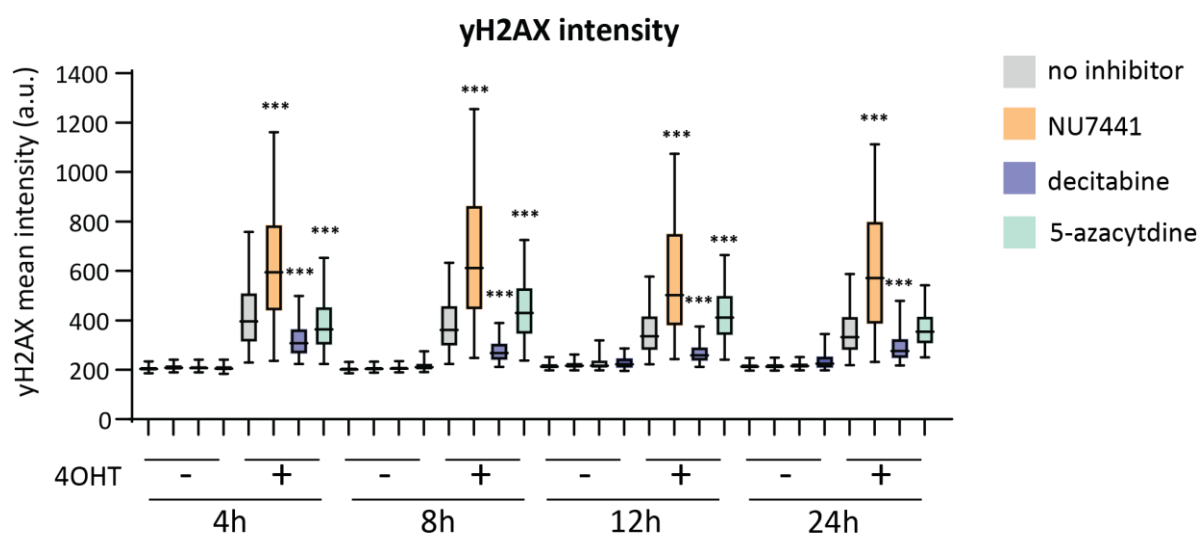


Figure 27: Decitabine blocks formation of γH2AX foci also upon 24 hours of persistent AsiSI expression. DIvA cells were pretreated with the indicated inhibitors for 1 hour, then 300 nM of 4-OHT was added to the cell culture media and incubated for the indicated times. Cells were then fixed and stained with an antibody raised against Ser139-P of H2AX. At least 2000 nuclei were analysed. Stars indicate statistical significance (*** P value <0.001 ; **** P value <0.0001).

2.6.4 Modelling of AsiSI – induced breakage and translocations by C-Fusion 3D upon decitabine or NU7441 treatment

The previous data merely indicate that decitabine and NU7441 affect the signaling of AsiSI-DSBs, in fact quantification of γH2AX foci provides information on modulation of AsiSI-dependent DNA

Results

damage response, induced by the above mentioned drugs. To confirm their influence in the actual formation of DSBs and their impact on translocations, we decided to use a method, developed in our lab, which combines labelling of genomic regions with fluorescence *in situ* hybridization technique (FISH), together with high-content microscopy and automated image analysis to detect chromosome breakage and chromosome translocations (Minneker et al., in preparation).

The method detects breaks and chromosome rearrangements, by probing two different genomic loci with 3 or 4 colored FISH probes and by measuring the Euclidean distances among the fluorescent probes (detectable microscopically as spots). Specifically two genomic regions whose translocation frequency (in this case two AsiSI loci) we are interested in calculating, are labelled with Green (488-dUTP labelled) and Red (568-dUTP labelled) probes, flanking one AsiSI site, whereas the second region is detected with FarRed (647- dUTP labelled) and Blue (405- dUTP labelled) probes, flanking the 2nd AsiSI site (Figure 28B). A chromosome break is defined when Green and Red probes are spatially separated with a distance higher than the background distance computed in the 99% of unchallenged cells. Definition of chromosome translocations satisfies more criteria: Green and Red spots distance is above the threshold, FarRed and Blue probes (used to probe a second genomic region) are also separated, and Green and FarRed spots lie in a distance lower than the given threshold, indicating spatial juxtaposition of the translocating partner loci.

When we induce AsiSI nuclear transfer for 24 hours, we observe that 2 μ M of decitabine significantly blocks the formation of AsiSI-DSBs at two different AsiSI sites and thereby prevents the formation of translocations with AsiSI site located at *mis12*. On the other hand, DNAPK inhibition leads to high frequency of broken chromosomes, increasing the possibility to form translocations (Figure 28C and Figure 28D).

To confirm relative frequencies of breakage among treatments, we decided to run a qPCR on an AsiSI site located in proximity of *mis12* locus: in case of a cleaved AsiSI sites, one can expect a futile PCR amplification; vice versa an intact locus will provide a productive amplification by primers flanking the AsiSI site. By doing so, we validated that in condition of 4-OHT-induced DSBs, the treatment with NU7441 led to a lower amplification compared to control (cells challenged only with 4-OHT), reminiscent of a higher frequency of broken DNA molecules. In line with our FISH-based results and γ H2AX foci staining, decitabine treatment reduces DSBs occurrence, as no amplification difference compared to an intact locus was detected (Figure 28A).

Results

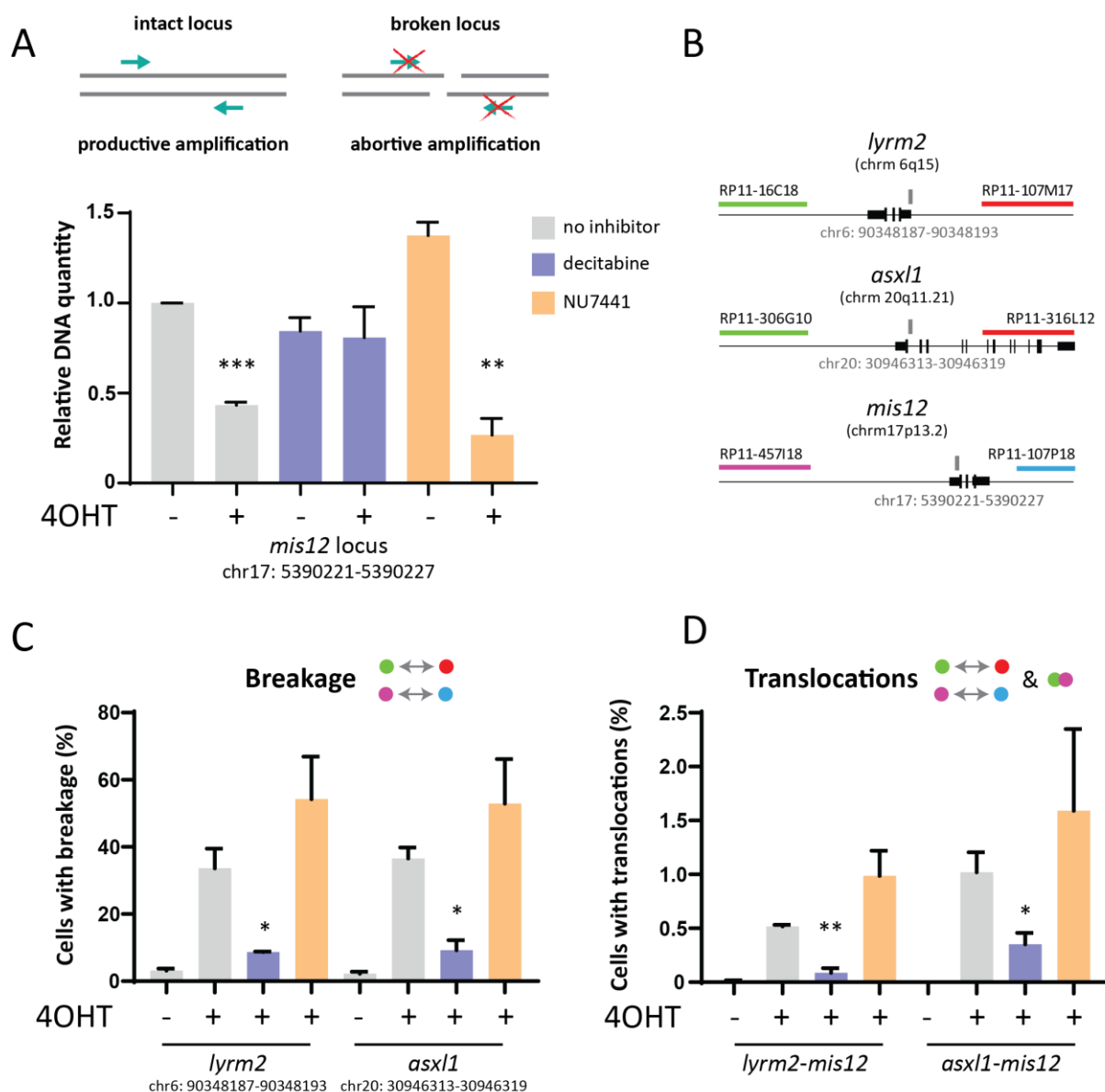


Figure 28: Decitabine blocks AsiSI-DSBs and AsiSI induced translocations. **A.** DiVa cells were pretreated with the indicated inhibitors for 1 hour, then 300 nM of 4-OHT was added to the cell culture media and cells were incubated for 24 hours. gDNA was extracted and qPCR using primers flanking an AsiSI at *mis12* (chr17: 5390221-5390227, in hg19 reference genome) was performed and normalized on *gapdh*. Fold differences relative to the amplification of an intact locus in control conditions (no inhibitor, no 4-OHT treatment) are calculated and shown, together with standard deviations of the mean of two biological experiments. Differences were analysed with unpaired t test and stars indicate P value=0.0004 (no inhibitor, plus 4-OHT; compared to no inhibitor, minus 4-OHT) and P value=0.0056 (plus NU7441, plus 4-OHT; compared to plus NU7441, minus 4-OHT). **B.** Schematic of FISH probes used in the following experiment. Breakage was computed as separation of Green and Red spot, used to probe a same locus; translocations were defined when breakage occurred and Green spot (probing the centromeric regions of the indicated loci) was in spatial vicinity with FarRed probe used to detect the telomeric region of *mis12* locus. **C.** Cells harboring AsiSi breaks were computed for having: 1) same Green and Red spot number per nucleus (Green=Red=2 for *lyrm2* locus; Green=Red=3 for *asx1* locus) and 2) Green-Red spots pair distances above threshold were defined according to default distances in 99% of unchallenged cells. The threshold value depends on the probe pairs used (threshold >1.25 for *lym2* locus and threshold >1.6 for *asx1* locus). DSBs in decitabine treated cells are significantly decreased in comparison with DSBs in cells challenged only with 4-OHT (*lyrm2*, P value=0.0271; *asx1*, P value=0.0128) **D.** Cells with translocations were selected in agreement with previous criteria and including the following filter: Green-FarRed spots pair distances are lower than threshold values. Chromosome translocations in decitabine treated cells are significantly decreased compared to translocations in cells challenged only with 4-OHT (*lyrm2*, P value=0.0059; *asx1*, P value=0.0048). At least 4000

Results

cells per condition were analyzed and error bars indicate standard deviation of the mean of two independent experiments.

Altogether, these data show that decitabine and NU7441 treatments, coupled with HT-FISH methodology, can be successfully employed to screen for decrease and increase of AsiSI-DSBs and AsiSI-induced translocations.

Importantly, we demonstrated that the DIvA cell line is a feasible system to model chromosome breakage and chromosome translocations. However, how changes in the acetylation status of chromatin environment surrounding an AsiSI-DSBs influence its propensity to translocate remain to be fully understood.

2.6.5 Chromosome translocations occur preferentially at sites with hypo-acetylated histones upon the formation of DSBs

Our data indicate that in absence of HDAC1, acetylation marks are retained onto chromatin and that DSB mobility is impaired and LacO-TetO translocations are decreased (Figure 21C, and Figure 24B). Therefore, we decided to use DIvA system to induce DSBs in different context of hyper-acetylated or hypo-acetylated chromatin and observe how these impact formation of AsiSI-DSBs and translocations. Recently, Legube's laboratory has mapped changes in the chromatin landscape upon formation of DSBs (Clouaire et al. 2018). To select AsiSI cleaved sites, they focused on a set of 80 DSBs defined by BLESS, which were significantly detected upon 4-OHT treatment (high read count in 1 Kbp window). Then, they performed CHIP-seq analysis for 20 histone marks, including histone variants, post-translation histone modifications, linker and core histone, providing a snapshot of the undamaged and damaged chromatin after 4 hours treatment of 4-OHT.

Among those markers, it was carried out genome wide profiling of acetylation on K56 of histone H3 and K12 and K16 of histone H4 that are erased from chromatin in HDAC1 and HDAC2-dependent manner. In the analyzed base pair window of +/- 500 bp from the cleavage site, DSBs formation did not provoke significant enrichment or depletion at AsiSI sites, at least at population level (Figure 29A). Yet, analyzing DSBs-induced acetylation changes at individual AsiSI sites, we have observed all possible scenarios. In fact, upon formation of DSBs, some sites did not show any changes in histone acetylation levels, whereas other sites showed high depletion or enrichment in all of the three acetyl marks analyzed, or even combination of such chromatin changes (Figure 29C, Figure 29D).

Results

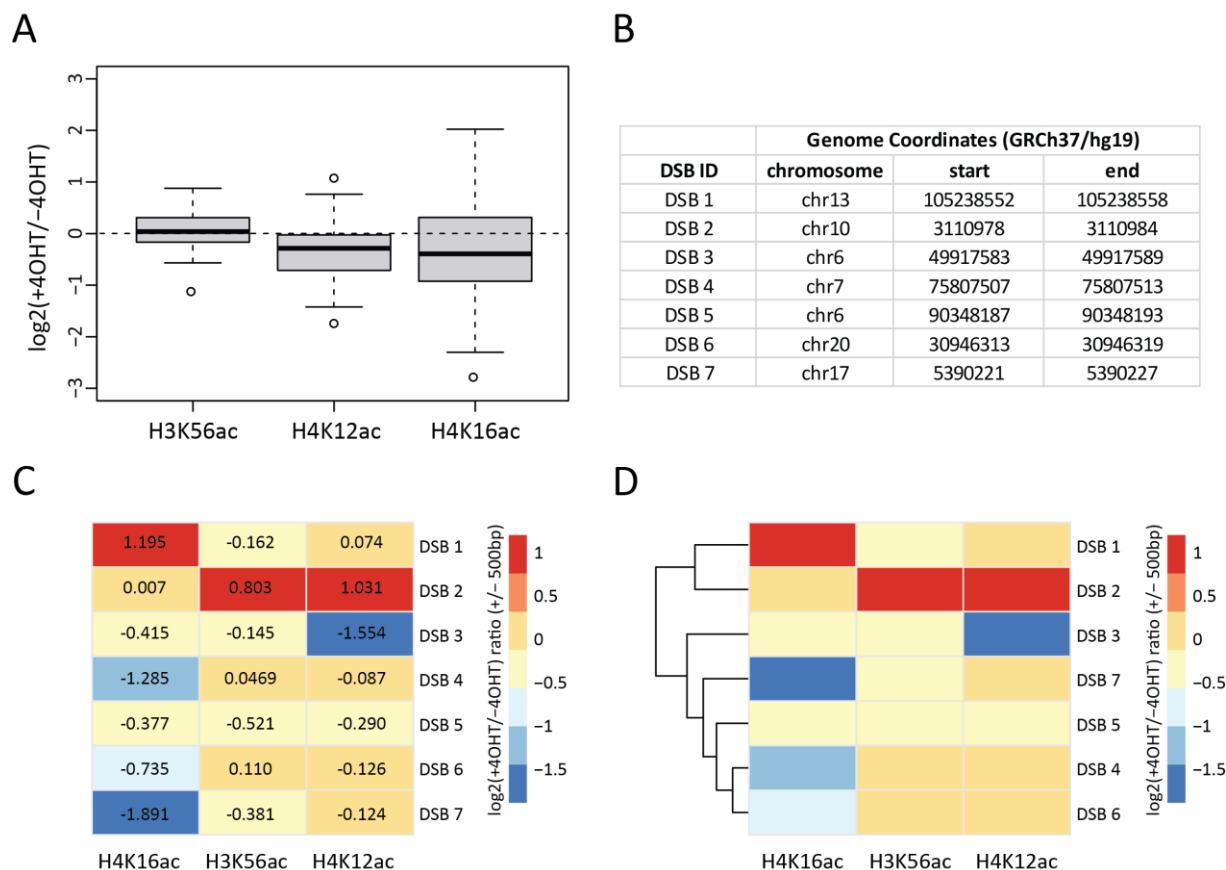


Figure 29: DSBs-induced changes of H3K56ac, H4K12ac and H4K16ac over 1 Kbp window around DSBs. **A.** Box plot represents H3K56ac, H4K12ac and H4K16ac signal ratio (expressed as \log_2) between damaged (+4-OHT) and undamaged (-4-OHT) chromatin for 80 cleaved AsiSI sites, selected by BLESS analysis; analyzed base pair window of 1 Kbp centered on AsiSI cut site. No significant changes were observed upon DSBs for the indicated acetyl histone marks. **B.** Genome coordinates of AsiSI sites analyzed in translocations-capture assay, to assess how breakage and translocations frequencies correlate with changes in the acetylation status of the chromatin environment. **C.** Heatmap shows \log_2 ratio between +4-OHT and -4-OHT treated chromatin for the indicated acetyl histone marks at selected DSBs, in 1 Kbp window. Values of enrichment or depletion are reported. **D.** Same heatmap as in C, but DSBs are clustered based on the average of the \log_2 ratios of the analyzed chromatin changes.

By knowing the status of acetylation of each AsiSI sites, specifically whether they become hypo-acetylated or hyper-acetylated upon DSB formation, we asked how such DSB-induced changes in the acetylation status of the surrounding chromatin, do influence the probability of those loci to form chromosome translocations.

For this purpose, we chose an AsiSI site which serves as constant translocation partner (DSB7 on chr7p13.2, chr17:5390221-5390227, hg19) and assessed the frequency of translocations of other AsiSI sites, featuring different levels in acetylation at H3K56, H4K12 and -K16. Thus, we used the aforementioned FISH-based tool to detect chromosome breakage and translocations after 24h stimulation of AsiSI-nuclear transfer.

Results

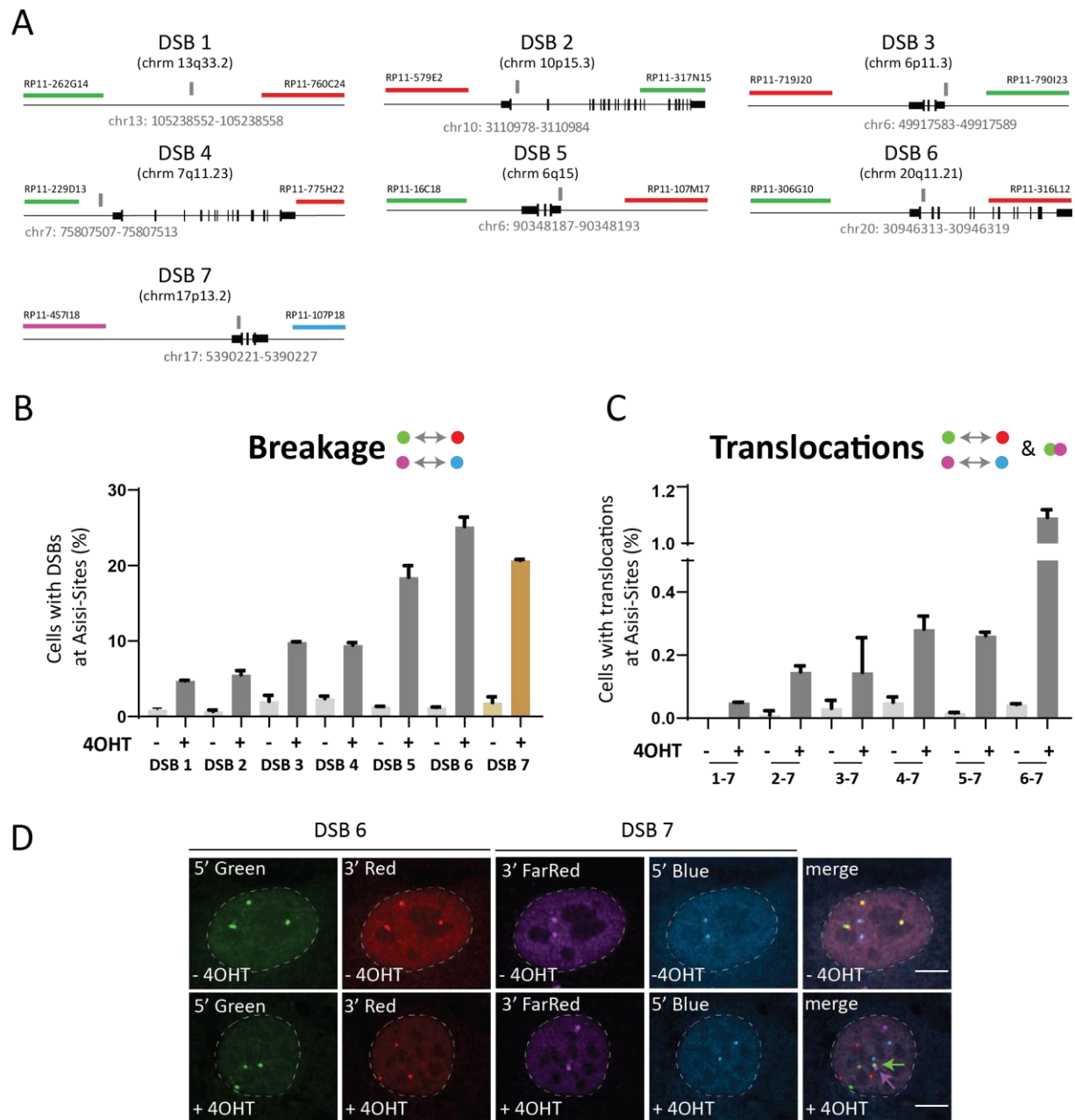


Figure 30: Asisi-induced chromosome breaks and translocations are more frequent at sites, which lose H4K16ac upon DSB formation. **A.** Schematic design of FISH probes labelling DSBs, used to study the dependency of Asisi-induced translocations with changes in acetylation upon DSBs formation. BAC probes are labelled in “Green” by 488-labelled dUTPs, in “Red” by 568-labelled dUTPs, in “FarRed” by 647-labelled dUTPs and in “Blue” by 405-labelled dUTPs. Asisi site at *mis12* is marked by FarRed and Blue probes and it is used as constant translocation partner. **B.** Cells harboring chromosome breakage are defined to have Green-Red spot pair distances (or FarRed-Blue spot pair distances) above a threshold given by the default spot pair distances computed in 99% of unchallenged cells. **C.** Cells harboring a translocation junction are selected by having breakage in both loci and Green-FarRed spot pair distances below the previously defined threshold. At least 5000 nuclei per condition have been analysed per biological replicate (n=2). **D.** Representative images of nuclei having intact loci (-4-OHT) or broken and translocating loci (+4-OHT). Example comes from loci referred as DSB#6 and DSB#7.

We have noticed that breakage and translocations accumulate with higher frequency at sites with DSB-induced loss of acetyl histone marks (this observation is more striking especially for H4K16), suggesting an inverse dependency on the status of acetylation and the frequency of chromosome translocations

Results

(Figure 30). In fact, it seems that translocations (Figure 30C) highly occur at sites which become deacetylated upon DSBs (Figure 29C), hinting to a protective role of chromatin acetylation in preventing the formation of these rearrangements. This observation is in agreement with our previous result showing a decreased translocation frequency in HDAC1 loss of function experiments. However, whether the hypo-acetylation observed at certain AsiSI-DSBs is due to the mere deacetylase activity of HDAC1 or due to the synergistic function of HDAC1 and HDAC2 remain to be explored, as well as the link between high frequency of translocations and deacetylation of the chromatin environment where those chromosome rearrangements occur.

2.6.5.1 Fast and slow repair rates of DSBs do not correlate with difference in acetyl histone marks

According to our previous data of mobility of a broken LacO-I-SceI locus in absence of inhibition of HDAC1, depletion in H4K16 acetylation might enhance the mobility of DSB, increasing the risk of engaging a translocating partner. The possibility that DSBs with hypo-acetylated histones in their vicinity explore a larger volume does not exclude another scenario where DSBs are slowly (or poorly) repaired in hypo-acetylated chromatin, thereby increasing the chances for an unfaithful joining with a heterologous DSB.

To assess whether differences in the acetylation status of chromatin and differences in the frequency of translocations might be caused by differential repair rates of those DSBs, we made use of some data generated by another PhD student in the lab, who is interested in dissecting how 3D genome organization, chromatin and genomic contexts might influence the repair kinetics of DSBs induced via various means; to start, he has employed AsiSI-degron system to induce AsiSI-DSBs and followed their repair by sBLISS technique (Bouwman et al. 2020). Through an *in situ* ligation reaction and sequencing, this method allows capturing DSBs genome wide. AsiSI-degron cells allow induction of DSB and monitoring of repair events by adding auxin to the cell culture media, triggering TIR1-mediated degradation of the tagged enzyme, as also showed in Figure 26A. We have monitored degradation of AsiSI enzyme and repair of AsiSI-DSBs in a time course experiments where samples were collected after 0', 15', 30', 60' and 120' with 500ng/μl of auxin treatment.

A previous model has described a biphasic behavior of the repair of IR-induced DSBs and, thereby, has identified a fast and slow components (Metzger and Iliakis 1991; H. Wang et al. 2001). In agreement with this model, by calculating the residual fraction of AsiSI-DSBs at given time points, we have noticed that after 30 min, only 25% of fast repair DSBs remain unrepaired, whereas 50% of the slow repaired AsiSI sites are already resealed.

The observed clearance of AsiSI-DSBs suggests a type of repair that well fits the proposed model, allowing us to cluster three groups of AsiSI sites undergoing a “fast” repair, or a “slow” repair and some other which have shown intermediate characteristics.

Results

We wondered whether these differences in the repair kinetics across different AsiSI-DSBs are associated with changes in hypo-acetylated or hyper-acetylated chromatin status upon DSBs formation, such to explain different frequency in chromosome translocations. Therefore, we analyzed the degree of chromatin changes between the two classes of DSBs repair; as control, we plotted changes in H2BK120Ub, showing a lower abundance on sites repaired rapidly; this aligns with the switch from H2BK120-Ubiquitination to H2BK120-Acetylation in response to DSBs formation, previously characterized (Clouaire et al. 2018).

However, when we quantified DSBs-induced changes in H3K56ac, H4K12ac and H4K16ac, we did not observe significant differences between fast or slowly repaired AsiSI sites (Fig 31B).

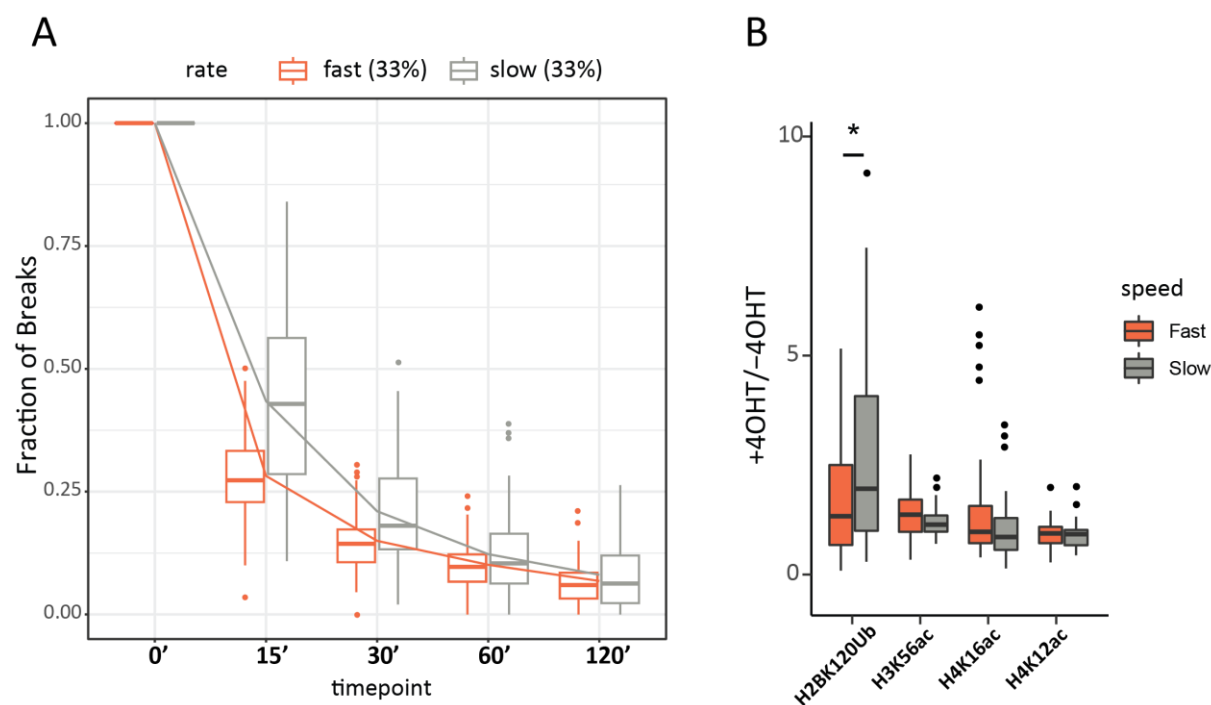


Figure 31: AsiSI-DSBs exhibit two rates of repair which are not influenced by different acetylation status of the chromatin surrounding DSBs. **A.** Box plots represent the residual fraction of breaks after induction of AsiSI degradation (+aux) in the 2 classes of repair rate, fast and slow. Specifically the DSBs were ranked from the highest contribution of the fast component to the lowest. Therefore, the 33% of top ranked sites were classified as fast repaired, while the 33% of bottom ranked are the ones where the fast component has the least contribution, and therefore defined as slow repaired sites. The number of breaks is normalized on the 1st time point, condition where DSBs were induced but no repair was triggered yet (time 0). **B.** Box plots represent the ratio of changes for the indicated histone marks between damaged and undamaged chromatin, classified for the two groups of repair rate.

We also verified whether individual DSBs, with different frequency of translocations, are repaired at different rate: however, the fitting of the model includes a subgroup of the ones analyzed in Figure 30C, and, for those, no differences in repair kinetics were detectable (data not shown).

Thus, we excluded that the acetylation status surrounding AsiSI-DSBs does affect the repair kinetics of the same breaks, giving rise to the possibility that upstream events of the translocation process are

Results

influenced by DSBs-induced changes in acetyl histone marks, as well as we observed for HDAC1-dependent mobility of a broken LacO locus (Figure 23 and Figure 24).

As final goal we wanted to check whether perturbation of the chromatin context also affects the occurrence of cancer initiating translocations. Specifically, we aimed to address whether a hyper-acetylated chromatin environment, achieved via HDACs inhibition, might decrease the formation of translocations recurrently found in patients. In this regard, we decided to assess how HDAC inhibition influence the frequency of etoposide-induced translocations.

2.7 HDAC inhibition reduces the frequency of Etoposide-induced *MLL* translocations

Etoposide is used in chemotherapy as a powerful cytostatic drug, because it triggers cell apoptosis by covalently trapping Topoisomerases 2 on DNA and leading to the formation of SSBs and DSBs (Kerrigan et al. 1987). Because of this intrinsic genomic instability, treatment with Topoisomerase inhibitors is highly associated with the risk of developing a secondary leukemia, such as t-AML (therapy-related Acute Myeloid Leukemia), which is characterized by having short latency and poor prognosis. Etoposide-induced leukemia is formed as consequence of chromosome translocations harboring at *MLL* locus and recurrent partner genes.

An important focus of our lab was to dissect mechanistic steps in the formation of etoposide-induced chromosome translocations, but to do so we firstly addressed key determinants in modulating etoposide-induced genome instability. We sought to interfere with some cellular mechanisms, which could potentially modulate the etoposide-induced genome instability with the scope of finding suppressors of etoposide-mediated *MLL*-translocations.

Our previous results have shown that lack or inhibition of HDAC1 led to a reduction of translocation between two artificially integrated genomic loci, such Lac operator and Tet operator repeats. Therefore, we decided to inhibit histone deacetylases and assess how changes in the acetylation status of chromatin interfere with the occurrence of oncogenic *MLL*- translocations, such as the ones induced by etoposide. To model the contribution of the chromatin environment in the incidence of oncogenic etoposide-induced translocations, we used our FISH-based method to probe the 5' end of the *MLL* locus with a BAC labelled in Green/488-dUTP and another one labelled in Red/568-dUTP for the 3' of *MLL* gene (Figure 32A). The 3' end of a translocation partner gene (*AF4*) was probed via a BAC labelled in FarRed/647dUTP (Figure 32A), as described in (Gothe et al. 2019).

To assess whether histone deacetylases affect the frequency of etoposide-induced translocations between *MLL* and a partner gene, such as *AF4*, we decided to treat SKM-1 cells with etoposide (10 μ M, for 6 hours) and finally release them in media containing HDACs inhibitors, such as TSA or SAHA (both at final concentrations of 250 nM and 500 nM). Two days later, cells were spun and fixed on coverslips, and then FISH was performed.

Results

Quantification of spot pairs distances have shown that inhibition of HDACs by TSA or SAHA does not affect the breakage at *MLL*, in fact we quantified similar percentage of cells with green-red probes apart in etoposide challenged cells or in cells receiving the co-treatments. Nevertheless, cells treated with etoposide and released in media supplemented with HDACs inhibitors have shown a reduced frequency of *MLL-AF4* translocation in a dose dependent manner and with a more potent effect achieved upon SAHA treatment (up to three-fold reduction; Figure 32C). This suggests that inhibiting HDAC1-related function, and likely preventing deacetylation status of the locus, it reduces the formation of etoposide-induced *MLL* translocations, confirming our previous result obtained by probing LacO-TetO translocations.

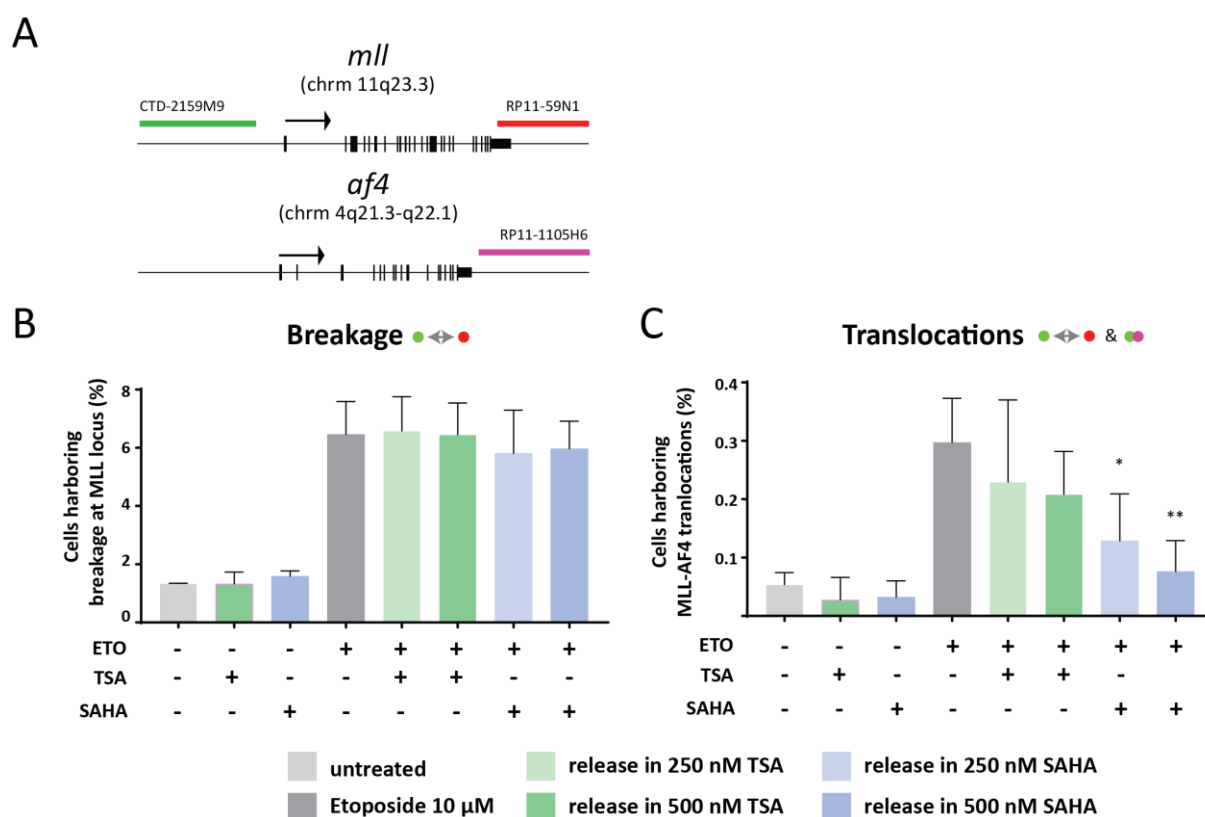


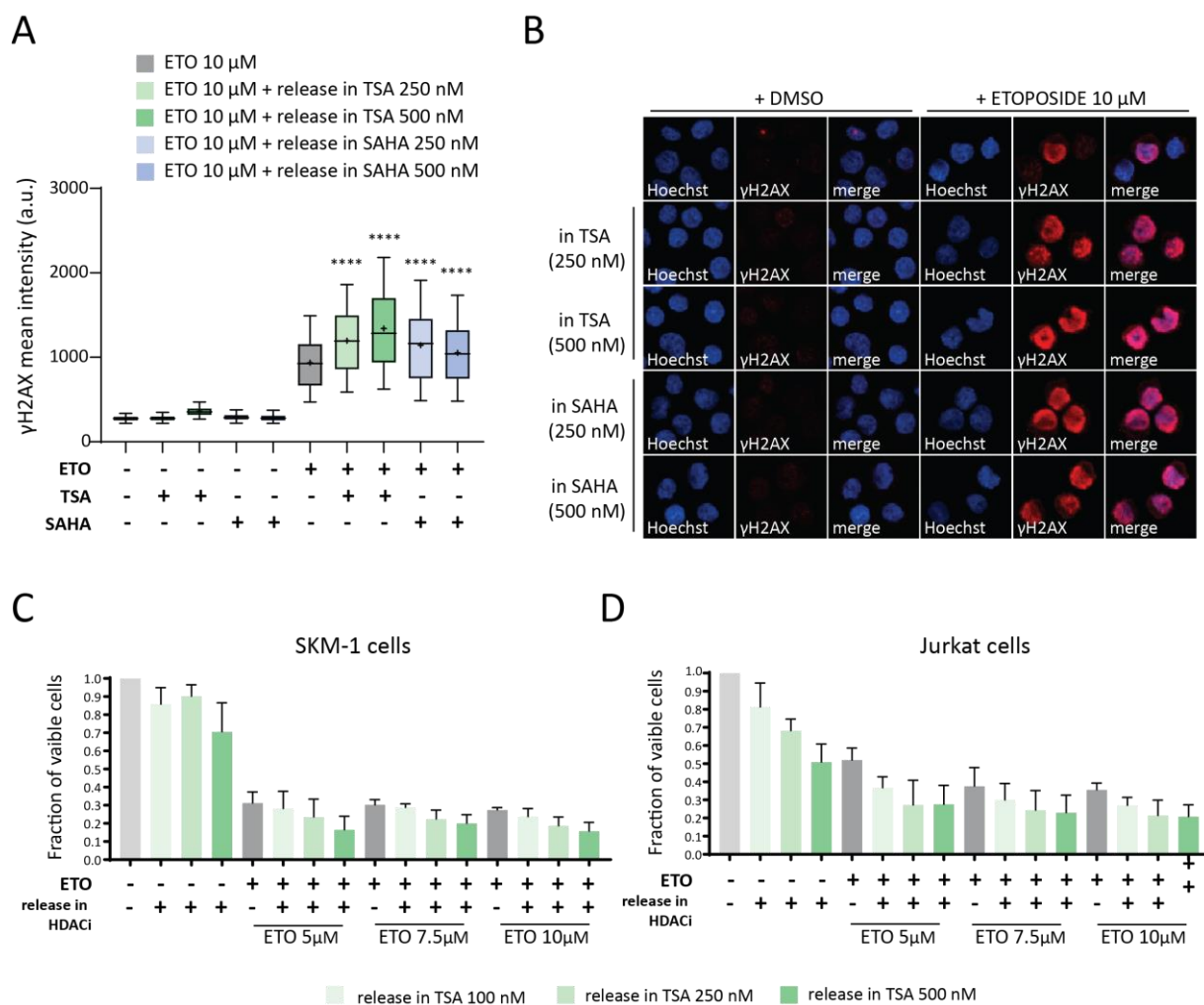
Figure 32: TSA and SAHA treatment reduce etoposide-induced MLL translocations. A. Schematic representation of FISH based probes labelling *MLL* gene and 3' end of *AF4* gene. *MLL* recurrent breakpoint cluster region is labelled with flanking green probe (5' end) and red probe (3' end). The 3' end of *af4* gene was labelled with FarRed probe. Black arrows indicate transcription directionality of the loci. B. SKM1 cells were treated with 10 μ M of etoposide for 6h and then released in media supplied or not with TSA or SAHA at the final concentrations of 250 nM or 500 nM. After 2 days, FISH was performed and high-throughput imaging and automated image analysis allowed counting cells with breakage at *MLL* and *MLL-AF4* translocations. Nuclei with 2 spots of each FISH probes were filtered in the analysis and a breakage event at *MLL* locus was quantified when cells had Green-Red pair distances above 1.2 μ m. C. Translocations were quantified for having Green-FarRed pair distances lower than 1.2 μ m. The cut off was based on the green-red pair distances of 99% of unchallenged cells. The fitness of cells challenged with etoposide is generally quite low compared unchallenged cells; this makes the numbers of nuclei included in the analysis quite different: compared to cells receiving or not etoposide treatment: we analyzed more than 4000 cells non treated; vice versa this number drops to 500-1000 cells in cells receiving etoposide treatment. Error bars indicate standard deviation of the averages of two independent experiments (n=2). Stars indicate *P* value of difference between cells treated only with eto and eto+SAHA 250 nM (*P* value=0.0254) or eto+SAHA 500 nM (*P* value=0.0059).

Results

An explanation of the reduced frequency of etoposide-induced translocations upon HDACs inhibition could be the reduced efficacy of Top2 inhibitors as DNA damage agent. In chemotherapy, this is particularly detrimental because it might lead to increase the dose of the drug or the length of the therapy to counteract this fading effect of etoposide treatment.

However, from our FISH data, we could rule out this possibility because the percentage of cells harboring breakage at *MLL* locus was nearly identical between conditions where cells were treated only with etoposide and cells undergoing Top2 and HDAC inhibition (Figure 32B).

To be sure that the reduction in *MLL* translocations observed upon HDACs inhibition was not due to a milder cytostatic effect of etoposide per se triggered by TSA and SAHA, we decided to quantify the viability of cells, by measuring their capability to metabolize a bioluminescent substrate. Importantly, we observed that double treatment with TSA rather potentiates the toxic effect induced by etoposide treatment in cell viability (Figure 33C). This enhanced effect in genome instability was confirmed also by quantification of phosphorylation of Ser139 at H2AX, which is not reduced upon double inhibitors treatments, but instead it is boosted up when etoposide-treated cells are also challenged by inhibition of histone deacetylases (TSA and SAHA treatments), explaining the diminished cell viability in these cells (Figure 33A, Figure 33B).



Results

Figure 33: TSA and SAHA treatments potentiate etoposide-induced genome instability and decrease cell viability. **A.** SKM-1 cells were treated for 6h with etoposide (10 μ M) and released in media with TSA or SAHA, both concentrated 250 and 500 nM. Cells were fixed 48h later and γ H2AX staining was performed. Box plots represent 5-95 percentiles of γ H2AX intensity of at least 500 nuclei. Median and mean are indicated with a black line or a black cruise, respectively. **B.** Example images of nuclear γ H2AX intensity, quantified in A. **C.** SKM-1 cells were treated with etoposide at the indicated concentrations for 6 hours and released in media supplement with different concentrations of TSA (100 nM, 250 nM and 500 nM). Plots indicate the fraction of viable cells measured 2 days after the release, by incubating a redox dye for at least 2h. Cell viability is measured as the cell capability to metabolize the redox dye and convert it in a fluorescent product. Error bars indicate standard deviation of the mean of two biological replicates. **D.** As in C. but cell viability was measured in Jurkat cells. Error bars represent standard deviation of the average of technical triplicates.

This additive effect in decreasing cells viability mediated by combined treatment of etoposide and TSA was observed also with other HDACs inhibitors, SAHA and MS-275 (Figure appendix 4). To assess the universality of the observed reduction of etoposide-induced translocations upon TSA and SAHA, found in SKM-1 cells, we tried to recapitulate the same finding in another hematopoietic cell lines, such as the Jurkat cells. Similarly to SKM-1, upon combined treatments of etoposide and HDACs inhibitor, Jurkat cells showed reduced fitness (Figure 33D).

Together these data suggest that the reduction in *MLL* translocations, observed upon Top2- poison and histone deacetylases inhibition, was likely not due to a decreased etoposide-induced genome instability, but rather to events subsequent to DSBs formation. Although we have not tested in the context of etoposide-induced DSBs and translocation, our previous findings hint that interfering with the acetylation status of the chromatin environment might influence the dynamics of a DSB and thereby its participation in the formation of a chromosome translocation.

To shade light on other key determinants of the process of etoposide-induced translocations, we continued by perturbing other cellular functions and assessed their involvement in etoposide-induced DDR.

2.8 Investigating key determinants of etoposide-mediated genome instability

The mechanism of formation of therapy - related translocations upon etoposide treatment is linked to the effect of TOP2-poisoning, which stabilizes TOP2 cleavage complexes (TOP2ccs), preventing religation of the double strand ends and giving rise to DPC (DNA-Protein Crosslinks) adducts. So far, I have described an involvement of chromatin factors in modulating the frequency of t-*MLL* translocations. In this paragraph, I am presenting our effort in dissecting the mechanisms underlying etoposide-induced DNA fragility.

It is likely that the presence of Topoisomerase 2 enzymes is *per se* crucial in genome instability triggered by etoposide, because they represent the targets upon which the posing effect is carried out. Furthermore, accumulation of torsional stress due to travelling, along the genome, of transcriptional bubble and

Results

replication fork, or direct collisions between TOP2-cleavage complexes (TOP2ccs) and transcriptional or replication machineries, can pose a threat to genome integrity by generating free DSBs, which might undergo translocations.

Finally, it is possible that repair mechanisms and proteolysis dependent metabolism of TOP2ccs affect genome stability by revealing the broken double strand ends, which are engaged in phosphodiesterase binding with the catalytic residues of TOP2 homodimer.

To verify whether the aforementioned pathways and factors contribute to TOP2-related genome instability, we decided to investigate whether tuning down these processes with specific inhibitor or, siRNAs for key factors, could alleviate the etoposide-induced DNA damage response. As surrogate of etoposide-mediated DNA damage, we quantified the nuclear intensity of Ser139-phosphorylation of H2AX.

2.8.1 Etoposide-induced genome instability depends on both Topoisomerase 2 alpha and beta

Topoisomerase 2 are the enzymes which become covalently trapped upon etoposide treatment; therefore, removal of the drug targets abrogate etoposide-induced γ H2AX and RPA phosphorylation (this latter parameter has been quantified for each of the cell lines, but it has been shown only for U2OS cell line as example, in Figure appendix 4). Further, we have observed a different contribution of TOP2A and TOP2B, with a stronger effect in relieving etoposide-induced breakage upon TOP2A KD, in HeLa, HCT and U2OS cells (Figure 34); while MCF-7 cells and progenitor cells positive for CD34 marker have shown similar dependency on both TOP2A and TOP2B, regarding etoposide-induced damage. Other evidence, obtained by another PhD student in the lab of Dr. Vassilis Roukos (Henrike Johanna Gothe), confirm that both isoforms of Topoisomerases 2 enzymes contribute to etoposide-induced genome instability, however the relative contribution is dependent on the levels of TOP2A and TOP2B in the different cell lines.

Results

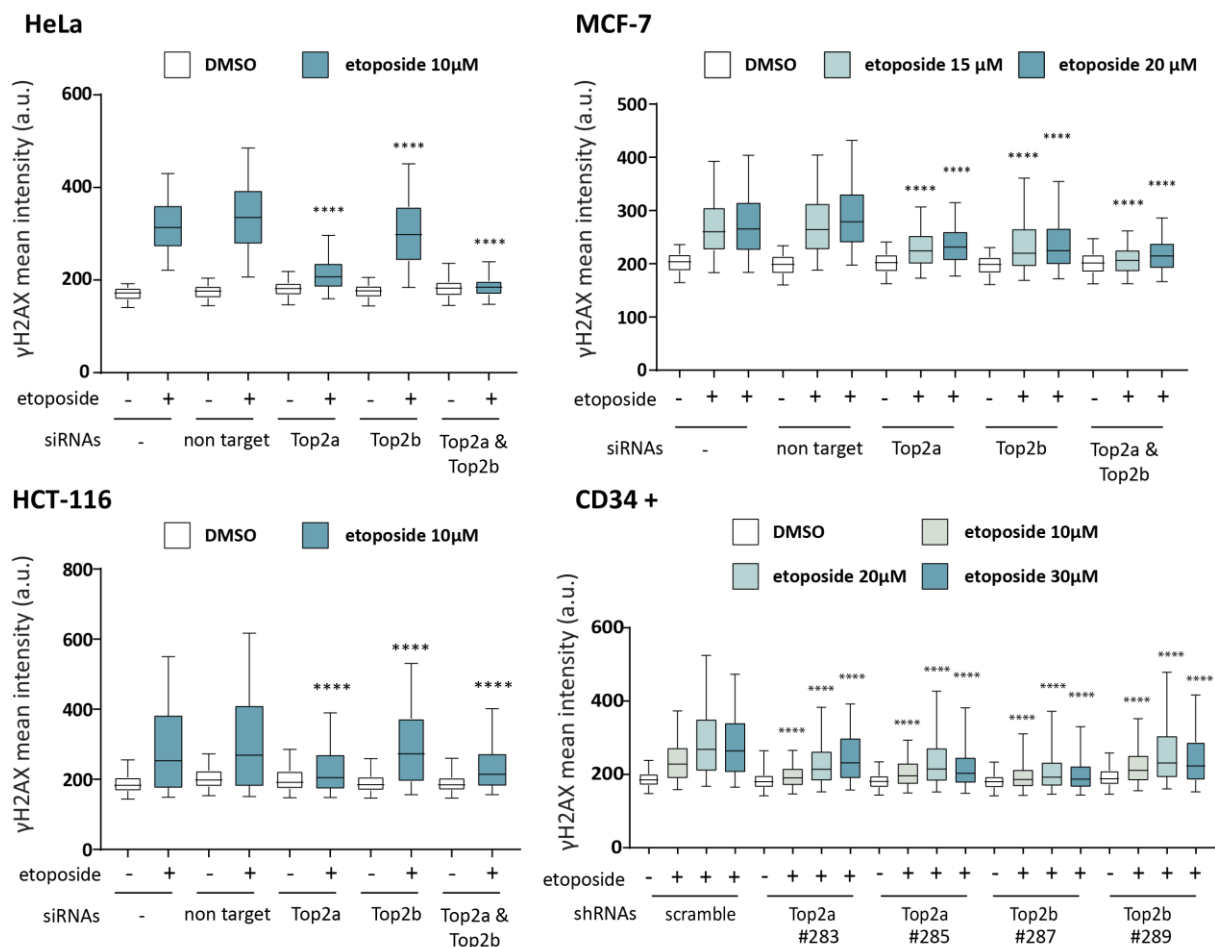


Figure 34: Both TOP2A and TOP2B determine etoposide-mediated phosphorylation of H2AX. Box plots show γ H2AX levels upon etoposide treatment, in cells with lower levels of TOP2A and/or TOP2B. HeLa, MCF-7 and HCT-116 cells were transfected with siRNA targeting Topoisomerase 2 alpha and beta isoforms and 72 hours later, etoposide at the indicated final concentrations was added for 4h. Cells were then fixed and immunofluorescence to detect phosphorylation of H2AX (and phosphorylation of RPA, not shown) was performed. CD34 positive progenitors, isolated from patients' samples, were transduced with lentiviral vectors encoding GFP and short harpins RNAs for Top2A or Top2B. Five days upon infection cells were treated with 10, 20 or 30 μ M of etoposide for 4 hours and γ H2AX was imaged and automatically quantified in GFP positive cells (at least 700 per condition). Representative box plot of two independent experiments is shown. Statistical significance was calculated with One Way ANOVA test and Tukey test.

Results

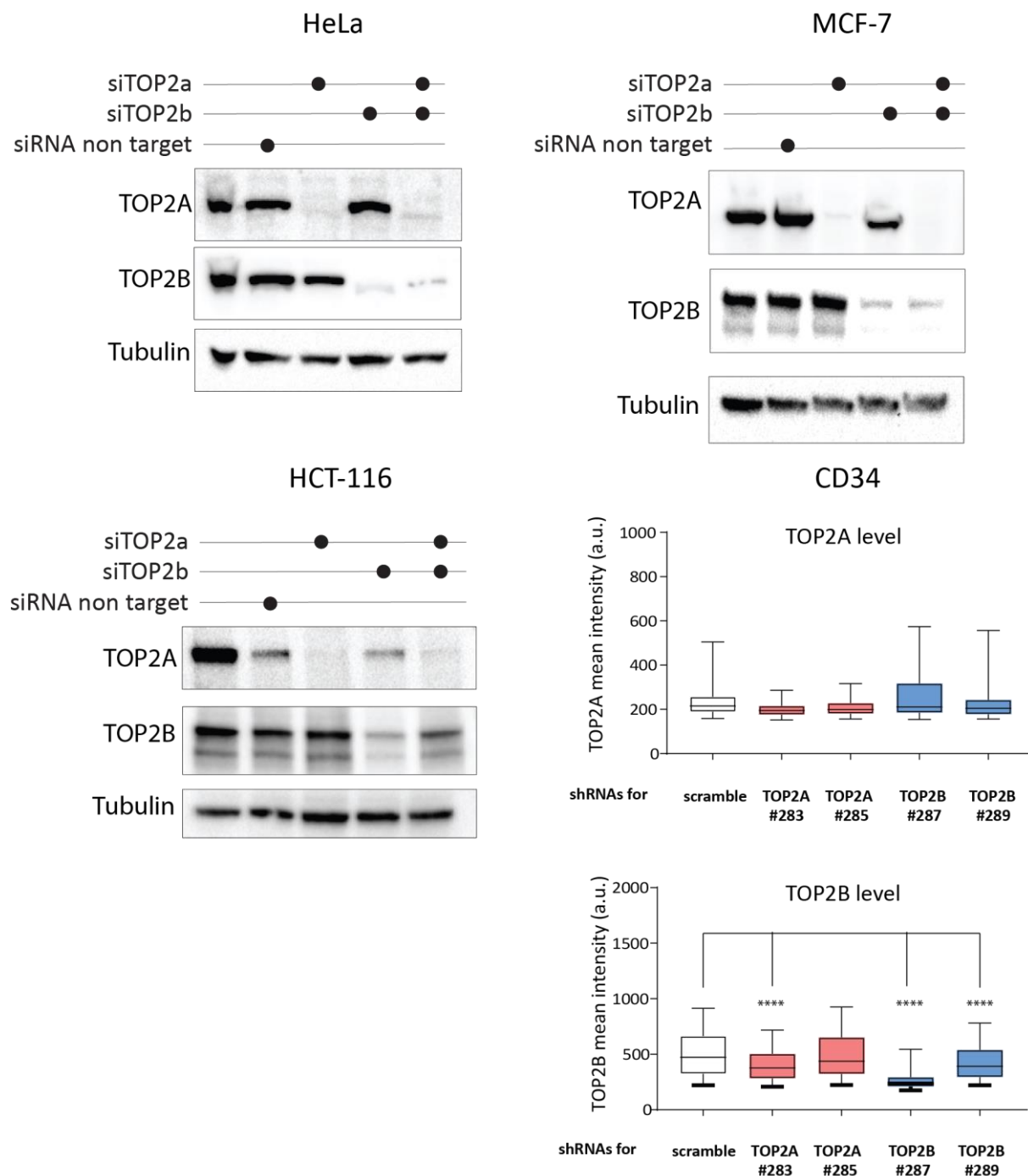


Figure 35: TOP2A and TOP2B levels upon siRNAs or shRNAs exposure in the indicated cell lines. Immunoblot analysis shows TOP2A and TOP2B protein levels upon 72 hours of transfection with targeted siRNA, in HeLa, MCF-7 and HCT-116 cell lines. In CD34+ cells, TOP2 levels were monitored by immunofluorescence upon 5 days of transduction with shRNAs against Top2 enzymes.

2.8.2 Transcription and replication are contributors of Etoposide-induced DNA damage

To investigate whether transcription and replication metabolisms impinge on etoposide-mediated γ H2AX foci formation, we decided to interfere with RNAPII elongation by pretreatment with actinomycin D and 5,6-Dichlorobenzimidazole 1- β -D-ribofuranoside, DRB (respectively with 100 nM and 200 μ M); while triptolide (2 μ M) was used to hamper transcription initiation. Inhibition of replication was achieved by pretreatment with 20 μ M of aphidicolin. Block of transcription and replication was monitored by checking the levels of incorporation of EU (Figure 36A, Figure 36B) and EdU (Figure 36C, Figure 36D) upon transcription and replication inhibitions.

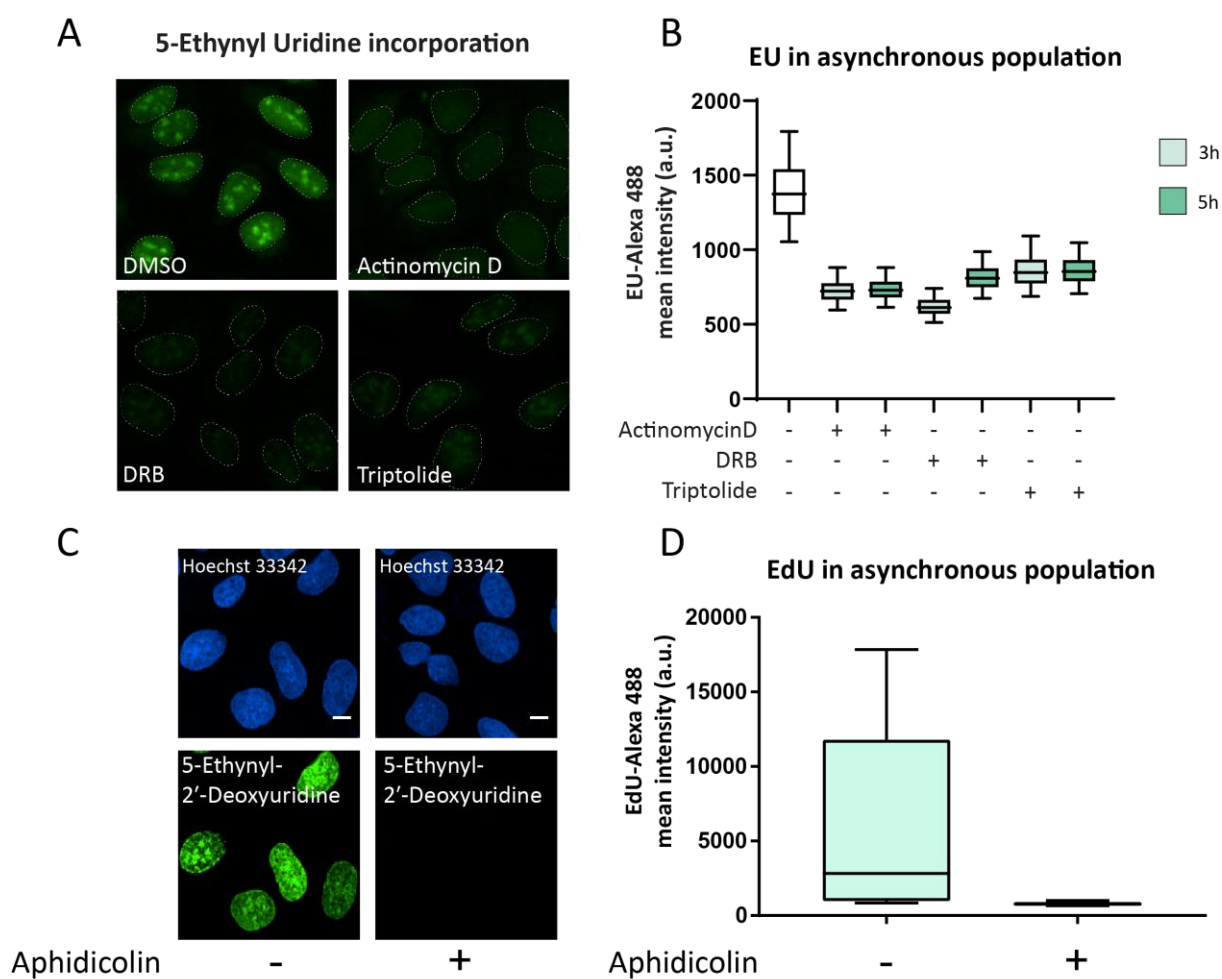


Figure 36: Transcription and replication inhibition prevent DNA incorporation of Ethynyl Uridine and 5-Ethynyl-2'-Deoxyuridine, respectively. **A.** Representative pictures of EU intensity upon 3 hours block of transcription. **B.** Quantification of EU nuclear intensity upon 3 or 5 hours treatment with actinomycin D (100 nM), DRB (200 μ M) and triptolide (2 μ M). **C.** Representative pictures of EdU staining upon replication inhibition. **D.** Quantification of EdU nuclear intensity upon 3 hours treatment with 20 μ M of aphidicolin.

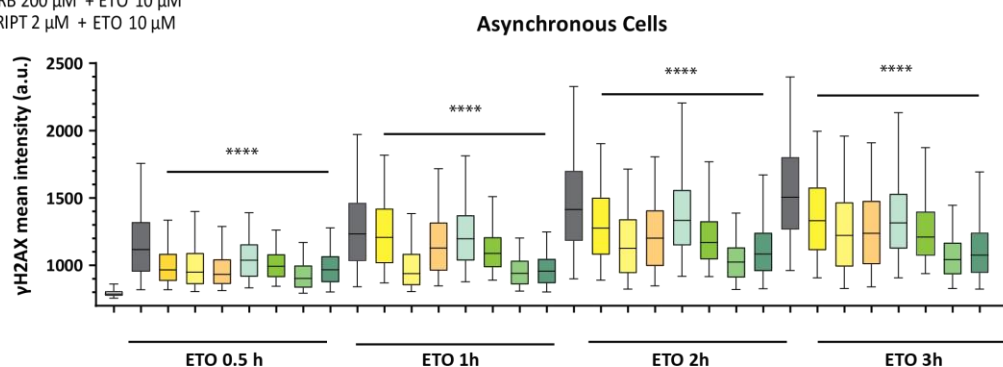
Upon 3h pretreatment with single or double inhibitors (aphidicolin and each transcriptional inhibitor), U2OS cells were challenged with etoposide for different time and DNA damage response was monitored by quantification of γ H2AX levels (and pRPA levels, not shown).

Results

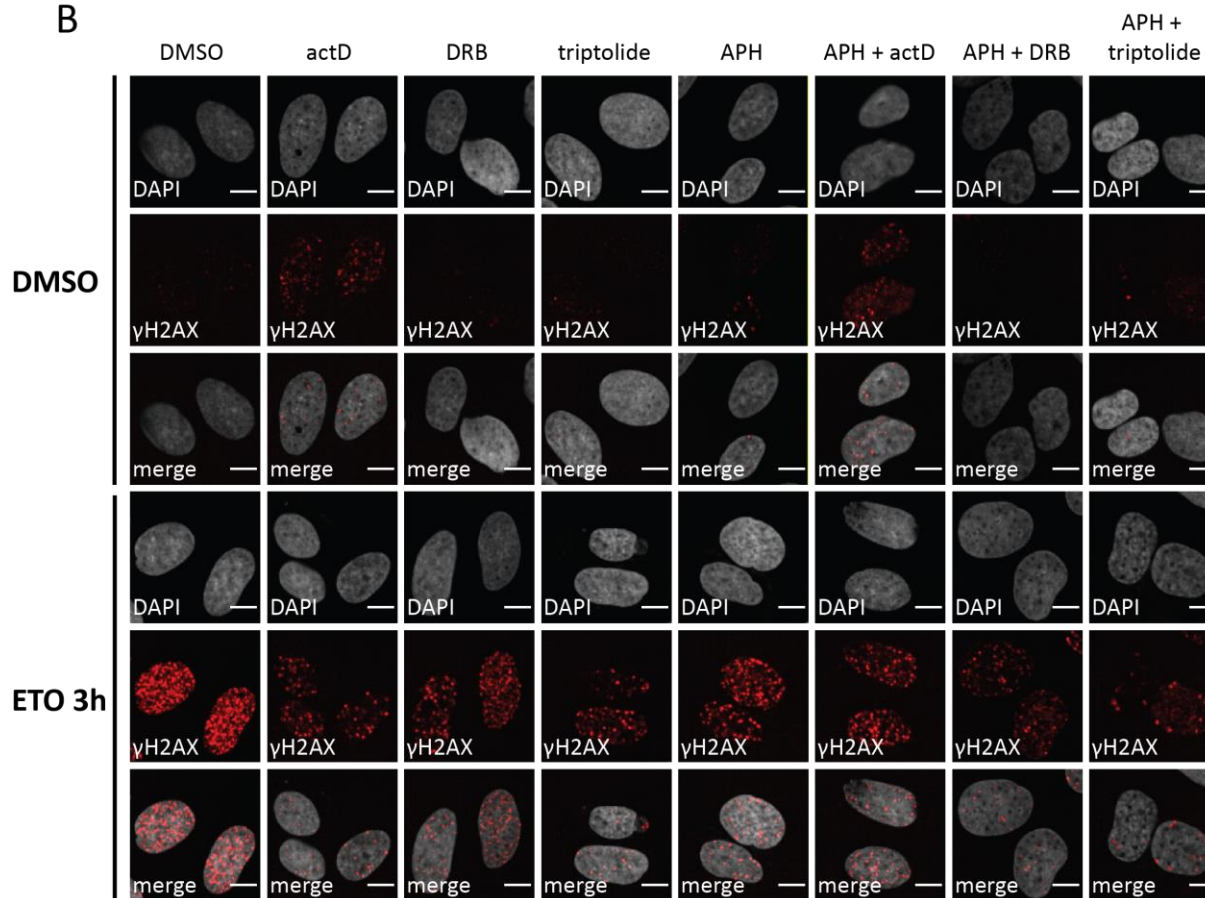
Results show that etoposide-induced DDR is greatly relieved when transcription or replication are shut down (Figure 37A). Furthermore, double inhibition with transcription inhibitor and aphidicolin highlights that both transcription and replication tune the DNA Damage Response triggered upon etoposide treatment, suggesting that clashes between Top2 trapped on DNA and transcription and/or replication machineries are contributors of DNA fragility.

A

- w/o inhibitor + ETO 10 μ M
- Act 100 nM + ETO 10 μ M
- DRB 200 μ M + ETO 10 μ M
- TRIPT 2 μ M + ETO 10 μ M
- APH 20 μ M + ETO 10 μ M
- APH 20 μ M + Act 100 nM + ETO 10 μ M
- APH 20 μ M + DRB 200 μ M + ETO 10 μ M
- APH 20 μ M + TRIPT 2 μ M + ETO 10 μ M



B



Results

Figure 37: Transcription and replication inhibition reduces etoposide-mediated DNA damage. **A.** U2OS cells were pre-treated for 3 hours with actinomycin D (100 nM), DRB (200 μ M), triptolide (2 μ M), aphidicolin (20 μ M), or combined treatment of aphidicolin (to block replication) and each of the transcription inhibitors. Without removing inhibitors, cells were challenged with 10 μ M of Etoposide for the indicated time (30 min, 1 hour, 2 hours, and 3 hours). Box Plot shows 5-95 percentile range of γ H2AX intensity for all the etoposide-treated conditions and untreated cells (DMSO). To simplify the graph, DDR triggered by only transcription and/or replication inhibition is not shown, but representative images are shown in **B.** At least 1000 nuclei per condition were analyzed. **B.** Images show γ H2AX foci triggered upon 3 hours treatment with etoposide. Cells with replication and transcription inhibition show reduced DDR signaling. Scale bar indicates 10 μ m.

2.8.3 VCP and proteasome system are enhancers of Etoposide-induced genome instability

Transcription and replication processes are not unique contributors of etoposide-induced chromosome breakage, in fact DSBs can arise also during the metabolism of removal of TOP2 stalled onto chromatin, as consequence of the physiological metabolism of repair of the etoposide-induced lesion. Resolution of TOP2ccs can occur via nucleolytic processing of the DNA sequence where Top2 is stalled or by TDP2-mediated hydrolysis of 5' phosphotyrosyl bound by which topoisomerase is covalently linked to the 5' termini of DNA (Pommier et al. 2016; Ledesma et al. 2009). However, how DNA repair enzymes distinguish between functional or abortive TOP2ccs is an open question. It is possible that TOP2, engaged in an abortive cleavage complex, has a different conformation compared to the functional one, or that TOP2 might be post-translationally modified by sumoylation or ubiquitination upon etoposide treatment (Mao, Desai, and Liu 2000; Mao et al. 2001). In line with this latter hypothesis, it has been predicted that TDP2 contains an ubiquitin associated (UBA)-like domain and in the catalytic domain has been inferred a SUMO-interacting motif (SIM). Those modifications might induce 26-proteasome dependent degradation and facilitate the accessibility to the 5' terminus by TDP2 in order to cut off the 5' phosphotyrosyl bound (Mao et al. 2001). Therefore, we sought to investigate whether the proteasome system could be involved in modulating etoposide-dependent DNA damage response. However, proteasome-related functions are downstream the removal of trapped Top2 from chromatin. A possible candidate in this step is VCP (Valosin-containing protein), a hexameric segregase that targets ubiquitinated proteins through specific ubiquitin adaptors proteins. By ATP-hydrolysis, VCP/p97 segregates and evicts substrate from cellular compartments, facilitating downstream degradation by proteasome system. Beside its well characterized role in ER-associated degradation, VCP plays functions in many different contexts and cellular processes: during cell cycle regulation, during transcription and replication processes and in DNA damage response (van den Boom and Meyer 2018). VCP is also a player in DSBs repair: during HR, it regulates the association of Rad51-Rad52 complex (Bergink et al. 2013), and it extracts Ku70/Ku80, facilitating Homologous Recombination (Meerang et al. 2011; van den Boom et al. 2016). The involvement of VCP in the resolution of other type of lesions is recently started to be elucidated: recently, for example, it has been shown that p97, together with SPRTN, is recruited at the site of Top1ccs and they found TEX264 as adaptor protein that bridges this interaction (Fielden et al. 2020).

This prompted us to hypothesize that VCP and proteasome play a role in repairing etoposide-induced TOP2ccs. Therefore, we explored whether VCP and proteasome, influence etoposide-induced DNA

Results

damage signaling, by pretreating the cells with specific inhibitors (NMS-873 to block VCP and MG132 for proteasome inhibition) prior etoposide treatment. Surprisingly, we have observed that the inhibition of VCP or proteasome does not enhance etoposide-induced genome instability; on the contrary, we have quantified significant reduction of the nuclear intensity of γ H2AX when cells were pretreated with NMS-873 or MG132 (Figure 38A, Figure 38B, Figure 38D). We confirmed this observation in different cell lines (adherent U2OS, Cal51 and the lymphoblastoid TK6) and it is a phenomenon independent of doses of etoposide utilized. VCP knockdown also showed diminished levels of γ H2AX upon etoposide treatment (Figure 38C).

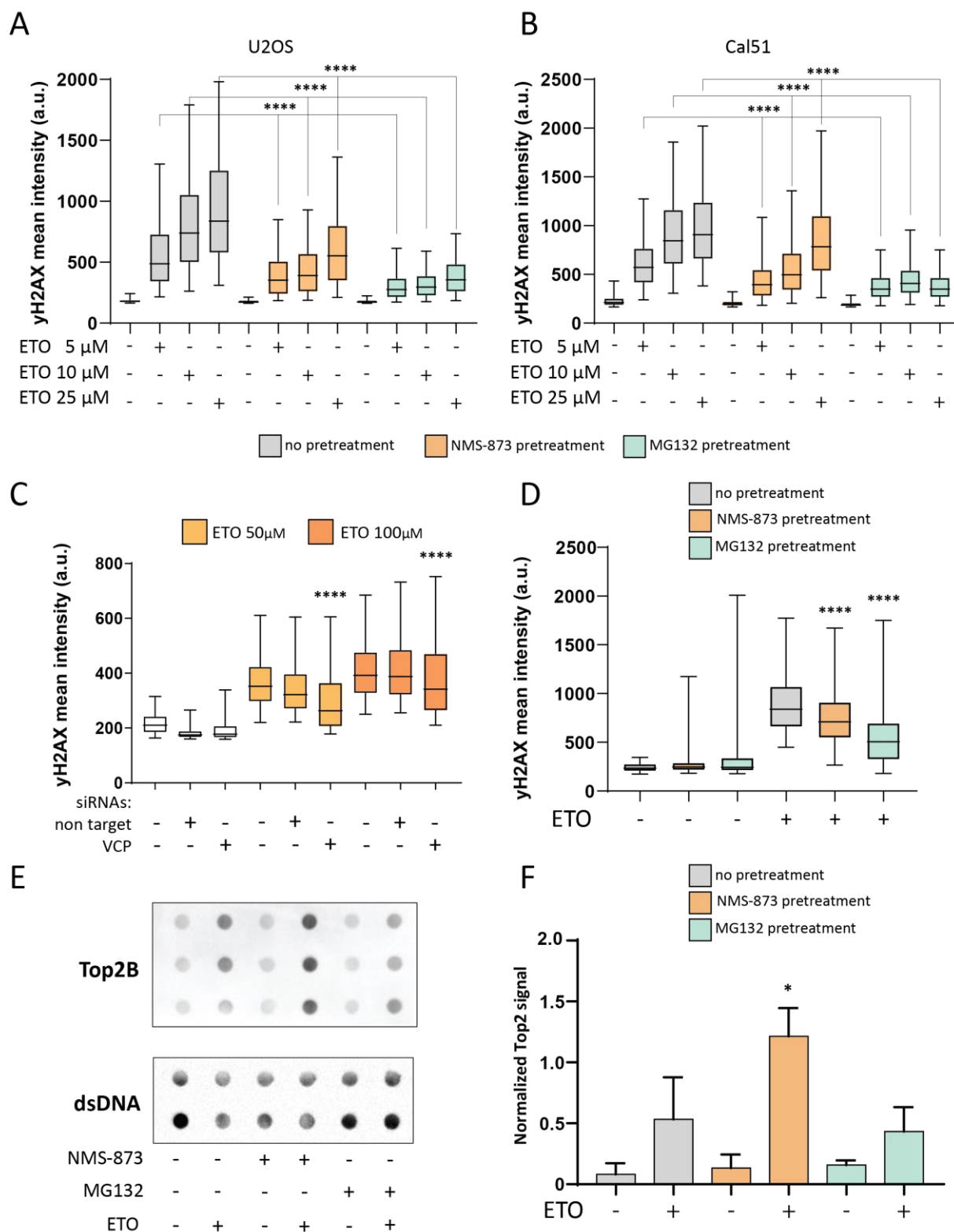


Figure 38: VCP and proteasome inhibitions reduce etoposide-mediated genome instability. **A.** U2OS cells were pre-treated for 3 hours with 5 μ M of NMS-873 and 2.5 μ M of MG132, then etoposide was added at the indicated concentrations; after 3 more hours, cells were fixed and γ H2AX staining was performed. Box plots show 5 to 95 percentile of the nuclear intensity of γ H2AX quantified in at least 800 nuclei per condition of two biological replicates. Stars indicate P value <0.0001 . **B.** As in A, Cal51 cells were pre-treated for 3 hours with 5 μ M of NMS-873 and 2.5 μ M of MG132, then etoposide was added at the indicated concentrations; after 3 more hours cells were fixed and γ H2AX staining was performed. Nuclear intensity of γ H2AX quantified in at least 1500 nuclei per

Results

condition of two biological replicates. Stars indicate P value < 0.0001 . **C.** Cal51 cells were transfected with 30 nM siRNA against VCP, then 48h later treatment with 50 μ M or 100 μ M of etoposide for 3h. Nuclear intensity of γ H2AX was quantified in at least 10000 nuclei per condition. **D.** TK6 cells were pre-treated for 3 hours with 2.5 μ M of NMS-873 and 2.5 μ M of MG132, then etoposide was added at the final concentration of 20 μ M; after 4 more hours cells were spun down and fixed and γ H2AX staining was performed. Box plots show 5 to 95 percentile of the nuclear intensity of γ H2AX quantified in at least 1500 nuclei per condition of two biological replicates. Stars indicate P value < 0.0001 . **E.** TK6 cells were treated as in **D.** and then immediately lysed in MB buffer (6 M GTC, 10 mM Tris-HCl (pH 6.5), 20 mM EDTA, 4% Triton X100, 1% Sarkosyl and 1% dithiothreitol) to collect free dsDNA and DNA covalently bound to proteins. dsDNA was quantified by QUBIT and 800 ng of DNA-proteins samples were used for dotblot analysis. Membranes were incubated with antibodies against Top2B and dsDNA, in figure a representative image with triplicates for Top2B staining and duplicates for dsDNA. **F.** Quantification of normalized Top2B signal from three independent experiments is shown in figure. Stars indicate P value = 0.0129.

This hints that interfering with the repair system to resolve stalled TOP2ccs might be beneficial for the cells, which can cope better when DNA-protein adducts accumulate, and eventually they get reversed, rather than when TOP2ccs are processed, thereby revealing free DSBs.

To demonstrate that VCP is involved in TOP2ccs extraction and that upon its inhibition DNA termini are engaged in a complex with the Topoisomerase enzyme, preventing being recognized as free DSBs, we decided to detect TOP2ccs upon isolation of free dsDNA and DNA bound to proteins, in cells pretreated or not with inhibitors for VCP and MG132. As hypothesized, we could observe higher accumulation of TOP2 signal in cells treated with NMS-873 and etoposide, compared cells challenged only with the TOP2 poison or in combination with MG132 treatment (Figure 38E, Figure 38F). It is intriguing to observe that proteasome inhibition does not lead to the same accumulation of TOP2 on DNA, the reason behind this is not understood yet. However, similarly to our finding, a recent work had shown that TOP2ccs can be rapidly reversed and block of proteolytic processing of trapped TOP2 prevents from etoposide-induced genome instability, potentially explaining the phenomenon of acquired tumor-resistance to Topoisomerase poisons (Sciascia et al. 2020).

To conclude, VCP is indeed involved in a multitude of molecular and cellular process and we found it constitutes a possible determinant for the formation of the TOP2-related DSBs that initiate the formation of therapy related *MLL* translocations, however how it targets substrate-specificity remains to be elucidated.

Chapter 3 – Discussion

Even though directly associated with tumorigenesis and in several cases can directly cause cancer, cellular and molecular determinants of the etiology of chromosome fusions remain poorly understood. This gap is probably due to the fact that chromosome translocations are rare events and therefore monitoring their formation in physiological conditions is difficult. To overcome this limitation various cellular systems have been developed to quantify their frequency. However, the approaches established so far preclude to elucidate which steps of translocations formation are fostered or hindered by the depletion of a given factor. In fact, those experimental assays are able to quantify the last step in the formation of a chromosome translocation, namely the illegitimate repair of heterologous DSBs, while lacking the ability of investigating upstream events such as the spatial dynamics of broken ends, the partner search, the synapsis of DSBs and finally inaccurate repair.

Recently, it has been generated a cell-based system where targeted formation of DSBs mediated by the endonuclease I-SceI is triggered at integrated sites flanked by LacO and TetO sequences. Labelling of broken chromosome ends is achieved by tethering of fluorescent proteins (GFP and mCherry) fused to their respective repressors (LacR and TetR) and formation of chromosome translocations is probed in real time (Roukos et al. 2013; Roukos, Burgess, and Misteli 2014). LacO/LacR tethering system has previously allowed studying spatial dynamics of DSBs in different organisms and cellular models. In this system, combination of TetO/TetR tool, in combination with fluorescent reporters, have allowed studying motion properties of distinct DSBs, revealing, for instance that DSBs undergoing translocations move faster compared to non-translocating DSBs. High-throughput imaging and automated image analysis permit also to calculate the frequency of DSBs pairing and thereby to track not only motion characteristics of a given DSBs, but also to assess further steps of a translocation process, such as when two broken DNA ends come together and persistent in a synapsis.

Therefore, alteration of a given molecular pathway in such system allows not only addressing whether the studied process and/or factor affects the frequency of chromosome translocations, but also to dissect in which steps of the formation of chromosome rearrangement is involved. Hence, in this project we have attempted to investigate the role of chromatin environment in the mechanism underlying the formation of chromosomal rearrangements.

3.1 Chromatin – related functions influence chromosome translocation frequency

Previously, Burman and colleagues have identified that H3K4me facilitates the frequency of chromosome translocations upon irradiation showing that overexpression of the relative histone methyltransferases ASH2L or SET7/9 make chromosomes more prone to break (Burman et al. 2015). This study proposes that the increased predisposition to breakage accounts for the increased translocation frequency, without investigating events downstream the formation of DSBs. In our project

Discussion

we aimed to characterize what happens during downstream events the formation of DSBs. Our epigenetic drugs-based screening has revealed that inhibition of class I of HDACs leads to decreased frequency of translocations between LacO and TetO loci (Figure 8). We validated that the decrease in translocation frequency specifically occurs at doses of deacetylase inhibitors that provoke increased intensity of fluorescent proteins, which we interpreted as increased expression level due to an increased global relaxation of the chromatin status. Together this leads us to hypothesize that chromatin hyperacetylation, upon HDACs inhibition, might suppress the formation of chromosome translocations.

3.2 A cell-based system for the spatial and temporal controlled formation of I-SceI-induced DSBs

To dig into the mechanism, we decided to point out which histone deacetylase drives this effect. However to investigate the respective role of each histone deacetylases on translocation formation, it was pivotal that cells experienced the same amount of DSBs. A limitation of the cellular system described above is that the pool of cells was transfected with a vector encoding I-SceI enzyme. This limitation would preclude assessing the relative contribution of chromatin factors in translocation formation, considering the fact that those rearrangements are difficult to quantify. To circumvent this, we generated an inducible tool that controls in space and in time the formation of DSBs, via a Dox-inducible expression of I-SceI. Furthermore we thought to control where the enzyme resides after expression, by cloning the nuclear binding domain of the glucocorticoid receptor (GR) in tandem with the endonuclease. Last, we sought to equip the chimeric construct also of an auxin-inducible degron (AID) or a destabilization degron (DD) tags, which could enable us to degrade I-SceI and monitor DSBs repair. Thus, we selected a clone carrying the GR construct fused at the C-terminus, and holding a DD tag at N-terminus. Among all, the selected clone (renamed Superduo) allows a better I-SceI transits to the nucleus and induction of 53BP1 foci, surrogates of DSBs (Figure 11B); specific induction of DSBs at LacO array (Figure 14B, Figure 14C) and DSBs repair occurring already 12 hours after inducing I-SceI degradation (Figure 12).

Kinetic experiments revealed that to I-SceI nuclear transfer (Figure 13A) corresponds to a progressive accumulation of 53BP1 foci (Figure 13B), both peaking 4 hours of dex treatment. However direct quantification of DSBs formation by LM-PCR revealed a plateau already after 3 hours (Figure 14A). It is reasonable that the kinetics of accumulation of 53BP1 foci is delayed compared to the actual formation of DSBs, being 53BP1 a repair marker, which transduce to effectors proteins the real presence of DSB lesions.

Nonetheless, the kinetic of accumulation of I-SceI-induced DSBs is comparable to DSBs generated also by endonucleases in other cellular systems (Soutoglou et al. 2007; Iacovoni et al. 2010).

Discussion

However, when we compared to frequencies of chromosome translocations induced via inducible I-SceI expression or via I-SceI electroporation, we have observed that the Dox-inducible system recovers lower frequency of chromosome translocations compared to the canonical system where I-SceI is overexpressed through electroporation (Figure 15).

This might be due to the fact that in this latter we assist to generation of persistent DSBs as I-SceI is largely expressed and gives rise to many cleavage cycles; whereas when we induce I-SceI-breaks by doxycycline we have observed that 53BP1 foci reach rapidly a plateau, which eventually tends to revert towards lower 53BP1 counts (observed also in other time course experiments, not shown). We envision that as cells progress into cell cycle, the nuclear concentration of I-SceI molecules diminishes (due to extrusion of I-SceI from the dissolved nuclear membrane), giving higher chances for a correct repair of the broken ends, and accounting for a reduced translocations frequency. From this we concluded that our Dox-inducible system is not able to recover enough chromosome translocations to quantify differences among different chromatin environments and we relied on another molecular tool based on electroporation of a GFP-tag version of I-SceI endonuclease. Yet, we have induced DSBs via Dox-triggered I-SceI in order to characterize DSBs motion properties in unperturbed or hyper-acetylated chromatin environments (Figure 23 and Figure 24).

3.3 HDAC1 plays a major role in the formation of chromosome translocations

Our results have showed that members of class I histone deacetylases might be required for the process of formation of chromosome translocations, in fact, when inhibited we have observed a decrease in the translocation frequencies. To characterize which histone deacetylases play a role in this phenomenon we followed two complementary approaches: in the first, we have perturbed chromatin organization in a global scale via specific HDACs knock down (Figure 21); the second way aimed to locally modify the chromatin status surrounding the DSB site via tethering of specific histone deacetylases (Figure 22). Altogether the data hint that HDAC1 might act as facilitator in the process of formation of chromosome translocations. Absence of HDAC1 significantly decreases the formation of LacO-TetO translocations, whereas targeting of HDAC1, as fusion with LacR, to the breaks site lead to higher translocations events in comparison with tethering of only LacR or when fused with N-truncated form of HDAC1.

It is quite intriguing that depletion of HDAC2 did not trigger the same changes in translocation frequency, in fact not only HDAC1 and HDAC2 co-exist in the same corepressor complexes, but, we and others have observed that depletion of HDAC1 stabilizes HDAC2 protein levels and vice versa (Zupkovitz et al. 2006; Lagger et al. 2002). However, other studies have also shown independent functions between the two histone deacetylases (Dovey, Foster, and Cowley 2010; Hagelkruys et al. 2014; Somanath, Herndon Klein, and Knoepfler 2017), including HDAC1-specific regulation of H3K56ac levels. Therefore, it is possible that only HDAC1-related functions are implicated in the

Discussion

formation of chromosome translocations; whereas, in HDAC1 knock down condition, HDAC2, becoming steadier, might conversely hamper the decrease in translocation frequency.

Similarly, when we investigated whether chromatin acetylation affects DSBs mobility, we have observed again that HDAC1 loss of function impairs mobility of a broken LacO-I-SceI locus (Figure 23 and Figure 24). On the other hand, depletion of HDAC2 causes only a milder reduction of DSB motion properties (Figure 24), probably not sufficient to induce changes in translocation frequency (Figure 21C) that are recovered at frequency similar to control cells with unperturbed chromatin state. In case of double knock down of HDAC1 and HDAC2, the effect in DSB movement mirrors the one observed in cells carrying only HDAC1 depletion, suggesting that the HDAC1 is the driving regulator in DSB dynamics. Together, this might hint that in absence of HDAC1, hyper-acetylation of chromatin environment makes DSBs less mobile and thereby less prone to translocate. To validate this finding it will be important to follow a complementary approach which consists of overexpressing HDAC1 to assess whether broken LacO-I-SceI loci shows an increased displacement compared to control conditions; alternatively, it is fundamental to assess whether local delivery of HDAC1 (for instance through LacO/LacR tethering system) at break site can lead as well to enhanced DSBs movement. However, it is also possible that chromatin hypo-acetylation increases translocation frequency, by leading to a more defective repair, we are discussing it in paragraph 3.5.

Surprisingly, targeting of Tip60 led also to an increase in chromosome translocations frequency (which however is not significant, due to a wide standard deviation). Because we did not observe an opposite and complementary behavior between HDAC1 and Tip60 tethering, in future would be interesting to assess the contribution of other histone acetyltransferases, such as CBP/p300 or MOF, that together with Tip60, are respectively responsible for acetyl group deposition on residues K56 of H3 and K16 of H4, histone marks erased in HDAC1, and HDAC2, -dependent manner (Das et al. 2009; Taipale et al. 2005; G. G. Sharma et al. 2010).

Moreover, it is also worth to note that induction of chromatin domains occurred only in a small pool of cells; we cover this in the following paragraph (3.4), where we discuss assays to address the functionality of chimeric mCherryLacR-chromatin modifiers constructs.

3.4 Functional validation of tethering of mCherryLacR-chromatin modifiers

Local change of the chromatin environment, where a DSB hits, was achieved by employing the high binding affinity of Lac Repressor for its DNA cognate, namely tandem repeats of LacO operator integrated in our system. Constructs are also tagged with mCherry, therefore, targeting on the LacO array was visible as a bright spot (glowing in mCherry channel) already 12h after washing out IPTG from the media culture. Then, to proof the induction of specific chromatin environment at LacO locus we pursue three different approaches not curbed by the need of amplifying repetitive genomic region, such instead we would have faced by performing ChIP on the LacO repeats adjacent to the breakpoint

Discussion

region. In fact, a common a direct way to verify the formation of chromatin domains upon artificial tethering of histone modifiers is to directly quantify by ChIP, any enrichment or depletion mediated respectively by a certain chromatin “writer” or “eraser” upon binding to the genomic locus.

Upon tethering of histone modifiers, we measured the size of the array as surrogate of the status of condensation of the chromatin, and we have observed, as expected, a more condensed locus when HDAC1 was tethered, compared to control condition or in condition of Tip60 targeting (Figure 18).

However, when HDAC1- or Tip60 were tethered, the LacO locus did not show differences of sensitivity to I-SceI enzyme, in fact we did not observe changes in 53BP1 localization or in DSBs captured events (Figure 16 and Figure 19), suggesting equal chromatin accessibility. A possible explanation can be given by a previous work showing that loss of Tip60 increases 53BP1 localization at DNA damage sites and end joining events (M. L. Li et al. 2019), suggesting the targeting of Tip60 to the break site might mitigate 53BP1 accumulation. Moreover, recovering of DSBs events through LM-PCR is comparable across tethering of histone modifiers: only a slightly lower fraction of DSBs can be detected upon tethering of mouse HDAC1 that, anyhow, is not significantly different from control conditions.

An important difference to be considered is that arrays size upon tethering of chromatin modifiers was carried out in condition of cells not experiencing DSBs formation. Whereas, measure of 53BP1-array colocalization or DSBs quantification by LM-PCR, upon targeting of histone modifiers to the locus, were carried out upon I-SceI cleavage, which might have saturated DSBs formation at a given locus, precluding the possibility to assess how the chromatin status impacts I-SceI recruitment and breakage formation. Indeed, while we have used the full cut capability of I-SceI, (i.e. when fully expressed and transferred into the nucleus), other researchers have performed a similar assay, by using the leakage of the enzyme (when I-SceI is expressed, but nuclear transfer is not triggered), so that to exclude plateau of I-SceI cleavage activity (Soutoglou et al. 2007; Burman et al. 2015). Nonetheless, we have tried to assess differences in chromatin accessibility upon only induction of I-SceI expression (Dox- condition), but we obtained only futile and not specific amplification near to background levels, which was quite difficult to interpret.

Finally, we have observed an enrichment or depletion of H4panAc from the site of the array in a small fraction of cells, when we tried by microscopy to quantify deposition or removal of acetylmarks from histone proteins (Figure 20). However, independently of the chromatin modifiers tethered, Lac array was carrying either H4panAc with higher signal in comparison to background signal, or same intensity as background level or absence of signal. Altogether, this suggests that induction of functional hyper-acetylated or hypo-acetylated chromatin domains occurs only in a small pool of cells, and the fact that all chromatin status were detectable independently of the tethered factors, suggests that chromatin environment is dynamically shaped and presumably we just observed a snapshot of it.

Discussion

To overcome the limitations of being able to modify chromatin acetylation at LacO-I-SceI site only in a small fraction of cells, one could pursue a different strategy to induce local tethering of chromatin modifiers by using a catalytic inactive Cas9 enzyme (dCas9) fused with HDAC1, Tip60 and mutants and deliver the chimeric constructs by sgRNAs in proximity of DSBs. A big advantage of this method comes from being suitable with various sources of DSBs induction, included, for instance, the delivery of histone modifiers to strongly cut AsiSI sites. Recently, tethering of dCas9-HDACs or HATs was successfully performed by targeting respectively HDAC3 or p300 in order to manipulate H3K27 acetylation levels (Kwon et al. 2017; Hilton et al. 2015). Furthermore, in our specific project, targeting chromatin modifiers to any genomic sites of interest, through a sgRNA, unbounds by the difficulty of amplifying repetitive sequences, as we encountered in our system where LacR-mediated targeting was restricted to LacO repeats.

3.5 AsiSI endonuclease induces DSBs in various chromatin contexts

To validate our results and explore whether HDAC1 plays role not in DSB mobility, but rather it affects the repair kinetics of broken ends, we have finally used a previously characterized cellular system, based on AsiSI endonuclease, to generate DSBs genome wide and in various chromatin domains. In this case, we sought of using HT-4C FISH methodology that based on 3D distances of colored FISH probes, allowed us to quantify chromosome breakage and chromosome translocations frequencies at AsiSI sites characterized by different chromatin acetylation upon the induction of AsiSI-DSBs (Clouaire et al. 2018).

To do so, firstly we tested the feasibility of our FISH-based method to dynamically quantify chromosome translocations, by using modulators of DSBs frequency and thereby translocation rates, such as DNAPK inhibitor and decitabine, a specific inhibitor of DNMT enzymes. DNAPK inhibitor treatment leads to persistent DSBs and DDR activation and it has been already used to positively screen for increment of translocation frequency in this project and in (Roukos et al. 2013); on the other hand AsiSI cleavage is blocked by methylated cytosine, therefore it was surprising that upon decitabine treatment, which should evoke a more robust AsiSI cut activity because of hypo-methylated sites, we actually observed a block of AsiSI-DSB formation.

An explanation for this effect comes from a work which highlights that upon decitabine treatment, hemi-methylates CpGs are increased due to DNMT1 trapping at newly synthesized strands, where decitabine gets incorporated. Because, TET proteins have enzymatic preference for hemi-methylated templates, they get recruited at those loci, provoking an effect of dilution of TDG and BER enzymes, with the dramatic effect of tuning down the active cycle of demethylation (Chowdhury et al. 2015). It is possible that this underlies the resistance mechanisms of certain tumors which display a weak response upon DNMT inhibitors treatment and increased methylation was observed in more than half of the patients (Giri and Aittokallio 2019). Unexpectedly, though, in our attempt to modulate and screen AsiSI-induced

Discussion

translocations, decitabine treatment turned out being an important control to screen for negative accumulation of AsiSI triggered chromosome breakage and rearrangements.

When AsiSI induces DSBs, at certain loci it can perturb the levels of H3K56ac, H4K12ac and H4K16ac, which are erased in HDAC1/2 dependent manner (Miller et al. 2010). For a subgroup of these genomic loci, we have observed that to a stronger depletion of acetyl histone marks, especially for H4K16ac, corresponds a higher frequency of chromosome translocations, with a bait DSB (Figure 30). In order to address whether a decreased occupancy of acetyl marks correlates with a defective repair process that might explain the high frequency of chromosome translocations, we performed repair kinetics experiments, by inducing AsiSI-DSBs and, then, monitoring repair events at different time points by sBLISS. Data showed that fractions of DSBs retained over time were well fitting a previous model, proposed by Iliakis and colleagues to describe the repair of IR-induced DSBs. They observed that repair of such lesions takes place in a biphasic manner and it relies on two parameters: “fast” and “slow” components that give the name to our groups where we classified AsiSI-breaks, according precisely whether they were repaired with a faster or slower rate. Iliakis and colleagues identified that during the first 30 minutes breaks are repaired with a fast rate by NHEJ, then, a slow component takes over but unlikely reflects homologous recombination repair (Metzger and Iliakis 1991; H. Wang et al. 2001). Similarly, after 0.5 hour, DSBs repaired in a fast mode account for only one quarter of the total breaks quantified at time point 0, when the repair process was not induced yet; whereas half of slow breaks persist still after 30 minutes. However, we were not able to account for differences in DSBs- induced histone acetylation changes, (nor for the chromatin landscape, prior DSBs induction, data not shown) for the two classes of DSBs repair (Figure 31).

In future, the data set of AsiSI sites for translocations detection must be increased to give robustness to our working model, which currently suggests an involvement of HDAC1 function in enhancing the DSBs mobility and, possibly, ends synapsis events and not in the regulation of DSBs repair.

To strengthen this hypothesis and in line with decreased mobility of a broken LacO-I-SceI locus, in condition of hyper-acetylated chromatin, a future direction would be to induce AsiSI-DSBs at selected loci, by CRISPR-Cas9 system and observe mobility and fusion frequency of 53BP1 foci, for the purpose tagged with a fluorescent protein. This will ultimately assess whether DSBs show distinct motion properties dictated by changes in the acetylation status of the chromatin environment where they arise, which, then, might result in different frequencies of chromosome translocations.

As ultimate goal, it is pivotal to decipher which histone deacetylase is responsible for changes in the acetyl marks at level of AsiSI-DSBs, in fact it has been shown that in absence of both HDAC1 and HDAC2, chromatin retains acetyl group at level of K56 on H3 and K12 and K16 on H4 (Miller et al. 2010). Our findings hint that HDAC1 is the main responsible for the formation of chromosome translocations; therefore, profiling the occupancy of the two histone deacetylases, upon AsiSI-DSBs

formation (by ChIP-seq or Cut&Run-seq) is important and it might reveal a differential DSB-dependent recruitment of HDAC1 and HDAC2 that might, then, influence distinctive translocation frequencies.

3.6 HDACs inhibition decreases etoposide-induced *MLL* translocations

During my doctoral research, as collaborative project, I have confirmed and identified novel contributors of etoposide-induced genome instability. We have characterized the involvement of Topoisomerases α and β in triggering H2AX-phosphorylation upon etoposide treatment (Figure 34). In fact, stalling of Topoisomerases can lead to DSBs formation especially when DNA-protein adducts collide with ongoing transcription and replication. We have observed, indeed, that tuning down of such processes relieves etoposide-induced DDR (Figure 37). We have also demonstrated that inhibition of VCP, ATP-dependent segregase, and of proteasome system, also decreases genomic instability triggered by etoposide. The molecular key underlying this is given by the fact that VCP inhibition blocks TOP2ccs extraction from chromatin, thereby decreasing free double strand ends and associated H2AX phosphorylation (Figure 38; Fielden et al. 2020).

Moreover, in the scenario of identifying determinants of etoposide-induced fragility and recurrent translocations we tested the involvement of histone deacetylases in the formation of *MLL* translocations. Understanding how chromatin environment surrounding the etoposide-induced lesion contributes to the formation of t-*MLL* translocations has high significance in the context of discovering molecules and mechanisms able to counteract the occurrence of etoposide-driven *MLL* translocations. Identification of epigenetic inhibitors, which reduces etoposide-induced translocations, might constitute potential targets of clinical trial of a co-treatment based on Topoisomerase 2 and epigenetic inhibitors, for patients with high risk of developing a second tumor. Similar to our previous results showing that HDACs inhibition decreases the frequency of LacO-TetO translocations, treatment of etoposide and release in media with TSA or SAHA accounts for a reduction of *MLL-AF4* translocations. Intriguingly, this occurs in conditions that do not mitigate etoposide-induced genome instability, nor *MLL* breakage, and it suggests that HDACs inhibition protects from the formation of chromosome translocations by acting on steps downstream DSBs formation. This is particularly relevant considering that counteracting the risk of formation of therapy-related translocations cannot occur by decreasing breakage susceptibility, because this would reduce the cytotoxic effect of chemotherapeutic and thereby preclude to erase the primary tumor.

To conclude, our findings point to a role of histone hyper-acetylation in downstream events of DSB formation, specifically in the decreasing DSBs mobility and thereby their propensity to synapse and to form chromosome translocations.

Chapter 4 – Material & Methods

4.1 Material

Indication of the main reagents and equipment, used in this PhD thesis, are embodied in the text of the method section.

4.2 Methods

4.2.1 Generation of Dox-inducible cell line for space and time control of I-SceI enzyme

4.2.1.1 Cloning of GR-I-SceI degron constructs in lentiviral pLenti CMV TRE 3G

To control the induction of I-SceI-DSBs, we decided to restrict, in time and space, the enzymatic activity of I-SceI endonuclease by a Tet-On inducible promoter, which becomes activated when supplementing the culture media with doxycycline. Instead, I-SceI cellular localization is controlled via dexamethasone, which binds the nuclear binding domain of the glucocorticoid receptor (GR), fused in tandem to I-SceI, and it shuttles the enzyme into the nucleus. For the purpose of studying repair kinetics of I-SceI-DSB, we also decided to fuse a degron tag allowing to provoke I-SceI degradation. For this latter, in frame with the GR-I-SceI, we cloned an auxin inducible degron (AID) or a destabilization degron (DD): both allow proteasome-dependent degradation of the target protein, but with slightly different mechanisms. In case of the Auxin-Inducible Degron, when auxin is added to the cell culture media, it binds AID tag and promotes OsTIR1/Cul1-dependent ubiquitination and, therefore, proteasome-dependent degradation of the target protein. Viceversa, culturing the cells in presence of a ligand, Shield1, protects from I-SceI-DD proteolysis. In fact, if the ligand is washed out from the cell culture media, destabilization and degradation of the target protein are achieved.

To achieve the best results in terms of induction of I-SceI-DSBs and to rule out protein conformation defects, constructs were designed to have two regulatory elements, namely GR, DD or AID, which were arranged in each possible configurations, so that each tag was fused at the N- or C- terminus of I-SceI coding sequence. Specifically, cell lines carrying a Dox-inducible expression of the following constructs were generated: 1) GR-I-SceI-DD, 2) DD-I-SceI-GR, 3) GR-I-SceI-AID, 4) AID-I-SceI-GR.

Because each construct shares two or three elements, for the cloning was used GeneArt® Seamless Cloning and Assembly Kit (Invitrogen, #A14603), which employs 5'-exonuclease activity, as well as polymerase and ligase reactions to fill up the nicks and join DNA segments which, as result, will be cloned in different configurations. Pivotal for this type of simultaneous multiple cloning is the amplification of each individual element with oligo primers containing, not only a small linker (encoding for the peptide Ser-Ala-Ser-Ala-Gly, allowing proper folding of each element), but, mainly, sequences homologous to the adjacent cassette (Table 7 and Figure appendix 1). Then, combination of the amplified cassettes will determine the directionality by which the assorted elements are cloned. Importantly, the first and the last element of the chimeric fusion are amplified with oligos which introduce, respectively, compatible DNA ends to KpnI- or EcoRV-digestion; both enzymes were used

Material and Methods

to linearize the entry vector, pENTR1A (Addgene, #17398). Templates of the PCR reaction are: pLVX-PTuner (Clontech #632173; to amplify DD); I-SceI-GR-RFP (Addgene, #17654; to amplify I-SceI and GR); pCDH-CuO-AID-HANLSISceI-EF1-CymR-T2A-Puro (to amplify AID),

PCR reaction

| Component of reaction | | Amount |
|-----------------------------|-------------|------------------|
| DNA template | 50 ng | ~ 1 μ l |
| dNTPS (25 mM) | 250 μ M | 0.5 μ l |
| Forward primer (10 μ M) | 0.2 μ M | 1 μ l |
| Reverse primer (10 μ M) | 0.2 μ M | 1 μ l |
| Pfu Ultra II Polymerase | | 1 μ l |
| Buffer Pfu Ultra II 10X | | 5 μ l |
| NFW | | up to 50 μ l |

PCR cycles programme

| Step | Temperature | Time | |
|-----------------|-------------|--------|-----------|
| denaturation | 95 °C | 2 min | 30 cycles |
| denaturation | 95 °C | 20 sec | |
| annealing | 60 °C | 20 sec | |
| extension | 72 °C | 20 sec | |
| final extension | 72 °C | 3 min | |
| | | | |

PCR products were cleaned up via QIAquick PCR Purification Kit (Qiagen, #28106) and fragments size was inspected via gel electrophoresis (Figure appendix 1). The seamless cloning consisted of recombination reactions set up in 10 μ l (final volume) at room temperature (RT) for 30 min, using roughly 100 ng of each PCR product and 60 ng of a KpnI/EcoRV-digested pENTR1A plasmid, containing a Kanamycin resistance gene. Then, 3 μ l of reaction were used to transform DH10B T1 Phage-resistant cells (Thermo Scientific, #123311013).

Sequencing confirmed successful integration of the correct integration and orientation into the pENTR1A plasmid for the constructs: GR-I-SceI-DD, GR-I-SceI-AID and AID-I-SceI-GR.

The DD-I-SceI-GR chimeric fusion have shown a mismatch in the DD elements, which was successfully corrected via QuikChange II Site-Directed Mutagenesis Kit (Agilent, 200523) by using primers #57 and #58, as following:

PCR-based mutagenesis reaction

| Component of reaction | Amount |
|---------------------------------|------------------|
| Buffer Pfu Ultra 10X | 2.5 μ l |
| DNA template | ~25 ng |
| Forward primer #57 (10 μ M) | 0.65 μ l |
| Reverse primer #58 (10 μ M) | 0.65 μ l |
| dNTPs mix | 0.5 μ l |
| Pfu Ultra Polymerase | 0.5 μ l |
| NFW | up to 25 μ l |

PCR cycles programme

| Step | Temperature | Time | |
|--------------|-------------|--------|-------------|
| denaturation | 95 °C | 30 sec | x 12 cycles |
| denaturation | 95 °C | 30 sec | |
| annealing | 55 °C | 1 min | |
| extension | 72 °C | 13 min | |

Material and Methods

Commonly, transformation and replication of DNA vectors happen in *dam*⁺ bacteria background, where Dam methylase catalyses the transfer of a methylgroup to the N6 position of the adenine when in GATC sequence. Thus, after site-directed mutagenesis, parental vector was restricted out by DpnI enzyme, which degrades methylated, or hemimethylated plasmids. Then, the newly mutagenized vector, insensitive to DpnI digestion, was transformed in *Stbl3* bacteria cells, and corrected sequence was confirmed by sequencing using primer #49.

To facilitate the screening of different clones, a HA tag was integrated upstream of each construct via a protocol by Zhang and colleagues, developed to clone sgRNAs oligos into lentiviral transfer vectors (Shalem et al. 2014) (Sanjana, Shalem, and Zhang 2014). The strategy is based on annealing two complementary oligos with overhangs compatible with the ones generated by the restriction enzyme which nicks the vector at the site where oligo duplex will be cloned. To the purpose, a HA tag was designed with KpnI-compatible ends in order to introduce the tag at the N-terminus, in frame with the coding sequence of the full GR-I-SceI degradation tags constructs. Briefly, 5' end phosphorylation of the DNA oligos (mediated by T4-Polynucleotide Kinase, NEB, #M0201), then annealing of the two complementary sequences (primers #47 and #48) and ligation into previously KpnI-digested and dephosphorylated vectors, containing the GR-I-SceI-degron fusions, were performed.

Material and Methods

Oligos Phosphorylation and Annealing reaction

| Component of reaction | amount |
|----------------------------------|-------------|
| Forward primer #47 (100 μ M) | 1 μ l |
| Reverse primer #48 (100 μ M) | 1 μ l |
| Buffer T4 ligation 10X | 1 μ l |
| T4 PNK | 0.5 μ l |
| NFW | 6.5 μ l |

PCR cycles programme

| Step | Temperature | Time |
|--------------------|-------------|--------|
| phosphorylation | 37 °C | 30 min |
| annealing | 95 °C | 5 min |
| Ramp down to 25 °C | 5 °C/min | |

Digestion and dephosphorylation of pENTR1A with GR-I-SceI degnon

| Component of reaction | amount |
|-----------------------|---------------|
| pENTR1A vector | 5 μ g |
| KpnI | 2 μ l |
| Buffer Cut Smart 10X | 5 μ l |
| NFW | To 50 μ l |

Enzymatic digestion is carried out for at least 30 minutes at 37 °C, and then a dephosphorylating step (for 10 min at 37 °C) blocked re-ligation of the linearized plasmid.

| Component of reaction | amount |
|---|---------------|
| KpnI-digestion reaction | 50 μ l |
| Antarctic Phosphatase Reaction Buffer 10X | 1 μ l |
| Antarctic Phosphatase | 1 μ l |
| NFW | To 60 μ l |

After Antarctic Phosphatase (NEB, #B0289S) inactivation for 5 minutes at 75 °C, quick ligation reaction (Quick Ligation™ Kit, NEB, #M2200) was set up as described in the table below and carried out for 5 minutes at RT.

| Component of reaction | amount |
|---|------------------|
| Digested and dephosphorylated DNA vector | 50 ng |
| Phosphorylated and annealed HA-oligo duplex | 100 nM |
| Buffer Quick Ligation 2X | 5 μ l |
| Quick Ligase | 1 μ l |
| NFW | up to 10 μ l |

Material and Methods

Heat-shock treatment allowed transformation of chemically competent Stbl3 bacteria cells (One Shot® Stbl3™, Invitrogen, #C737303) with 4 ul of ligation reaction, positive clones were isolated from Kanamycin selective LB-agar plates.

Final goal was to restrict the expression of the GR-I-SceI degron constructs via a Tetracycline – Responsive Element, which becomes activated in presence of doxycycline. Therefore, all HA-GR-I-SceI- degron constructs were cloned through a LR reaction into a destination lentiviral vector with a TetON- inducible promoter, pLenti CMV-TRE3G (pLenti CMVTRE3G Neo DEST, w813-1, depositer Eric Campeau). Specifically, 150 ng of entry vector and 150 ng of destination plasmid (1:1 ratio) are incubated with 1 µl of LR Clonase II enzyme mix (Gateway® LR Clonase® II Enzyme mix, Thermo Fisher Scientific, #11791100) in a final volume of 5 µl, adjusted with TE buffer, pH 8. The LR reaction was incubated overnight at 25 °C constant.

As common feature of gateway destination vectors, the propagation of the empty pLenti CMV-TRE3G vector requires *ccdB* survival cells and co-selection on LB-media enriched of chloramphenicol and ampicillin. The chloramphenicol resistance cassette and the *ccdB* gene are located between the homology arms (attR1 and attR2), so that during the LR reaction, the fusion constructs get successfully cloned into destination lentiviral vectors, while the toxic gene and the selection cassette recombine into the entry vector within attL1 and attL2 as by-product of the reaction. Then, to select positive clones, it was sufficient to grow the transformed bacteria on plate containing only ampicillin, whereas empty destination vectors or entry vectors are negatively selected out.

The pLenti CMV-TRE 3G vector contains a neomycin resistance gene, therefore, upon integration of the lentiviral vector, cells can be positively selected by culturing with media containing G418 antibiotic.

4.2.1.2 Infection of NIH3T3 duo cells with Dox-inducible lentiviral vectors for the expression of GR-I-SceI constructs

A TetON promoter is regulated via binding of doxycycline to a reverse tetracycline-transactivator (rtTA), inducing a conformational change, by which Tet repressor (rtTA) can engage the TRE promoter and turn on the transcription. Therefore, to generate Dox-inducible cell lines for the expression of the GR-I-SceI-degron, we proceeded with co-infection of pLenti CMV-TRE3G (expressing the inducible I-SceI chimeric fusions) and pLenti CMV rtTA3 (pLenti CMV rtTA3 Blast, w756-1, Addgene, #26429) carrying, respectively, neomycin and blasticidin resistance gene for the mammalian selection.

To produce viral vectors, HEK293T cells were transfected with 3rd generation packaging vectors (pMDLg/pRRE, pRSV-Rev, pMD2.G) and lentiviral plasmids carrying the transgenes (namely CMV-TRE3G- HA-I-SceI chimeric constructs or CMV rtTA3) between long terminal repeat (LTR) sequences, which promote the stable integration in the genome of the host cell line. Specifically, in transfection mix A we diluted 5 µg of DNA of each packaging vector and 8 µg of pLenti CMV rtTA3 or pLenti CMV-

Material and Methods

TRE3G, in 450 μ l of Opti-MEM (Gibco, #31985070); whereas transfection mix B contained 30 μ l of transfection reagent XtremeGENE HP (Sigma-Aldrich, #6366236001) in 450 μ l of Opti-MEM. Single incubation for 5 minutes of each mix was followed by 20 minutes incubation of the joint solutions; hence, the transfection mix was added dropwise to 10 cm dish of HEK293T cells. A day later, we replaced the culture media with fresh one containing TET-free FBS, to avoid unscheduled transcription activation of Tet-ON promoter and recipient NIH3T3 duo cells were seeded with 60% confluence to be transduced on the next day. Finally, the media culture from donor HEK293T cells was cleaned out via 0.45 μ m filter and $\sim 3 \times 10^5$ NIH3T3 cells were co-transduced by adding 8 μ g/ml of Polybrene (Merck, #TR-1003-G) to the viral soups carrying regularly the transgene CMV-rtTA3 and, distinctly, each of the CMV-TRE3G- I-SceI constructs. Selective pressure was applied 2 days after the infection by adding to the media 10 μ g/ml of Blasticidin (Invivogen, #ant-bl-1) and 600 μ g/ml of G418 (Invivogen, #ant-gn-1), to favor the growth of cells carrying the integration of CMV-rtTA3 and CMV-TRE-I-SceI. Pools of polyclonal cells were frozen down 3 and 5 days after antibiotic selection. Finally a drop containing few cells was spread out in a 15 cm plate, thus we could derive monoclonal cell lines by colonies picking. Clones were selected based on the expression and nuclear localization of I-SceI, revealed by HA-immunostaining.

4.2.2 Generation of stable cells lines for the overexpression of mCherry-LacR-chromatin modifiers

4.2.2.1 Two steps cloning strategy

To assess whether changes in the chromatin status in proximity of a DSB might influence its motion properties, or its probability to fuse with another chromosome ends, we decided to employ artificial tethering of specific chromatin modifiers near to I-SceI-DSB. This can be achieved because in NIH3T3 duo cells, an I-SceI site is flanked by Lac operator repeated sequences which can be bound, with high affinity, by Lac Repressor, in absence of IPTG. Therefore, we have employed the LacO/LacR recognition system to target directly HDACs and HATs at DSB sites. Furthermore, cloning a fluorescent protein in frame with the LacR (e.g. GFP or mCherry) allows visualization of chromatin dynamics and organization of the genomic region where the LacO-I-SceI locus is integrated. Therefore, we decided to clone chromatin modifiers into a p-mCherry-C1 based vector (Clontech), where LacR was previously cloned at the C-terminus of mCherry coding region.

Then, we digested the vector by KpnI/BamHI and dephosphorylate by Alkaline Phosphatases as described above. Then, coding sequences of HDAC1, -2, -3 (humans) and HDAC1 WT and mutant (mouse), have been PCR amplified with oligos containing the KpnI and BamHI restriction sites, respectively at the forward and reverse primers. TIP60 WT and mutant (human), and GCN5 WT and mutant (mouse) were cloned with a similar strategy with the exception of KpnI and MfeI used as rescription enzymes for cloning the HAT enzymes in frame with mCherry-LacR. Template of the PCR

Material and Methods

reaction were pMSCVpuro-Gcn5 and pMSCVpuro-Gcn5 (D608A) (Addgene #63706 and # 63707) to get out respectively, GCN5 WT and the enzymatic dead mutant isoforms; Tip60 ORF was amplified from DNA vector pENTR223.1, belonging to “The ORFeome Collaboration” database (GenBank BC117167). Linearized vectors and PCR fragments were ligated by a quick ligation, carried out as aforesaid, and 4 µl of reaction were transformed into chemically competent Stbl3 cells; then, clones were selected in kanamycin-LB-agar plates. Site-specific mutagenesis was performed as described in paragraph to generate a catalytic dead mutant of mCherry-LacR-Tip60 fusion. Primers #61 and #62 were used to introduce point mutations at catalytic residues (Q377A and G380A) (Ikura et al. 2000).

Finally, to generate stable cell line carrying overexpression of mCherry-LacR-chromatin modifiers protein fusion, we sought to clone the chimeric constructs under the control of CMV promoter, into retroviral vectors pQCXIN and pQCXIP, which differ for the mammalian resistance gene, in fact they carry respectively neomycin and puromycin selective cassette. To do so, we proceeded as following:

- mCherry-LacR-hHDACs vectors were digested with AgeI and BamHI; same pair of enzymes was used to linearize the retroviral vector pQCXIP.
- mCherry-LacR-mHDACs (WT and mut) constructs were amplified with primers (#3 and #4) containing cut sites for NotI and BamHI; then, PCR products and pQCXIP were digested with the same enzymes pair and gel purified via QIAquick Gel Extraction Kit (Qiagen, #28706).
- mCherry-LacR-Tip60 (WT and Q377A,G380A mutant) and mCherry-LacR-GCN5 (WT and D608A mutant) vectors were digested by AgeI and MfeI, while pQCXIP was digested with AgeI and EcoRI. MfeI and EcoRI generate DNA ends, which are compatible during the ligation reaction.

Digested fragments were ligated into retroviral vectors, previously linearized with corresponding enzyme pairs. Upon isolation of positive colonies in Ampicillin-selective media, we confirmed the final vectors by restriction reaction (Figure appendix 2 and 3) and sequencing.

4.2.2.2 Infection with retroviral vectors to over-express mCherry-LacR-chromatin modifiers

Viral transduction was carried out as already described with the exception that Platinum-GP Packaging cell line (Plat GP) derived from HEK293T cell line was used as donor cell line for the production of retrovirus. Plat GP cells stably express gag and pol retroviral genes; therefore, together with 8 µg of vector carrying the transgene, cells were transfected with 2 µg of pVSVG vector expressing the envelop protein VSV-G. Then, NIH3T3 duo parental cell lines were virally transduced with pQCXIN vector and clones resistant to G418 (600 µg/ml) were selected. On the other hand, NIH3T3 duo cells expressing I-SceI upon Dox- stimulus were resistant to G418 (used to select clones with integration of Tet-ON-I-SceI constructs), therefore these cell line was transduced with pQCXIP-based vectors and puromycin selection (2 µg/ml, Invivogen, #ant-pr-1) was applied two days after the infection. Positive clones were

Material and Methods

screened based on mCherry nuclear intensity and, upon IPTG removal, on the ability to form a fluorescent spot, confirming binding of LacR to the Lac Operator repeats.

4.2.3 Cell Maintenance

NIH3T3 cells were cultured in Dulbecco's modified Eagle's medium (DMEM, Gibco, # 21969-035), supplemented with 10% Fetal Bovin Serum (Gibco, #16050-122), 2 mM L-glutamine (Gibco, #25030-024) and 100 U/ml penicillin – streptomycin mix (Gibco, #15140-122). NIH3T3 carrying Dox-tunable expression of I-SceI were cultured as the parental cell line with the exception of Tet-approved FBS usage (Biochrom, #S0115). NIH3T3 overexpressing LacR-constructs were cultured in media supplemented with 5 mM of Isopropyl β -D-1-thiogalactopyranoside (IPTG, Sigma-Aldrich, #I5502) which prevents LacR binding to lac operator repeated sequences and rulling out roadblocks for replication and transcription processes. U2OS cells, carrying the integration of LacO-I-SceI-TetO sequence at two different genomic locations, were cultured in DMEM, supplemented with 10% Fetal Bovin Serum, 2 mM L-glutamine and 100 U/ml penicillin – streptomycin mix, a short reselection of the cells was achieved using 200 μ g/ml of hygromycin. DIvA cells, a U2OS-derived cell line, is cultured with similar conditions. This cell line is generated from Legube and colleagues by stable tranfection of pBABE HA–AsiSI–ER (Iacovoni et al. 2010) and cultured in DMEM enriched with puromycin (1 μ g/ml), for clone selection's purpose. Similarly, AID-DIvA cells were transfected with AID-AsiSI-ER plasmid and positive cells were selected with G418 at a final concentration of 800 μ g/ml. HEK293T and Platinum Retroviral Packaging cells, Plat-GP (based on 293T cells) were grown in DMEM with 10% FBS, 2 mM L-glutamine and 100 U/ml of Pen/Strep and were used as donor cell line for lentiviral transduction. When at 80-90% confluency, HEK293T and PlatGP cells were diluted at 1:10 ratio; while NIH3T3 and U2OS-derived cells were split at 1:3 ratio. SKM-1 is a human myelodysplastic cell line, derived, in 1989, from the peripheral blood of a patient with acute monoblastic leukemia. SKM-1 cells were cultured in Roswell Park Memorial Institute (RPMI) 1640 media (Gibco, #21875-034) supplemented with 20% FBS, 2 mM L-glutamine and 100 U/ml of Pen/Strep mix. SKM-1 cells were passed every 2-3 days and maintained to a cell density of 0.5- 2 x 10⁶/ml. To assess modulators of etoposide-induced genome instability, we cultured and performed experiments in various adherent cells: U2OS, HeLa and Cal51 (grown in DMEM with 10% FBS, 2 mM L-glutamine and 100 U/ml of Pen/Strep) and HCT-116 cultured in RMP1 suplmented with 10% FBS, 2 mM L-glutamine and 100 U/ml of Pen/Strep. Two lymphoblastoid lines were also used in this study: TK6 cells (cultured in RPM1 media with 5% of Horse FBS, 1 mM sodium pyruvate, 2mM L-glutamine and 100 U/ml of Pen/Strep) and Jurkat cells (grown in RPM1 with 10% FBS, 2 mM L-glutamine and 100 U/ml of Pen/Strep). Finally, CD34 positive cells were isolated from peripheral blood of patients and maintained in IMDM media supplemented with the following cytokines: SCF 100 ng/mL, FLT3 50 ng/mL, TPO 50 ng/mL, IL3 20 ng/mL (Peprotech, 300-

Material and Methods

07, 300-19, 300-20, 200-03). A cell density of 0.5×10^6 cells/ mL was maintained. All cell lines were cultured at temperature of 37°C and atmosphere of 95% air and 5% CO₂.

4.2.4 Drug treatments

4.2.4.1 Induction and repair of DSBs

In Superduo cells, 4 µg/ml of doxycycline (Sigma-Aldrich, D9891) 1 mM of Shield1 (Takara/Clontech, #632189), were used to induce the expression of DD-I-SceI-GR fusion; then nuclear transfer was achieved via 5 µM of dexamethasone (Sigma-Aldrich, #D4902).

In DIvA and AID-DIvA systems, treatment with 300 nM of 4-Hydroxytamoxifen (4-OHT, Sigma-Aldrich, #H7904) allows AsiSI-dependent DSBs formation; time of treatment was assay-specific. Repair of DSBs was induced by degradation of AsiSI enzyme through auxin treatment (500 µg/ml final concentration, Sigma-Aldrich, #I5148), in AID-DIvA cell line.

etoposide (Sigma Aldrich, #E1383) was used as DNA damage agent in a variety of cell lines and therefore time and doses of treatments are cell lines- and assay- specific. To quantify etoposide-induced *MLL* translocations in SKM-1 cells, etoposide-induced DSBs were elicited upon 6h treatment with 10 µM of Top2 poison. To assess etoposide-induced DNA damage response, ETO was added for 4h at the final concentration of 10 µM in HCT and HeLa, 15 and 20 µM in MCF-7 and 10, 20 and 30 µM in CD34 positive cells, prior depletion of Top2A and Top2B levels. The role of transcription and replication processes in etoposide-induced damage was assessed in U2OS, challenged with 10 µM of etoposide for 30 min or 1 hour, 2 or 3 hours. The role of VCP and proteasome in etoposide-induced genome instability was assessed in U2OS and Cal51 with 3h treatment of etoposide at 5, 10 and 25 µM final, or TK6 challenged for 4h with 20 µM of Top2inhibitor. Cal51 cells were exposed for 3 hours to 50 and 100 µM final of etoposide, upon VCP knockdown.

4.2.4.2 Induction of chromatin domains

To induce tethering of mCherry-LacR-chromatin modifiers, IPTG was removed from the cell culture media by five washes with pre-warmed PBS. Already 12 hours later, binding of the Lac Repressor to the array is visible microscopically as a red spot.

4.2.4.3 Chemical Inhibitors

Histone deacetylases inhibition was carried out overnight by using Thricostatin A, TSA (3 µM, Cayman Chemicals, #Cay89730), and SAHA (5 µM, Cayman Chemicals, #Cay10009929), prior induction of I-SceI-DSBs in Superduo system. SKM-1 cells were released from etoposide in media supplemented with 250 nM or 500 nM of TSA or SAHA. For cell viability, 100 nM concentration was included in the assay.

Material and Methods

MS-275 (Cayman Chemicals, #13284) was also used at the final concentration of 100, 250 and 500 nM. Then, cell viability was checked 2 days later according to manufactures instructions (CellTiter-Blue® Cell Viability Assay, Promega #G8080).

DNAPKI inhibitors (NU7441, Selleckchem, #S2638) and decitabine (Cayman Chemicals, #Cay11166) have been used, respectively, as enhancer and suppressor of AsiSI induced –genome instability. Pretreatment for 1 hour with 5 μ M NU7441 and 2 μ M decitabine was carried out before eliciting AsiSI-nuclear transfer (adding 4-OHT to the cell culture media). 5-azacytidine (Cayman Chemicals, #Cay11164), analog of decitabine, was used at 2 μ M final dose.

To interfere with transcriptional process the following inhibitors were used as treatment prior etoposide incubation. Concentration and time of treatments were optimized. Finally, actinomycin D (Cayman Chemicals, #11421-5) was used at the final concentration of 100 μ M, 5,6-Dichlorobenzimidazole 1- β -D-ribofuranoside, DRB (Cayman Chemicals, #10010302-10) was used 200 μ M while triptolide (Sigma-Aldrich, #T3652) was used at the final concentration of 2 μ M. Inhibition of replication was achieved by pretreatment with 20 μ M of aphidicolin (Sigma-Aldrich, #A4487). Pretreatment with the indicated inhibitors was carried out 3 hours prior etoposide damage. Ongoing transcription and replication was monitored by quantifying the level of EU (5-Ethynyl Uridine) or EdU (5-Ethynyl-2'-deoxyuridine) incorporation. The uridine and thymidine analogs are added to cells 30 min or 10 min, respectively, prior fixation at the final concentration of 1 mM and 10 μ M, accordingly. Detection of EU and EdU was performed by click-labelling reaction of 488-fluoroazide, according to manufactures instructions (Click-iT™ RNA Alexa Fluor™ 488 Imaging Kit, Invitrogen #C10329; Click-iT™ EdU Alexa Fluor™ 488 Imaging Kit, Invitrogen #C10337).

Inhibition of VCP and proteasome system was achieved by 3 hours treatment prior etoposide incubation with 5 μ M of NMS-873 (Selleckchem, #S7285) and 2.5 μ M of MG132 (Sigma Aldrich, #M7449) in adherent cell lines. In TK6 cells, conditions of incubation are identical with the exception that 2.5 μ M of NMS-873 were used.

4.2.5 Immunofluorescence assay

Adherent cells were grown either on coverslips, or on 96- and 384- well microscopy plates (PerkinElmer, #6005550 and #6057300) and fixed with 4% paraformaldehyde (PFA, Sigma-Aldrich, #158127) for at least 10 minutes. Suspension cells were grown and treated in flasks, then transferred to poly-L-Lysine (PLL) -coated coverslips, or wells and, just prior fixation, cells were spun down by pulse centrifugation (normally 15 seconds at 400g). Then, for 20 minutes, PFA (8%) was added to a same volume of culture media in order to reach a final concentration of 4% PFA, upon 1:1 dilution. Residual PFA was washed out by three PBS cycles of 5 minutes each and lipid cell membrane permeabilization was achieved in 5 minutes by incubation with a detergent solution composed of 0.3% Triton in 1X PBS (Triton X100,

Material and Methods

Sigma-Aldrich, #T8787). After three PBS washes, permeabilized cells were incubated for 1h with PBS supplemented with 3% BSA (Sigma-Aldrich, #A3294), in order to block aspecific binding sites. Target-specific antibodies were also diluted in 3% BSA-PBS solution and incubation was carried out overnight at +4°C, or at least for a couple of hours at RT, in a humidified chamber. Then, 1h dark incubation with secondary antibodies followed by three cycles of PBS washing to remove unbound primary antibodies. Secondary antibodies solutions were also removed by three PBS washes and Hoechst 33342 (Molecular Probes, #H3570) at concentration of 5 µg/ml was used for DNA staining. After 10 minutes, microscopy plates were washed with PBS and ready for images acquisition. Coverslips specimens were inverted on microscopy glass slides (neoLab Migge GmbH, # 1-6274), where they were left to dry on few drops of Mowiol-DABCO solution. Antibodies used in immunofluorescence assays are listed below, in table 1.

Table 1 - Antibodies used in immunofluorescence

| PROTEIN TARGET | SUPPLIER | CATALOG NUMBER | DILUTION |
|--|-------------------|-------------------|----------|
| HA, RAT MONOCLONAL (3F10) | Roche | cat # 11867423001 | 1:500 |
| 53BP1, RABBIT POLYCLONAL | Novus Biologicals | cat # 100-304 | 1:2000 |
| PHOSPHO-H2A.X (SER139), MOUSE MONOCLONAL | Millipore | cat # 05-636 | 1:1000 |
| ACETYL-HISTONE H4 (PAN), RABBIT POLYCLONAL | Millipore | cat # 06-866 | 1:2000 |
| TOP2A (C-15), GOAT POLYCLONAL | Santa Cruz | cat # sc-5346 | 1:200 |
| TOP2B (H-286), RABBIT POLYCLONAL | Santa Cruz | cat # sc-13059 | 1:200 |
| ALEXA FLUOR 647 ANTI-RAT IGG, RAISED IN CHICKEN | Mol. Probes | cat # 21472 | 1:1000 |
| ALEXA FLUOR 568 ANTI-RABBIT IGG, RAISED IN GOAT | Life technologies | cat # A11011 | 1:1000 |
| ALEXA FLUOR 488 ANTI-RABBIT IGG, RAISED IN GOAT | Mol. Probes | cat # A11034 | 1:1000 |
| ALEXA FLUOR 568 ANTI MOUSE IGG, RAISED IN DONKEY | Mol. Probes | cat # A10037 | 1:1000 |
| ALEXA FLUOR 488 ANTI MOUSE IGG, RAISED IN DONKEY | Life technologies | cat # A21202 | 1:1000 |
| ALEXA FLUOR 568 ANTI GOAT IGG, RAISED IN DONKEY | Mol. Probes | cat # A11057 | 1:1000 |

4.2.6 Cytoskeletal extraction

To shed light on the role of specific factors in genome maintenance often it is useful to probe for the molecular pools of proteins in the vicinity of the DNA lesions, and therefore, associated with chromatin. Even in absence of DSBs, sometimes it becomes extremely convenient to isolate the chromatin-associated fraction when, for example, it is required to detect proteins, such as histone, that are tightly held to chromatin, but also they are found abundantly in the nucleoplasmatic fraction. A way to detect only the pool of protein tightly associated with chromatin is by washing out both the cytoplasmic portion and the loosely nuclear retained portion by Cytoskeletal (CSK) buffer supplemented with 0.1% Triton. Specifically before PFA fixation, cells were washed twice with cold PBS and with two extra washes of 1 minute with freshly prepared CSK buffer supplemented with protease inhibitors. Then, non-fixed cells were quickly incubated for 2 minutes with CSK buffer with 0.5% Triton and finally treated with 4% PFA, for 20 minutes. In case of pre-extracted cells, permeabilization was achieved with 0.5% of Nonidet-P40 (NP40). Following, we operated with a standard immunofluorescence protocol.

4.2.7 siRNAs knockdown

HDACs and VCP protein levels were tuned down via a double reverse transfection using 20 or 30 nM final of siRNAs and 2.5 μ l of transfection reagent (Dharmafect1), both diluted separately in 100 μ l each of Opti-MEM for 5 minutes. Then two mixes were joint together and incubated for 20 more minutes to allow the formation of RNA-containing lipo- based complexes which can melt with lipid bilayer of cellular membrane. Finally, 200 μ l of the final mix was added drop-wise to roughly 3×10^5 cells (NIH3T3 or Cal51) and media was exchanged at least six hours later. The amount of siRNAs was dependent on whether a second round of reverse transfection has followed (for NIH3T3 cells, then 20 nM siRNA) or not (for Cal51 cells, 30 nM), after 2 days from the first transfection. Experiments, or direct harvesting of cells, were carried out 24h later the second round of reverse transfection (or already 48 h after the single siRNAs transfection for Cal51 cells). All siRNAs were purchased from Dharmacon as SMARTpool ON-Targetplus. HeLa, HCT116, MCF-7 and U2OS were transfected with 30 nM of siRNAs against Top2A and Top2B for 72h, then cells were challenged with etoposide. Top2A and Top2B are validated selected siRNA purchased from Ambion, Life Technologies. Sequences of the siRNAs used in this thesis are reported in table 2. Knockdown efficiency was determined by Western blot analysis of protein levels.

Table 2 - siRNAs target sequences

| mRNA Target | target sequence | catalog number |
|-------------|--------------------------|------------------|
| non target | UGGUUUACAUGUCGACUAA | D-001810-10-05 |
| | UGGUUUACAUGUUGUGUGA | |
| | UGGUUUACAUGUUUUCUGA | |
| | UGGUUUACAUGUUUUCUA | |
| mHDAC1 | AUAAACGCAUUGCCUGUGA | L-040287-02-0005 |
| | UCAAGAAGAGGUCAAGUU | |
| | UGACCAACCAGAACACUAA | |
| | GAACUCUUCUAAUCUCAA | |
| mHDAC2 | CCAAUGAGUUGCCAUUAA | L-046158-02-0005 |
| | CAAUUGGCUGGAGGACUA | |
| | ACAGGAGACUUGAGGGUA | |
| | CAAAAGUGAUGGAGAUGUA | |
| mHDAC3 | GGGAAUGUGUUGAAUAUGU | L-043553-02-0005 |
| | CGGCAGACCUCCUGACGUA | |
| | AAGUUGAUGUGGAGAUUUA | |
| | GCACCCGCAUCGAGAAUCA | |
| mHDAC6 | GGAUGACCCUAGUGUAUUA | L-043456-02-0005 |
| | GCAGUUUGCGGUUGAGUAA | |
| | CUAAAUCAAGAUGGCUAA | |
| | UAAUGGAACUCAGCACAUA | |
| VCP | GCAUGUGGGUGCUGACUUA | L-008727-00-0005 |
| | CAAUUGGCUGGUGAGUCU | |
| | CCUGAUUGCUCGAGCUGUA | |
| | GUAAUCUCUUCGAGGUUA | |
| TOP2A | s: CAACUUGAUGUGCGUGAAAtt | S14309- ASO26WA3 |
| | as: UUCACGCACAUCAAGUUGgg | |
| TOP2B | s: GAGUGUACACUGAUUUAtt | S108-ASO26WA4 |
| | as: UUAUAUCAGUGUACACUCca | |

4.2.8 Silencing of Top2A and Top2B via shRNAs in CD34+

CD34+ cells were infected, according to protocol already described in paragraph 4.2.1.2, with lentiviral vectors encoding GFP-shRNAs for the two TOP2 isoforms. Specifically 2 shRNAs were used to induce silencing of Top2A and other 2 for Top2B targeting. After 5 days after transduction, etoposide treatment was performed. Vectors were purchased from OriGene, # # TR30023.

4.2.9 Western blot analysis

To evaluate knockdown efficiency and, consequently, to assess changes in the chromatin status, cells were harvested by trypsinization step or directly by cells scraping with cold PBS. A same number of cells was lysed on ice with a modified RIPA buffer (supplemented with a cocktail of protease inhibitors) and pulse-sonicated with 5 cycles (30 seconds ON, 30 seconds OFF). Because of the higher salt concentration (450 mM of NaCl, instead of 150 mM final concentration), a modified RIPA buffer should also bring in solution the tighter chromatin-bound protein fraction. Yet, assessing changes in the acetylation level of histone proteins was challenging. Therefore, the following modifications have been adopted: i) lysis buffer was supplemented with 5 mM of Sodium Butyrate, a potent HDACs inhibitor; ii) the cytoplasmatic fraction was removed from the total lysate by a CSK pre-extraction step, which was used to lyse the cells; iii) 1 hour of benzonase digestion of the nucleic acids was implemented to improve chromatin solubilization. In both cases, I proceeded with 15 minutes centrifugation (21,000 g, 4 °C), and clarified supernatants were collected and quantified by Bradford reagent (Quick Start™ Bradford 1X Dye Reagent, Biorad, #5000205). For Western blot inspection, between 10-15 µg of total protein lysates were pre-mixed with NuPAGE™ LDS sample buffer 4X (Thermo Scientific, # NP0007), supplemented with 1 mM of dithiothreitol (DTT), and boiled for 10 minutes at 90 °C. Then, protein samples were separated on precast gels with a polyacrylamide gradient 4%-15% for 1h at 135 V. Wet transfer on PVDF or Nitrocellulose membranes (for histone proteins) was performed at 200 mA constant for 1.5 hour. Non-specific sites were blocked by 30-60 minutes incubation with 5% milk dissolved in PBS, and then membranes were incubated overnight in a cold room with primary antibodies dilutions. Next day, three washes, with PBS-Tween 0.1% of 5 minutes each, preceded 1h incubation with secondary antibodies. Membranes were, then, washed three times with PBS-T and specific signals were detected by ECL-based chemiluminescence reagent containing a peroxidase's substrate (WesternBright™ Sirius, Advansta, #K-12043-D20 or SuperSignal™ West Pico PLUS Chemiluminescent Substrate, Thermo Scientific, #34577).

Protease inhibitors cocktail (cOmplete, EDTA-free, Sigma-Aldrich, #11873580001) was added in each lysis buffer; specifically, RIPA buffer consisted of 50 mM Tris-HCl pH 7.5, 150 mM NaCl, 1 mM EDTA, 1% NP-40, 0.1% Na-deoxycholate, then each lysate was supplemented with further 500 mM of NaCl to solubilize the chromatin bound fraction. CSK buffer was composed by 10 mM PIPES, 300 mM sucrose, 100 mM NaCl, 3 mM MgCl. All antibodies were diluted in blocking solution (5% milk-PBS), with the exception of unmodified histone H3 and antibodies against acetylated histones, for which BSA was utilized instead of milk and TBS is used as solvent.

Table 3 - Antibodies used in Western and dot blotting

| PROTEIN TARGET | SUPPLIER | CATALOG NUMBER | DILUTION |
|---|----------------------|-----------------|----------|
| HDAC1, RABBIT POLYCLONAL | Affinity Bioreagents | cat # PA1-860 | 1:1000 |
| HDAC2 (3F3), MOUSE MONOCLONAL | Upstate-Millipore | cat # 05814 | 1:1000 |
| HDAC3, MOUSE MONOCLONAL | Cell Signaling | cat # 3949 | 1:1000 |
| HDAC6 (D21B10), RABBIT POLYCLONAL | Cell signaling | cat # 7612 | 1:1000 |
| ACETYL K56-HISTONE H3, RABBIT POLYCLONAL | Millipore | cat # 07-677 | 1:1000 |
| ACETYL-HISTONE H4 (PAN), RABBIT POLYCLONAL | Millipore | cat # 06-866 | 1:1000 |
| ACETYL K16- HISTONE H4, RABBIT POLYCLONAL | Active Motif | cat # 39167 | 1:1000 |
| ACETYL K12- HISTONE H4, RABBIT POLYCLONAL | Abcam | cat # ab46983 | 1:1000 |
| HISTONE H3 (UNMODIFIED), RABBIT POLYCLONAL | Abcam | cat # ab1791 | 1:2000 |
| VCP, RABBIT POLYCLONAL | Cell Signaling | cat # 2648 | 1:500 |
| TOP2A (C-15), GOAT POLYCLONAL | Santa Cruz | cat # sc-5346 | 1:200 |
| TOP2B (A-12), MOUSE MONOCLONAL | Santa Cruz | cat # sc-365071 | 1:200 |
| DS-DNA [3519 DNA], MOUSE MONOCLONAL | Abcam | cat # ab27156 | 1:2000 |
| TUBULIN, MOUSE MONOCLONAL | Sigma-Aldrich | cat # T5168 | 1:5000 |
| VINCULIN, MOUSE MONOCLONAL | Sigma-Aldrich | cat # v9264 | 1:5000 |
| ANTI-MOUSE IGG, HRP-LINKED, RAISED IN HORSE | Cell Signaling | cat #7074 | 1:1000 |
| ANTI-RABBIT IGG, HRP-LINKED, RAISED IN GOAT | Cell Signaling | cat #7074 | 1:1000 |
| ANTI-GOAT IGG. HRP-LINKED, RAISED IN DONKEY | Santa Cruz | cat #sc-2056 | 1:1000 |

4.2.10 TOP2ccs detection assay

For isolation of TOP2ccs, a million of TK6 cells was directly lysed in 700 μ l of MB buffer (6M of GTC, 10 mM TrisCl pH 6.5 and 20 mM EDTA, 4% Triton, 1% Sarcosyl and 1% DTT) and incubated on ice for at least 5 minutes. A same volume of absolute ice cold EtOH was added to each sample and precipitation at max speed for at least 25 min allowed pelleting DNA and protein covalently bound to the DNA (DPC), while free proteins resided in the supernatant. At this point, the pellet was still not well visible, but it got clearer by washing twice with 1 ml of 75% EtOH. When most of EtOH is evaporated, DNA/DPC mixes were resuspended in 300 μ l supplemented with 8 mM of NaOH. Resuspension was carried overnight at 4 °C and yet for 2 hours at 37 °C, before quantification and loading on dotblot. dsDNA was measured by QUBIT (Qubit™ dsDNA HS Assay Kit, #Q32851) and 800 ng were spotted on Nylon membrane, positively charged or on Nitrocellulose membrane, previously equilibrated in 2XSSC. The amount of samples was diluted in a same volume among samples and each dilution was applied to a primed apparatus. When all samples run through the wells, membrane for dsDNA detection was incubated at 85 °C for 10 min in order to fix the free DNA. A blocking step was carried out and, then, same procedure for Western blot detection was followed.

4.2.11 Screening set up

NIH3T3 cells carrying the integration of LacO and TetO repeats (at density of 1×10^6 per reaction), were gently resuspended in 100 μ l of Amaxa kit R (Lonza, #VVCA-1001) and electroporated with 10 μ g of I-SceI vector using Nucleofector® 2b Device (Lonza, #AAB-1001). Several reactions were pooled together and released in media containing epigenetic inhibitors from Cayman library #Item No. 11076 at different concentrations, according to literature. One day later genomic DNA extraction was carried out and qPCR performed, as described in paragraph 4.2.12.

4.2.12 qPCR

To detect chromosome translocations between LacO and TetO repeats, genomic DNA was extracted from cells normally 24h after I-SceI transfection, by using DNeasy Blood & Tissue Kit (Qiagen, #69506), according to manufacturing conditions. Genomic DNA was eluted from column, in 50 μ l of NFW and diluted to 30 ng/ μ l. DNA was quantified by NanoDrop™ 2000 (Thermo Scientific). Because of the rare occurrence of chromosome translocations, ~60 ng of DNA were amplified for 45 cycles, via a 2-steps protocol, in a CFX96 Real-Time PCR Detection System (Bio-Rad). Oligos used to amplify LacO-TetO translocations are #267 and #247 from Table 7. Melting curve was used to check homogeneity of amplicons. Translocation frequencies were computed as fold change of Ct values between test conditions and a control sample from cells challenged with I-SceI digestion. 2 fold serial dilutions were used for standard curve and to correct for the efficiency of primers amplification. We used GAPDH as reference gene (oligos # 248 and #249) for normalization purpose and each sample was quantified in triplicate by using the Pfaffl equation:

$$E \text{ of LacO-TetO}^{-(Ct_{ctrl} - Ct_{test})} / E \text{ of GAPDH}^{-(Ct_{ctrl \text{ reference}} - Ct_{test \text{ reference}})}$$

where E is the amplification efficiency determined by the formula $E = 10^{-1/\text{slope of standard curve}}$

Components and conditions of PCR reaction are described in the following tables:

| Component of reaction | amount |
|------------------------------|-------------|
| SsoFast EvaGreen Supermix 2X | 10 μ l |
| Forward primer (10 μ M) | 1.5 μ l |
| Reverse primer (10 μ M) | 1.5 μ l |
| Genomic DNA ~60 ng | 2 μ l |
| NFW | 5 μ l |

| Step | Temperature | Time | |
|----------------------|-------------|--------|-----|
| Initial denaturation | 98 °C | 30 sec | |
| Denaturation | 98 °C | 10 sec | x45 |
| Annealing/Extension | 56.7 °C | 10 sec | |

Similarly as above, amplification of *mis12* locus is carried out using 60 ng of genomic DNA. Relative quantifications were computed by subtractions of Ct values from one of control sample (gnDNA of unchallenged cells, no inhibitors, no DSBs), then normalized on GAPDH DNA and corrected for the efficiency of amplification of primer pairs for *mis12* and *gapdh*, respectively # 1183-1184 and #564-

Material and Methods

565. All oligos sequences are listed in Table 7. Melting curves served to check amplicons specificity. Details of amplification cycles are given in the next table:

| Step | Temperature | Time | |
|----------------------|-------------|--------|-----|
| Initial denaturation | 95 °C | 2 min | |
| Denaturation | 95 °C | 5 sec | x45 |
| Annealing/Extension | 60 °C | 10 sec | |

4.2.13 Chromatin condensation assay

To address the induction of chromatin domains, we assessed the status of chromatin condensation as measure of a functional tethering of chromatin modifiers. NIH3T3, stably expressing mCherry-LacR-chromatin modifiers chimeric fusions, were seeded in microscopy plate upon removal of IPTG to allow binding of the LacR constructs to the LacO locus. Cells were then fixed after 16h, DNA staining was carried out as described in paragraph 4.2.5 and imaging of mCherry and DAPI channels were acquired by Leica AF7000 microscope. Images were exported as TIFF files for further image analysis. Through ImageJ software, ROIs were drawn for the LacO-LacR array (visible as a bright spot in the cell nucleus via microscope inspection of mCherry channel) and to delimitate the nucleus itself. Areas of the two objects were measured individually for each cell and the ratio of Spot/Nucleus was computed.

4.2.14 Chromatin enrichment or depletion of acetyl-histone marks measured by IF

To observe events of enrichment or depletion of acetyl-marks at the tethering site, we decided to exploit U2OS cells with a double integration of LacO-I-SceI-TetO, which consists of 10 Kbp tandem arrays of the Lac operator sequence, therefore the size of fluorescent spot can facilitate discern increase, decrease or no changes of acetyl marks signals at the array site. Thus, those cells were electroporated by Nucleofector™ Kit V (Lonza, #VCA-1003) and seeded in 96-well microscopy plate. Then, 12, 24 or 36 hours later, cells were treated with Cytoskeletal extraction (CSK) buffer, prior paraformaldehyde fixation. Then, immunofluorescence with H4panAc Ab was carried out as described in paragraph 4.2.5. Catalog number and dilution of the mentioned antibody are listed in table 1. Images were acquired by Opera Phenix System and exported through Harmony software as TIFF for further analysis. For analysis: a) enrichment events were scored as increased signals localizing at the array site; b) depletion of Ac-marks corresponded to a *lacuna* of the signal at the array site; c) no changes were scored when the acetyl mark-Ab did not show any difference in comparison with nuclear background levels at the array site.

4.2.15 Chromatin accessibility by Ligation-Mediated PCR

To verify the formation of chromatin domains, we decided to check I-SceI-accessibility to chromatin by monitoring the level of I-SceI-DSBs as readout of the assay. At least 18h before inducing I-SceI-DSBs, cells were transiently transfected by electroporation with 10 µg of vectors expressing mCherry-LacR, mCherry-LacR-mHDAC1 WT, mCherry-LacR-mHDAC1 mut, mCherry-LacR-hHDAC1, mCherry-LacR-hTip60. Doxycycline (4 µg/ml), Shield1 (1 mM) and dexamethasone (5 µM) were added, on the next day, for 12 hours; then, gnDNA was extracted from cells, quantified by Qubit dsDNA HS Assay Kit (Thermo Fisher, #Q32851), and aliquoted to preserve the overhang ends. Asymmetric oligos (#559 and #560) were phosphorylated and annealed in equimolar ratio, how previously described (Soutoglou et al. 2007; Lemaître et al. 2014) Then, oligo duplex was diluted 40 times (250 nM) and aliquots were cold stored. Ligation reaction was carried at RT for 1h in 30 µl final, using 600 ng of gnDNA and 3 µl of phosphorylated adaptor (25 nM final). Finally, the reaction was diluted 100 times in 300 µl final and 2 µl were used as template for the qPCR reaction. Primers designed on Lac operator sequence and on the ligated adaptor (# 250 and #571) allow quantifying double strand ends in Dox- and Dex- treated samples (cut), compared to untreated samples (uncut). Reaction components and cycles of amplification are identical the ones indicated in paragraph 4.2.12, with only one modification: plate reading was carried out after 5 seconds denaturation at 77 °C. Nonetheless time and concentration of oligo adaptors were titrated to reduce self-ligation of adaptors, the introduction of this small trick (5 seconds at 77 °C) before fluorescence reading, have allowed to reduce the quantification of concatamer molecules. GAPDH amplification was used as reference gene for normalization scope and each samples was quantified in triplicate as following:

$$E \text{ of LacO-LM-Adaptor}^{(Ct_{ctrl} - Ct_{test})} / E \text{ of GAPDH}^{(Ct_{ctrl \text{ reference}} - Ct_{test \text{ reference}})}$$

Because the efficiency of primers (calculated by 1 to 4 serial dilutions) was near 100% for both targets ($E_{test}=E_{gapdh}=2$), the above equation gets simplified according to the Livak method, which imply that the number of copies of PCR products doubles at each cycle of amplification, as following:

$$\begin{aligned} \text{Normalized ratio} &= 2^{(Ct_{ctrl} - Ct_{test})} / 2^{(Ct_{ctrl \text{ reference}} - Ct_{test \text{ reference}})} \\ &= 2^{\Delta Ct_{test}} / 2^{\Delta Ct_{gapdh}} \\ &= 2^{\Delta \Delta Ct} \end{aligned}$$

Oligos sequences used in this assay are listed in Table 7.

4.2.16 DSB Motion: experimental procedure and analysis

For live cell imaging, NIH3T3 cells were carefully washed from IPTG (5 PBS-washes) to allow the binding of the mCherry-LacR construct; then $\sim 3 \times 10^4$ cells were seeded in 8-wells plates (μ -Slide 8 Well high, Ibidi, #80806) and treated with TSA (3 μ M) or SAHA (5 μ M). Whereas, in case of HDACs depletion, NIH3T3 were transfected with siRNA for HDAC1, HDAC2 or both, as described in siRNA transfection section, and cultured them in presence of IPTG. Then, 18h before dox-I-SceI induction, binding of mCherry-LacR was triggered, and 300 μ l of cell suspension (1×10^5 /ml confluency) were seeded. In both cases, next day, DSBs were triggered by inducing I-SceI expression and nuclear transfer, adding 4 μ g/ml of doxycycline and dexamethasone (plus Shield-1 1 μ M), then 5-6 hours later images were acquired by using Visitron System, equipped with VisiView® Software. Briefly, 33 frames with a lag time of 15 seconds were acquired for 561 channel and brightfied. Specifically for the mCherry channel, 3 z-stacks, with 1 μ m of step size, were used for full detection of the nuclear volume. Importantly, LacO-I-SceI genomic locus, when bound with the mCherry-LacR construct, can be visualized microscopically as a spot, with fluorescent signal which raises over the background fluorescence representing unbound mCherry-LacR molecules. Analysis was carried out on maximal projected images and ROIs were generated around each cells, trough ImageJ software. On duplicated selected cell, stack registration was applied and TrackMate plugin was used to compute x and y coordinates for each centroid of defined spots. Specifically, ‘Dog Detector’, implemented in TrackMate, allows to quickly segmenting spots of small size (~ 5 pixels). For our purposes, the detection parameters were set to have 0.5 micron of blob diameter, and sub-pixel localization; according to the signal/noise intensity of each cell or conditions, threshold was set up to 2 to 8. Quality or mean intensity of spots were occasionally used to filters out false detected spots. Then x and y coordinates of selected spots, were tracked trough LAP tracker, which is a robust method to track single particles in live cell time lapse sequences (Jaqaman et al. 2008). Tracking happens in 2 steps: tracks segments are generated by frame to frame linking of spots, then, in case of missing detection in one frame, a linking “cost” (due to a gap-closing segment) is calculated which is proportional to the square distance between source and target spots. However, to calculate mean square displacement tracks, it was necessary to compute x and y positions of spots for each acquired frame, therefore in the analysis gap closing was not permitted. Then, through a customized script, mean square displacement (MSD) is calculated in batch from x and y positions of individual particle per ROI, detected in each lag time. Mean square displacement is defined as the squared distance traveled by the particle over time interval in 2D (d is calculated from x and y positions). Specifically, Δd^2 (μm^2) is a function of the time interval Δt (s): $\Delta d^2 = \{d(t) - d(t + \Delta t)\}^2$.

4.2.17 Fluorescent labelling of BAC probes

Bacterial Artificial Chromosomes (BACs), containing large portion of human genomic regions (~200 Kbp average size), were purchased by CHORI and the correct identity was confirmed by PCR. Specifically, two BACs per genomic location were chosen, spanning the 5'- and 3' of a translocating gene or upstream and downstream to a given AsiSI site. BACs minipreps were performed using ZR BAC DNA Miniprep Kit (Zymo Research, # D4048), while big preparations of BACs DNA were obtained with NucleoBond® Xtra BAC kit (Macherey-Nagel, 740436). Fluorescent labelling of BAC probes was achieved through incorporation of fluorophores-conjugated dUTPs, via a nick translation reaction performed according to kit's protocol (Abbott, #7J0001). This reaction combines DNase and DNA polymerase I activities to nick the DNA, remove nucleotides in 5'-3' directionality and elongate with fluorophores-conjugated dUTPs. Specifically, Chromatide AlexaFluor 488-5-dUTP, AlexaFluor 568-5-dUTP, AlexaFluor 647-AHA-dUTP (ThermoFisher Scientific, #C11397, #C11399, #A32763) are used to label BAC probes in Green, Red, and FarRed, correspondingly; while Blue-labelled probes were obtained through incorporation of CF405S-dUTP from Biotium (#40004). BAC probes used in this study are indicated in Table 4.

Table 4 - BAC probes

| GENOMIC REGION PROBED | BAC ID |
|-----------------------|-------------|
| DSB 1 - CENTROMERIC | RP11-262G14 |
| DSB 1 - TELOMERIC | RP11-760C24 |
| DSB 2 - CENTROMERIC | RP11-317N15 |
| DSB 2 - TELOMERIC | RP11-579E2 |
| DSB 3 - CENTROMERIC | RP11-790I23 |
| DSB 3 - TELOMERIC | RP11-719J20 |
| DSB 4 - CENTROMERIC | RP11-229D13 |
| DSB 4 - TELOMERIC | RP11-775H22 |
| DSB 5 - CENTROMERIC | RP11-16C18 |
| DSB 5 - TELOMERIC | RP11-107M17 |
| DSB 6 - CENTROMERIC | RP11-306G10 |
| DSB 6 - TELOMERIC | RP11-316L12 |
| DSB 7 - CENTROMERIC | RP11-107P18 |
| DSB 7 - TELOMERIC | RP11-457I18 |
| MLL-5' | CTD-2159M9 |
| MLL-3' | RP11-59N1 |
| AF4-5' | RP11-711J3 |

4.2.18 Fluorescence *In Situ* Hybridization (FISH)

For FISH experiments, cells were fixed according standard procedure described in previous section. Thus, cell permeabilization was carried out with 0.5% Saponin-0.5% Triton X-100 in PBS for 20 minutes, for suspension cells, whereas the incubation time was extended for 5 more minutes, for U2OS-derived cells. Upon 3 washes with PBS of 5 minutes each, 0.1M HCl was added for 15 minutes to allow denaturation of DNA double helix; then, a wash with 2X saline-sodium citrate (2X SSC) buffer was carried out for 10 minutes and finally cells were incubate for at least 30 minutes with 50% formamide/in 2XSSC.

For probe preparation, 80 ng of labelled-BAC DNA were mixed with 3 µg of COT1 human DNA (GeneON, #3001) and 20 µg of yeast tRNA (Thermo Fisher, #AM7118) and, consequently, ethanol-precipitated with 1/10 V of 3M NaOAc pH 5.3 and 2 volumes of ice cold absolute ethanol. Upon 20 minutes of centrifugation at maximum speed, pellet was dried in SpeedVac Vacuum Concentrators for a couple of minutes; then, resuspended in 7 µl (per coverslip), or 12 µl or 30 µl (per well of 384-well and 96-well plates, respectively) of hybridization buffer (10% dextran sulfate, 50% formamide, 2XSSC, and 1% Tween-20). Volumes and amounts are scaled-up according to the number of experimental samples. Finally, formamide-pretreated cells and FISH probes, dissolved in hybridization solution, are incubated together at 85 °C for 5 minutes (for coverslips) or 10 minutes (for microscopy plates); then hybridization is achieved during O/N incubation at 37 °C. Next day, the excess of fluorescent probes is diluted out with 2XSSC, and FISH samples are washed with gradually less stringent steps with pre-warmed 1XSSC buffer (three times) and 0.1X SSC (three times), heated up at 45 °C. For 96- or 384-well microscopy plates, DNA was stained by Hoechst33342 (Sigma-Aldrich) for 10 minutes, when a “Blue” FISH probe (CF405S-dUTP) was not included. Coverslips, instead, were mounted on microscopy slide by using Vectashield mounting medium, already containing DAPI (Vector Laboratories, H-1000), and sealed by picodent twinsil (Picodent, 1300 1000). Images of FISH samples were acquired by a spinning disk Opera Phenix High Content Screening System (PerkinElmer).

4.2.19 Imaging and image analysis

The Opera Phenix™ High Content Screening System (PerkinElmer) offers transmission illumination and four laser lines: 405 nm, 488 nm, 561 nm, 640 nm and emission filters can be chosen among the following range: (435 - 480) nm, (435 - 550) nm, (500 – 550) nm, (570 – 630) nm, (650 – 760) nm. The system hold 2 detectors, specifically two 16 bit sCMOS cameras and the Synchrony Optics which, combining a fast spinning microlens disc and the pinhole disc, allow imaging of fluorophores in the neighboring emission bands, reducing signals crosstalk, without compromising speed and sensitivity acquisition.

For imaging of FISH preparations, water 40X objective (N.A. 1.1) in confocal mode and camera with binning 2 were used. To detect the whole nuclear volume, and to not exclude detection of any FISH

Material and Methods

probes, 13 z-stacks with 0.5 μm step width were used for imaging SKM-1 cells; whereas FISH preparations of DIvA cells were imaged with 7 z-stacks of 0.6 μm step size. Then, Alexa 488, Alexa 568, Alexa 647 channels (500 ms, 100% laser power) were used for imaging 3-color FISH, while 4-color FISH was performed without DNA staining and 405-labelled probes were detected by using Turquoise channel (700 ms 100% laser power). At least 2000 DIvA cells or 7000 SKM1 cells per condition were imaged and analysed.

Immunofluorescence images were acquired either by the spinning disk Opera Phenix system, or by Operetta CLS High-Content Analysis System and or by widefield AF700 Leica microscope.

Features of the Opera Phenix microscope are described just above. The Operetta CLS High-Content Analysis System is, instead, a widefield microscope a laser-autofocus, a Xenon lamp (300W), a brightfield option (LED) and a 14-bit CCD camera, with 1.3 megapixel. Likewise, the Opera Phenix system, Operetta is fully automated and it is furnished with various filters to detect a wide spectrum from Alexa405/DAPI to Alexa647/DRAQ5.

The AF700 widefield system (Leica Biosystems) allows imaging with transmitted light or in fluorescence modality. Specifically, brightfield, phase contrast, differential interference contrast and polarisation contrast are methods for transmission light acquisition. To acquire in fluorescence mode, acquisition is performed by using the following filter cubes: A4/Blue; L5/Green; N3/Red; Y5/FarRed; TRI to use with a fast filter wheel, which allows fast multicolor imaging. Each filter cube is composed by an excitation filter, a dichroic mirror and an emission filter, which, correspondingly, allow band pass for selecting the excitation light, to filter the other emitted wavelengths and to emit fluorescence for the selected excited light. The CCD camera (Hamamatsu) is set up different field diaphragm (FD) sizes, defining the field of view and ensuring proper illumination. The microscope is equipped with LAS AF software (Leica Biosystems), which consents images visualization and saving the measurement in format (.lif) compatible for image analysis performed by using Image J software.

In case of high-throughput imaging by Opera, a 40X water objective NA 1.1 with camera binning of 2 (fitting 299 nm/pixel) served for images acquisition. mCherry and Alexa 647 lasers were excited for 200 ms (with 100% laser power), while, normally, Alexa 488 and HOECHST 33342 filters acquired for 60 ms exposure time with 50% of laser power. To image NIH3T3- derived cell lines 3 z stacks, with 1 μm of step width, were normally used. For images taken by the widefield AF700, we used a 63X immersion oil objective (NA 1.4) and A4, L5 and N3 filter cubes to acquire respectively DAPI, 488 and 568 fluorescences.

As image analyzer, Harmony® Software, version 4.8 (PerkinElmer) was used for quantification of fluorescence signals of images obtained with Opera Phenix system or Operetta microscope. Standard and customized building blocks allow analysis and quantification of the fluorescence intensity for the acquired channels in the measurement. Usually, nuclei were segmented based on Hoescht33342 signal

Material and Methods

of maximally projected images and using different algorithms and thresholds according to cell types. For instance, for U2OS and NIH3T3- derived cells were used method B, threshold 0.4 and object area $>130 \mu\text{m}^2$; whereas nuclei of suspension cells were detected by using method A, threshold 0.2 and object area $> 30 \mu\text{m}^2$. Nuclei at the border of field of acquisition are excluded from the analysis if not present as whole *objects*; this subpopulation is called “Nuclei Selected”. Number of spots and fluorescence intensities of a given channel are measured in the selected region of interest (Nuclei Selected). In immunofluorescence, spot detection of 53BP1 foci is achieved by “find spots” function and method B.

4.2.19.1 FISH image analysis

The entire methodology is based on high-throughput measurement of spatial distances among centroids of fluorescently labelled probes (which appears as spots) in interphase nuclei.

Briefly, in case of 4 colors FISH, nuclei segmentation was performed by using the background of FISH probe labelled employing 647-conjugated-dUTPs and method B allowed defining the following parameters: common threshold 0.57, object area $>130 \mu\text{m}^2$ splitting coefficient 10.6, individual threshold 0.40 and contrast > 0.04 .

FISH probes are visible in interphase nuclei as defined spots, which are detected via C algorithm with the following settings: radius ≤ 3.0 px, uncorrected spot threshold >1.0 , distance ≥ 2.7 px, spot peak radius 0.0 px. Contrast was set differently for each labelled probes:

| Channel | Green Spots-Alexa 488 | Red Spots-Alexa 568 | FarRed Spots-Alexa 647 | Blue Spots-Alexa 405 |
|---------|-----------------------|---------------------|------------------------|----------------------|
| Value > | 0.34 | 0.25 | 0.28 | 0.21 |

Euclidian distances in 3D were calculated between spot maximum points of each probe pairs. Defining distances in control cells enables us to set a threshold above which we identify breaks and, in the same nucleus, to screen for rare genomic rearrangements. Briefly, we utilize a pair of fluorescent probes labelled with 488 and 568 dUTPs (named “Green” and “Red”, respectively) across a breakpoint region and the distance among these, in unchallenged cells, defines the cut-off above which a DSB lies at that given genomic region (“Green” and “Red” spots are a-part).

The usage of a third and a fourth colored probes (labelled with 647-dUTP, “FarRed”, or with 405-dUTPs, “Blue”) allows to outline the 3’ and 5’ ends of a second chromosome region. We quantify translocations when two criteria are satisfied: in a given nucleus, (i) the genomic distances between Green-Red spots and between FarRed-Blue spots are above the threshold; (ii) the 5’ end of one locus lies in proximity of the 3’ end of the second chromosome region (with a distance lower than the cut off). Fine segmentation of the nuclear volume by imaging acquisition in Z-stacks mode allows to resolves distances in 3D which would be otherwise masked.

4.3. Supplementary methods

In this section experiments performed by and bioinformatics analysis by IMB Bioinformatics Core Facility are briefly described to complement methodologies relevant for the data presented in this dissertation.

4.3.1 ChIP-seq data analysis

Raw data of H3K56Ac, H4K12Ac, H4K16Ac and H2BK120Ub ChIP-seq were generated from a U2OS-derived cell line characterized by genotypic integration and expression of AsiSI-ER. Dataset (in Table 5) are public available and download from Array Express E-MTAB-5817. The bioinformatic analysis was performed following the methods described in (Clouaire et al. 2018).

Boxplots and heatmaps in Figure 29 are generated by quantifying the \log_2 ratio of reads count in cut vs uncut conditions ($\log_2(+4\text{OHT}/-4\text{OHT})$) in a window of $\pm 500\text{bp}$ centered on the AsiSI breaks site.

Table 5 – Public available datasets used in this study

| Source Name | Compound | Dose (nanomolar) | Immunoprecipitate | Data file |
|----------------|--------------------|------------------|---|-----------|
| H2BK120ac_mOHT | None | None | Anti-acetyl-Histone H2B (Lys120) Antibody (Millipore 07-564) | FASTQ |
| H2BK120ac_pOHT | 4-hydroxytamoxifen | 300 | Anti-acetyl-Histone H2B (Lys120) Antibody (Millipore 07-564) | FASTQ |
| H2BK120ub_mOHT | None | None | Ubiquityl-Histone H2B (Lys120) D11 (Cell signaling 5546) | FASTQ |
| H2BK120ub_pOHT | 4-hydroxytamoxifen | 300 | Ubiquityl-Histone H2B (Lys120) D11 (Cell signaling 5546) | FASTQ |
| H3K56ac_mOHT | None | None | Anti-Histone H3 (acetyl K56) antibody [EPR996Y] (Abcam ab76307) | FASTQ |
| H3K56ac_pOHT | 4-hydroxytamoxifen | 300 | Anti-Histone H3 (acetyl K56) antibody [EPR996Y] (Abcam ab76307) | FASTQ |
| H4K12ac_mOHT | None | None | Anti-Histone H4 (acetyl K12) antibody (Abcam ab46983) | FASTQ |
| H4K12ac_pOHT | 4-hydroxytamoxifen | 300 | Anti-Histone H4 (acetyl K12) antibody (Abcam ab46983) | FASTQ |
| H4K16ac_mOHT | None | None | Anti-acetyl-Histone H4 (Lys16) Antibody (Millipore 07-329) | FASTQ |
| H4K16ac_pOHT | 4-hydroxytamoxifen | 300 | Anti-acetyl-Histone H4 (Lys16) Antibody (Millipore 07-329) | FASTQ |

4.3.2 DSB repair kinetics by sBLISS

U2OS cells expressing AID-AsiSI-ER were treated with 300nM final concentration of 4-OHT for 4h, then IAA was added or not for 15 min, 30 min, 60 min or 120 min at the final concentration of 500ng/ μl . sBLISS was performed as described in (Bouwman et al. 2020), with the exception that A-tailing reaction

Material and Methods

was performed after blunting of DNA DSB ends in fixed nuclei. A-tailing was carried out using Klenow Fragment (3'→5' exo-, NEB #M0212), at 37 °C for 1 h and 300 rpm. Consequently, DNA DSB-end labelling was achieved using sBLISS linkers containing one thymine overhang at the 3' end of the reverse oligo. Downstream steps were carried out with 150 ng of DNA template input from each sample. Sequencing data processing was carried out as previously described using BlissNP (Bouwman et al. 2020; Gothe et al. 2019).

4.3.2.1 AsiSI-DSB repair kinetics - model

Modeling of AsiSI-DSBs was carried as described in (Metzger and Iliakis 1991), according to the following equation:

$$\text{FAR} = A \times 10^{-at} + B \times 10^{-bt}$$

FAR corresponds to the number of residual breaks at any time. In the initial work, they measured DSB repair, through an asymmetric field inversion gel electrophoresis technique, where the amount of DNA ¹⁴C-labelled released during electrophoresis was used as measure of residual DSBs at given time.

Then, the parameters indicate: A is number of breaks at a given AsiSI site at 0 min; *a* is the rate at which the fast component repair the breaks; B is number of breaks at a given AsiSI site at 60 min; *b* is the rate at which the slow component repair the breaks. For each AsiSI-DSB it has been evaluated how much *a* component describe the number of breaks for that given site. Then, all DSBs have been ranked according to their *a* parameter and the top 50% are the ones repaired mainly according to the fast component.

Material and Methods

Table 6 - Plasmids used in this study

| #Roukos Lab database | Vector Name | Source | Purpose |
|----------------------|---|------------------------|---|
| 21 | pMDLg/pRRE | Addgene #12251 | packaging vectors for viral production (Gifts from Holger Richly) |
| 22 | pRSV-REV | Addgene #12253 | |
| 23 | pMD2.G | Addgene #12259 | |
| 108 | pVSG | | pacakaging vector for viral production |
| 6 | pLenti CMV rtTAE3 Blast (w756-1) | Addgene #26429 | Tetracycline repressor A3 mutant |
| 1 | pENTR1A | Addgene #17398 | |
| 2 | pLentiCMV Tre 3G Neo Dest | Eric Campeau | TetON-promoter |
| / | pLVX-PTuner | Clontech #632173 | amplify DD |
| / | I-SceI-GR-RFP | Addgene #17654 | amplify GR and I-SceI |
| / | pCDH-CuO-AID-HANLSISceI-EF1-CymR-T2A-Puro | Roukos Lab | amplify AID |
| 38 | HA_GR_I-SceI_DD_inpLenti CMVTre3GNeo | Roukos Lab, this study | Dox- inducible I-SceI degran |
| 39 | HA_DD_I-SceI_GR_inpLentiCMVTre3GNeo | | |
| 40 | HA_GR_I-SceI_AID_inpLentiCMVTre3GNeo | | |
| 41 | HA_AID_I-SceI_GR_inpLentiCMVTre3GNeo | | |
| 121 | pEGFP_HA2nls_I-SceI | | I-SceI-DSBs in GFP + cells |
| 25 | pMSCVpuro-Gcn5(D608A) | Addgene 63707 | amplify GCN5 WT and mut |
| 26 | pMSCVpuro-Gcn5 | Addgene 63706 | |
| 14 | mCherryLacRNLS_hHDAC1 | Roukos Lab, this study | Chromatin Modifiers are in frame with mCherryLacR |
| 15 | mCherryLacRNLS_hHDAC2 | | |
| 16 | mCherryLacRNLS_hHDAC3 | | |
| 17 | mCherryLacRNLS_mHDAC1 wt | | |
| 18 | mCherryLacRNLS_mHDAC1 mutant | | |
| 32 | mCherryLacR_nls_Tip60 wt | | |
| 35 | mCherryLacR_nls_STOPfixed | | |
| 52 | mCherryLacR-nls-TIP60 (Q377A and G380A) | | |
| 54 | mCherryLacR-nls-GCN5 wt | | |

Material and Methods

| | | | |
|------------|--|------------------------|---|
| 55 | mCherryLacR-nls-GCN5 (D608A) | | |
| 98 | pQCXIP_mCherryLacR_hHDAC2 | | |
| 99 | pQCXIP_mCherryLacR_hHDAC3 | | |
| 100 | pQCXIP_mCherryLacR_mHDAC1 wt | | |
| 101 | pQCXIP_mCherryLacR_mHDAC1 mutant | | |
| 102 | pQCXIP_mCherryLacR_TIP60 wt | Roukos Lab, this study | to generate stable cell lines overexpressing mCherry-LacR-chromatin modifiers |
| 103 | pQCXIP_mCherryLacR_TIP60 (Q377A and G380A) | | |
| 104 | pQCXIP_mCherryLacR_mGC5 wt | | |
| 105 | pQCXIP_mCherryLacR_mGCN5 (D608A) | | |
| 106 | pQCXIP_mCherryLacR_hHDAC1 | | |
| 107 | pQCXIP_mCherryLacRSTOP | | |
| 283 | pGFP-C-shLenti TOP2A TL308699A | | |
| 285 | pGFP-C-shLenti TOP2A TL308699C | OriGene - TL308699C | |
| 287 | pGFP-C-shLenti TOP2B TL308698A | OriGene - TL308698A | to transduce dsCD34 + cells and induce silencing of Top2A and Top2B isoforms |
| 289 | pGFP-C-shLenti TOP2B TL308698C | OriGene - TL308698C | |
| 291 | pGFP-C-shLenti scramble | OriGene | |

Material and Methods

Table 7 - Oligos sequence used in this study

| # Roukos Lab database | Primer ID | Primer Sequence | purpose |
|-----------------------|----------------------|--|---|
| 3 | F_NotI_mChLacmHDAC1 | GCGCGCGGCCGCCCATGGTGTAGCAAGGGCGAGG | |
| 4 | R_BamHI_mChLacmHDAC1 | GCG CGG ATC CTC AGG CCA ACT TGA CCT C | cloning mHDAC1_wt&mut in pQCXIN vector |
| 11 | F_1a_Vec-GR | cagtcgactggatccggtacCATGTACCGGGTATCGGA | |
| 12 | R_1a_I-SceI-GR | GTT TTT CAT GCC AGC ACT AGC TGA TCT AGA TCC GGT GGA TCC AAA | to amplify GR, downstream vec- KpnI |
| 13 | F_1b_GR-I-SceI | CCGGATCTAGATCAGCTAGTGTGGCATGAAAAACATCAAAAAAACAG | |
| 14 | R_1b_DD-I-SceI | CCT GCA CTC CCA TGC CAG CAC TAG CTG ATT TCA GGA AAG TTT CGG AGG AG | to amplify I-SceI, upstream of DD |
| 15 | F_1c_I-SceI-DD | GAAATCAGCTAGTGTGGCATGGGAGTGCAGGTGGAAACCATCTCCCCAG- | |
| 16 | R_1c_Vec-DD | AAG AAA GCT GGG TCT AGA TTC ATT CCG GTT TTA GAA GCT CCA CAT CG | to amplify DD with I-SceI upstream |
| 17 | F_2a_Vec-DD | caattcagtcgactggatccggtacCATGGGAGTGCAGGTGGAAACCATC | |
| 18 | R_2a_I-SceI-DD | GTT TTT CAT GCC AGC ACT AGC TGA TTC CGG TTT TAG AAG CTC CAC ATC | to amplif DD with I-SceI downstream |
| 19 | F_2b_DD-I-SceI | CCGGAATCAGCTAGTGTGGCATGAAAAACATCAAAAAAAC | |
| 20 | R_2b_GR-I-SceI | CCC GCG GTA GCC AGC ACT AGC TGA TTT CAG GAA AGT TTC GGA GG | to amplify I-SceI, downstream of DD |
| 21 | F_2c_I-SceI-GR | CCTGAAATCAGCTAGTGTGGCTACCGGGTATCGGAAATGTCTTC | |
| 22 | R_2c_Vec-GR | AGA AAG CTG GGT CTA GAT TCA TCT AGA TCC GGT GGA TCC AAA TTT TTG | to amplify GR then EcoRV-vec |
| 23 | R_3b_AID-I-SceI | CGA CAC TGC CCA TGC CAG CAC TAG CTG ATT TCA GGA AAG TTT CGG AG | to amplify I-SceI, upstream AID, use with FW #13 |
| 24 | F_3c_AID-Vec | CTTTCCTGAAATCAGCTAGTGTGGCATGGGAGTGTGAGCTGAATCT | |
| 25 | R_3c_Vec-AID | CAA GAA AGC TGG GTC TAG ATT CAA GCT CTG CTC TTG CAC TTC TC | to amplify AID, upstream vec |
| 26 | F_4a_Vec-AID | gtcgactggatccggtacCATGATGGGAGTGTGAGCTGAATC | |
| 27 | R_4a_I-SceI-AID | GTT TTT CAT GCC AGC ACT AGC TGA AGC TCT GCT CTT GCA CTT CTC CAT C | to amplify AID, upstream I-SceI |
| 28 | F_4b_AID-I-SceI | GAGCAGAGCTCAGCTAGTGTGGCATGAAAAACATCAAAAAAAC | to amplify I-SceI, upstream GR, use with RV #20 |
| 41 | For_LacR_seq | CAA ACA GGA TTT TCG CCT GC | sequencing |
| 42 | Rev_pQCXIN_seq | GCT TCC AGA GGA ACT GCT T | sequencing pQCXIN |

Material and Methods

| | | | |
|-------------|------------------------------------|---|--|
| 47 | For_KpnI-HA-KpnI | CATGtaccatcacgatgttctgactatgCGGTAC | |
| 48 | Rev_KpnI-HA-KpnI | CCGCATAGTCAGGAACATCGTATGGGTACATGGTAC | oligo to insert HA tag upstream GR-IsceI-degradation constructs |
| 49 | F_pENTR1A_Seq | TAA ACT GCC AGG CAT CAA ACT | sequencing pENTR1A |
| 57 | F_C2_pENTR1A_extraG_mut | GAC TAT GCG GGT ACC ATG GGA GTG CAG GTG GAA ACC | to insert an extra G in DD-IsceI-GR construct |
| 58 | R_C2_pENTR1A_extraG_mut | GGT TTC CAC CTG CAC TCC CAT GGT ACC CGC ATA GTC | |
| 61 | F_Tip60_Q377A_G380A | GCC TCC CTA CGC GCG CCG GGC CTA CGG CAA GC | to build TIP60 catalytic mutant |
| 62 | R_Tip60_Q377A_G380A | GCT TGC CGT AGG CCC GGC GCG CGT AGG GAG GC | |
| 246 | LacO FW | 5'-GCCACATGTGGAATTGTG-3' | LacO-TetO translocations |
| 247 | TetO RV | 5'-TCGACTTTCACCTTTCTCTAT-3' | |
| 248 | GAPDH FW | 5'-GGGGCTGGCATTGCTCTCAATGA-3' | reference locus in murine cell line |
| 249 | GAPDH RV | 5'-TCAGGTTTCCATCCCCACATACCA-3' | |
| 250 | LM-IsceI | 5'-CATCCTACATCGTAGTGATGC-3' | LM-PCR at LacO-I-IsceI locus |
| 571 | Lacrepeats_Soutoglou_Dorn_Sengupta | TGTGGAATTGTGAGGGGATA | |
| 559 | adaptator 1 LMPCR | gcatcactacgatgtaggatg | ligatable oligos at LacO-I-IsceI broken locus |
| 560 | adaptator 2 LMPCR | catcctacatcgtagtgatgcttat | |
| 1183 | MIS12 FW | GACTGGCATAAGCGTCTTCG | to monitor DSB induction at mis12 locus |
| 1184 | MIS12 RV | CGGCTTGATCAGTATTTGCCG | |
| 864 | GAPDH-ie-1 FW | gggaggtagagggtgatgt | reference locus in human cell line |
| 865 | GAPDH-ie-1 RV | GAGGCAGGGATGATGTTCTG | |

Chapter 5 – References

- Adimoolam, Shanthi, Mint Sirisawad, Jun Chen, Patti Thiemann, James M. Ford, and Joseph J. Buggy. 2007. “HDAC Inhibitor PCI-24781 Decreases RAD51 Expression and Inhibits Homologous Recombination.” *Proceedings of the National Academy of Sciences* 104 (49): 19482–87. <https://doi.org/10.1073/pnas.0707828104>.
- Aguilera, Andrés, and Belén Gómez-González. 2017. “DNA-RNA Hybrids: The Risks of DNA Breakage during Transcription.” *Nature Structural and Molecular Biology* 24 (5): 439–43. <https://doi.org/10.1038/nsmb.3395>.
- Aguilera, Andrés, and Pablo Huertas. 2003. “Cotranscriptionally Formed DNA:RNA Hybrids Mediate Transcription Elongation Impairment and Transcription-Associated Recombination.” *Molecular Cell* 12 (3): 711–21. <http://www.ncbi.nlm.nih.gov/pubmed/14527416>.
- Aguzzi, Adriano, and Matthias Altmeyer. 2016. “Phase Separation: Linking Cellular Compartmentalization to Disease.” *Trends in Cell Biology* 26 (7): 547–58. <https://doi.org/10.1016/j.tcb.2016.03.004>.
- Albuquerque, Claudio P., Guoliang Wang, Nancy S. Lee, Richard D. Kolodner, Christopher D. Putnam, and Huilin Zhou. 2013. “Distinct SUMO Ligases Cooperate with Esc2 and Slx5 to Suppress Duplication-Mediated Genome Rearrangements.” *PLoS Genetics* 9 (8). <https://doi.org/10.1371/journal.pgen.1003670>.
- Albuquerque, Claudio Ponte De, Jason Liang, Nathaniel James Gaut, and Huilin Zhou. 2016. “Molecular Circuitry of the SUMO (Small Ubiquitin-like Modifier) Pathway in Controlling Sumoylation Homeostasis and Suppressing Genome Rearrangements.” *Journal of Biological Chemistry* 291 (16): 8825–35. <https://doi.org/10.1074/jbc.M116.716399>.
- Allfrey, V. G., R Faulkner, and A E Mirsky. 1964. “Acetylation and Methylation of Histones and their possible role in the regulation of RNA synthesis.” *Proceedings of the National Academy of Sciences* 51 (5): 786–94. <https://doi.org/10.1073/pnas.51.5.786>.
- Amaral, Nuno, Taehyun Ryu, Xiao Li, and Irene Chiolo. 2017. “Nuclear Dynamics of Heterochromatin Repair.” *Trends in Genetics* 33 (2): 86–100. <https://doi.org/10.1016/j.tig.2016.12.004>.
- Arab, Khelifa, Emil Karaulanov, Michael Musheev, Philipp Trnka, Andrea Schäfer, Ingrid Grummt, and Christof Niehrs. 2019. “GADD45A Binds R-Loops and Recruits TET1 to CpG Island Promoters.” *Nature Genetics* 51 (2): 217–23. <https://doi.org/10.1038/s41588-018-0306-6>.
- Aten, Jacob A. 2004. “Dynamics of DNA Double-Strand Breaks Revealed by Clustering of Damaged Chromosome Domains.” *Science* 303 (5654): 92–95. <https://doi.org/10.1126/science.1088845>.
- Aymard, François, Marion Aguirrebengoa, Emmanuelle Guillou, Biola M Javierre, Beatrix Bugler, Vincent Rocher, Jason S Iacovoni, et al. 2017. “Genome-Wide Mapping of Long-Range Contacts Unveils Clustering of DNA Double-Strand Breaks at Damaged Active Genes.” *Nature Publishing Group* 24 (4): 353–61. <https://doi.org/10.1038/nsmb.3387>.
- Aymard, François, Beatrix Bugler, Christine K. Schmidt, Emmanuelle Guillou, Pierre Caron, Sébastien Briois, Jason S. Iacovoni, et al. 2014. “Transcriptionally Active Chromatin Recruits Homologous Recombination at DNA Double-Strand Breaks.” *Nature Structural and Molecular Biology* 21 (4): 366–74. <https://doi.org/10.1038/nsmb.2796>.
- Baarlink, Christian, Matthias Plessner, Alice Sherrard, Kohtaro Morita, Shinji Misu, David Virant, Eva Maria Kleinschmitz, et al. 2017. “A Transient Pool of Nuclear F-Actin at Mitotic Exit Controls Chromatin Organization.” *Nature Cell Biology* 19 (12): 1389–99. <https://doi.org/10.1038/ncb3641>.
- Baldeyron, Céline, Gaston Soria, Danièle Roche, Adam J.L. Cook, and Geneviève Almouzni. 2011. “HP1 α Recruitment to DNA Damage by P150CAF-1 Promotes Homologous Recombination Repair.” *Journal of Cell Biology* 193 (1): 81–95. <https://doi.org/10.1083/jcb.201101030>.

References

- Barlow, Jacqueline H, Robert B. Faryabi, Elsa Callén, Nancy Wong, Amy Malhowski, Hua Tang Chen, Gustavo Gutierrez-Cruz, et al. 2013. "Identification of Early Replicating Fragile Sites That Contribute to Genome Instability." *Cell* 152 (3): 620–32. <https://doi.org/10.1016/j.cell.2013.01.006>.
- Belin, Brittany J., Terri Lee, and R. Dyche Mullins. 2015. "DNA Damage Induces Nuclear Actin Filament Assembly by Formin-2 and Spire-1/2 That Promotes Efficient DNA Repair." *ELife* 4 (AUGUST2015): 1–16. <https://doi.org/10.7554/eLife.07735>.
- Belmont, Andrew S., Gang Li, Gail Sudlow, and Carmen Robinett. 1999. "Visualization of Large-Scale Chromatin Structure and Dynamics Using the Lac Operator/Lac Repressor Reporter System." *Methods in Cell Biology* 58 (58): 203–22. [https://doi.org/10.1016/s0091-679x\(08\)61957-3](https://doi.org/10.1016/s0091-679x(08)61957-3).
- Bennardo, Nicole, Anita Cheng, Nick Huang, and Jeremy M. Stark. 2008. "Alternative-NHEJ Is a Mechanistically Distinct Pathway of Mammalian Chromosome Break Repair." *PLoS Genetics* 4 (6). <https://doi.org/10.1371/journal.pgen.1000110>.
- Berger, Michael F., Michael S. Lawrence, Francesca Demichelis, Yotam Drier, Kristian Cibulskis, Andrey Y. Sivachenko, Andrea Sboner, et al. 2011. "The Genomic Complexity of Primary Human Prostate Cancer." *Nature* 470 (7333): 214–20. <https://doi.org/10.1038/nature09744>.
- Bergink, Steven, Tim Ammon, Maximilian Kern, Lothar Schermelleh, Heinrich Leonhardt, and Stefan Jentsch. 2013. "Role of Cdc48/P97 as a SUMO-Targeted Segregase Curbing Rad51-Rad52 Interaction." *Nature Cell Biology* 15 (5): 526–32. <https://doi.org/10.1038/ncb2729>.
- Bertos, Nicholas R., Benoit Gilquin, Gordon K.T. Chan, Tim J. Yen, Saadi Khochbin, and Xiang Jiao Yang. 2004. "Role of the Tetradecapeptide Repeat Domain of Human Histone Deacetylase 6 in Cytoplasmic Retention." *Journal of Biological Chemistry* 279 (46): 48246–54. <https://doi.org/10.1074/jbc.M408583200>.
- Bhaskara, Srividya, Brenda J. Chyla, Joseph M. Amann, Sarah K. Knutson, David Cortez, Zu Wen Sun, and Scott W. Hiebert. 2008. "Deletion of Histone Deacetylase 3 Reveals Critical Roles in S Phase Progression and DNA Damage Control." *Molecular Cell* 30 (1): 61–72. <https://doi.org/10.1016/j.molcel.2008.02.030>.
- Bhaskara, Srividya, Vincent Jacques, James R. Rusche, Eric N. Olson, Bradley R. Cairns, and Mahesh B. Chandrasekharan. 2013. "Histone Deacetylases 1 and 2 Maintain S-Phase Chromatin and DNA Replication Fork Progression." *Epigenetics & Chromatin* 6 (1): 27. <https://doi.org/10.1186/1756-8935-6-27>.
- Bhaskara, Srividya, Sarah K. Knutson, Guochun Jiang, Mahesh B. Chandrasekharan, Andrew J. Wilson, Siyuan Zheng, Ashwini Yenamandra, et al. 2010. "Hdac3 Is Essential for the Maintenance of Chromatin Structure and Genome Stability." *Cancer Cell* 18 (5): 436–47. <https://doi.org/10.1016/j.ccr.2010.10.022>.
- Bickmore, Wendy A., and Peter Teague. 2002. "Influences of Chromosome Size, Gene Density and Nuclear Position on the Frequency of Constitutional Translocations in the Human Population." *Chromosome Research* 10 (8): 707–15. <https://doi.org/10.1023/A:1021589031769>.
- Blattmann, Claudia, Susanne Oertel, Volker Ehemann, Markus Thiemann, Peter E. Huber, Marc Bischof, Olaf Witt, et al. 2010. "Enhancement of Radiation Response in Osteosarcoma and Rhabdomyosarcoma Cell Lines by Histone Deacetylase Inhibition." *International Journal of Radiation Oncology Biology Physics* 78 (1): 237–45. <https://doi.org/10.1016/j.ijrobp.2010.03.010>.
- Bolden, Jessica E., Melissa J. Peart, and Ricky W. Johnstone. 2006. "Anticancer Activities of Histone Deacetylase Inhibitors." *Nature Reviews Drug Discovery* 5 (9): 769–84. <https://doi.org/10.1038/nrd2133>.
- Boom, Johannes van den, and Hemmo Meyer. 2018. "VCP/P97-Mediated Unfolding as a Principle in Protein Homeostasis and Signaling." *Molecular Cell* 69 (2): 182–94.

References

- <https://doi.org/10.1016/j.molcel.2017.10.028>.
- Boom, Johannes van den, Markus Wolf, Lena Weimann, Nina Schulze, Fanghua Li, Farnusch Kaschani, Anne Riemer, et al. 2016. "VCP/P97 Extracts Sterically Trapped Ku70/80 Rings from DNA in Double-Strand Break Repair." *Molecular Cell* 64 (1): 189–98. <https://doi.org/10.1016/j.molcel.2016.08.037>.
- Bouwman, Britta A.M., Federico Agostini, Silvano Garnerone, Giuseppe Petrosino, Henrike J. Gothe, Sergi Sayols, Andreas E. Moor, et al. 2020. "Genome-Wide Detection of DNA Double-Strand Breaks by in-Suspension BLISS." *Nature Protocols* 15 (12): 3894–3941. <https://doi.org/10.1038/s41596-020-0397-2>.
- Branco, Miguel R, and Ana Pombo. 2006. "Intermingling of Chromosome Territories in Interphase Suggests Role in Translocations and Transcription-Dependent Associations." Edited by Peter Becker. *PLoS Biology* 4 (5): e138. <https://doi.org/10.1371/journal.pbio.0040138>.
- Braunstein, Miriam, Alan B. Rose, Scott G. Holmes, C. David Allis, and James R. Broach. 1993. "Transcriptional Silencing in Yeast Is Associated with Reduced Nucleosome Acetylation." *Genes and Development* 7 (4): 592–604. <https://doi.org/10.1101/gad.7.4.592>.
- Brownell, James E., Jianxin Zhou, Tamara Ranalli, Ryuji Kobayashi, Diane G. Edmondson, Sharon Y. Roth, and C. David Allis. 1996. "Tetrahymena Histone Acetyltransferase A: A Homolog to Yeast Gcn5p Linking Histone Acetylation to Gene Activation." *Cell* 84 (6): 843–51. [https://doi.org/10.1016/S0092-8674\(00\)81063-6](https://doi.org/10.1016/S0092-8674(00)81063-6).
- Burgess, Rebecca C., Bharat Burman, Michael J. Kruhlak, and Tom Misteli. 2014. "Activation of DNA Damage Response Signaling by Condensed Chromatin." *Cell Reports* 9 (5): 1703–18. <https://doi.org/10.1016/j.celrep.2014.10.060>.
- Burman, Bharat, Zhuzhu Z. Zhang, Gianluca Pegoraro, Jason D. Lieb, and Tom Misteli. 2015. "Histone Modifications Predispose Genome Regions to Breakage and Translocation." *Genes and Development* 29 (13): 1393–1402. <https://doi.org/10.1101/gad.262170.115>.
- Canela, Andres, Yaakov Maman, Shar yin N. Huang, Gordana Wutz, Wen Tang, Guido Zagnoli-Vieira, Elsa Callen, et al. 2019. "Topoisomerase II-Induced Chromosome Breakage and Translocation Is Determined by Chromosome Architecture and Transcriptional Activity." *Molecular Cell* 75 (2): 252-266.e8. <https://doi.org/10.1016/j.molcel.2019.04.030>.
- Canela, Andres, Yaakov Maman, Seolkyoung Jung, Nancy Wong, Elsa Callen, Amanda Day, Kyong-Rim Kieffer-Kwon, et al. 2017. "Genome Organization Drives Chromosome Fragility." *Cell* 170 (3): 507-521.e18. <https://doi.org/10.1016/j.cell.2017.06.034>.
- Canela, Andres, Sriram Sridharan, Nicholas Sciascia, Anthony Tubbs, Paul Meltzer, Barry P. Sleckman, and André Nussenzweig. 2016. "DNA Breaks and End Resection Measured Genome-Wide by End Sequencing." *Molecular Cell* 63 (5): 898–911. <https://doi.org/10.1016/j.molcel.2016.06.034>.
- Caridi, Christopher P., Carla D'Agostino, Taehyun Ryu, Grzegorz Zapotoczny, Laetitia Delabaere, Xiao Li, Varandt Y. Khodaverdian, et al. 2018. "Nuclear F-Actin and Myosins Drive Relocalization of Heterochromatic Breaks." *Nature* 559 (7712): 54–60. <https://doi.org/10.1038/s41586-018-0242-8>.
- Cheblal, Anaïs, Kiran Challa, Andrew Seeber, Kenji Shimada, Haruka Yoshida, Helder C. Ferreira, Assaf Amitai, and Susan M. Gasser. 2020. "DNA Damage-Induced Nucleosome Depletion Enhances Homology Search Independently of Local Break Movement." *Molecular Cell* 80 (2): 311-326.e4. <https://doi.org/10.1016/j.molcel.2020.09.002>.
- Chiarle, Roberto, Yu Zhang, Richard L. Frock, Susanna M. Lewis, Benoit Molinie, Yu-jui Ho, Darienne R. Myers, et al. 2011. "Genome-Wide Translocation Sequencing Reveals Mechanisms of Chromosome Breaks and Rearrangements in B Cells." *Cell* 147 (1): 107–19. <https://doi.org/10.1016/j.cell.2011.07.049>.
- Chiolo, Irene, Aki Minoda, Serafin U. Colmenares, Aris Polyzos, Sylvain V. Costes, and Gary H.

References

- Karpen. 2011. "Double-Strand Breaks in Heterochromatin Move Outside of a Dynamic HP1a Domain to Complete Recombinational Repair." *Cell* 144 (5): 732–44. <https://doi.org/10.1016/j.cell.2011.02.012>.
- Chou, Danny M., Britt Adamson, Noah E. Dephoure, Xu Tan, Amanda C. Nottke, Kristen E. Hurov, Steven P. Gygi, M. P. Colaiacovo, and Stephen J. Elledge. 2010. "A Chromatin Localization Screen Reveals Poly (ADP Ribose)-Regulated Recruitment of the Repressive Polycomb and NuRD Complexes to Sites of DNA Damage." *Proceedings of the National Academy of Sciences* 107 (43): 18475–80. <https://doi.org/10.1073/pnas.1012946107>.
- Chowdhury, Basudev, Andrew McGovern, Yi Cui, Samrat Roy Choudhury, Il Hoon Cho, Bruce Cooper, Timothy Chevassut, Amy C. Lossie, and Joseph Irudayaraj. 2015. "The Hypomethylating Agent Decitabine Causes a Paradoxical Increase in 5-Hydroxymethylcytosine in Human Leukemia Cells." *Scientific Reports* 5 (1i): 1–8. <https://doi.org/10.1038/srep09281>.
- Chuang, Chien-Hui, Anne E Carpenter, Beata Fuchsova, Terezina Johnson, Primal de Lanerolle, and Andrew S Belmont. 2006. "Long-Range Directional Movement of an Interphase Chromosome Site." *Current Biology* 16 (8): 825–31. <https://doi.org/10.1016/j.cub.2006.03.059>.
- Chubb, Jonathan R, Shelagh Boyle, Paul Perry, and Wendy A Bickmore. 2002. "Chromatin Motion Is Constrained by Association with Nuclear Compartments in Human Cells." *Current Biology* 12 (6): 439–45. [https://doi.org/10.1016/S0960-9822\(02\)00695-4](https://doi.org/10.1016/S0960-9822(02)00695-4).
- Chung, Daniel K.C., Janet N.Y. Chan, Jonathan Strecker, Wei Zhang, Sasha Ebrahimi-Ardebili, Thomas Lu, Karan J. Abraham, Daniel Durocher, and Karim Mekhail. 2015. "Perinuclear Tethers License Telomeric DSBs for a Broad Kinesin- and NPC-Dependent DNA Repair Process." *Nature Communications* 6. <https://doi.org/10.1038/ncomms8742>.
- Churikov, Dmitri, Ferose Charifi, Nadine Eckert-Boulet, Sonia Silva, Marie Noelle Simon, Michael Lisby, and Vincent Géli. 2016. "SUMO-Dependent Relocalization of Eroded Telomeres to Nuclear Pore Complexes Controls Telomere Recombination." *Cell Reports* 15 (6): 1242–53. <https://doi.org/10.1016/j.celrep.2016.04.008>.
- Clouaire, Thomas, Vincent Rocher, Anahita Lashgari, Coline Arnould, Marion Aguirrebengoa, Anna Biernacka, Magdalena Skrzypczak, et al. 2018. "Comprehensive Mapping of Histone Modifications at DNA Double-Strand Breaks Deciphers Repair Pathway Chromatin Signatures." *Molecular Cell* 72 (2): 250-262.e6. <https://doi.org/10.1016/j.molcel.2018.08.020>.
- Cohen, Haim Y., Siva Lavu, Kevin J. Bitterman, Brian Hekking, Thomas A. Imahiyerobo, Christine Miller, Roy Frye, Hidde Ploegh, Benedikt M. Kessler, and David A. Sinclair. 2004. "Acetylation of the C Terminus of Ku70 by CBP and PCAF Controls Bax-Mediated Apoptosis." *Molecular Cell* 13 (5): 627–38. [https://doi.org/10.1016/S1097-2765\(04\)00094-2](https://doi.org/10.1016/S1097-2765(04)00094-2).
- Cohen, Haim Y., Christine Miller, Kevin J. Bitterman, Nathan R. Wall, Brian Hekking, Benedikt Kessler, Konrad T. Howitz, Myriam Gorospe, Rafael De Cabo, and David A. Sinclair. 2004. "Calorie Restriction Promotes Mammalian Cell Survival by Inducing the SIRT1 Deacetylase." *Science* 305 (5682): 390–92. <https://doi.org/10.1126/science.1099196>.
- Cohen, Sarah, Nadine Puget, Yea Lih Lin, Thomas Clouaire, Marion Aguirrebengoa, Vincent Rocher, Philippe Pasero, Yvan Canitrot, and Gaëlle Legube. 2018. "Senataxin Resolves RNA:DNA Hybrids Forming at DNA Double-Strand Breaks to Prevent Translocations." *Nature Communications* 9 (1). <https://doi.org/10.1038/s41467-018-02894-w>.
- Cowell, I. G., Z. Sondka, K. Smith, K. C. Lee, C. M. Manville, M. Sidorcuk-Lesthurge, H. A. Rance, et al. 2012. "Model for MLL Translocations in Therapy-Related Leukemia Involving Topoisomerase II -Mediated DNA Strand Breaks and Gene Proximity." *Proceedings of the National Academy of Sciences* 109 (23): 8989–94. <https://doi.org/10.1073/pnas.1204406109>.
- Cremer, T., and Marion Cremer. 2010. "Chromosome Territories." *Cold Spring Harbor Perspectives in Biology* 2 (3): a003889–a003889. <https://doi.org/10.1101/cshperspect.a003889>.
- Crisanti, M. Cecilia, Africa F. Wallace, Veena Kapoor, Fabian Vandermeers, Melissa L. Dowling,

References

- Luana P. Pereira, Kara Coleman, et al. 2009. “The HDAC Inhibitor Panobinostat (LBH589) Inhibits Mesothelioma and Lung Cancer Cells in Vitro and in Vivo with Particular Efficacy for Small Cell Lung Cancer.” *Molecular Cancer Therapeutics* 8 (8): 2221–31. <https://doi.org/10.1158/1535-7163.MCT-09-0138>.
- Cristini, Agnese, Matthias Groh, Maiken S. Kristiansen, and Natalia Gromak. 2018. “RNA/DNA Hybrid Interactome Identifies DXH9 as a Molecular Player in Transcriptional Termination and R-Loop-Associated DNA Damage.” *Cell Reports* 23 (6): 1891–1905. <https://doi.org/10.1016/j.celrep.2018.04.025>.
- Cristini, Agnese, Giulia Ricci, Sébastien Britton, Simona Salimbeni, Shar yin Naomi Huang, Jessica Marinello, Patrick Calsou, et al. 2019. “Dual Processing of R-Loops and Topoisomerase I Induces Transcription-Dependent DNA Double-Strand Breaks.” *Cell Reports* 28 (12): 3167–3181.e6. <https://doi.org/10.1016/j.celrep.2019.08.041>.
- Crossley, Madzia P., Michael Bocek, and Karlene A. Cimprich. 2019. “R-Loops as Cellular Regulators and Genomic Threats.” *Molecular Cell* 73 (3): 398–411. <https://doi.org/10.1016/j.molcel.2019.01.024>.
- Csink, Amy K., and Steven Henikoff. 1998. “Large-Scale Chromosomal Movements during Interphase Progression in *Drosophila*.” *Journal of Cell Biology* 143 (1): 13–22. <https://doi.org/10.1083/jcb.143.1.13>.
- Das, Chandrima, M. Scott Lucia, Kirk C. Hansen, and Jessica K. Tyler. 2009. “CBP/P300-Mediated Acetylation of Histone H3 on Lysine 56.” *Nature* 459 (7243): 113–17. <https://doi.org/10.1038/nature07861>.
- Dias, Joana N.R., Sandra I. Aguiar, Diane M. Pereira, Ana S. André, Lurdes Gano, João D.G. Correia, Belmira Carrapiço, et al. 2018. “The Histone Deacetylase Inhibitor Panobinostat Is a Potent Antitumor Agent in Canine Diffuse Large B-Cell Lymphoma.” *Oncotarget* 9 (47): 28586–98. <https://doi.org/10.18632/oncotarget.25580>.
- Difilippantonio, Michael J., Jie Zhu, Hua Tang Chen, Eric Meffre, Michel C. Nussenzweig, Edward E. Max, Thomas Ried, and André Nussenzweig. 2000. “Dna Repair Protein Ku80 Suppresses Chromosomal Aberrations and Malignant Transformation.” *Nature* 404 (6777): 510–14. <https://doi.org/10.1038/35006670>.
- Difilippantonio, Simone, Eric Gapud, Nancy Wong, Ching Yu Huang, Grace Mahowald, Hua Tang Chen, Michael J. Kruhlak, et al. 2008. “53BP1 Facilitates Long-Range DNA End-Joining during V(D)J Recombination.” *Nature* 456 (7221): 529–33. <https://doi.org/10.1038/nature07476>.
- Dimitrova, Nadya, Yi Chun M. Chen, David L. Spector, and Titia De Lange. 2008. “53BP1 Promotes Non-Homologous End Joining of Telomeres by Increasing Chromatin Mobility.” *Nature* 456 (7221): 524–28. <https://doi.org/10.1038/nature07433>.
- Dion, Vincent, Véronique Kalck, Chihiro Horigome, Benjamin D. Towbin, and Susan M. Gasser. 2012. “Increased Mobility of Double-Strand Breaks Requires Mec1, Rad9 and the Homologous Recombination Machinery.” *Nature Cell Biology* 14 (5): 502–9. <https://doi.org/10.1038/ncb2465>.
- Doil, Carsten, Niels Mailand, Simon Bekker-Jensen, Patrice Menard, Dorthe Helena Larsen, Rainer Pepperkok, Jan Ellenberg, et al. 2009. “RNF168 Binds and Amplifies Ubiquitin Conjugates on Damaged Chromosomes to Allow Accumulation of Repair Proteins.” *Cell* 136 (3): 435–46. <https://doi.org/10.1016/j.cell.2008.12.041>.
- Dovey, Oliver M., Charles T. Foster, and Shaun M. Cowley. 2010. “Histone Deacetylase 1 (HDAC1), but Not HDAC2, Controls Embryonic Stem Cell Differentiation.” *Proceedings of the National Academy of Sciences of the United States of America* 107 (18): 8242–47. <https://doi.org/10.1073/pnas.1000478107>.
- Downs, Jessica A., Stéphane Allard, Olivier Jobin-Robitaille, Ali Javaheri, Andréanne Auger, Nathalie Bouchard, Stephen J. Kron, Stephen P. Jackson, and Jacques Côté. 2004. “Binding of Chromatin-Modifying Activities to Phosphorylated Histone H2A at DNA Damage Sites.” *Molecular Cell* 16

References

- (6): 979–90. <https://doi.org/10.1016/j.molcel.2004.12.003>.
- Dundr, Miroslav, Jason K. Ospina, Myong Hee Sung, Sam John, Madhvi Upender, Thomas Ried, Gordon L. Hager, and A. Gregory Matera. 2007. “Actin-Dependent Intranuclear Repositioning of an Active Gene Locus in Vivo.” *Journal of Cell Biology* 179 (6): 1095–1103. <https://doi.org/10.1083/jcb.200710058>.
- Duquette, Michelle L., Phuong Pham, Myron F. Goodman, and Nancy Maizels. 2005. “AID Binds to Transcription-Induced Structures in c-MYC That Map to Regions Associated with Translocation and Hypermutation.” *Oncogene* 24 (38): 5791–98. <https://doi.org/10.1038/sj.onc.1208746>.
- Durrin, Linda K., Randall K. Mann, Paul S. Kayne, and Michael Grunstein. 1991. “Yeast Histone H4 N-Terminal Sequence Is Required for Promoter Activation in Vivo.” *Cell* 65 (6): 1023–31. [https://doi.org/10.1016/0092-8674\(91\)90554-C](https://doi.org/10.1016/0092-8674(91)90554-C).
- Eot-Houllier, Grégory, Géraldine Fulcrand, Laura Magnaghi-Jaulin, and Christian Jaulin. 2009. “Histone Deacetylase Inhibitors and Genomic Instability.” *Cancer Letters* 274 (2): 169–76. <https://doi.org/10.1016/j.canlet.2008.06.005>.
- Escribano-Díaz, Cristina, Alexandre Orthwein, Amélie Fradet-Turcotte, Mengtan Xing, Jordan T.F. Young, Ján Tkáč, Michael A. Cook, et al. 2013. “A Cell Cycle-Dependent Regulatory Circuit Composed of 53BP1-RIF1 and BRCA1-CtIP Controls DNA Repair Pathway Choice.” *Molecular Cell* 49 (5): 872–83. <https://doi.org/10.1016/j.molcel.2013.01.001>.
- Fenaux, Pierre. 2005. “Inhibitors of DNA Methylation: Beyond Myelodysplastic Syndromes.” *Nature Clinical Practice Oncology* 2 (SUPPL. 1): 36–44. <https://doi.org/10.1038/ncponc0351>.
- Ferguson, David O., Joann M. Sekiguchi, Sandy Chang, Karen M. Frank, Yijie Gao, Ronald A. DePinho, and Frederick W. Alt. 2000. “The Nonhomologous End-Joining Pathway of DNA Repair Is Required for Genomic Stability and the Suppression of Translocations.” *Proceedings of the National Academy of Sciences of the United States of America* 97 (12): 6630–33. <https://doi.org/10.1073/pnas.110152897>.
- Fielden, John, Katherine Wiseman, Ignacio Torrecilla, Shudong Li, Samuel Hume, Shih Chieh Chiang, Annamaria Ruggiano, et al. 2020. “TEX264 Coordinates P97- and SPRTN-Mediated Resolution of Topoisomerase 1-DNA Adducts.” *Nature Communications* 11 (1): 1–16. <https://doi.org/10.1038/s41467-020-15000-w>.
- Flotho, C., R. Claus, C. Batz, M. Schneider, I. Sandrock, S. Ihde, C. Plass, C. M. Niemeyer, and M. Lübbert. 2009. “The DNA Methyltransferase Inhibitors Azacitidine, Decitabine and Zebularine Exert Differential Effects on Cancer Gene Expression in Acute Myeloid Leukemia Cells.” *Leukemia* 23 (6): 1019–28. <https://doi.org/10.1038/leu.2008.397>.
- Fradet-Turcotte, Amélie, Marella D. Canny, Cristina Escribano-Díaz, Alexandre Orthwein, Charles C.Y. Leung, Hao Huang, Marie Claude Landry, et al. 2013. “53BP1 Is a Reader of the DNA-Damage-Induced H2A Lys 15 Ubiquitin Mark.” *Nature* 499 (7456): 50–54. <https://doi.org/10.1038/nature12318>.
- Fraga, Mario F., Esteban Ballestar, Ana Villar-Garea, Manuel Boix-Chornet, Jesus Espada, Gunnar Schotta, Tiziana Bonaldi, et al. 2005. “Loss of Acetylation at Lys16 and Trimethylation at Lys20 of Histone H4 Is a Common Hallmark of Human Cancer.” *Nature Genetics* 37 (4): 391–400. <https://doi.org/10.1038/ng1531>.
- Galati, Elena, Maria C. Bosio, Daniele Novarina, Matteo Chiara, Giulia M. Bernini, Alessandro M. Mozzarelli, Maria L. García-Rubio, et al. 2021. “VID22 Counteracts G-Quadruplex-Induced Genome Instability.” *Nucleic Acids Research* 49 (22): 12785–804. <https://doi.org/10.1093/nar/gkab1156>.
- Gao, Ge, and David I. Smith. 2014. “Very Large Common Fragile Site Genes and Their Potential Role in Cancer Development.” *Cellular and Molecular Life Sciences* 71 (23): 4601–15. <https://doi.org/10.1007/s00018-014-1753-6>.
- Gao, Yijie, David O. Ferguson, Wei Xie, John P. Manis, Jo Ann Sekiguchi, Karen M. Frank, Jayanta

References

- Chaudhuri, James Horner, Ronald A. DePinho, and Frederick W. Alt. 2000. "Interplay of P53 and DNA-Repair Protein XRCC4 in Tumorigenesis, Genomic Stability and Development." *Nature* 404 (6780): 897–900. <https://doi.org/10.1038/35009138>.
- Ghezraoui, Hind, Marion Piganeau, Benjamin Renouf, Jean-Baptiste Renaud, Annahita Sallmyr, Brian Ruis, Sehyun Oh, et al. 2014. "Chromosomal Translocations in Human Cells Are Generated by Canonical Nonhomologous End-Joining." *Molecular Cell* 55: 829–42. <https://doi.org/10.1016/j.molcel.2014.08.002>.
- Ginno, Paul A., Paul L. Lott, Holly C. Christensen, Ian Korf, and Frédéric Chédin. 2012. "R-Loop Formation Is a Distinctive Characteristic of Unmethylated Human CpG Island Promoters." *Molecular Cell* 45 (6): 814–25. <https://doi.org/10.1016/j.molcel.2012.01.017>.
- Giri, Anil K., and Tero Aittokallio. 2019. "DNMT Inhibitors Increase Methylation in the Cancer Genome." *Frontiers in Pharmacology* 10 (APR): 1–11. <https://doi.org/10.3389/fphar.2019.00385>.
- Glozak, Michele A., Nilanjan Sengupta, Xiaohong Zhang, and Edward Seto. 2005. "Acetylation and Deacetylation of Non-Histone Proteins." *Gene* 363 (1–2): 15–23. <https://doi.org/10.1016/j.gene.2005.09.010>.
- Gong, Fade, and Kyle M Miller. 2013. "Mammalian DNA Repair: HATs and HDACs Make Their Mark through Histone Acetylation." *Mutation Research - Fundamental and Molecular Mechanisms of Mutagenesis* 750: 23–30. <https://doi.org/10.1016/j.mrfmmm.2013.07.002>.
- Goodarzi, Aaron A, Angela T Noon, Dorothee Deckbar, Yael Ziv, Yosef Shiloh, Markus Löbrich, and Penny A Jeggo. 2008. "ATM Signaling Facilitates Repair of DNA Double-Strand Breaks Associated with Heterochromatin." *Molecular Cell* 31 (2): 167–77. <https://doi.org/10.1016/j.molcel.2008.05.017>.
- Gore, Steven D. 2005. "Combination Therapy with DNA Methyltransferase Inhibitors in Hematologic Malignancies." *Nature Clinical Practice Oncology* 2 (SUPPL. 1): 30–35. <https://doi.org/10.1038/ncponc0346>.
- Gothe, Henrike Johanna, Britta Annika Maria Bouwman, Eduardo Gade Gusmao, Rossana Piccinno, Giuseppe Petrosino, Sergi Sayols, Oliver Drechsel, et al. 2019. "Spatial Chromosome Folding and Active Transcription Drive DNA Fragility and Formation of Oncogenic MLL Translocations." *Molecular Cell* 75 (2): 267-283.e12. <https://doi.org/10.1016/j.molcel.2019.05.015>.
- Gray, Jhanelle, Christopher L. Cubitt, Shumin Zhang, and Alberto Chiappori. 2012. "Combination of HDAC and Topoisomerase Inhibitors in Small Cell Lung Cancer." *Cancer Biology and Therapy* 13 (8): 614–22. <https://doi.org/10.4161/cbt.19848>.
- Groh, Tomas, Jan Hrabeta, Mohammed Ashraf Khalil, Helena Doktorova, Tomas Eckschlager, and Marie Stiborova. 2015. "The Synergistic Effects of DNA-Damaging Drugs Cisplatin and Etoposide with a Histone Deacetylase Inhibitor Valproate in High-Risk Neuroblastoma Cells." *International Journal of Oncology* 47 (1): 343–52. <https://doi.org/10.3892/ijo.2015.2996>.
- Haberland, Michael, Mayssa H. Mokalled, Rusty L. Montgomery, and Eric N. Olson. 2009. "Epigenetic Control of Skull Morphogenesis by Histone Deacetylase 8." *Genes and Development* 23 (14): 1625–30. <https://doi.org/10.1101/gad.1809209>.
- Haberland, Michael, Rusty L. Montgomery, and Eric N. Olson. 2009. "The Many Roles of Histone Deacetylases in Development and Physiology: Implications for Disease and Therapy." *Nature Reviews Genetics* 10 (1): 32–42. <https://doi.org/10.1038/nrg2485>.
- Hagelkruys, Astrid, Sabine Lager, Julia Krahmer, Alexandra Leopoldi, Matthias Artaker, Oliver Pusch, Jürgen Zezula, et al. 2014. "A Single Allele of Hdac2 but Not Hdac1 Is Sufficient for Normal Mouse Brain Development in the Absence of Its Paralog." *Development (Cambridge)* 141 (3): 604–16. <https://doi.org/10.1242/dev.100487>.
- Hajji, N., K. Wallenborg, P. Vlachos, J. Füllgrabe, O. Hermanson, and B. Joseph. 2010. "Opposing

References

- Effects of HMOF and SIRT1 on H4K16 Acetylation and the Sensitivity to the Topoisomerase II Inhibitor Etoposide.” *Oncogene* 29 (15): 2192–2204. <https://doi.org/10.1038/onc.2009.505>.
- Hajji, N., K. Wallenborg, P. Vlachos, U. Nyman, O. Hermanson, and B. Joseph. 2008. “Combinatorial Action of the HDAC Inhibitor Trichostatin A and Etoposide Induces Caspase-Mediated AIF-Dependent Apoptotic Cell Death in Non-Small Cell Lung Carcinoma Cells.” *Oncogene* 27 (22): 3134–44. <https://doi.org/10.1038/sj.onc.1210976>.
- Hakim, Ofir, Wolfgang Resch, Arito Yamane, Isaac Klein, Kyong Rim Kieffer-Kwon, Mila Jankovic, Thiago Oliveira, et al. 2012. “DNA Damage Defines Sites of Recurrent Chromosomal Translocations in B Lymphocytes.” *Nature* 484 (7392): 69–74. <https://doi.org/10.1038/nature10909>.
- Hauer, Michael H., Andrew Seeber, Vijender Singh, Raphael Thierry, Ragna Sack, Assaf Amitai, Mariya Kryzhanovska, et al. 2017. “Histone Degradation in Response to DNA Damage Enhances Chromatin Dynamics and Recombination Rates.” *Nature Structural and Molecular Biology* 24 (2): 99–107. <https://doi.org/10.1038/nsmb.3347>.
- Hilton, Isaac B., Anthony M. D’Ippolito, Christopher M. Vockley, Pratiksha I. Thakore, Gregory E. Crawford, Timothy E. Reddy, and Charles A. Gersbach. 2015. “Epigenome Editing by a CRISPR-Cas9-Based Acetyltransferase Activates Genes from Promoters and Enhancers.” *Nature Biotechnology* 33 (5): 510–17. <https://doi.org/10.1038/nbt.3199>.
- Hnisz, Denes, Abraham S Weintraub, Daniel S Day, Anne-laure Valton, Rasmus O Bak, Charles H Li, Johanna Goldmann, et al. 2016. “Activation of Proto-Oncogenes by Disruption of Chromosome Neighborhoods” 351 (6280): 3812–14.
- Hoeijmakers, Jan H J. 2009. “DNA Damage, Aging, and Cancer,” 1475–85.
- Horigome, Chihiro, Denise E. Bustard, Isabella Marcomini, Neda Delgoshai, Monika Tsai-Pflugfelder, Jennifer A. Cobb, and Susan M. Gasser. 2016. “PolySUMOylation by Siz2 and Mms21 Triggers Relocation of DNA Breaks to Nuclear Pores through the Slx5/Slx8 STUBL.” *Genes and Development* 30 (8): 931–45. <https://doi.org/10.1101/gad.277665.116>.
- Huang, Cheng Ran Lisa, Anna M. Schneider, Yunqi Lu, Tejasvi Niranjana, Peilin Shen, Matoya A. Robinson, Jared P. Steranka, et al. 2010. “Mobile Interspersed Repeats Are Major Structural Variants in the Human Genome.” *Cell* 141 (7): 1171–82. <https://doi.org/10.1016/j.cell.2010.05.026>.
- Huen, Michael S.Y., Robert Grant, Isaac Manke, Kay Minn, Xiaochun Yu, Michael B. Yaffe, and Junjie Chen. 2007. “RNF8 Transduces the DNA-Damage Signal via Histone Ubiquitylation and Checkpoint Protein Assembly.” *Cell* 131 (5): 901–14. <https://doi.org/10.1016/j.cell.2007.09.041>.
- Huyen, Yentram, Omar Zgheib, Richard A. DiTullio, Vassilis G. Gorgoulis, Panayotis Zacharatos, Tom J. Petty, Emily A. Sheston, Hestia S. Mellert, Elena S. Stavridi, and Thanos D. Halazonetis. 2004. “Methylated Lysine 79 of Histone H3 Targets 53BP1 to DNA Double-Strand Breaks.” *Nature* 432 (7015): 406–11. <https://doi.org/10.1038/nature03114>.
- Hwang, Ji Young, Stephanie Smith, Audrey Ceschia, Jordi Torres-Rosell, Luis Aragon, and Kyungjae Myung. 2008. “Smc5-Smc6 Complex Suppresses Gross Chromosomal Rearrangements Mediated by Break-Induced Replications.” *DNA Repair* 7 (9): 1426–36. <https://doi.org/10.1016/j.dnarep.2008.05.006>.
- Iacovoni, Jason S., Pierre Caron, Imen Lassadi, Estelle Nicolas, Laurent Massip, Didier Trouche, and Gaëlle Legube. 2010. “High-Resolution Profiling of γ H2AX around DNA Double Strand Breaks in the Mammalian Genome.” *The EMBO Journal* 29 (8): 1446–57. <https://doi.org/10.1038/emboj.2010.38>.
- Iannelli, Fabio, Alessandro Galbiati, Ilaria Capozzo, Quan Nguyen, Brian Magnuson, Flavia Micheli, Giuseppina D’Alessandro, et al. 2017. “A Damaged Genome’s Transcriptional Landscape through Multilayered Expression Profiling around in Situ-Mapped DNA Double-Strand Breaks.” *Nature Communications* 8 (May): 1–7. <https://doi.org/10.1038/ncomms15656>.

References

- Ikura, Tsuyoshi, Vasily V Ogryzko, Mikhail Grigoriev, Regina Groisman, Jin Wang, Masami Horikoshi, Ralph Scully, Jun Qin, and Yoshihiro Nakatani. 2000. "Involvement of the TIP60 Histone Acetylase Complex in DNA Repair and Apoptosis." *Cell* 102 (4): 463–73. [https://doi.org/10.1016/S0092-8674\(00\)00051-9](https://doi.org/10.1016/S0092-8674(00)00051-9).
- Ikura, Tsuyoshi, Satoshi Tashiro, Akemi Kakino, Hiroki Shima, Naduparambil Jacob, Ravindra Amunugama, Kristine Yoder, et al. 2007. "DNA Damage-Dependent Acetylation and Ubiquitination of H2AX Enhances Chromatin Dynamics." *Molecular and Cellular Biology* 27 (20): 7028–40. <https://doi.org/10.1128/mcb.00579-07>.
- Jacquet, Karine, Amélie Fradet-Turcotte, Nikita Avvakumov, Jean Philippe Lambert, Céline Roques, Raj K. Pandita, Eric Paquet, et al. 2016. "The TIP60 Complex Regulates Bivalent Chromatin Recognition by 53BP1 through Direct H4K20me Binding and H2AK15 Acetylation." *Molecular Cell* 62 (3): 409–21. <https://doi.org/10.1016/j.molcel.2016.03.031>.
- Jakob, B., J. Splinter, M. Durante, and G. Taucher-Scholz. 2009. "Live Cell Microscopy Analysis of Radiation-Induced DNA Double-Strand Break Motion." *Proceedings of the National Academy of Sciences of the United States of America* 106 (9): 3172–77. <https://doi.org/10.1073/pnas.0810987106>.
- Jaqaman, Khuloud, Dinah Loerke, Marcel Mettlen, Hirotaka Kuwata, Sergio Grinstein, Sandra L. Schmid, and Gaudenz Danuser. 2008. "Robust Single-Particle Tracking in Live-Cell Time-Lapse Sequences." *Nature Methods* 5 (8): 695–702. <https://doi.org/10.1038/nmeth.1237>.
- Kaidi, Abderrahmane, Brian T. Weinert, Chunaram Choudhary, and Stephen P. Jackson. 2019. "Human SIRT6 Promotes DNA End Resection Through CtIP Deacetylation." Edited by Jennifer Sills. *Science* 364 (6437): 247–247. <https://doi.org/10.1126/science.aax4558>.
- Karagiannis, T. C., and A. El-Osta. 2006. "Modulation of Cellular Radiation Responses by Histone Deacetylase Inhibitors." *Oncogene* 25 (28): 3885–93. <https://doi.org/10.1038/sj.onc.1209417>.
- Kato, Lucia, Nasim A. Begum, A. Maxwell Burroughs, Tomomitsu Doi, Jun Kawai, Carsten O. Daub, Takahisa Kawaguchi, Fumihiko Matsuda, Yoshihide Hayashizaki, and Tasuku Honjo. 2012. "Nonimmunoglobulin Target Loci of Activation-Induced Cytidine Deaminase (AID) Share Unique Features with Immunoglobulin Genes." *Proceedings of the National Academy of Sciences of the United States of America* 109 (7): 2479–84. <https://doi.org/10.1073/pnas.1120791109>.
- Kerrigan, Donna, Joseph M. Covey, Eugene J. Tilchen, and Kurt W. Kohn. 1987. "Topoisomerase II-Mediated DNA Breaks and Cytotoxicity in Relation to Cell Proliferation and the Cell Cycle in NIH 3T3 Fibroblasts and LI210 Leukemia Cells." *Cancer Research* 47 (8): 2050–55.
- Kilic, Sinan, Aleksandra Lezaja, Marco Gatti, Eliana Bianco, Jone Michelena, Ralph Imhof, and Matthias Altmeyer. 2019. "Phase Separation of 53 BP 1 Determines Liquid-like Behavior of DNA Repair Compartments ." *The EMBO Journal* 38 (16): 1–17. <https://doi.org/10.15252/embj.2018101379>.
- Kim, Hee Yeon, Seung Ah Choi, Eun Jung Koh, Kyung Hyun Kim, Ji Hoon Phi, Ji Yeoun Lee, and Seung Ki Kim. 2021. "Combination Treatment of CI-994 With Etoposide Potentiates Anticancer Effects Through a Topoisomerase II-Dependent Mechanism in Atypical Teratoid/Rhabdoid Tumor (AT/RT)." *Frontiers in Oncology* 11 (July). <https://doi.org/10.3389/fonc.2021.648023>.
- Klein, Isaac A., Wolfgang Resch, Mila Jankovic, Thiago Oliveira, Arito Yamane, Hirotaka Nakahashi, Michela Di Virgilio, et al. 2011. "Translocation-Capture Sequencing Reveals the Extent and Nature of Chromosomal Rearrangements in B Lymphocytes." *Cell* 147 (1): 95–106. <https://doi.org/10.1016/j.cell.2011.07.048>.
- Kolas, Nadine K., J. Ross Chapman, Shinichiro Nakada, Jarkko Ylanko, Richard Chahwan, Frédéric D. Sweeney, Stephanie Panier, et al. 2007. "Orchestration of the DNA-Damage Response by the RNF8 Ubiquitin Ligase." *Science* 318 (5856): 1637–40. <https://doi.org/10.1126/science.1150034>.
- Krawczyk, P. M., T. Borovski, J. Stap, T. Cijssouw, R. ten Cate, J. P. Medema, R. Kanaar, N. A.P.

References

- Franken, and J. A. Aten. 2012. “Chromatin Mobility Is Increased at Sites of DNA Double-Strand Breaks.” *Journal of Cell Science* 125 (9): 2127–33. <https://doi.org/10.1242/jcs.089847>.
- Krumm, Andrea, Christina Barckhausen, Pelin Kucuk, Karl Heinz Tomaszowski, Carmen Loquai, Jorg Fahrner, Oliver Holger Kramer, Bernd Kaina, and Wynand Paul Roos. 2016. “Enhanced Histone Deacetylase Activity in Malignant Melanoma Provokes RAD51 and FANCD2-Triggered Drug Resistance.” *Cancer Research* 76 (10): 3067–77. <https://doi.org/10.1158/0008-5472.CAN-15-2680>.
- Krummel, Kurt A., Lewis R. Roberts, Masako Kawakami, Thomas W. Glover, and David I. Smith. 2000. “The Characterization of the Common Fragile Site FRA16D and Its Involvement in Multiple Myeloma Translocations.” *Genomics* 69 (1): 37–46. <https://doi.org/10.1006/geno.2000.6321>.
- Kwon, Deborah Y., Ying Tao Zhao, Janine M. Lamonica, and Zhaolan Zhou. 2017. “Locus-Specific Histone Deacetylation Using a Synthetic CRISPR-Cas9-Based HDAC.” *Nature Communications* 8 (May): 1–8. <https://doi.org/10.1038/ncomms15315>.
- Lagger, Gerda, Dónal O’Carroll, Martina Rembold, Harald Khier, Julia Tischler, Georg Weitzer, Bernd Schuettengruber, et al. 2002. “Essential Function of Histone Deacetylase 1 in Proliferation Control and CDK Inhibitor Repression.” *EMBO Journal* 21 (11): 2672–81. <https://doi.org/10.1093/emboj/21.11.2672>.
- Lamm, Noa, Samuel Rogers, and Anthony J. Cesare. 2021. “Chromatin Mobility and Relocation in DNA Repair.” *Trends in Cell Biology* xx (xx): 1–13. <https://doi.org/10.1016/j.tcb.2021.06.002>.
- Lange, Titia De. 2005. “Shelterin: The Protein Complex That Shapes and Safeguards Human Telomeres.” *Genes and Development* 19 (18): 2100–2110. <https://doi.org/10.1101/gad.1346005>.
- LaRocque, Jeannine R., and Maria Jasin. 2010. “Mechanisms of Recombination between Diverged Sequences in Wild-Type and BLM-Deficient Mouse and Human Cells.” *Molecular and Cellular Biology* 30 (8): 1887–97. <https://doi.org/10.1128/MCB.01553-09>.
- Ledesma, Felipe Cortes, Sherif F. El Khamisy, Maria C. Zuma, Kay Osborn, and Keith W. Caldecott. 2009. “A Human 5’-Tyrosyl DNA Phosphodiesterase That Repairs Topoisomerase-Mediated DNA Damage.” *Nature* 461 (7264): 674–78. <https://doi.org/10.1038/nature08444>.
- Lee, Kihoon, and Eun Lee Sang. 2007. “Saccharomyces Cerevisiae Sae2- and Tel1-Dependent Single-Strand DNA Formation at DNA Break Promotes Microhomology-Mediated End Joining.” *Genetics* 176 (4): 2003–14. <https://doi.org/10.1534/genetics.107.076539>.
- Lemaître, Charlène, Anastazja Grabarz, Katerina Tsouroula, Leonid Andronov, Audrey Furst, Tibor Pankotai, Vincent Heyer, et al. 2014. “Nuclear Position Dictates DNA Repair Pathway Choice.” *Genes & Development* 28 (22): 2450–63. <https://doi.org/10.1101/gad.248369.114>.
- León-Ortiz, Ana María, Stephanie Panier, Grzegorz Sarek, Jean-Baptiste Vannier, Harshil Patel, Peter J. Campbell, and Simon J. Boulton. 2018. “A Distinct Class of Genome Rearrangements Driven by Heterologous Recombination.” *Molecular Cell* 69 (2): 292-305.e6. <https://doi.org/10.1016/j.molcel.2017.12.014>.
- Li, Guo, Yuan Tian, and Wei-Guo Zhu. 2020. “The Roles of Histone Deacetylases and Their Inhibitors in Cancer Therapy.” *Frontiers in Cell and Developmental Biology* 8 (September): 1–34. <https://doi.org/10.3389/fcell.2020.576946>.
- Li, Mischa Longyin, Qinqin Jiang, Natarajan V. Bhanu, Junmin Wu, Weihua Li, Benjamin A. Garcia, and Roger A. Greenberg. 2019. “Phosphorylation of TIP60 Suppresses 53BP1 Localization at DNA Damage Sites.” *Molecular and Cellular Biology* 39 (1). <https://doi.org/10.1128/MCB.00209-18>.
- Lin, Chunru, Liuqing Yang, Bogdan Tanasa, Kasey Hutt, Bong gun Ju, Kenny Ohgi, Jie Zhang, et al. 2009. “Nuclear Receptor-Induced Chromosomal Proximity and DNA Breaks Underlie Specific Translocations in Cancer.” *Cell* 139 (6): 1069–83. <https://doi.org/10.1016/j.cell.2009.11.030>.

References

- Lisby, Michael, Uffe H. Mortensen, and Rodney Rothstein. 2003. "Colocalization of Multiple DNA Double-Strand Breaks at a Single Rad52 Repair Center." *Nature Cell Biology* 5 (6): 572–77. <https://doi.org/10.1038/ncb997>.
- Liu, Yun, Ramesh Subrahmanyam, Tirtha Chakraborty, Ranjan Sen, and Stephen Desiderio. 2007. "A Plant Homeodomain in Rag-2 That Binds Hypermethylated Lysine 4 of Histone H3 Is Necessary for Efficient Antigen-Receptor-Gene Rearrangement." *Immunity* 27 (4): 561–71. <https://doi.org/10.1016/j.immuni.2007.09.005>.
- Lottersberger, Francisca, Roos Anna Karssemeijer, Nadya Dimitrova, and Titia de Lange. 2015. "53BP1 and the LINC Complex Promote Microtubule-Dependent DSB Mobility and DNA Repair." *Cell* 163 (4): 880–93. <https://doi.org/10.1016/j.cell.2015.09.057>.
- Lu, Huiming, Janapriya Saha, Pauline J. Beckmann, Eric A. Hendrickson, and Anthony J. Davis. 2019. "DNA-PKcs Promotes Chromatin Decondensation to Facilitate Initiation of the DNA Damage Response." *Nucleic Acids Research* 47 (18): 9467–79. <https://doi.org/10.1093/nar/gkz694>.
- Luijsterburg, Martijn S., Christoffel Dinant, Hannes Lans, Jan Stap, Elzbieta Wiernasz, Saskia Lagerwerf, Daniël O. Warmerdam, et al. 2009. "Heterochromatin Protein 1 Is Recruited to Various Types of DNA Damage." *Journal of Cell Biology* 185 (4): 577–86. <https://doi.org/10.1083/jcb.200810035>.
- Luijsterburg, Martijn S., Inge de Krijger, Wouter W. Wiegant, Rashmi G. Shah, Godelieve Smeenk, Anton J.L. de Groot, Alex Pines, et al. 2016. "PARP1 Links CHD2-Mediated Chromatin Expansion and H3.3 Deposition to DNA Repair by Non-Homologous End-Joining." *Molecular Cell* 61 (4): 547–62. <https://doi.org/10.1016/j.molcel.2016.01.019>.
- Magis, Alessio De, Stefano G. Manzo, Marco Russo, Jessica Marinello, Rita Morigi, Olivier Sordet, and Giovanni Capranico. 2019. "DNA Damage and Genome Instability by G-Quadruplex Ligands Are Mediated by R Loops in Human Cancer Cells." *Proceedings of the National Academy of Sciences of the United States of America* 116 (3): 816–25. <https://doi.org/10.1073/pnas.1810409116>.
- Mani, Ram Shankar, Scott A. Tomlins, Kaitlin Callahan, Aparna Ghosh, Mukesh K. Nyati, Sooryanarayana Varambally, Nallasivam Palanisamy, and Arul M. Chinnalyan. 2009. "Induced Chromosomal Proximity and Gene Fusions in Prostate Cancer." *Science* 326 (5957): 1230. <https://doi.org/10.1126/science.1178124>.
- Mann, Bhupinder S., John R. Johnson, Martin H. Cohen, Robert Justice, and Richard Pazdur. 2007. "FDA Approval Summary: Vorinostat for Treatment of Advanced Primary Cutaneous T-Cell Lymphoma." *The Oncologist* 12 (10): 1247–52. <https://doi.org/10.1634/theoncologist.12-10-1247>.
- Mao, Yong, Shyamal D. Desai, and Leroy F. Liu. 2000. "SUMO-1 Conjugation to Human DNA Topoisomerase II Isozymes." *Journal of Biological Chemistry* 275 (34): 26066–73. <https://doi.org/10.1074/jbc.M001831200>.
- Mao, Yong, Shyamal D. Desai, Chun Yuan Ting, Jaulang Hwang, and Leroy F. Liu. 2001. "26 S Proteasome-Mediated Degradation of Topoisomerase II Cleavable Complexes." *Journal of Biological Chemistry* 276 (44): 40652–58. <https://doi.org/10.1074/jbc.M104009200>.
- Marcomini, Isabella, Kenji Shimada, Neda Delgosaie, Io Yamamoto, Andrew Seeber, Anais Cheblal, Chihiro Horigome, Ulrike Naumann, and Susan M. Gasser. 2018. "Asymmetric Processing of DNA Ends at a Double-Strand Break Leads to Unconstrained Dynamics and Ectopic Translocation." *Cell Reports* 24 (10): 2614–2628.e4. <https://doi.org/10.1016/j.celrep.2018.07.102>.
- Marnef, Aline, Anne Laure Finoux, Coline Arnould, Emmanuelle Guillou, Virginie Daburon, Vincent Rocher, Thomas Mangeat, Philippe E. Mangeot, Emiliano P. Ricci, and Gaëlle Legube. 2019. "A Cohesin/HUSH- And LINC-Dependent Pathway Controls Ribosomal DNA Double-Strand Break Repair." *Genes and Development* 33 (17–18): 1175–90. <https://doi.org/10.1101/gad.324012.119>.
- Marnef, Aline, and Gaëlle Legube. 2021. "R-Loops as Janus-Faced Modulators of DNA Repair."

References

- Nature Cell Biology* 23 (4): 305–13. <https://doi.org/10.1038/s41556-021-00663-4>.
- Matthews, Adam G.W., Alex J. Kuo, Santiago Ramón-Maiques, Sunmi Han, Karen S. Champagne, Dmitri Ivanov, Mercedes Gallardo, et al. 2007. “RAG2 PHD Finger Couples Histone H3 Lysine 4 Trimethylation with V(D)J Recombination.” *Nature* 450 (7172): 1106–10. <https://doi.org/10.1038/nature06431>.
- Meaburn, Karen J, Tom Misteli, and Evi Soutoglou. 2007. “Spatial Genome Organization in the Formation of Chromosomal Translocations.” *Seminars in Cancer Biology* 17 (1): 80–90. <https://doi.org/10.1016/j.semcancer.2006.10.008>.
- Meerang, Mayura, Danilo Ritz, Shreya Paliwal, Zuzana Garajova, Matthias Bosshard, Niels Mailand, Pavel Janscak, Ulrich Hübscher, Hemmo Meyer, and Kristijan Ramadan. 2011. “The Ubiquitin-Selective Segregase VCP/P97 Orchestrates the Response to DNA Double-Strand Breaks.” *Nature Cell Biology* 13 (11): 1376–82. <https://doi.org/10.1038/ncb2367>.
- Mertens, Fredrik, Bertil Johansson, Thoas Fioretos, and Felix Mitelman. 2015. “The Emerging Complexity of Gene Fusions in Cancer.” *Nature Reviews Cancer*. <https://doi.org/10.1038/nrc3947>.
- Metzger, L., and G. Iliakis. 1991. “Kinetics of DNA Double-Strand Break Repair throughout the Cell Cycle as Assayed by Pulsed Field Gel Electrophoresis in CHO Cells.” *International Journal of Radiation Biology* 59 (6): 1325–39. <https://doi.org/10.1080/09553009114551201>.
- Miller, Kyle M, Jorrit V Tjeertes, Julia Coates, Gaëlle Legube, Sophie E Polo, Sébastien Britton, and Stephen P Jackson. 2010. “Human HDAC1 and HDAC2 Function in the DNA-Damage Response to Promote DNA Nonhomologous End-Joining.” *Nature Structural & Molecular Biology* 17 (99): 1144–51. <https://doi.org/10.1038/nsmb.1899>.
- Miné-Hattab, Judith, Vincent Recamier, Ignacio Izeddin, Rodney Rothstein, and Xavier Darzacq. 2017. “Multi-Scale Tracking Reveals Scale-Dependent Chromatin Dynamics after DNA Damage.” *Molecular Biology of the Cell* 28 (23): 3323–32. <https://doi.org/10.1091/mbc.E17-05-0317>.
- Miné-Hattab, Judith, and Rodney Rothstein. 2012. “Increased Chromosome Mobility Facilitates Homology Search during Recombination.” *Nature Cell Biology* 14 (April): 510. <https://doi.org/10.1038/ncb2472>.
- Mitelman, Felix, Bertil Johansson, and Fredrik Mertens. 2007. “The Impact of Translocations and Gene Fusions on Cancer Causation.” *Nature Reviews Cancer* 7 (4): 233–45. <https://doi.org/10.1038/nrc2091>.
- Mizuno, Ken’Ichi, Izumi Miyabe, Stephanie A. Schalbetter, Antony M. Carr, and Johanne M. Murray. 2013. “Recombination-Restarted Replication Makes Inverted Chromosome Fusions at Inverted Repeats.” *Nature* 493 (7431): 246–49. <https://doi.org/10.1038/nature11676>.
- Montgomery, Rusty L., Christopher A. Davis, Matthew J. Potthoff, Michael Haberland, Jens Fielitz, Xiaoxia Qi, Joseph A. Hill, James A. Richardson, and Eric N. Olson. 2007. “Histone Deacetylases 1 and 2 Redundantly Regulate Cardiac Morphogenesis, Growth, and Contractility.” *Genes and Development* 21 (14): 1790–1802. <https://doi.org/10.1101/gad.1563807>.
- Mosler, Thorsten, Francesca Conte, Gabriel M.C. Longo, Ivan Mikicic, Nastasja Kreim, Martin M. Möckel, Giuseppe Petrosino, et al. 2021. “R-Loop Proximity Proteomics Identifies a Role of DDX41 in Transcription-Associated Genomic Instability.” *Nature Communications* 12 (1): 1–17. <https://doi.org/10.1038/s41467-021-27530-y>.
- Nagashima, Ryosuke, Kayo Hibino, S. S. Ashwin, Michael Babokhov, Shin Fujishiro, Ryosuke Imai, Tadasu Nozaki, et al. 2019. “Single Nucleosome Imaging Reveals Loose Genome Chromatin Networks via Active RNA Polymerase II.” *Journal of Cell Biology* 218 (5): 1511–30. <https://doi.org/10.1083/jcb.201811090>.
- Neumann, Frank R, Vincent Dion, Lutz R Gehlen, Monika Tsai-Pflugfelder, Roger Schmid, Angela Taddei, and Susan M Gasser. 2012. “Targeted INO80 Enhances Subnuclear Chromatin

References

- Movement and Ectopic Homologous Recombination.” *Genes & Development* 26 (4): 369–83. <https://doi.org/10.1101/gad.176156.111>.
- Neves, H, C Ramos, M G da Silva, A Parreira, L Parreira, C. Chomienne, Kathy Howe, et al. 1999. “The Nuclear Topography of ABL, BCR, PML, and RARalpha Genes: Evidence for Gene Proximity in Specific Phases of the Cell Cycle and Stages of Hematopoietic Differentiation.” *Blood* 93 (4): 1197–1207. <http://www.ncbi.nlm.nih.gov/pubmed/9949162>.
- Ng, Huck Hui, David N. Ciccone, Katrina B. Morshead, Marjorie A. Oettinger, and Kevin Struhl. 2003. “Lysine-79 of Histone H3 Is Hypomethylated at Silenced Loci in Yeast and Mammalian Cells: A Potential Mechanism for Position-Effect Variegation.” *Proceedings of the National Academy of Sciences of the United States of America* 100 (4): 1820–25. <https://doi.org/10.1073/pnas.0437846100>.
- Niehrs, Christof, and Brian Luke. 2020. “Regulatory R-Loops as Facilitators of Gene Expression and Genome Stability.” *Nature Reviews Molecular Cell Biology* 21 (3): 167–78. <https://doi.org/10.1038/s41580-019-0206-3>.
- Nikiforova, M. N., J. R. Stringer, R. Blough, M. Medvedovic, J. A. Fagin, and Y. E. Nikiforov. 2000. “Proximity of Chromosomal Loci That Participate in Radiation-Induced Rearrangements in Human Cells.” *Science* 290 (5489): 138–41. <https://doi.org/10.1126/science.290.5489.138>.
- Nowell, C. 1962. “The Minute Chromosome (Ph1) in Chronic Granulocytic Leukemia.” *Blut Zeitschrift Für Die Gesamte Blutforschung* 8 (2): 65–66. <https://doi.org/10.1007/BF01630378>.
- Nussenzweig, André, and Michel C. Nussenzweig. 2010. “Origin of Chromosomal Translocations in Lymphoid Cancer.” *Cell* 141 (1): 27–38. <https://doi.org/10.1016/j.cell.2010.03.016>.
- Osborne, Cameron S., Lyubomira Chakalova, Karen E. Brown, David Carter, Alice Horton, Emmanuel Debrand, Beatrix Goyenechea, et al. 2004. “Active Genes Dynamically Colocalize to Shared Sites of Ongoing Transcription.” *Nature Genetics* 36 (10): 1065–71. <https://doi.org/10.1038/ng1423>.
- Oshidari, Roxanne, Jonathan Strecker, Daniel K.C. Chung, Karan J. Abraham, Janet N.Y. Chan, Christopher J. Damaren, and Karim Mekhail. 2018. “Nuclear Microtubule Filaments Mediate Non-Linear Directional Motion of Chromatin and Promote DNA Repair.” *Nature Communications* 9 (1). <https://doi.org/10.1038/s41467-018-05009-7>.
- Paller, Channing J., Michel D. Wissing, Janet Mendonca, Anup Sharma, Eugene Kim, Hea Soo Kim, Madeleine S.Q. Kortenhorst, et al. 2014. “Combining the Pan-Aurora Kinase Inhibitor AMG 900 with Histone Deacetylase Inhibitors Enhances Antitumor Activity in Prostate Cancer.” *Cancer Medicine* 3 (5): 1322–35. <https://doi.org/10.1002/cam4.289>.
- Pan, Chun Hao, Ying Fang Chang, Ming Shuo Lee, B. Chen Wen, Jen Chung Ko, Sheng Kai Liang, and Mei Chih Liang. 2016. “Vorinostat Enhances the Cisplatin-Mediated Anticancer Effects in Small Cell Lung Cancer Cells.” *BMC Cancer* 16 (1): 1–11. <https://doi.org/10.1186/s12885-016-2888-7>.
- Parada, Luis A, Philip G Mcqueen, Peter J Munson, and Tom Misteli. 2002. “Conservation of Relative Chromosome Positioning in Normal and Cancer Cells Positioning of Translocated Chromosomes in AT-13 Lym-Phoma Cells and Comparing Them to the Arrangement Division of Computational Bioscience Center for Information Technology of The.” *Current Biology* 12 (02): 1692–97.
- Piazza, Aurèle, William Douglass Wright, and Wolf Dietrich Heyer. 2017. “Multi-Invasions Are Recombination Byproducts That Induce Chromosomal Rearrangements.” *Cell* 170 (4): 760-773.e15. <https://doi.org/10.1016/j.cell.2017.06.052>.
- Pierce, A. J., P. Hu, M. Han, N. Ellis, and M. Jasin. 2001. “Ku DNA End-Binding Protein Modulates Homologous Repair of Double-Strand Breaks in Mammalian Cells.” *Genes and Development* 15 (24): 3237–42. <https://doi.org/10.1101/gad.946401>.
- Pinzaru, Alexandra M., Mike Kareh, Noa Lamm, Eros Lazzarini-Denchi, Anthony J. Cesare, and

References

- Agnel Sfeir. 2020. “Replication Stress Conferred by POT1 Dysfunction Promotes Telomere Relocalization to the Nuclear Pore.” *Genes and Development* 34 (23–24): 1619–36. <https://doi.org/10.1101/gad.337287.120>.
- Pommier, Yves, Yilun Sun, Shar Yin N. Huang, and John L. Nitiss. 2016. “Roles of Eukaryotic Topoisomerases in Transcription, Replication and Genomic Stability.” *Nature Reviews Molecular Cell Biology* 17 (11): 703–21. <https://doi.org/10.1038/nrm.2016.111>.
- Raghavan, Sathees C., Ilan R. Kirsch, and Michael R. Lieber. 2001. “Analysis of the V(D)J Recombination Efficiency at Lymphoid Chromosomal Translocation Breakpoints.” *Journal of Biological Chemistry* 276 (31): 29126–33. <https://doi.org/10.1074/jbc.M103797200>.
- Raghavan, Sathees C., Patrick C. Swanson, Xiantuo Wu, Chih Lin Hsieh, and Michael R. Lieber. 2004. “A Non-B-DNA Structure at the Bcl-2 Major Breakpoint Region Is Cleaved by the RAG Complex.” *Nature* 428 (6978): 88–93. <https://doi.org/10.1038/nature02355>.
- Ramón-Maiques, Santiago, Alex J. Kuo, Dylan Carney, Adam G.W. Matthews, Marjorie A. Oettinger, Or Gozani, and Wei Yang. 2007. “The Plant Homeodomain Finger of RAG2 Recognizes Histone H3 Methylated at Both Lysine-4 and Arginine-2.” *Proceedings of the National Academy of Sciences of the United States of America* 104 (48): 18993–98. <https://doi.org/10.1073/pnas.0709170104>.
- Robbiani, Davide F., Anne Bothmer, Elsa Callen, Bernardo Reina-San-Martin, Yair Dorsett, Simone Difilippantonio, Daniel J. Bolland, et al. 2008. “AID Is Required for the Chromosomal Breaks in C-Myc That Lead to c-Myc/IgH Translocations.” *Cell* 135 (6): 1028–38. <https://doi.org/10.1016/j.cell.2008.09.062>.
- Rocha, Pedro P., Mariann Micsinai, Jung Hyun Rachel Kim, Susannah L. Hewitt, Patricia P. Souza, Thomas Trimarchi, Francesco Strino, Fabio Parisi, Yuval Kluger, and Jane A. Skok. 2012. “Close Proximity to Igh Is a Contributing Factor to AID-Mediated Translocations.” *Molecular Cell* 47 (6): 873–85. <https://doi.org/10.1016/j.molcel.2012.06.036>.
- Rogakou, Emmy P., Duane R. Pilch, Ann H. Orr, Vessela S. Ivanova, and William M. Bonner. 1998. “DNA Double-Stranded Breaks Induce Histone H2AX Phosphorylation on Serine 139.” *Journal of Biological Chemistry* 273 (10): 5858–68. <https://doi.org/10.1074/jbc.273.10.5858>.
- Roix, Jeffrey J., Philip G Mcqueen, Peter J Munson, Luis A Parada, and Tom Misteli. 2003. “Spatial Proximity of Translocation-Prone Gene Loci in Human Lymphomas” 34 (3): 287–91.
- Rother, Magdalena B., Stefania Pellegrino, Rebecca Smith, Marco Gatti, Cornelia Meisenberg, Wouter W. Wiegant, Martijn S. Luijsterburg, et al. 2020. “CHD7 and 53BP1 Regulate Distinct Pathways for the Re-Ligation of DNA Double-Strand Breaks.” *Nature Communications* 11 (1). <https://doi.org/10.1038/s41467-020-19502-5>.
- Roukos, Vassilis, Rebecca C Burgess, and Tom Misteli. 2014. “Generation of Cell-Based Systems to Visualize Chromosome Damage and Translocations in Living Cells.” *Nature Protocols* 9 (10): 2476–92. <https://doi.org/10.1038/nprot.2014.167>.
- Roukos, Vassilis, and Tom Misteli. 2014. “The Biogenesis of Chromosome Translocations.” *Nature Cell Biology* 16 (4): 293–300. <https://doi.org/10.1038/ncb2941>.
- Roukos, Vassilis, Ty C Voss, Christine K Schmidt, Seungtaek Lee, Darawalee Wangsa, and Tom Misteli. 2013. “Spatial Dynamics of Chromosome Translocations in Living Cells.” *Science (New York, N.Y.)* 341 (6146): 660–64. <https://doi.org/10.1126/science.1237150>.
- Rowley, Janet D. 1973. “A New Consistent Chromosomal Abnormality in Chronic Myelogenous Leukaemia Identified by Quinacrine Fluorescence and Giemsa Staining.” *Nature* 243 (5405): 290–93. <https://doi.org/10.1038/243290a0>.
- Ruiz, José F., Belén Gómez-González, and Andrés Aguilera. 2011. “AID Induces Double-Strand Breaks at Immunoglobulin Switch Regions and c-MYC Causing Chromosomal Translocations in Yeast THO Mutants.” *PLoS Genetics* 7 (2). <https://doi.org/10.1371/journal.pgen.1002009>.

References

- Ryu, Taehyun, Brett Spatola, Laetitia Delabaere, Katherine Bowlin, Hannah Hopp, Ryan Kunitake, Gary H. Karpen, and Irene Chiolo. 2015. "Heterochromatic Breaks Move to the Nuclear Periphery to Continue Recombinational Repair." *Nature Cell Biology* 17 (11): 1401–11. <https://doi.org/10.1038/ncb3258>.
- Sadler, J. R., H. Sasmor, and J. L. Betz. 1983. "A Perfectly Symmetric Lac Operator Binds the Lac Repressor Very Tightly." *Proceedings of the National Academy of Sciences of the United States of America* 80 (22 1): 6785–89. <https://doi.org/10.1073/pnas.80.22.6785>.
- Sanjana, Neville E., Ophir Shalem, and Feng Zhang. 2014. "Improved Vectors and Genome-Wide Libraries for CRISPR Screening." *Nature Methods* 11 (8): 783–84. <https://doi.org/10.1038/nmeth.3047>.
- Sarni, Dan, Takayo Sasaki, Michal Irony Tur-Sinai, Karin Miron, Juan Carlos Rivera-Mulia, Brian Magnuson, Mats Ljungman, David M. Gilbert, and Batsheva Kerem. 2020. "3D Genome Organization Contributes to Genome Instability at Fragile Sites." *Nature Communications* 11 (1): 1–12. <https://doi.org/10.1038/s41467-020-17448-2>.
- Sartori, Alessandro A., Claudia Lukas, Julia Coates, Martin Mistrik, Shuang Fu, Jiri Bartek, Richard Baer, Jiri Lukas, and Stephen P. Jackson. 2007. "Human CtIP Promotes DNA End Resection." *Nature* 450 (7169): 509–14. <https://doi.org/10.1038/nature06337>.
- Savage, John R.K. 1996. "Insight into Sites." *Mutation Research - Reviews in Genetic Toxicology* 366 (2): 81–95. [https://doi.org/10.1016/S0165-1110\(96\)90030-5](https://doi.org/10.1016/S0165-1110(96)90030-5).
- Schotta, Gunnar, Roopsha Sengupta, Stefan Kubicek, Stephen Malin, Monika Kauer, Elsa Callén, Arkady Celeste, et al. 2008. "A Chromatin-Wide Transition to H4K20 Monomethylation Impairs Genome Integrity and Programmed DNA Rearrangements in the Mouse." *Genes and Development* 22 (15): 2048–61. <https://doi.org/10.1101/gad.476008>.
- Schrank, Benjamin R., Tomas Aparicio, Yinyin Li, Wakam Chang, Brian T. Chait, Gregg G. Gundersen, Max E. Gottesman, and Jean Gautier. 2018. "Nuclear ARP2/3 Drives DNA Break Clustering for Homology-Directed Repair." *Nature* 559 (7712): 61–66. <https://doi.org/10.1038/s41586-018-0237-5>.
- Schultz, Linda B., Nabil H. Chehab, Asra Malikzay, and Thanos D. Halazonetis. 2000. "P53 Binding Protein 1 (53BP1) Is an Early Participant in the Cellular Response to DNA Double-Strand Breaks." *Journal of Cell Biology* 151 (7): 1381–90. <https://doi.org/10.1083/jcb.151.7.1381>.
- Sciascia, Nicholas, Wei Wu, Dali Zong, Yilun Sun, Nancy Wong, Sam John, Darawalee Wangsa, et al. 2020. "Suppressing Proteasome Mediated Processing of Topoisomerase II DNA-Protein Complexes Preserves Genome Integrity." *ELife* 9: 1–27. <https://doi.org/10.7554/eLife.53447>.
- Seeber, Andrew, Vincent Dion, and Susan M. Gasser. 2013. "Checkpoint Kinases and the INO80 Nucleosome Remodeling Complex Enhance Global Chromatin Mobility in Response to DNA Damage." *Genes and Development* 27 (18): 1999–2008. <https://doi.org/10.1101/gad.222992.113>.
- Shalem, Ophir, Neville E. Sanjana, Ella Hartenian, Xi Shi, David A. Scott, Tarjei S. Mikkelsen, Dirk Heckl, et al. 2014. "Genome-Scale CRISPR-Cas9 Knockout Screening in Human Cells." *Science* 343 (6166): 84–87. <https://doi.org/10.1126/science.1247005>.
- Sharma, Girdhar G., Sairei So, Arun Gupta, Rakesh Kumar, Christelle Cayrou, Nikita Avvakumov, Utpal Bhadra, et al. 2010. "MOF and Histone H4 Acetylation at Lysine 16 Are Critical for DNA Damage Response and Double-Strand Break Repair." *Molecular and Cellular Biology* 30 (14): 3582–95. <https://doi.org/10.1128/mcb.01476-09>.
- Sharma, Sreenath V., Diana Y. Lee, Bihua Li, Margaret P. Quinlan, Fumiyuki Takahashi, Shyamala Maheswaran, Ultan McDermott, et al. 2010. "A Chromatin-Mediated Reversible Drug-Tolerant State in Cancer Cell Subpopulations." *Cell* 141 (1): 69–80. <https://doi.org/10.1016/j.cell.2010.02.027>.
- Shen, Xuetong, Ryan Ranallo, Eugene Choi, and Carl Wu. 2003. "Involvement of Actin-Related Proteins in ATP-Dependent Chromatin Remodeling Ferases [HATs] or by ATP-Dependent

References

- Perturbations of Histone-DNA Interactions (the SWI/SNF Family of Protein Complexes) (See Fyodorov and Kadonaga, 2001; Neely." *Molecular Cell* 12: 147–55.
- Shi, Xuan-Yan, Wei Ding, Tie-Qiu Li, Yi-Xiong Zhang, and Shan-Chao Zhao. 2017. "Histone Deacetylase (HDAC) Inhibitor, Suberoylanilide Hydroxamic Acid (SAHA), Induces Apoptosis in Prostate Cancer Cell Lines via the Akt/FOXO3a Signaling Pathway." *Medical Science Monitor* 23 (December): 5793–5802. <https://doi.org/10.12659/MSM.904597>.
- Shimazaki, Noriko, Albert G. Tsai, and Michael R. Lieber. 2009. "H3K4me3 Stimulates the V(D)J RAG Complex for Both Nicking and Hairpinning in Trans in Addition to Tethering in Cis: Implications for Translocations." *Molecular Cell* 34 (5): 535–44. <https://doi.org/10.1016/j.molcel.2009.05.011>.
- Shogren-Knaak, Michael, Haruhiko Ishii, Jian-Min Sun, Michael J. Pazin, James R. Davie, and Craig L. Peterson. 2006. "Histone H4-K16 Acetylation Controls Chromatin Structure and Protein Interactions." *Science* 311 (5762): 844–47. <https://doi.org/10.1126/science.1124000>.
- Simsek, Deniz, Erika Brunet, Sunnie Yan-Wai Wong, Sachin Katyal, Yankun Gao, Peter J. McKinnon, Jacqueline Lou, et al. 2011. "DNA Ligase III Promotes Alternative Nonhomologous End-Joining during Chromosomal Translocation Formation." Edited by James E. Haber. *PLoS Genetics* 7 (6): e1002080. <https://doi.org/10.1371/journal.pgen.1002080>.
- Simsek, Deniz, and Maria Jasin. 2010. "Alternative End-Joining Is Suppressed by the Canonical NHEJ Component Xrcc4–Ligase IV during Chromosomal Translocation Formation." *Nature Structural & Molecular Biology* 17 (4): 410–16. <https://doi.org/10.1038/nsmb.1773>.
- Sirbu, Bianca M., Frank B. Couch, Jordan T. Feigerle, Srividya Bhaskara, Scott W. Hiebert, and David Cortez. 2011. "Analysis of Protein Dynamics at Active, Stalled, and Collapsed Replication Forks." *Genes & Development* 25 (12): 1320–27. <https://doi.org/10.1101/gad.2053211>.
- Smith, Michael J., Eric E. Bryant, Fraulin J. Joseph, and Rodney Rothstein. 2019. "DNA Damage Triggers Increased Mobility of Chromosomes in G1-Phase Cells." *Molecular Biology of the Cell* 30 (21): 2620–25. <https://doi.org/10.1091/mbc.E19-08-0469>.
- Smith, Michael J., Eric E. Bryant, and Rodney Rothstein. 2018. "Increased Chromosomal Mobility after DNA Damage Is Controlled by Interactions between the Recombination Machinery and the Checkpoint." *Genes and Development* 32 (17–18): 1242–51. <https://doi.org/10.1101/gad.317966.118>.
- Somanath, Priyanka, Rachel Herndon Klein, and Paul S. Knoepfler. 2017. "CRISPR-Mediated HDAC2 Disruption Identifies Two Distinct Classes of Target Genes in Human Cells." *PLoS ONE*. <https://doi.org/10.1371/journal.pone.0185627>.
- Soni, Aashish, Maria Siemann, Martha Grabos, Tamara Murmann, Gabriel E Pantelias, and George Iliakis. 2014. "Requirement for Parp-1 and DNA Ligases 1 or 3 but Not of Xrcc1 in Chromosomal Translocation Formation by Backup End Joining." *Nucleic Acids Research* 42 (10): 6380–92. <https://doi.org/10.1093/nar/gku298>.
- Soni, Aashish, Maria Siemann, Gabriel E. Pantelias, and George Iliakis. 2015. "Marked Contribution of Alternative End-Joining to Chromosome-Translocation-Formation by Stochastically Induced DNA Double-Strand-Breaks in G2-Phase Human Cells." *Mutation Research/Genetic Toxicology and Environmental Mutagenesis* 793 (November): 2–8. <https://doi.org/10.1016/j.mrgentox.2015.07.002>.
- Soutoglou, Evi, Jonas F. Dorn, Kundan Sengupta, Maria Jasin, Andre Nussenzweig, Thomas Ried, Gaudenz Danuser, and Tom Misteli. 2007a. "Positional Stability of Single Double-Strand Breaks in Mammalian Cells." *Nature Cell Biology* 9 (6): 675–82. <https://doi.org/10.1038/ncb1591>.
- Staszewski, Ori, Richard E. Baker, Anna J. Ucher, Raygene Martier, Janet Stavnezer, and Jeroen E.J. Guikema. 2011. "Activation-Induced Cytidine Deaminase Induces Reproducible DNA Breaks at Many Non-Ig Loci in Activated B Cells." *Molecular Cell* 41 (2): 232–42. <https://doi.org/10.1016/j.molcel.2011.01.007>.

References

- Sun, Yingli, Xiaofeng Jiang, Shujuan Chen, Norvin Fernandes, and Brendan D. Price. 2005. "A Role for the Tip60 Histone Acetyltransferase in the Acetylation and Activation of ATM." *Proceedings of the National Academy of Sciences of the United States of America* 102 (37): 13182–87. <https://doi.org/10.1073/pnas.0504211102>.
- Sun, Yingli, Xiaofeng Jiang, Ye Xu, Marina K Ayrapetov, Lisa A Moreau, Johnathan R Whetstine, Brendan D Price, Nat Cell, and Biol Author. 2009. "Histone H3 Methylation Links DNA Damage Detection to Activation of the Tip60 Tumor Suppressor HHS Public Access Author Manuscript." *Nat Cell Biol* 11 (11): 1376–82. <https://doi.org/10.1038/ncb1982.Histone>.
- Sun, Yingli, Ye Xu, Kanaklata Roy, and Brendan D. Price. 2007. "DNA Damage-Induced Acetylation of Lysine 3016 of ATM Activates ATM Kinase Activity." *Molecular and Cellular Biology* 27 (24): 8502–9. <https://doi.org/10.1128/mcb.01382-07>.
- Taccioli, Guillermo E., Gary Rathbun, Eugene Oltz, Thomas Stamato, Penny A. Jeggo, and Frederick W. Alt. 1993. "Impairment of V(D)J Recombination in Double-Strand Break Repair Mutants." *Science* 260 (5105): 207–10. <https://doi.org/10.1126/science.8469973>.
- Taipale, Mikko, Stephen Rea, Karsten Richter, Ana Vilar, Peter Lichter, Axel Imhof, and Asifa Akhtar. 2005. "HMOF Histone Acetyltransferase Is Required for Histone H4 Lysine 16 Acetylation in Mammalian Cells." *Molecular and Cellular Biology* 25 (15): 6798–6810. <https://doi.org/10.1128/mcb.25.15.6798-6810.2005>.
- Tang, Jiangbo, Nam Woo Cho, Gaofeng Cui, Erica M. Manion, Niraj M. Shanbhag, Maria Victoria Botuyan, Georges Mer, and Roger A. Greenberg. 2013. "Acetylation Limits 53BP1 Association with Damaged Chromatin to Promote Homologous Recombination." *Nature Structural and Molecular Biology* 20 (3): 317–25. <https://doi.org/10.1038/nsmb.2499>.
- Taplick, Jan, Vladislav Kurtev, Karin Kroboth, Markus Posch, Thomas Lechner, and Christian Seiser. 2001. "Homo-Oligomerisation and Nuclear Localisation of Mouse Histone Deacetylase 1." *Journal of Molecular Biology* 308 (1): 27–38. <https://doi.org/10.1006/jmbi.2001.4569>.
- Tarhini, Ahmad A., Haris Zahoor, Brian McLaughlin, William E. Gooding, John C. Schmitz, Jill M. Siegfried, Mark A. Socinski, and Athanassios Argiris. 2013. "Phase I Trial of Carboplatin and Etoposide in Combination with Panobinostat in Patients with Lung Cancer." *Anticancer Research* 33 (10): 4475–82.
- Taunton, Jack, Christian A. Hassig, and Stuart L. Schreiber. 1996. "A Mammalian Histone Deacetylase Related to the Yeast Transcriptional Regulator Rpd3p." *Science* 272 (5260): 408–11. <https://doi.org/10.1126/science.272.5260.408>.
- Therizols, Pierre, Robert S. Illingworth, Celine Courilleau, Shelagh Boyle, Andrew J. Wood, and Wendy A. Bickmore. 2014. "Chromatin Decondensation Is Sufficient to Alter Nuclear Organization in Embryonic Stem Cells." *Science* 346 (6214): 1238–42. <https://doi.org/10.1126/science.1259587>.
- Thompson, Jeffrey S., Xuefeng Ling, and Michael Grunstein. 1994. "Histone H3 Amino Terminus Is Required for Telomeric and Silent Mating Locus Repression in Yeast." *Nature* 369 (6477): 245–47. <https://doi.org/10.1038/369245a0>.
- Torres-Rosell, Jordi, Ivana Sunjevaric, Giacomo De Piccoli, Meik Sacher, Nadine Eckert-Boulet, Robert Reid, Stefan Jentsch, Rodney Rothstein, Luis Aragón, and Michael Lisby. 2007. "The Smc5–Smc6 Complex and SUMO Modification of Rad52 Regulates Recombinational Repair at the Ribosomal Gene Locus." *Nature Cell Biology* 9 (8): 923–31. <https://doi.org/10.1038/ncb1619>.
- Tsai, Albert G., Haihui Lu, Sathees C. Raghavan, Markus Muschen, Chih-Lin Hsieh, and Michael R. Lieber. 2008. "Human Chromosomal Translocations at CpG Sites and a Theoretical Basis for Their Lineage and Stage Specificity." *Cell* 135 (6): 1130–42. <https://doi.org/10.1016/j.cell.2008.10.035>.
- Tsouroula, Katerina, Audrey Furst, Melanie Rogier, Vincent Heyer, Anne Maglott-Roth, Alexia

References

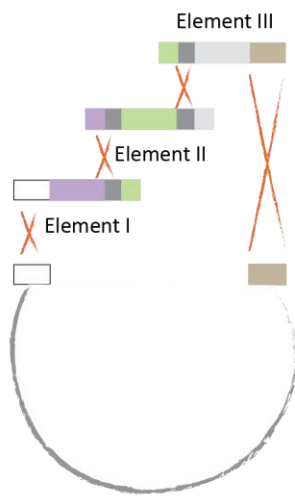
- Ferrand, Bernardo Reina-San-Martin, and Evi Soutoglou. 2016. “Temporal and Spatial Uncoupling of DNA Double Strand Break Repair Pathways within Mammalian Heterochromatin.” *Molecular Cell* 63 (2): 293–305. <https://doi.org/10.1016/j.molcel.2016.06.002>.
- Tubbs, Anthony, and André Nussenzweig. 2017. “Endogenous DNA Damage as a Source of Genomic Instability in Cancer.” *Cell* 168 (4): 644–56. <https://doi.org/10.1016/j.cell.2017.01.002>.
- Tumbar, Tudorita, and Andrew S. Belmont. 2001. “Interphase Movements of a DNA Chromosome Region Modulated by VP16 Transcriptional Activator.” *Nature Cell Biology* 3 (2): 134–39. <https://doi.org/10.1038/35055033>.
- Tumbar, Tudorita, Gail Sudlow, and Andrew S. Belmont. 1999. “Large-Scale Chromatin Unfolding and Remodeling Induced by VP16 Acidic Activation Domain.” *Journal of Cell Biology* 145 (7): 1341–54. <https://doi.org/10.1083/jcb.145.7.1341>.
- Vazquez, Berta N, Joshua K Thackray, Nicolas G Simonet, Noriko Kane-Goldsmith, Paloma Martinez-Redondo, Trang Nguyen, Samuel Bunting, Alejandro Vaquero, Jay A Tischfield, and Lourdes Serrano. 2016. “SIRT 7 Promotes Genome Integrity and Modulates Non-homologous End Joining DNA Repair .” *The EMBO Journal* 35 (14): 1488–1503. <https://doi.org/10.15252/embj.201593499>.
- Verdel, André, Sandrine Curtet, Marie Paule Brocard, Sophie Rousseaux, Claudie Lemerrier, Minoru Yoshida, and Saadi Khochbin. 2000. “Active Maintenance of MHD2/MHDAC6 Histone-Deacetylase in the Cytoplasm.” *Current Biology* 10 (12): 747–49. [https://doi.org/10.1016/S0960-9822\(00\)00542-X](https://doi.org/10.1016/S0960-9822(00)00542-X).
- Verschure, Pernelle J., Ineke van der Kraan, Wim de Leeuw, Johan van der Vlag, Anne E. Carpenter, Andrew S. Belmont, and Roel van Driel. 2005. “In Vivo HP1 Targeting Causes Large-Scale Chromatin Condensation and Enhanced Histone Lysine Methylation.” *Molecular and Cellular Biology* 25 (11): 4552–64. <https://doi.org/10.1128/mcb.25.11.4552-4564.2005>.
- Wang, Guan, Holly Edwards, J. Timothy Caldwell, Steven A. Buck, William Y. Qing, Jeffrey W. Taub, Yubin Ge, and Zhihong Wang. 2013. “Panobinostat Synergistically Enhances the Cytotoxic Effects of Cisplatin, Doxorubicin or Etoposide on High-Risk Neuroblastoma Cells.” *PLoS ONE* 8 (9). <https://doi.org/10.1371/journal.pone.0076662>.
- Wang, Huichen, Zhao Chong Zeng, Tu Anh Bui, Eiichiro Sonoda, Minoru Takata, Shunichi Takeda, and George Iliakis. 2001. “Efficient Rejoining of Radiation-Induced DNA Double-Strand Breaks in Vertebrate Cells Deficient in Genes of the RAD52 Epistasis Group.” *Oncogene* 20 (18): 2212–24. <https://doi.org/10.1038/sj.onc.1204350>.
- Wang, Minli, Weizhong Wu, Wenqi Wu, Bustanur Rosidi, Lihua Zhang, Huichen Wang, and George Iliakis. 2006. “PARP-1 and Ku Compete for Repair of DNA Double Strand Breaks by Distinct NHEJ Pathways.” *Nucleic Acids Research* 34 (21): 6170–82. <https://doi.org/10.1093/nar/gkl840>.
- Wang, Yuxiang, Jie Yang, Aaron T. Wild, Wei H. Wu, Rachna Shah, Carla Danussi, Gregory J. Riggins, et al. 2019. “G-Quadruplex DNA Drives Genomic Instability and Represents a Targetable Molecular Abnormality in ATRX-Deficient Malignant Glioma.” *Nature Communications* 10 (1). <https://doi.org/10.1038/s41467-019-08905-8>.
- Watanabe, Takaaki, Michael Marotta, Ryusuke Suzuki, Scott J. Diede, Stephen J. Tapscott, Atsushi Niida, Xiongfong Chen, et al. 2017. “Impediment of Replication Forks by Long Non-Coding RNA Provokes Chromosomal Rearrangements by Error-Prone Restart.” *Cell Reports* 21 (8): 2223–35. <https://doi.org/10.1016/j.celrep.2017.10.103>.
- Weinstock, David M., and Maria Jasin. 2006. “Alternative Pathways for the Repair of RAG-Induced DNA Breaks.” *Molecular and Cellular Biology* 26 (1): 131–39. <https://doi.org/10.1128/mcb.26.1.131-139.2006>.
- Wells, Christina E., Srividya Bhaskara, Kristy R. Stengel, Yue Zhao, Bianca Sirbu, Benjamin Chagot, David Cortez, et al. 2013. “Inhibition of Histone Deacetylase 3 Causes Replication Stress in

References

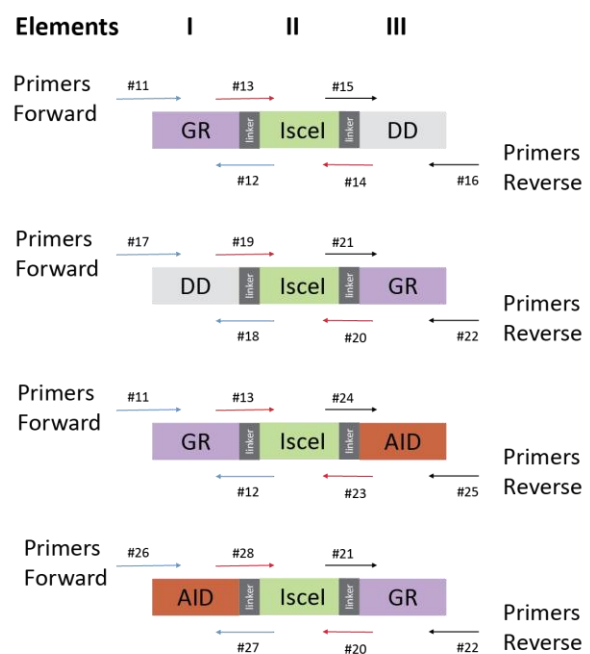
- Cutaneous T Cell Lymphoma.” *PLoS ONE* 8 (7). <https://doi.org/10.1371/journal.pone.0068915>.
- Whalen, Jenna M., Nalini Dhingra, Lei Wei, Xiaolan Zhao, and Catherine H. Freudenreich. 2020. “Relocation of Collapsed Forks to the Nuclear Pore Complex Depends on Sumoylation of DNA Repair Proteins and Permits Rad51 Association.” *Cell Reports* 31 (6): 107635. <https://doi.org/10.1016/j.celrep.2020.107635>.
- Yamaguchi, Tepei, Fabien Cubizolles, Yu Zhang, Nina Reichert, Hubertus Kohler, Christian Seiser, and Patrick Matthias. 2010. “Histone Deacetylases 1 and 2 Act in Concert to Promote the G1-to-S Progression.” *Genes and Development* 24 (5): 455–69. <https://doi.org/10.1101/gad.552310>.
- Yang, Wen Ming, Carla Inouye, Yingying Zeng, David Bearss, and Edward Seto. 1996. “Transcriptional Repression by YY1 Is Mediated by Interaction with a Mammalian Homolog of the Yeast Global Regulator RPD3.” *Proceedings of the National Academy of Sciences of the United States of America* 93 (23): 12845–50. <https://doi.org/10.1073/pnas.93.23.12845>.
- Yang, X. J., and E. Seto. 2007. “HATs and HDACs: From Structure, Function and Regulation to Novel Strategies for Therapy and Prevention.” *Oncogene* 26 (37): 5310–18. <https://doi.org/10.1038/sj.onc.1210599>.
- Yang, Xiang-Jiao, and Edward Seto. 2008. “The Rpd3/Hda1 Family of Lysine Deacetylases: From Bacteria and Yeast to Mice and Men.” *Nature Reviews Molecular Cell Biology* 9 (3): 206–18. <https://doi.org/10.1038/nrm2346>.
- Yu, Kefei, Frederic Chedin, Chih Lin Hsieh, Thomas E. Wilson, and Michael R. Lieber. 2003. “R-Loops at Immunoglobulin Class Switch Regions in the Chromosomes of Stimulated B Cells.” *Nature Immunology* 4 (5): 442–51. <https://doi.org/10.1038/ni919>.
- Zagelbaum, Jennifer, Allana Schooley, Junfei Zhao, Benjamin R Schrank, Elsa Callen, Shan Zha, Max E Gottesman, et al. 2021. “ARP2/3- and Resection-Coupled Genome Reorganization Facilitates Translocations.” *BioRxiv*, January, 2021.10.22.465487. <https://doi.org/10.1101/2021.10.22.465487>.
- Zhang, Feng, Mehrdad Khajavi, Anne M. Connolly, Charles F. Towne, Sat Dev Batish, and James R. Lupski. 2009. “The DNA Replication FoSTeS/MMBIR Mechanism Can Generate Genomic, Genic and Exonic Complex Rearrangements in Humans.” *Nature Genetics* 41 (7): 849–53. <https://doi.org/10.1038/ng.399>.
- Zhang, Yu, and Maria Jasin. 2011. “An Essential Role for CtIP in Chromosomal Translocation Formation through an Alternative End-Joining Pathway.” *Nature Structural & Molecular Biology* 18 (1): 80–84. <https://doi.org/10.1038/nsmb.1940>.
- Zhang, Yu, Rachel Patton McCord, Yu Jui Ho, Bryan R. Lajoie, Dominic G. Hildebrand, Aline C. Simon, Michael S. Becker, Frederick W. Alt, and Job Dekker. 2012. “Spatial Organization of the Mouse Genome and Its Role in Recurrent Chromosomal Translocations.” *Cell* 148 (5): 908–21. <https://doi.org/10.1016/j.cell.2012.02.002>.
- Zhu, Songli, Mohammadjavad Paydar, Feifei Wang, Yanqiu Li, Ling Wang, Benoit Barrette, Tadayoshi Bessho, Benjamin H. Kwok, and Aimin Peng. 2020. “Kinesin Kif2C in Regulation of DNA Double Strand Break Dynamics and Repair.” *ELife* 9: 1–22. <https://doi.org/10.7554/eLife.53402>.
- Zupkovitz, Gordin, Julia Tischler, Markus Posch, Iwona Sadzak, Katrin Ramsauer, Gerda Egger, Reinhard Grausenburger, et al. 2006. “Negative and Positive Regulation of Gene Expression by Mouse Histone Deacetylase1.” *Molecular and Cellular Biology* 26 (21): 7913–28. <https://doi.org/10.1128/mcb.01220-06>.

Appendix 1

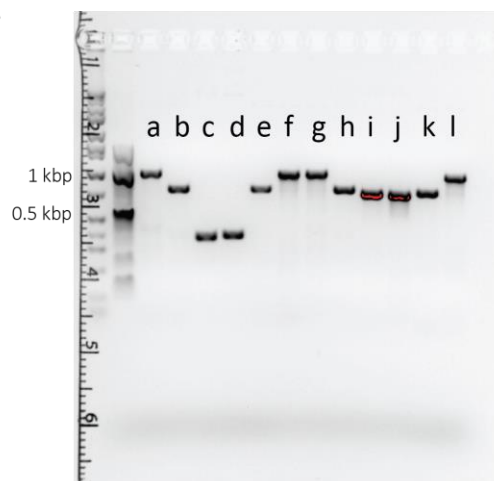
A



B



C



| | | |
|------------|--|---------------|
| a: #11-#12 | | GR-I-SceI-DD |
| b: #13-#14 | | |
| c: #15-#16 | | |
| d: #17-#18 | | DD-I-SceI-GR |
| e: #19-#20 | | |
| f: #21-#22 | | |
| g: #11-#12 | | GR-I-SceI-AID |
| h: #13-#23 | | |
| i: #24-#25 | | |
| j: #26-#27 | | AID-I-SceI-GR |
| k: #28-#20 | | |
| l: #21-#22 | | |

* 100 bp DNA Ladder

Figure Appendix 1: Cloning of Dox-inducible I-SceI degron constructs using Gibson assembly and seamless cloning strategy. **A.** Each elements contain homologues sequences with the adjacent one. **B.** Schematic of primer designing for each respective constructs. **C.** Amplification with the respective primers pair (each containing specific overhangs) is confirmed by gel electrophoresis. Expected size for GR cassette: 930 bp; I-SceI cassette: 705 bp; DD cassette: 327 bp; AID cassette: 627 bp.

Appendix 2

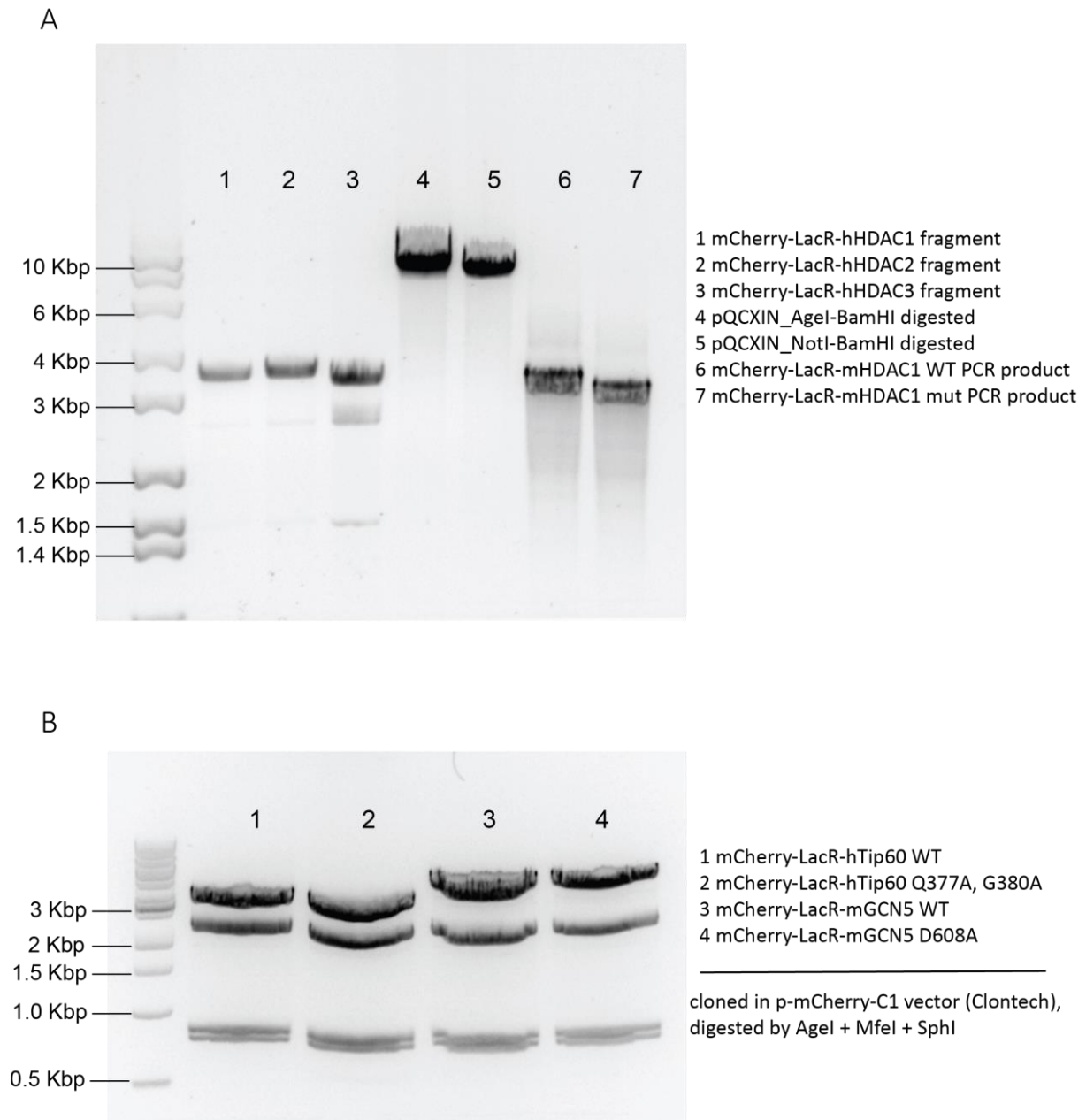


Figure Appendix 2: mCherry-LacR-constructs' fragments size inspection, prior cloning in retroviral expression vector. A. Gel electrophoresis confirms mCherry-LacR-hHDACs digestion pattern (upon AgeI and BamHI double digestion, lines 1, 2 and 3); pQCXIN vectors digested with AgeI and MfeI (line 4) or with NotI and BamHI (line 5), to clone respectively human HDACs and the mouse HDACs in frame with mCherry-LacR; PCR products size of mCherry-LacR mHDAC1 WT and mut amplified by primers #3 and #4 (lines 6 and 7). Expected size: line 1 3318 bp, line 2 3336 bp; line3 3156 bp, line 6 3288 bp; line 7 3138bp. **B.** Gel electrophoresis for size inspection and to gel extract the fragments encoding for mCherry-LacR-hTIP60 WT and MUT and mCherry-LacR-GCN5 WT and mut. Fragments were selectively digested by AgeI and MfeI and the vector was furtherly fragmented by SphI. Expected size: line 1 and 2: 3394 bp (AgeI/MfeI fragment); whereas line 3 and 4:4345 (AgeI/MfeI fragment), then 2175 bp, 816 bp, 763 bp, 72 bp (not visible on the gel) are common in each lines.

Appendix 3

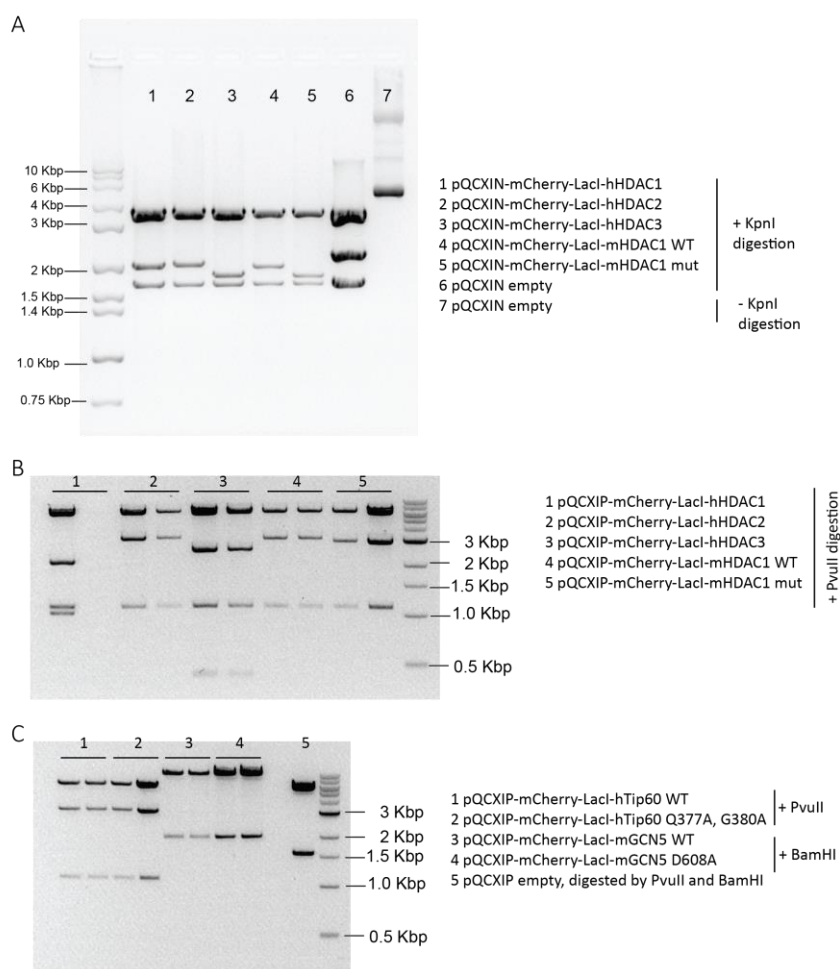


Figure Appendix 3: Expression vectors are confirmed by restriction pattern. **A.** Final pQCXIN expression vectors containing mCherry-LacR-HDACs constructs were confirmed by KpnI digestion pattern. Expected size: **B.** PvuII digestion profile confirm for 2 colonies of pQCXIP-mCherry-LacR-HDACs (upper gel) and pQCXIP-mCherry-LacR-TIP60 constructs (lower gel). pQCXIP-mCherry-LacR-GCN5 constructs were restricted by BamHI enzyme. Expected size in table below:

| fig | line | enzyme | plasmid | Fragments size (bp) |
|--------------|------|--------|---------------------------------------|----------------------------|
| A | 1 | KpnI | pQCXIN + mCherry-LacR hHDAC1 | 3557; 3518; 1941; 1668 |
| | 2 | | pQCXIN + mCherry-LacR hHDAC2 | 3557; 3518; 1959; 1668 |
| | 3 | | pQCXIN + mCherry-LacR hHDAC3 | 3557; 3511; 1779 1668 |
| | 4 | | pQCXIN + mCherry-LacR mHDAC1 WT | 3557; 3507; 1911; 1668 |
| | 5 | | pQCXIN + mCherry-LacR mHDAC1 mut | 3557; 3505; 1761; 1668 |
| | 6 | | pQCXIN empty | 3557; 2156; 1668 |
| B (upper) | 1 | PvuII | pQCXIP + mCherry-LacR hHDAC1 | 6201; 2055; 1104; 1012; 93 |
| | 2 | | pQCXIP+ mCherry-LacR hHDAC2 | 6201; 3085; 1104; 93 |
| | 3 | | pQCXIP + mCherry-LacR hHDAC3 | 6201; 2606; 1104; 414; 93 |
| | 4 | | pQCXIP + mCherry-LacR mHDAC1 WT | 6190; 3037; 1104; 93 |
| | 5 | | pQCXIP + mCherry-LacR mHDAC1 mut | 6188; 2877; 1104; 93 |
| B (lower) | 1/2 | PvuII | pQCXIP +mCherry-LacR-TIP60 wt and mut | 6201; 3123; 1104; 93 |
| | 3/4 | BamHI | pQCXIP +mCherry-LacR-GCN5 wt and mut | 9516; 1956 |

*The fragment of 93bp is not visible because it run out from gel.

Appendix 4

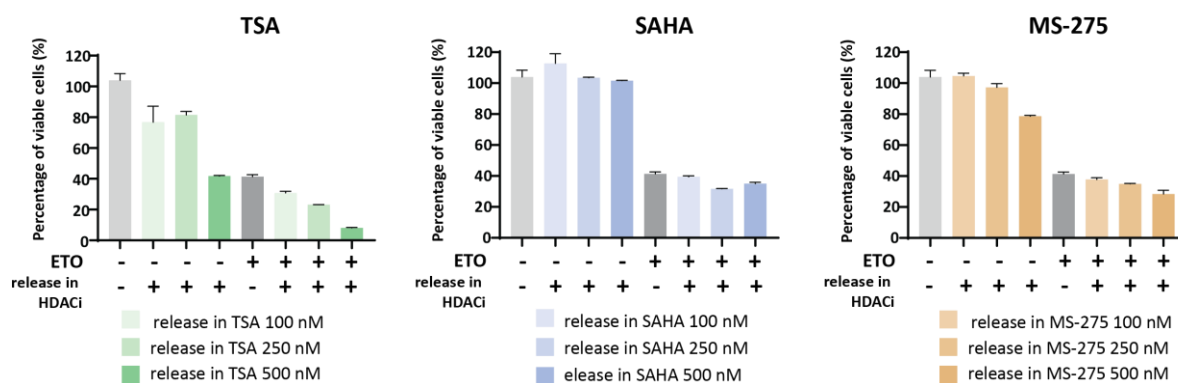


Figure Appendix 4: Cell viability upon etoposide and HDACs inhibitors in SKM-1 cells. SKM-1 cells were treated with 10 μ M of etoposide for 6 hours and released in media supplement with different concentrations of HDACs inhibitors. TSA, SAHA and MS-275 were used to inhibit histone deacetylases at the following concentrations: 100 nM, 250 nM and 500 nM. Cell viability was measured 2 days later by incubating a redox dye for at least 2h. Viability is measured as the cell capability to metabolize the redox dye and convert it in a fluorescent product. Error bars indicate standard deviation of the mean of technical triplicates.

List of abbreviations arranged in alphabetical order

4-OHT, 4-Hydroxytamoxifen
53BP1, p53 Binding Protein 1
 γ H2AX, phosphorylation of Histone H2AX on Ser139
AID, auxin inducible degron
Alt-EJ, alternative end joining
BAC, bacterial artificial chromosomes
BCR, breakpoint cluster region
BIR, break-induced replication
BLESS, Breaks Labeling, Enrichment on Streptavidin, and Sequencing
sBLISS, suspension- Breaks Labeling In Situ and Sequencing
BRCA1 Breast cancer early onset 1
CDKs, cycline-dependent kinases
ChIP, Chromatin Immunoprecipitation
CMV, cytomegalovirus
CRISPR-Cas9, Clustered Regularly Interspaced Short Palindromic Repeats-Cas9
DD, destabilization degron
DDR, DNA damage response
DEX, dexamethasone
DNAPK, DNA-dependent protein kinase
DNMT, DNA methyltransferase
DOX, doxycycline
DPC, DNA-protein crosslink
DRB, 5,6-Dichloro-1- β -d-ribofuranosylbenzimidazole
DSB, double-strand break
EdU, 5-Ethynyl-2'-deoxyuridine
ER, estrogen receptor
ETO, etoposide
EU, 5-Ethynyl Uridine
FISH, fluorescence *in situ* hybridization
GR, glucocorticoid receptor
gnDNA, genomic DNA
H3, Histone H3
H3K4me3, tri-methylation on lysine 4 of histone H3
H3K56ac, acetylation on lysine 56 of histone H3
H4K12ac, acetylation on lysine 12 of histone H4
H4K16ac, acetylation on lysine 16 of histone H4
HA-tag, hemagglutinin tag
HAT, histone acetyltransferase
HDAC, histone deacetylase
HP1, Histone protein 1
HR, homologous recombination
HT-FISH, High-throughput FISH
IF, immunofluorescence
IAA, indole-3-acetic acid
IPTG, Isopropyl- β -D-thiogalactoside
LacO, Lac Operator
LacR (=LacI), Lac Repressor
LM-PCR, Ligation Mediated PCR
MLL, mixed lineage leukemia gene
MRE11, meiotic recombination 11
NHEJ, non-homologous end joining
NuA4 complex, Nucleosome Acetylation complex
NuRD complex, Nucleosome Remodeling and Deacetylase complex
PBS, phosphate-buffer saline
PFA, paraformaldehyde
PLL, poly-L-lysine
pRPA, phosphorylation of replication protein A (phospho-Ser4/Ser8)
PTM, post-translational modification
qPCR, quantitative PCR

ROI, region of interest
RSS, recombination signal sequence
RT, room temperature
siRNAs, small interfering RNAs
SAHA, suberoylanilide hydroxamic acid
sBLISS, in-suspension Breaks Labeling In Situ and Sequencing
SSA, single-strand annealing
SSB, single-strand break
ssDNA, single strand DNA
SUMO, Small Ubiquitin-related MOdifier protein
SV40, simian virus 40
t-AML, therapy-acute myloid leukemia
TDP2, Tyrosyl-DNA phosphodiesterase 2
TetO, Tet Operator
TetR, Tet Repressor
TET ON promoter, Tetracycline ON promoter
TOP2, Topoisomerase 2
TOP2ccs, Topoisomerase 2 cleavage complexes
TSA, Trichostatin A
TSS, transcription start site
VCP, valosin-containing protein
WT, wild-type

List of figures

Chapter 1 - Introduction

Figure 1: DSB-repair pathways.

Figure 2: Chromosome translocations can cause gene deregulation.

Figure 3: DNA and chromatin features influencing breakage susceptibility and translocation formation.

Figure 4: Changes in chromatin organization influence mobility and locus positioning in eukaryotes.

Figure 5: Lysine Acetylation.

Figure 6: Organization of human Histone Deacetylase family and domains similarity with *S. cerevisiae* Rpd3 enzyme.

Figure 7: Cell system to induce and to quantify mechanistic steps of chromosome translocations in real time.

Chapter 2 - Results

Figure 8: Epigenetic inhibitors screening revealed many modulators of the translocations frequency.

Figure 9: Translocation frequency decreases upon reduction of the condensation state of chromatin structure

Figure 10: Dox- inducible system to generate DSBs in time and space controlled manner.

Figure 11: Dox-inducible expression of I-SceI endonuclease in various constructs configurations and controlled-induction of I-SceI-mediated DSBs.

Figure 12: Repair of I-SceI-induced DSBs.

Figure 13: Time and space control of I-SceI-DSBs.

Figure 14: I-SceI nuclear transfer progressively induces DSBs formation at LacO locus.

Figure 15: Comparison of two systems to induce DSBs and chromosome translocations.

Figure 16: Artificial tethering of specific chromatin modifiers at LacO-I-SceI site.

Figure 17: Chromatin changes upon tethering of histone deacetylases or histone acetyltransferases enzymes in proximity of a DSB.

Figure 18: Artificial tethering of specific chromatin modifiers influence the status of chromatin condensation of the locus.

Figure 19: Artificial tethering of HDAC1 or TIP60 does not lead to difference in chromatin accessibility.

Figure 20: Artificial tethering of HDAC1 and TIP60 induce changes in H4 Acetylation levels at Lac array.

Figure 21: HDAC1 depletion significantly decreases LacO-TetO translocation frequency.

Figure 22: Induction of chromatin domains influences the formation of LacO-TetO translocations.

Figure 23: HDACs inhibition enhanced the motion properties of a broken LacO-I-SceI locus.

Figure 24: HDAC1 depletion enhanced the motion properties of a broken LacO-I-SceI locus.

Figure 25: Controlled induction of AsiSI-DSBs.

Figure 26: AsiSI-induced γ H2AX is reduced upon decitabine treatment, while DNAPKi delays γ H2AX restoration.

Figure 27: Decitabine blocks formation of γ H2AX foci also upon 24 hours of persistent AsiSI expression.

Figure 28: Decitabine blocks AsiSI-DSBs and AsiSI induced translocations.

Figure 29: DSBs-induced changes of H3K56ac, H4K12ac and H4K16ac over 1 Kbp window around DSBs.

Figure 30: AsiSI-induced chromosome breaks and translocations are more frequent at sites, which lose H4K16ac upon DSB formation.

Figure 31: AsiSI-DSBs exhibit two rates of repair which are not influenced by different acetylation status of the chromatin surrounding DSBs.

Figure 32: TSA and SAHA treatment reduce etoposide-induced *MLL* translocations.

Figure 33: TSA and SAHA treatments potentiate etoposide-induced genome instability and decrease cell viability.

Figure 34: Both TOP2A and TOP2B determine etoposide-mediated phosphorylation of H2AX.

Figure 35: TOP2A and TOP2B levels upon siRNAs or shRNAs exposure in the indicated cell lines.

Figure 36: Transcription and replication inhibition prevent DNA incorporation of Ethynyl Uridine and 5-Ethynyl-2' Deoxyuridine, respectively.

Figure 37: Transcription and replication inhibition reduces etoposide-mediated DNA damage.

Figure 38: VCP and proteasome inhibitions reduce etoposide-mediated genome instability.

Appendices

Figure Appendix 1 - Cloning of Dox- inducible I-SceI degron constructs using Gibson assembly and seamless cloning strategy

Figure Appendix 2 - mCherry-LacR-constructs' fragments size inspection, prior cloning in retroviral expression vector

Figure Appendix 3 - Expression vectors are confirmed by restriction pattern

Figure Appendix 4 - Cell viability upon etoposide and HDACs inhibitors in SKM-1

Figure Appendix 5 - Depletion of Top2A mainly reduces etoposide-triggered H2AX and RPA phosphorylation in U2OS cells

List of tables

Table 1 - Antibodies used in immunofluorescence

Table 2 - siRNAs target sequences

Table 3 - Antibodies used in Western and dot blotting

Table 4 - BAC probes

Table 5 - Public available datasets used in this study

Table 6 - Plasmids used in this study

Table 7 - Oligos sequence used in this study

